PHYSICAL PROPERTIES OF THIN FILMS OF SODIUM TUNGSTEN BRONZES

by

Anastasios Travlos B.Sc. (Physics), M. Tech.

June 1984

A thesis submitted in partial fulfilment of the requirements for the degree of Doctor of Philosophy of the University of London.

Department of Electrical Engineering
Imperial College of Science and Technology
London

Abstract

Sodium Tungsten Bronze thin films are prepared by co-evaporation of WO_3 and sodium as well as insertion of the sodium from the vapour phase into evaporated WO_3 films.

Trasmission electron microscopy reveals that the films are polycrystalline, the size of their grains being a function of the rate of deposition and substrate temperature.

The sodium concentration of the films is determined by electrochemical extraction of the sodium from a small area of the film.

The optical properties of the films are studied as a function of the sodium concentration x, ($0 \leq x \leq 0.22$), in the wavelength range of 0.3μm to 4.5μm. The d.c. resistivity and thermoelectric power of the films are also measured in the temperature range of 220°K to 300°K.

The Na_xWO_3 films are treated as a collection of crystalline grains embedded in a matrix of disordered grain boundary material.

The grain material behaves as a degenerate semiconductor, whose degree of degeneracy is a function of x. Its optical properties are interpreted in terms of three interband electronic transitions : valence to conduction band, which gives rise to the main absorption edge and filled states of the conduction band to a higher lying conduction band and to the empty sodium states, which give rise to the blue colour of the films. The conduction and valence bands of WO_3 are separated by both an indirect and a larger direct gap whose magnitude depends on the crystal structure. The electronic band structure of Na_xWO_3 is derived from the band structure of WO_3 in a "rigid band" approximation for $x \leq 0.05$. For larger values of x, the band structure of WO_3 is deformed under the influence of the high sodium concentration.

The electrical properties of the films are dominated by the presence of the high density of grain boundaries.

Acknowledgements

I am deeply indebted to my supervisor Professor Mino Green for his contributions to the development of this work, his encouragement and enlightened advise throughout this work.

I would like to thank Dr. K.S. Kang for his assistance in the initial stages of this project and Mr. S. Biswas for his assistance in developing the computing programme.

My thanks are also due to Mrs D Abeysekera for typing the text.

I wish to acknowledge the award of a scholarship by "Alexandros S. Onasis" Foundation for part of this work.

I would also like to express my graditude to my parents for their moral and financial support throughout my education.

Contents

page

LIST OF TABLES

LIST OF FIGURES

Page

Page

Page

Page

Page

Page

CHAPTER 1

Introduction

Sodium tungsten bronze is one of the several non-stochiometric ternary metal oxides of the general formula M_xWO_3, where M is a metal or hydrogen and $0 \leq x \leq 1$, known as tungsten bronzes.

Sodium tungsten bronzes (Na_xWO_3) were first obtained at the beginning of the 19^{th} century [1]. Since then, several elements were found to form tungsten bronzes [2]. Because of their interesting physical and chemical properties, many research groups have been studying these compounds in recent years.

Several methods have been used to prepare tungsten bronzes : reduction of a sodium tungstate-tungsten trioxide mixture with hydrogen or other reducing agents [3], electrolytic reduction of a molten mixture of metal tungsten and tungstic acid [4], vapour-phase reaction of WO_3 and metals [5] as well as chemical reduction of metal tungstate, tungsten trioxide and tungsten metal in vaccum [6]. A review of the above methods of preparation of tungsten bronzes is given by Hussain [2].

In tungsten bronzes, the metal M is inserted in the WO_3 sublattice which consists of WO_6 corner-linked octahedra. The WO_6 octahedra can be arranged in different ways depending on the nature and the concentration of M. The structure of WO_3, which is considered as the host structure of M_xWO_3, shows five phase transitions in the temperature range -180°C to 900°C [7,8,9,10] : monoclinic $\xleftrightarrow{-52°C}$ triclinic $\xleftrightarrow{-17°C}$ monoclinic $\xleftrightarrow{467°C}$ orthorombic $\xleftrightarrow{680°C}$ tetragonal.

The structure of the above five phases of WO_3 can be obtained from the ideal ReO_3 structure (Fig. 1.1) by small displacement of the

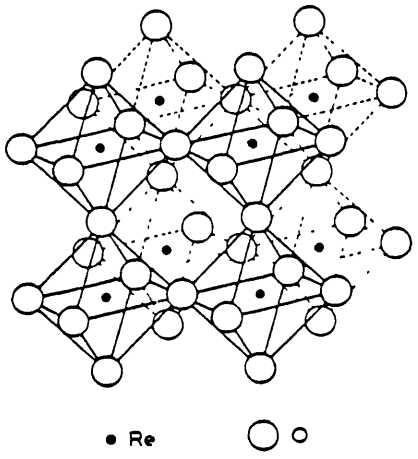

Fig. 1.1 : The ReO_3 structure (after Doumerc et. al [11]).

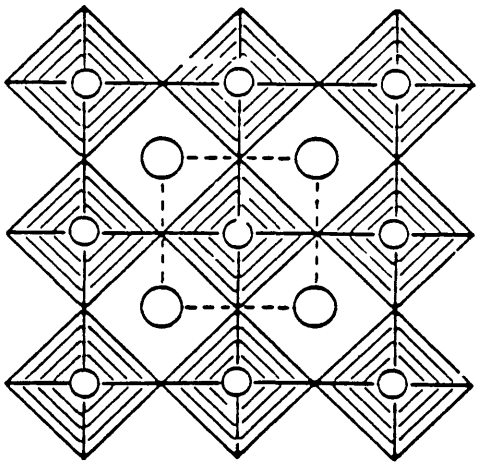

Fig. 1.2 : The structure of perovskite tungsten bronze. The large circles indicate interstitial metal atoms and the small circles tungsten atoms.(after Hussain [6])

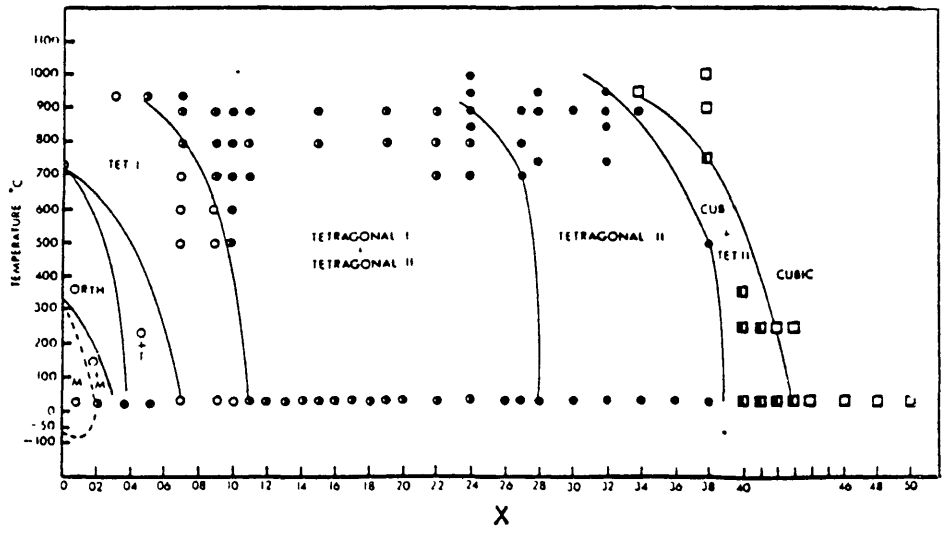

Fig. 1.3 : Phase diagram of Na_xWO_3 (after Ribnick [6]).

tungsten ions from the centre of the octahedra [2].

When all the interstitial sites, between the WO_6 octahedra, are filled by the sodium ions the perovskite structure with cubic unit cell is obtained. The perovskite structure of Na_xWO_3 is shown in Fig. (1.2). As the sodium content decreases, the perovskite structure is progressively distorted and several other phases with lower symmetry are obtained Fig. (1.3) shows the place diagram for Na_xWO_3 as a function of x, obtained by Ribnick et. al. [6]. THe lowering of the symmetry of the perovskite structure leads to tilting of the WO_6 octahedra and their rearrangement so that apart from the tetragonal channels, shown ın Fig. (1.2), channels of hexagonal, pentagonal and triangular cross-sections appear. Sodium ions can be accomodated in all of these channnels, except the triangular ones which are very small [2].

The electronic properties of tungsten bronzes, and in particular of Na_xWO_3, have been extensively investigated in the range of x-values $0.25 \leq x \leq 1$.

Nuclear magnetic resonance Knight shift measurements [12] and Hall effect measurements [13,14,15] show that the alkali atoms are fully ionised and the nearly free electrons are located in a delocalized conduction band.

Resistivity [13,15,16,17], heat capacity and magnetic susceptibility [18], Seebeck coefficient [13] and optical measurements [19,20,21] confirm that the current carries in tungsten bronzes are nearly free electrons.

The mechanism of band formation in tungsten bronzes has been explained in different ways. Goodenough [22, 23] assumes that the conduction band of tungsten bronzes arises from the tungsten atom array and that the alkali atoms act as donors to the otherwise empty conduction band. A similar interpretation was proposed by Sienko as well [16].

This model is in agreement with the experimentally obtained properties of the bronzes and theoretical band calculations [24,25,26].

On the other hand, Mackintosh [27] and Fuchs [28] postulate that the conduction band of tungsten bronzes is composed of overlapping alkali metal orbitals. This model has been, however, criticized mainly because it fails to account for the common behaviour of all tungsten bronzes irrespective of the particular metal ions inserted in the WO_3 lattice.

Tungsten bronzes with $x<0.25$ have not been systematically investigated mainly because of difficulties in obtaining appropriate single crystals. On the basis of the resistivity measurements on a few crystals [2,13,14], it is assumed that tungsten bronzes with $x \lesssim 0.25$ behave as semiconductors rather than metals and conflicting models have been proposed to explain this behaviour [29,30]. However, in view of the poor experimental substantiation of such a metal-nonmetal transition in tungsten bronzes, further investigation of their properties at low x-values is needed.

It should be pointed out that the properties of the dilute bronzes is not the only area in the tungsten bronze behaviour that is still ambiguous. The broad features of the behaviour of the tungsten bronzes are well accounted for by the Goodenough model. However, several questions such as the exact form of the band structure and the effect the insertion of alkali atoms has on it, as well as the scattering mechanism of charge carriers, are still unresolved.

Considerable attention has recently been given to thin film tungsten bronzes because of their technological applications in information display devices. These applications are based on the electrochromic properties of the WO_3 thin films. It has been shown that the insertion of Group I elements into WO_3 films results in tungsten bronze formation

and a change of the colour of the films, from transparent to blue. Several electrochemical electrochromic cells based upon the reversible insertion of Group I elements into WO_3 films have been fabricated and investigated [3 ,32,33,34,35].

The preparation and microstructure [36,37,38], the optical properties [38,39,40,41,42] and electrical properties [43,44,45,] of thin film tungsten bronzes have been the subject of several investigations. However, no systematic study of the properties of thin film tungsten bronzes as a function of their x-value and microstructure has been undertaken to date. The absence of such a study combined with the lack of information about the properties of dilute single crystal bronzes, has led to the proposition of different conflicting models in order to explain the electrochromic and other properties of the thin film tungsten bronzes.

Faughnan et. al. [33] propose that the electrons in H_xWO_3 films are localized at tungsten ion sites and the blue colour of these films arises from intervalency transition absorption. Deb [39] argues in favour of a colour centre formation in oxygen vacancies. Schirmer et. al. [41] believe that electron-phonon interaction is very strong in H_xWO_3 films and small polaron absorption is responsible for their colour. Green et. al. [32], on the other hand, explain the variation with x of the chemical potential of Na_xWO_3 films in terms of a free electron gas model.

It is the aim of this work to investigate the properties of Na_xWO_3 thin films as a function of their microstructure and their x-value. To this purpose, the microstructure of the films has been studied and methods to determine their x-value have been developed. The optical properties of the films have been determined in the photon energy range $0.4 \leq h\nu \leq 4eV$ by transmission and reflection measurements.

The resistivity and Seebeck coefficient of the films have also been determined as a function of the temperature.

REFERENCES

[1] F. Wöhler, Ann. Chim. Phys. 43, 29, (1823)

[2] A. Hussain, University of Stockholm Chem. Commun. 2, 1,(1978)

[3] E. Banks and A. Wold,"Preparative Inorganic Reactions" Ed. J. William, Interscience Publishers, (1968)

[4] G. Hägg, Z. Phys. Chem. B29, 192, (1935)

[5] M.J. Sienko, J. Ann. Chem. Soc. 81, 5556, (1959)

[6] A.S. Ribnick, B. Post and E. Banks, Nonstochiometric compounds, Advances in Chemistry, Series 39, 246, (1963)

[7] E. Salje, Acta Crystallogr. B33, 574, (1977)

[8] S. Tanisaki, J. Phys. Soc. Japan, 15, 573, (1960)

[9] W.L. Kehl, R.G. Hoy and D. Wahl, J. Appl. Phys. 33, 212, (1952)

[10] B.O. Loopstra and M.H. Rietveld, Acta Crystallogr. B25, 1420, (1969)

[11] J.P. Doumerc, Tungsten Bronzes : Fluorine or Tantalum substitution, "The Metal-Nonmetal Transition in Disordered Systems", Ed. L.R. Friedmann and D.P. Tungtall, (1968)

[12] W.H. Jones, E.A. Garbaty and R.G. Barnes, J. Chem. Phys. 36, 494, (1962)

[13] H.R. Shanks, P.H. Sidles and G.C. Danielson, "Advances in Chemistry" Series 39, Amer. Chem. Soc., 1963

[14] P.A. Lightsey, P.A. Lilienfeld and D.F. Holcomb, Phys. Rev. B, 14, 4730, (1976)

[15] L.D. Muhlestein and G.C. Danielson, Phys. Rev., 15, 825, (1967)

[16] M.J. Sienko, Non-Stoichiometric Compounds, Adv. Chem. Series 39, 224, (1963)

[17] L.D. Elleerbeck, H.R. Shanks, P.H. Sidles and G.C. Danielson, J. Chem. Phys. 35, 298, (1961)

[18] F.C. Zumsteg, Phys. Rev. B, 14, 1406, 1976

[19] P.G. Dickens, R.M.P. Quilliam and M.S. Whittingham, Mat. Res. Bull., 3, 941, 1968

[20] J.F. Owen, K.J. Teegarden and H.R. Shanks, Phys. Rev. B, 18, 3827, (1978)

[21] P. Camagni, A. Manara, G. Campagnoli, A. Gustinetti and A. Stella, Phys. Rev. B, 15, 4623, (1977)

[22] J.B. Goodenough, Metalic Oxides, Progress in Solid State Chemistry, H. Reiss, Pergamon Press, 5, 145, (1971)

[23] J.B. Goodenough, J. Appl. Phys., 37, 1415, (1966)

[24] D.W. Bullett, J. Phys. C., 16, 2197, (1983)

[25] P.W. Bullett, Solid State Commun., 46, 575, (1983)

[26] L. Kopp, B.N. Harmon and S.H. Liu, Solid State Commun., 22, 677, (1977)

[27] A.R. Mackintosh, J. Chem. Phys., 38, 1991, (1963)

[28] N.F. Mott, Phil. Mag., 35, 111, (1977)

[30] I. Webman, J. Jortner and M.H. Cohen, Phys. Rev. B, 13, 713, (1976)

[31] M.Green, W.C. Smith and J.A. Weiner, Thin Solid Films, 38, 89, (1976)

[32] M. Green and K. Kang, Solid State Ionics, 8, 281, (1983)

[33] B.W. Faughnan, R.S. Crandall and P.M. Heyman, RCA Rev. 36, 177, (1975)

[34] H.N. Hersch, W.E. Kramer and J.H. MsGee, Appli. Phys. Lett., 27, 646, (1975)

[35] H. Morita and H. Washida
Japanese J. Appl Phys., 19, L228, (1980)

[36] M. Shiojiri, T. Miyano and C. Kaito, Japanese J. Appl. Phys., 18, 1937, (1979)

[37] R. Le Bihan, G. Grandet and S. Paoli, Proc. 8th International Vaccum Congress, 409, (1980)

[38] L.A. Aleshina, A.D. Fofanov and O.N. Shivrin, Sov. Phys. Dokl., 27, (1972)

[39] S.K. Deb. Phil. Mag., 27, 801, (1973)

[40] A. Nakamura and S. Yamada, Appli. Phys., 24, 55, (1981)

[41] O.F. Schirmer, V. Wittwer, G. Baur and G. Brandt, J. Electrochem. Soc., 124, 748, (1977)

[42] V. Dallacasa, M. Manfredi and G. Schianchi, Thin Solid Films, 91, 1, (1982)

[43] M.R. Goulding and C.B. Thomas, Thin Solid Films, 62, 175, (1979)

[44] R.S. Crandall and B.W. Faughnan, Phys. Rev. Lett., 39, 232,(1977)

[45] K. Miyake, H. Kaneko and V. Teramoto, J. Appli. Phys., 53, 1511, (1982)

CHAPTER 2

FILM PREPARATION AND CHARACTERIZATION

Introduction

The major requirements in $Na_x WO_3$ films for accertaining their physical properties, are that they should be chemically pure and reproducible. Since the properties of the films depend in a complicated and not always well understood way, on the method of preparation, the achievement of the above requirements is not an easy task.

The main problems encountered are :

a) the minimization of the water contamination of the films

b) the reproducibility of the microstructure of the films and

c) the controllable variation of the sodium content of the films.

There are various methods, both chemical and physical, of depositiong thin films.

The chemical methods have not been used in the present study because of problems in controlling film parameters. On the other hand, from the physical methods, namely evaporation and sputtering, it was found [1] that the former offers the greater flexibility in control over

i) deposition rates and substrate temperature, which determine the film microstructure,

ii) Hydrogen contamination and

iii) Sodium insertion.

Therefore the method used throughout this study was the evaporation.

2.1.1. WO_3 Evaporation

a. Preparation of WO_3 powder

Commercially available WO_3 powder consists of 1μm agglomerates of small particles. In order to reduce the surface area and therefore the amount of water contained in a given mass of WO_3, the following heat treatment of the powder was undertaken : Analar grade WO_3 powder is packed into platinum crucible and heated at 1350°C for 15 hours after a preheat of 24 hours at 700°C to remove bound water. The resulting sintered mass consists of 50μm single crystallites.

b. Source

There is a variety of evaporation sources that can be used to evaporate WO_3. However, it has been found [1,2] that the best results are obtained using the chimney source.

The construction of the source used is shown in Fig. 2.1.1. A sheet of .002 inch molybdenum foil is spot welded to the stainless steel collars through which the heating current is passed. The WO_3 powder is contained inside a silica test-tube which fits closely into the source cavity.

Evaporation rates of 300Å /min to 2000 Å /min at currents of 50 to 65 Amps are possible with this source at 18 cm from the substrate.

c. Evaporation

The properties of the films depend in a critical way on the procedure

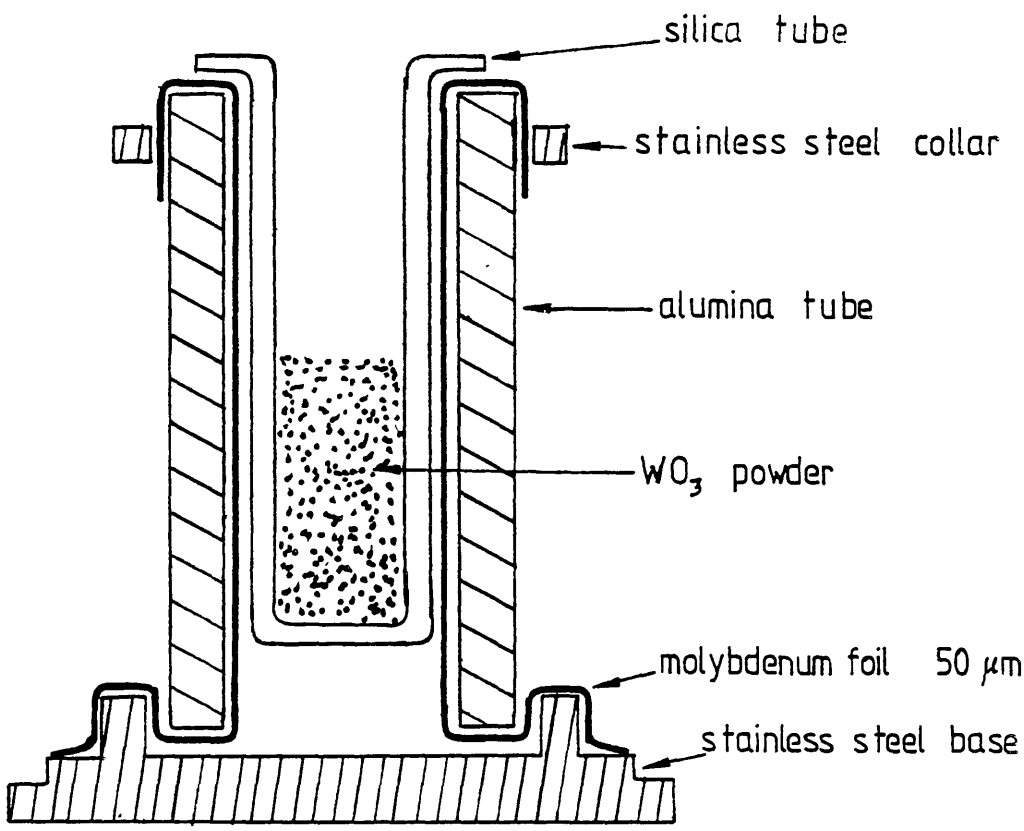

Fig. 2.1.1: The chimney source used in the evaporation of WO_3 films

of evaporation. The following procedure was found to be successful and was employed throughout the present study.

Films were deposited on silica and I.T.O coated glass slides. The slides were thoroughly cleaned with Tepol and water followed by a three minutes distilled water both in an ultrasonic tank and a then were cycled in a vapour decreasing unit (Sholet unit) in which iso-propyl alcohol (I.P.A) was continuously refluxed.

Once the clean slides were positioned onto the substrate heater the system was pumped down to less then 10^{-6} Torr.

A liquid nitrogen trap was used to minimize the water vapour present in the system.

The WO_3 powder was outgassed for 20 minutes at 900°C and then its temperature was gradually raised to 1200°C. By controlling the current passing through the source the desired constant rate of evaporation was achieved and then the substrates were exposed to the WO_3 vapour, opening the shutter which was masking them. The pressure of the chamber as well as the rate of evaporation and thickness of the film were continuously monitored.

During evaporation the pressure in the chamber rises to about 5×10^{-5} Torr where it remains constant for 3 to 5 minutes before it starts decreasing. If the substrates remain exposed to the vapour after the decrease in pressure, the films produced are slightly coloured and/or craze when exposed to atmosphere. Similar phenomena occur to films produced from WO_3 powder left over from the first evaporation or when the evaporation is carried out at pressures higher than 10^{-4} Torr or without the liquid nitrogen trap.

It has been pointed out [1] that the most important factor contributing to the crazing is the composition of the vapour. Ackerman and

Rauth [3] have determined the composition of the vapour of samples of initial compositions of O/W equal to 2.91, 2.931 and 2.956. All compositions except the last resulted in the solid system. $W_{20}O_{49}$ - $W_{20}O_{48}$ whereas the last sample produced $WO_{2.96}$. The first two oxides are found [4] to be unstable at 1 atmosphere pressure and below 585°C and 485°C. Therefore, it is most likely that prolonged heat treatment of WO_3 powder in vaccum leads to a loss of oxygen and hence production of unstable films. On the other hand, films produced at the first stages of evaporation from fresh WO_3 powder have been found [5] to have an O/W ratio equal to 2.96 ± 0.18.

The blue colouration of the films prepared either at higher than 10^{-4} Torr pressures and/or without the liquid nitrogen trap, is believed to be due to hydrogen bronze (H_xWO_3) formation. It has been established by Raudin [6], that the as-evaporated WO_3 films contain a certain amount of water, which decreases as the evaporation pressure decreases. This water bound on the films can become a source of H, provided that sufficient energy is available for its production. It is well known, for example, that H_xWO_3 can easily be formed by either U.V. irradiation [7], or the presence of moderate electric fields (10^4 V cm^{-1}) [5,8]. In these cases the energy required for H production from the water bound to the films is supplied by the U.V. photons or the electric field.

In the case of our films, however, the hydrogen production and its subsequent diffusion into the WO_3 lattice may occur in a different way. The surface of the films are found to be slightly non-stochiometric [3]. The oxygen of the water molecules can interact with the oxygen defficient WO_3 lattice liberating hydrogen which then diffuses into the film to form a bronze. Such a process is expected to be temperature dependent. Indeed, the colouration of the films is found to be strongly temperature

dependent. When transparent films are heated in vacuum at 60°C or higher they become blue and their colour deepens as their temperature increases. Further evidence in support of the hydrogen bronze formation is the fact that these blue WO_3 films can be bleached electrochemically. However, the exact mechanism of the process leading to H_xWO_3 formation is not well understood at the moment and further work is needed for its qualitative understanding.

On the basis of the above hypothesis it seems probable that all WO_3 films contain a certain amount of hydrogen. Therefore they should be described by the formula H_xWO_3. Depending on the particular way of preparation x can vary from less than 10^{-4} up to $x = 10^{-2}$.

Following the procedure described at the beginning of the section and taking into consideration the limitations presented above, one can produce films which are transparent and stable. Their thickness can be varied by changing the time and rate of evaporation but it is limited to about 1μm by the time taken for the WO_3 powder to become non-stochiometric and the deposition of an unstable film to begin.

2.1.2 $Na_x WO_3$ preparation

The requirements for our films were that they should be deposited on a transparent and insulation substrate, so that optical and electrical measurements could be performed and that they should posess a uniform distribution of sodium.

Two methods, satisfying the above requirements were used by the present study : i) co-evaporation of sodium and WO_3 and ii) insertion of sodium from the vapour in already deposited WO_3 films.

a) Co-evaporation of sodium and WO_3

Because of the large difference in the vapour pressures of sodium and WO_3, the two materials have to be evaporated from two different boats kept at different temperatures.

The source and method of evaporation of WO_3 was described in the previous section.

Sodium was evaporated from a molybdenum boat placed very near the chimney source of WO_3. Because the distance between the two sources is much smaller than the distance between source and substrate, the films produced are uniform both in thickness and sodium concentration.

Sodium is very reactive and therefore when exposed to air, even for a few minutes, a layer of sodium oxide is formed around it, which prevents the evaporation of sodium. To overcome this problem the following procedure was adopted : the sodium was heated to about $100^{o}C$ for ten minutes to outgas it and then the temperature was raised for a few seconds to $350^{o}C$. At this temperature the sodium is boiling and the oxide layer is broken. The temperature was then lowered to obtain the desired rate of

evaporation.

By controlling the rates of evaporation of the two materials a large range of possible values of sodium concentration can be obtained.

b) Insertion of Na in WO_3 films

Films prepared by the co-evaporation method cannot be heated above $60^{o}C$ because of the rapid outdiffusion of Na. Therefore for films in which the WO_3 host lattice had to be annealed, sodium was inserted after annealling using the following method.

The film and the sodium are placed inside a glass chamber as shown in Fig. 2.1.2. After its evacuation to about 10^{-3} Torr, the glass chamber is heated to $250^{o}C$. As in the previous method, the sodium has to be heated to $350^{o}C$ for a few seconds in order to break the oxide covering it. Once this is achieved the sodium vapour fills the chamber and sodium atoms diffuse into the film. In principle, one should be able to control the vapour pressure and consequently the amount of sodium inserted into the film, by controlling the temperature of the chamber. However, because of the high reactivity of sodium vapour and the high temperatures needed to break the oxide, one is very limited in the choice of materials and the design of the chamber, and as a result of these limitations the control of the amount of sodium diffusing into the film is restricted.

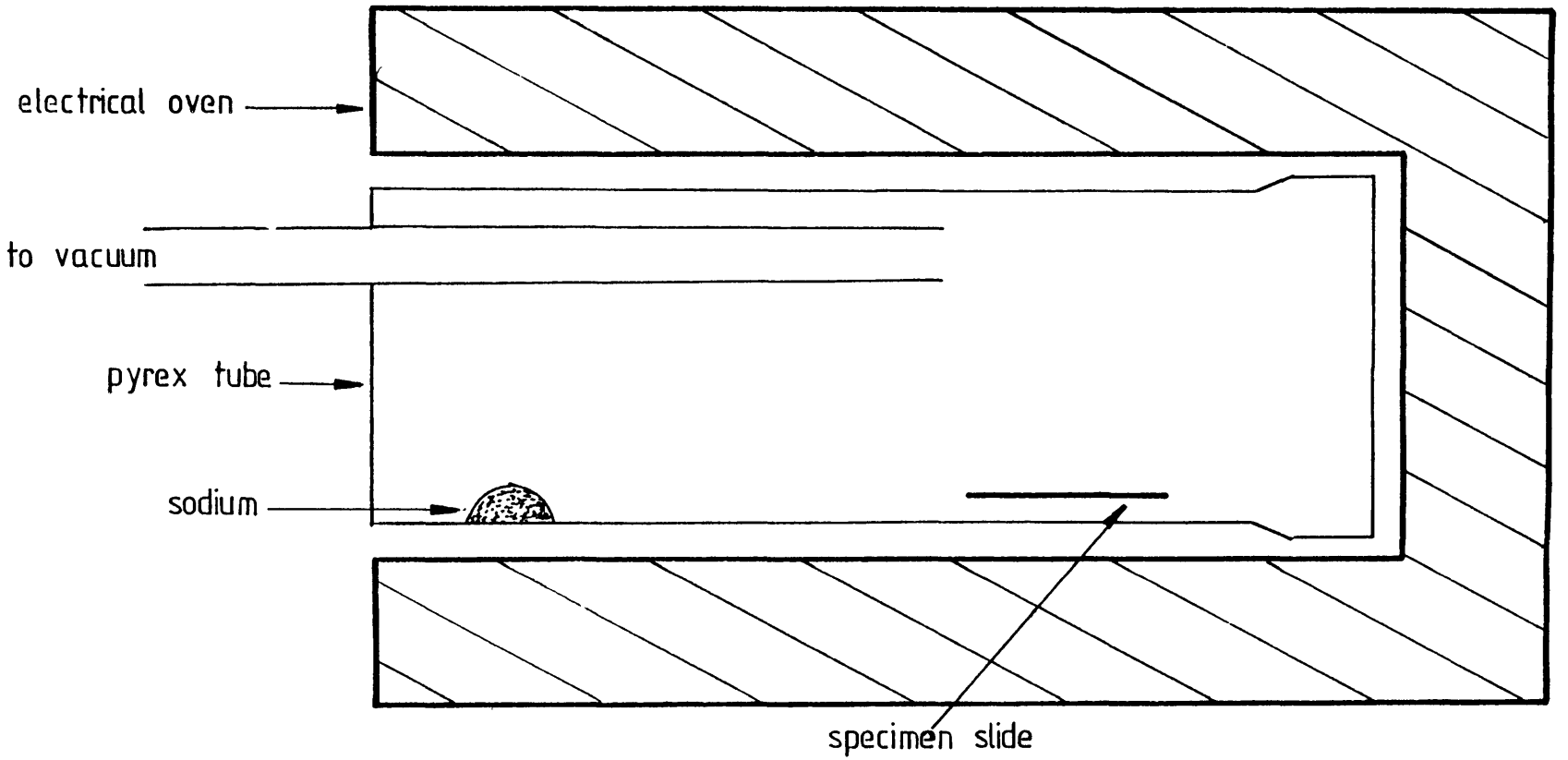

Fig. 2.1.2 : Apparatus used for sodium insertion from the vapour phase into WO_3 films

2.2 Film Characterisation

2.2.1 Micro structure.

The microstructure of the evaporated WO_3 films was examined under the 1 MeV. electron microscope and was found to be polycrystalline. The extent of crystallinity depends on the sustrate temperature and rate of evaporation.

WO_3 films were prepared at different sustrate temperatures and rates of deposition, on clean glass slides. The films were exposed to HF vapour in order to expose the grain boundaries and then floated off the slide in distilled water. During this process the film was usually broken up into small pieces the largest of which were caught on 400 mesh copper grids . Once mounted on the grid the film was left to dry in air for several hours before inserting it into the microscope.

The electron microscope was operated at 1000KV and the electron micrographs were taken in pseudo-dark field conditions in order to obtain adequate constast. In order to avoid excessive heating of the samples the electron beam was kept slightly out of focus.

Selected area diffrection patterns (S.A.D.P.) of the samples were also recorded. The wavelength of the electrons was 8.72×10^{-3} Å and the camera length, L , 240 ± 2cm.

Fig. 2.2.1 to 2.2.5 show electron migrographs (EMG) and selected area diffraction patterns (SADP) of different films.

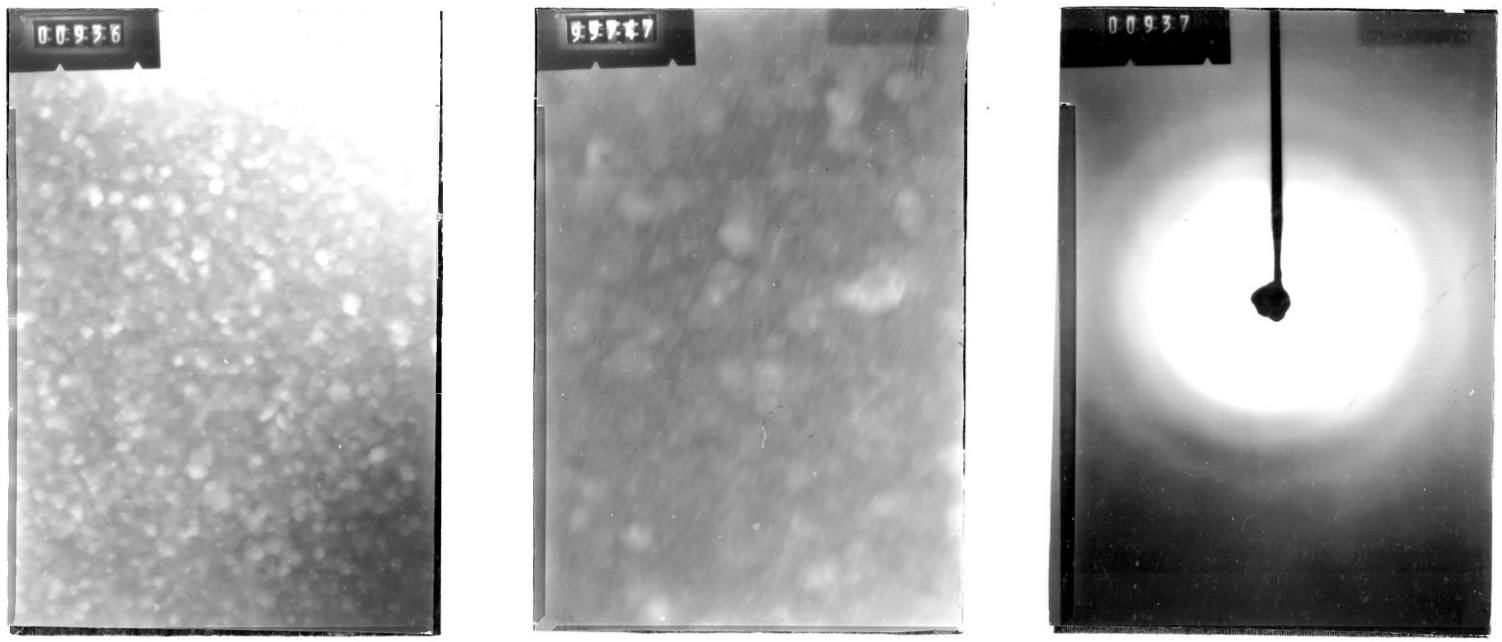

Fig. 2.2.1 : Electron micrographs and selected area diffraction pattern of WO_3 film. Thickness 1800Å, rate of evaporation 600Å/min, substrate temperature 60°C.

(a) EMG at 4×10^4 magnification

(b) EMG of the same area at 1.6×10^5 magnification

(c) SADP of the same area, camera length 248 ± 2 cm

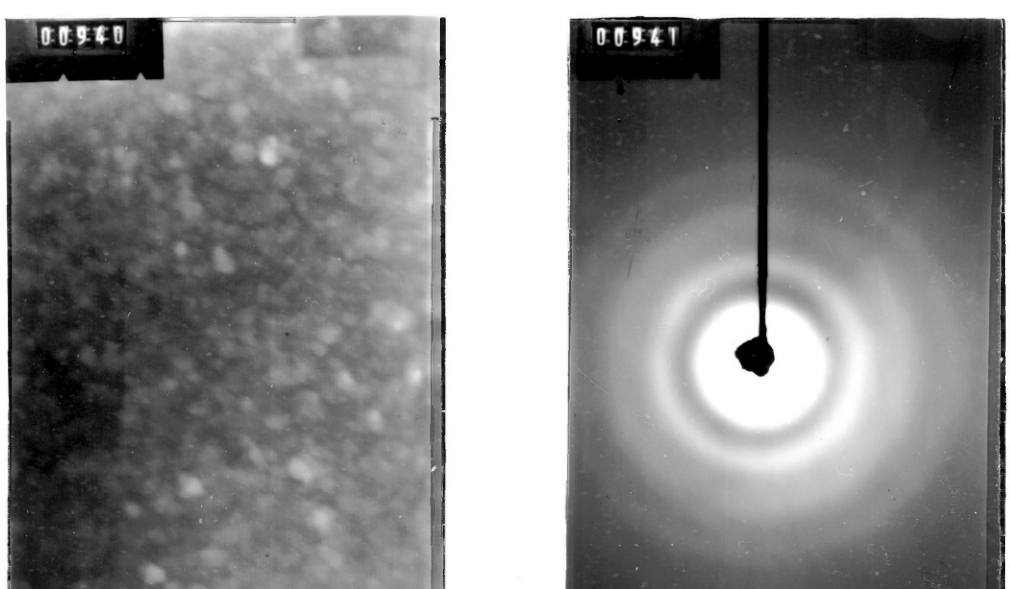

(a) (b)

Fig. 2.2.2 : Electron micrograph and selected area diffraction pattern of WO_3 film. Thickness 1800A, rate of evaporation 675Å/min, substrate temperature 120°C.

(a) EMG at 6.3×10^4 magnification

(b) SADP of the same area, camera length 248±2 cm

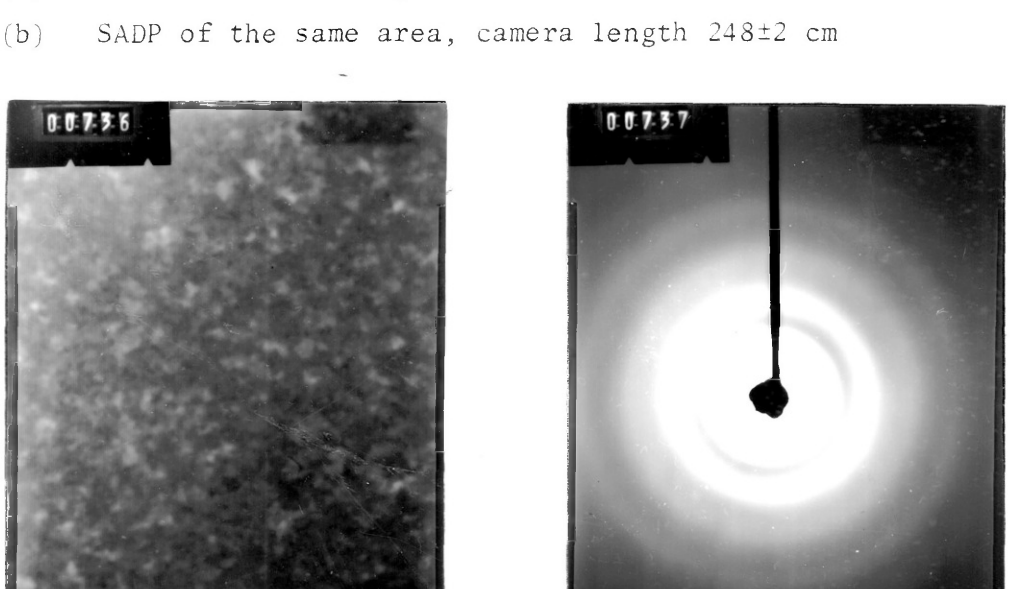

(a) (b)

Fig. 2.2.3 : Electron micrograph and selected area diffraction pattern of WO_3 film. Thickness 1600Å, rate of evaporation 640Å/min, substrate temperature 280°C.

(a) EMG at 10^5 magnification

(b) SADP of the same area, camera length 248±2 cm

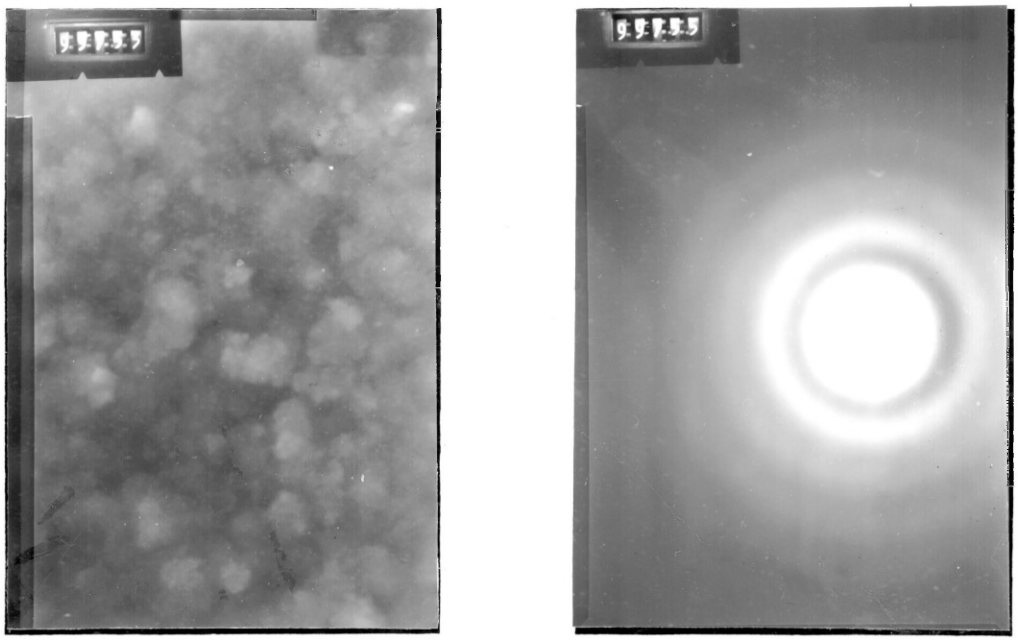

(a) (b)

Fig. 2.2.4 : Electron micrograph and selected area diffraction pattern of WO_3 film. Thickness 2000Å, rate of evaporation 380Å/min, substrate temperature 120°C.

(a) EMG at 10^5 magnification

(b) SADP of the same area, camera length 248±2 cm

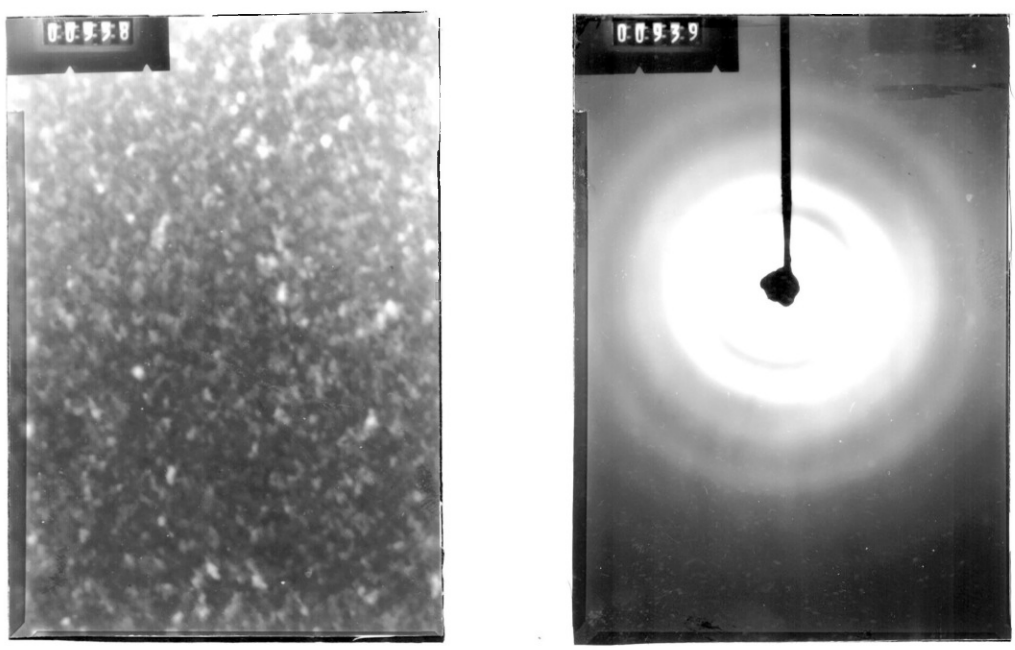

(a) (b)

Fig. 2.2.5 : Electron micrograph and selected area diffraction pattern of WO_3 film. Thickness 1700Å, rate of evaporation 390Å/min, substrate temperature 60°C.

(a) ENG at 4×10^4 magnification

(b) SADP of the same area, camera length 248±2 cm.

The common feature of all the diffraction patterns shown is that they consist of diffuse concentric rings, a pattern characteristic of amorphous materials. Because of the observation of these diffraction patterns many workers in the field (1, 2, 3, 4) assumed that the WO_3 films are amorphous. However, close examination of the electron micrographs do not justify such a conclusion.

Fig (2.2.1) shows E.M.G's of the same WO_3 film at different magnifications, which reveal that this film consists of small crystallites of mean size ~ 70Å which form aggregates of 300 to 500Å.

In Fig (2.2.1)(a) only the aggregates are visible, while in (b), both the aggregates and their internal structure are shown. The diffuse SADP arises from the fact that the crystallites are very small and randomly oriented.

An increase in the substrate temperature during the evaporation results in larger grains. Figs. (2.2.2) and (2.2.3) show E.M.G's of WO_3 films evaporated at approximately the same rate as the film on Fig. 2.2.1 but at substrate temperatures of 120°C and 300°C respectively.

Fig. 2.2.2 shows 500Å aggregates of grains, while Fig. (2.2.3) reveals individual grains of 120Å mean size.

Growth of the crystallites was also obtained by amealing small grain films. Annealling a film of initial grain size of ~ 50Å, at 500°C for 5 hours increases the size of the grains to about 2 - 3μm. At this size the grains are visible under the optical microscope.

The annealed films were not studied in the electron microscope because it proved extremely difficult to obtain large enough samples due to the very good adhesion of the film to the substrate.

The effect of the decrease in the evaporation rate is similar to the increase of the substrate temperature. Fig. (2.2.4) and (2.2.5) show

EMG's and SADP's of films evaporated at 120°C and 60°C respectively, but the rates of evaporation were lower than the previous examples, namely 380°Å/min and 390Å/min.

In both cases the dimensions of single grains and aggregates are larger than those of Figs. (2.2.1) and (2.2.2) which have been evaporated at the same substrate temperatures but at higher rates.

Fig (2.2.4) shows aggregates of 600-800Å in diameter, consisting of 100Å single grains.

Fig. (2.2.5) shows aggregates of 300Å in diameter, but individual grains are not resolved at this magnification.

Films evaporated at 60°C but with evaporation rates of 1000Å/min or higher did not show any structure when examined under the electron microscope. However, on the basis of the observations made on the films deposited with lower rates, we believe that these films are polycrystalline with mean grain size of 50Å or smaller.

Observations made by M. Shiojiri et al [9, 10], and K. Kang [1] tend to confirm our conclusions. M. Shiojiri et.al. report that WO_3 films prepared in a way similar to the one described above, are polycrystalline.

They estimate the m.g.s. of the films deposited at room temperature to be of the order of 20Å, while that of films which have been anealed at 300°C for ten hours to be a few hundreds of Å-units.

K. Kang [1]also estimates the size of crystallites in evaporated films to be less than 100Å . Moreover, he reports observations on the effect of substrate temperature and rate of deposition on the size of the crystallites that agree with our results.

Comparsion of the SADP's shown in Fig (2.2.1) to (2.2.5) with SADP's of films with larger grains [1, 9] reveals that the diffuse rings in our SADP's consist of several rings which had broadened and merged together.

Therefore the extraction of information about the size of the grains and their crystallo-graphic structure from the SADP's in Fig (2.2.1) to (2.2.5) is not possible.

2.2.2 Density of WO_3 Films

The density of crystalline WO_3 is known to be 7.3 gm/cm^3 [8,11]. On the other hand, reported values of the density of WO_3 films vary over a large range. At one end of the range M. Shiojiri et al [9] estimate the density of evaporated films to be 4.96 ± 0.45 gm/cm^3 and at the other end of the range K. Kang [1] found that the density of reactively sputtered WO_3 films is 6.9 ± 0.04 gm/cm^3.

From table 2.2.1, is apparent, that there is a strong correlation between the density and the method of preparation of the films. This relation can be understood in the light of the previous section where it has been shown that the films are polycrystalline and the size of the grains depends on the substrate temperature and rate of deposition. Polycrystalline films are composed of micro-crystallites among which regions of highly disordered material exist. Such regions, called grain boundaries, are expected to have different density than the grains. Therefore the density D of the film is given by the relation

$$D = \frac{D_G V_G + D_{GB} V_{GB}}{V_G + V_{GB}} \qquad (2.2.1)$$

where D_G and V_G are respectively the density and volume of the grains and D_{GB} and V_{GB} are the density and volume of the grain boundaries.
Eqn. (2.2.1) can also be written as

$$D = \frac{D_G + D_{GB} \dfrac{V_{GB}}{V_G}}{1 + \dfrac{V_{GB}}{VG}} \qquad (2.2.2)$$

Table 2.2.1: Density of WO_3 films

Density in gm/cm³	Grain size, L, in Å units	D_{GB} in gm/cm³ calculated equ.(2.2.4)	Method of Deposition	
4.96±0.45	20	3.9±0.47	evaporation T_s = 25°C rate = -	M. Shiorjiri et al [9]
6.2 ± 0.2	50	4.95±0.52	evaporation T_s = 60°C rate = -	K.S. Kang [1]
5.11	-	-	evaporation T_s = - rate = -	Zeller and Beyller [13]
6.5	-	-	evaporation T_s = 75°C rate= 600Å/min	S.K. Deb [8]
5.2	-	-	evaporation T_s = 100°C rate=1800Å/min	J.P. Randin [6]
6.9±0.04	250	4.62±0.2	r.f. sputtering T_s = 2000°C rate=50Å/min	K.S. Kang [1]

Assuming that D_G and D_{GB} are constants for all films then, it can be seen from eqn. (2.2.2) that the density of the films depends on the ratio $\frac{V_{GB}}{V_G}$. Since the volume occupied by the grains, V_G, is a function of their mean size which depends on the method of preparation the density, D , of the films should also be dependent on the method of preparation.

If the m.g.s. is L and the thickness of the grain boundary ℓ, where $\ell << L$, then

$$V_G \propto L^3$$

and

$$V_{GB} \propto L^2 \ell$$

therefore

$$\frac{V_{GB}}{V_G} = \frac{\kappa}{L} \qquad (2.2.3)$$

where κ is the product of the grain boundary thickness ℓ and some geometrical factor which depends in the shape of the grains. Green and Kang [12] have calculated κ from their thermodynamic data of sodium tungsten bronze thin films and they found it to be independent of grain size. Their value of κ is 44 ± 3Å.

Using eqn. (2.2.2) and (2.2.3) we find that

$$D = \frac{D_G + \frac{\lambda}{L} D_{GB}}{1 + \frac{\lambda}{L}} . \qquad (2.2.4)$$

From this equations and with κ = 44 ± 3Å, D_{GB} is calculated for the different values of D and L shown in table 2.2.1. These calculated values of D_{GB} are also shown in Table (2.2.1). The reasonable agreement which exists between these values is further evidence in support of the

polycrystalline nature of the WO_3 films. The small difference in the values of D_{GB} is mainly due to two factors : (i) uncertainty in the values of L and (ii) the different quantities of water which is bound to the films and which depends on the particular history of each film.

2.2.3 Determination of the sodium concentration in $Na_x WO_3$ films

The physical properties of sodium tungsten bronze are found to be a sensitive function of their sodium content. Therefore, in order to understand and interprete these physical properties in a coherent way, knowledge of Na concentration, i.e. the value of x, is an imperative necessity.

The direct measurement of x in the case of thin films is a very difficult task because of the small quantities of sodium which are to be detected. It is for this reason that most workers in the field of thin films of tungsten bronze rely on indirect methods of determination of the sodium content of the films [8,11]. However, such methods involve assumptions about certain of the properties of the films which either have not been determined experimentally, or may be functions of x themselves.

In order to determine x for every film unambiguously we measured it directly, using an electrochemical method.

There are two different sets of methods which one can use to measure the sodium content of $Na_x WO_3$ films, these are chemical and electrochemical. Chemical methods have not been used for routine measurement of x because of the following two limitations

a) In order to detect a few parts per million of sodium one has to work near the limits of accuracy of these methods and

b) All chemical methods involve the destruction of the film which is under examination and therefore one has to take all other physical measurements before the x-value is determined. Given the fact that Na outdiffuses continuously from the films, the determination of x several hours, even days, after the measurement of the other physical properties, severely limits its usefulness.

However, one of the chemical methods has been employed in order to verify the results obtained by the electrochemical method and it will be described later.

The electrochemical method we used is based on the well known [1,12, 15-19] electrochromic properties of WO_3 films. If electron and proton or Na or Li injecting contacts are made to a WO_3 film colouration of the film proceeds following the application of a small voltage, across the electrochemical cell formed in this way. The process is reversible and the film can be bleached if the applied voltage is reversed.

This behaviour of WO_3 films has been explained on the basis of tungsten bronze formation [15,1]. According to this theory, the protons or monovalent metal ions when injected into the film form a bronze which is coloured, while electrons injected from the other electrode preserve the charge neutrality of the film. Provided, therefore, that this process is the only, or the predominant one, during colouration, it can be used to determine the amount of sodium injected into or removed from a known volume of the film by measuring the charge injected or removed from the film.

We used the following experinental procedure in order to measure the sodium content of our films.

Two films were prepared from the same evaporation run. One was deposited on a silica substrate and was used for optical and electrical measurements and the other on an Indium Tin Oxide (I.T.O) coated glass slide, and was used for the sodium concentration measurement.

Films prepared in this way were examined for differences in the values of their optical and electrical parameters as well as differences in thickness and sodium concentration. There were repeatedly found to be identical within experimental error.

The film on I.T.O coated slide was placed in the apparatus shown

in Fig (2.2.6) and a small fraction of its volume was uncoloured. The apparatus shown in Fig (2.2.6) consists of two thick perspex plates which can be pressed together with four brass screws (not shown in the figure). The glass slide with the $Na_x WO_3$ film which is to be bleached is sandwiched between the two plates. A viton "O" - ring, compressed between the top plate and the slide prevents the liquid electrolyte from wetting the whole surface of the film. The liquid electrolyte is poured from the top, into the hole of the top perspex plate and a Pt wire is used as electrode. Electrical contact to the $120\Omega\square^{-1}$ I.T.O coating is made by silver dag paint.

The liquid electrolyte used was a saturated solution of NaCℓ in distilled water.

The extraction of sodium was performed under constant current conditions.

A Keithbey 616 electrometer was used as the constant current source while the potential difference between the two electrodes was continuously recorded on a JJ instruments 550 chart recorder. A schematic diagram of the instruments arrangement is shown in Fig (2.2.7).

Typical bleaching curves are shown in Fig (2.2.8). The same curves are plotted on a log-log scale in Fig (2.2.9).

The dynamics of bleaching of a WO_3 - liquid electrolyte electrochromic device is complicated because there are potentially several processes which can contribute to the bleaching current. These are : i) the out-diffusion of ions from the film, ii) the electrolysis of water and iii) the dissolution of the film .

We do not expect process (iii) to play an important role before the bleaching is complete. Randin [16] has measured the dissolution rate of WO_3 films using different electrolytes and he found it to be only 20Å/day under colour-bleach cycling conditions. In these measurements

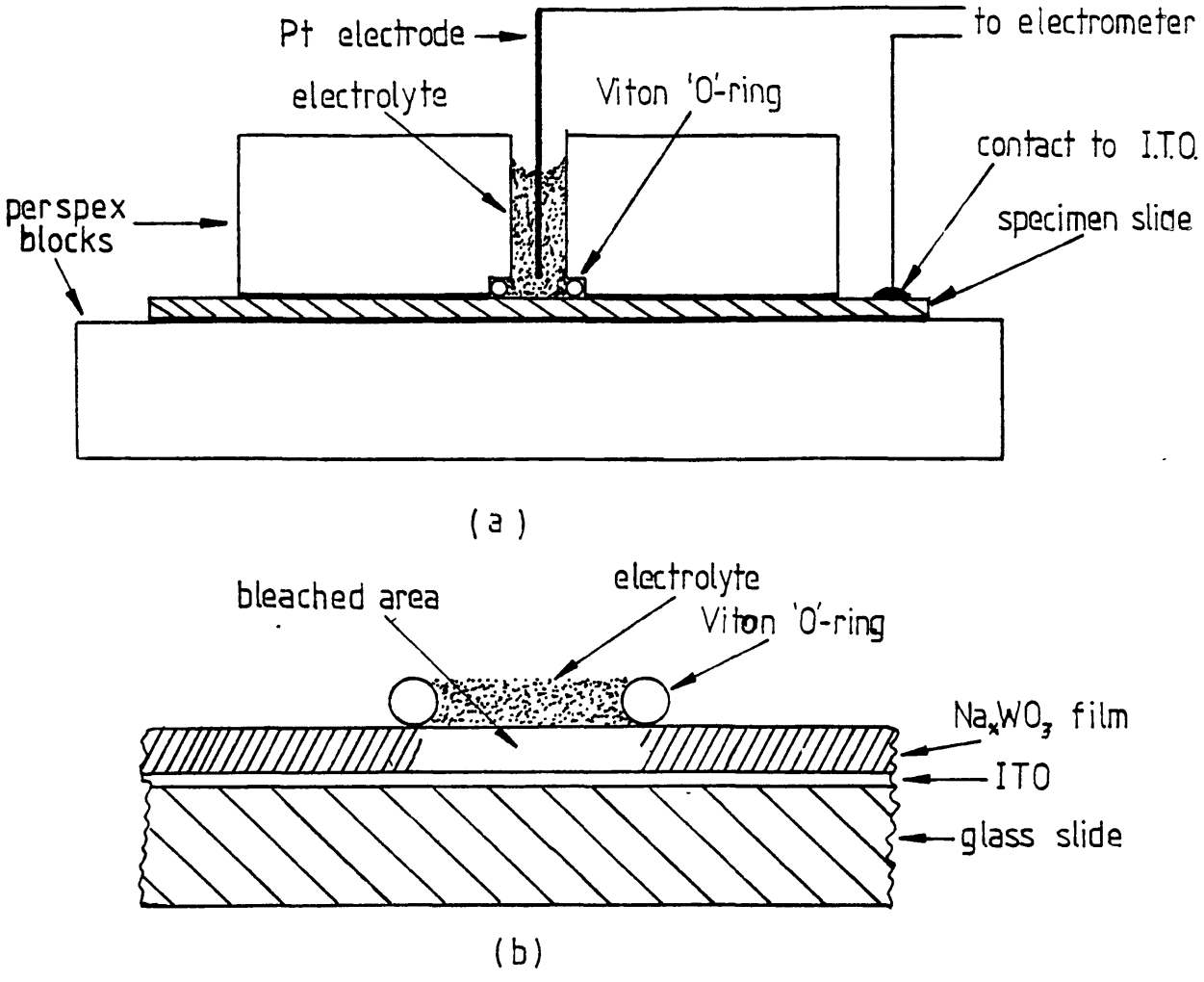

Fig. 2.2.6 : (a) Electrochemical cell used for the determination of the x-value of Na_xWO_3 films.

(b) Detail of the electrochemical cell showing the arrangement of the Na_xWO_3 and I.T.O. films on the glass substrate. The diameter of the bleached area is 3mm.

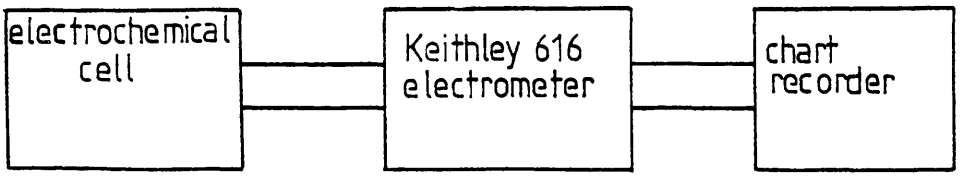

Fig. 2.2.7 : Schematic diagram of the instruments arrangement for the determination of the x-value of Na_xWO_3 films

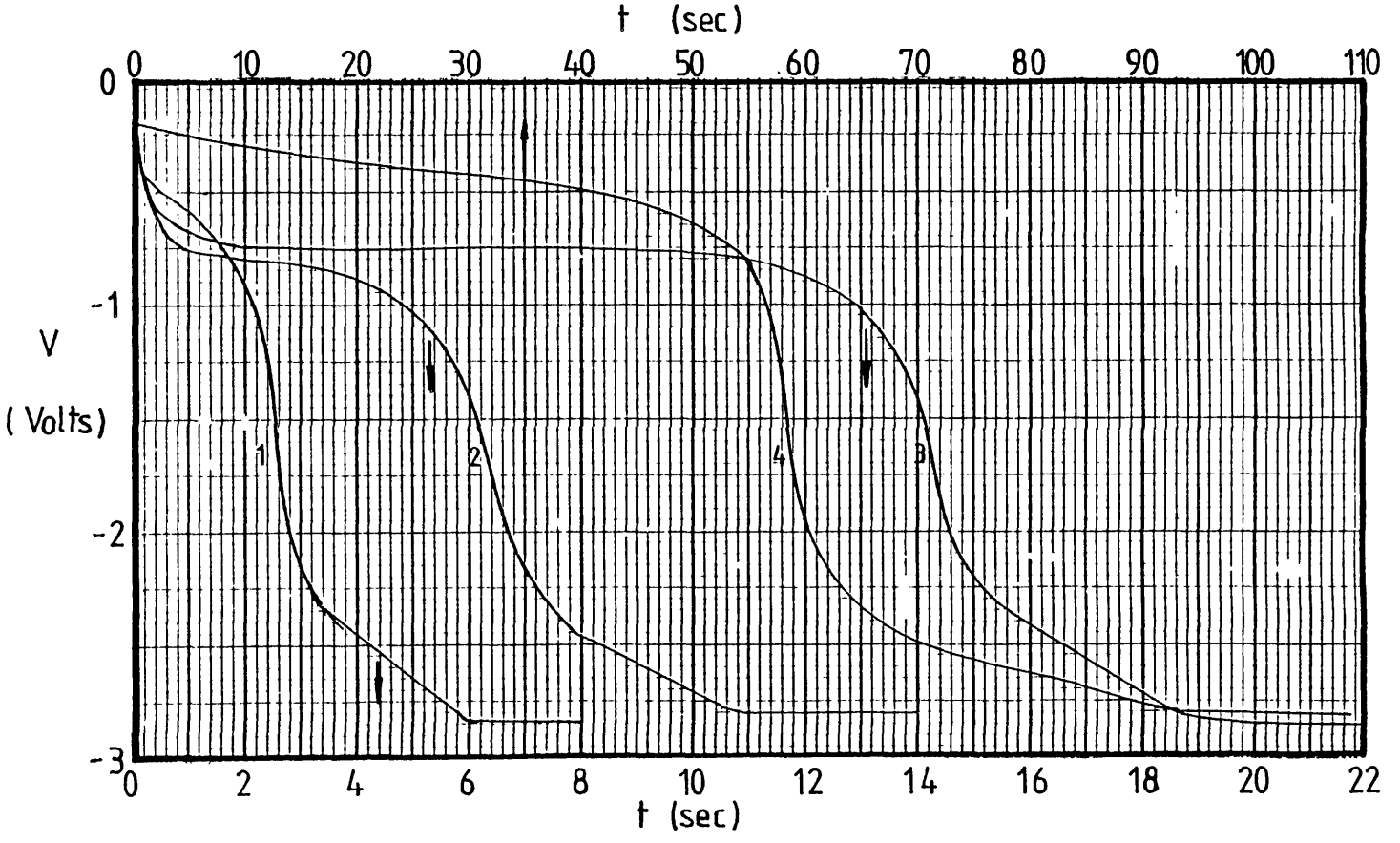

Fig. 2.2.8 : Typical bleaching curves of Na_xWO_3 films, at constant current (10^{-5}A) conditions. The volume of the bleached part of the film is : (1) $3.29\times10^{-12}m^3$, (2) $4.46\times10^{-12}m^3$, (3) $4.89\times10^{-12}m^3$ and (4) 6.75×10^{-12} m^3.

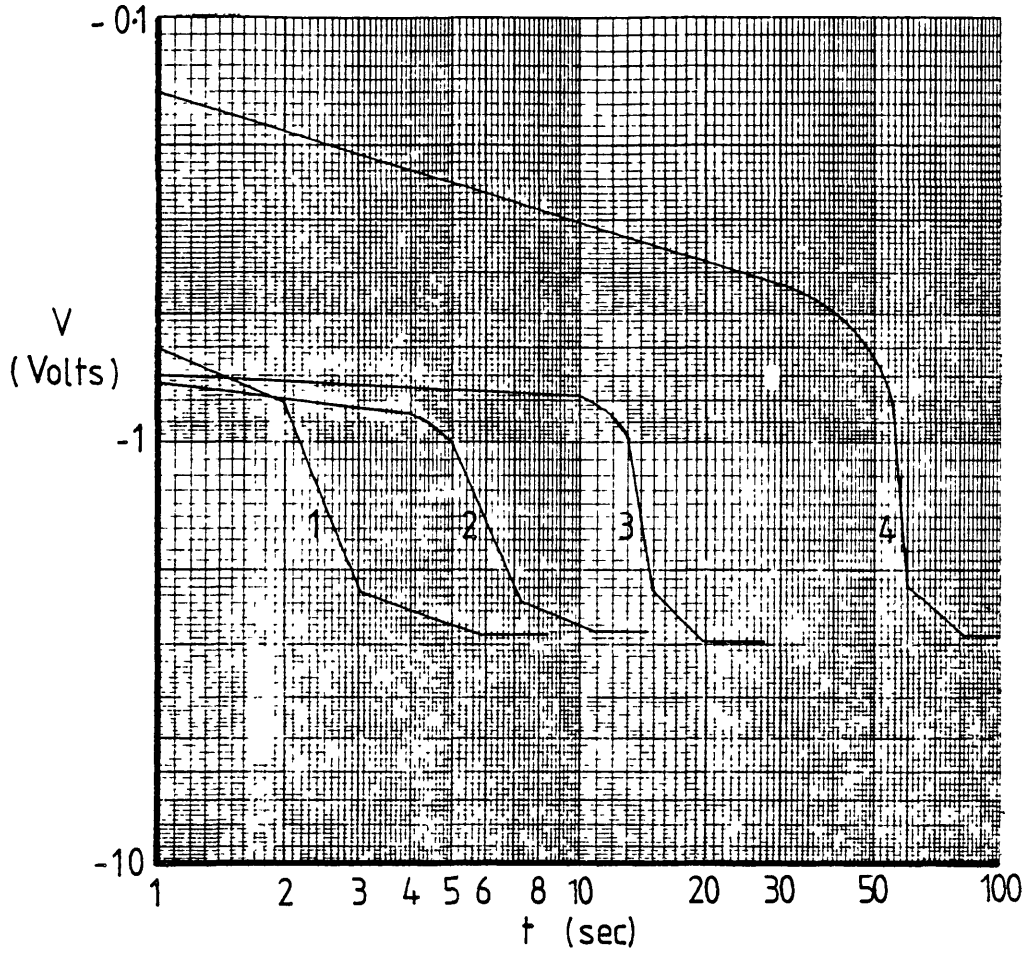

Fig. 2.2.9 : The bleaching curves of Fig. 2.2.8, plotted on a log-log scale. The constant bleaching current is 10^{-5}A and the volume of the bleached part of the film is : (1) 3.29×10^{-12}, (2) $4.46\times10^{-12}m^3$, (3) $4.89\times10^{-12}m^3$ and (4) $6.75\times10^{-12}m^3$.

the film was never completely bleached. Examination of our bleached films under the optical microscope did not show any sign of erosion. If, however, the current passing through the cell is not switched off after the completion of the extraction of sodium, the WO_3 film rapidly breaks-up.

On the other hand, the role played by the electrolysis of water is more difficult to predict. It cannot, however, start before the potential drop across the electrolyte is higher than 1.5 volts. Taking into account the high resistivity values of the bleached films ($10^8 \Omega cm$) we except this process to commence only when the voltage across the electrodes is approximately 2 volts.

As it can be seen from Fig (2.2.10) bleaching curves consist of five different sections. We believe that in the last two sections the current passing through the cell is mainly due to electrolysis of water, (i.e. oxygen evolution) while sections II and III represent the extraction of sodium and section I is governed by the response time of the electrical apparatus and the cell.

To verify this interpretation of the bleaching curves we performed the following experiment: Pure WO_3 films were placed in the apparatus and were coloured under constant current conditions. They were subsequently bleached under the same conditions by reversing the polarity of the applied voltage.

Two colouring and bleaching pulses of different duration are shown in Fig (2.2.11). The time required to extract the ions inserted into the film during the colouring pulse is equal to the time covered by sections I, II and III of the bleaching pulse. We therefore, conclude that all the sodium in the film is extracted at the end of section III of the curves and we use the corresponding time to calculate the value of x in the film.

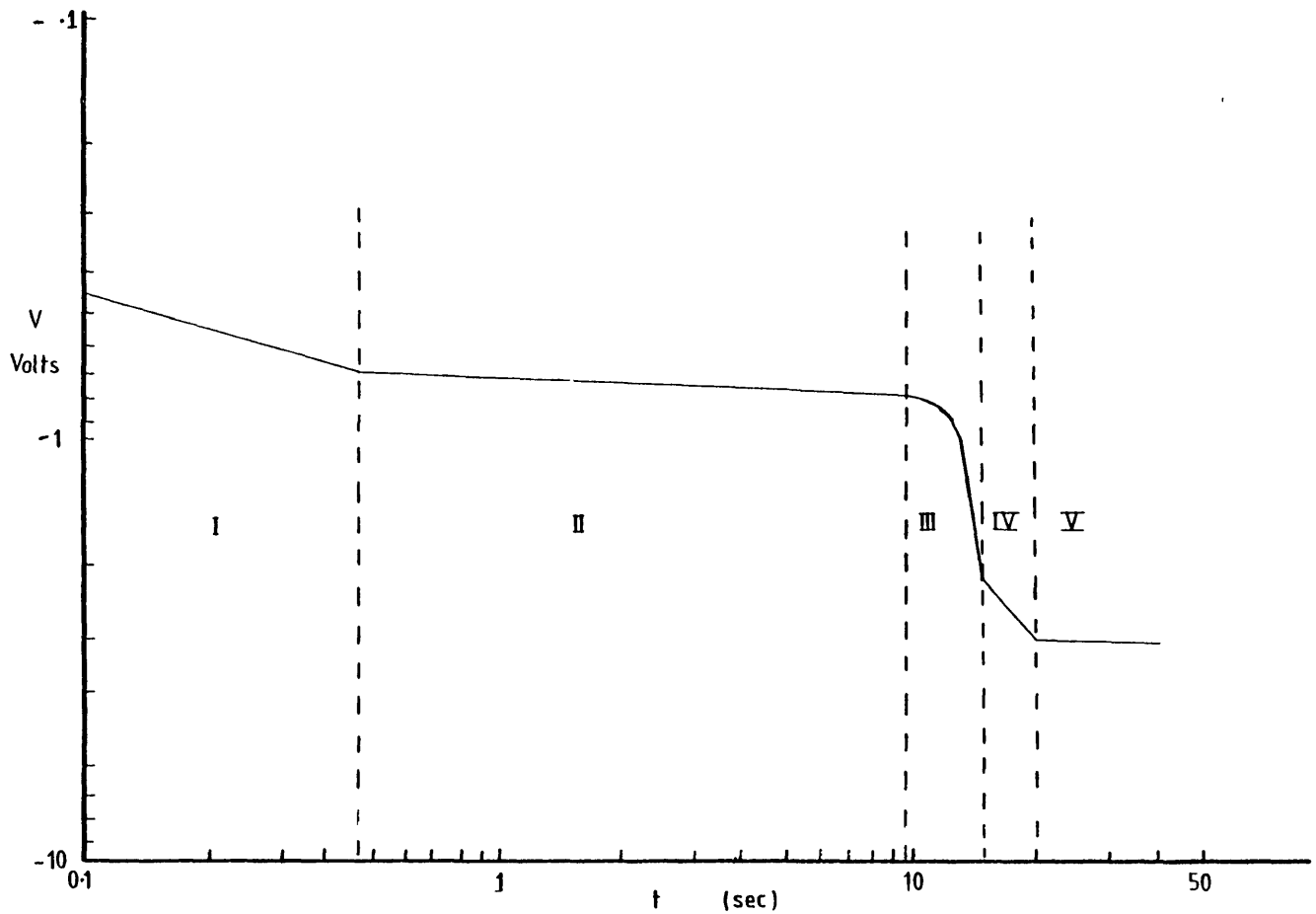

Fig. 2.2.10 : Bleaching curve of a Na_xWO_3 film at constant current conditions showing its five sections. Section (I) is governed by the response time of the apparatus, sections (II) and (III) represent the extraction of sodium and sections (IV) and (V) the oxygen evolution

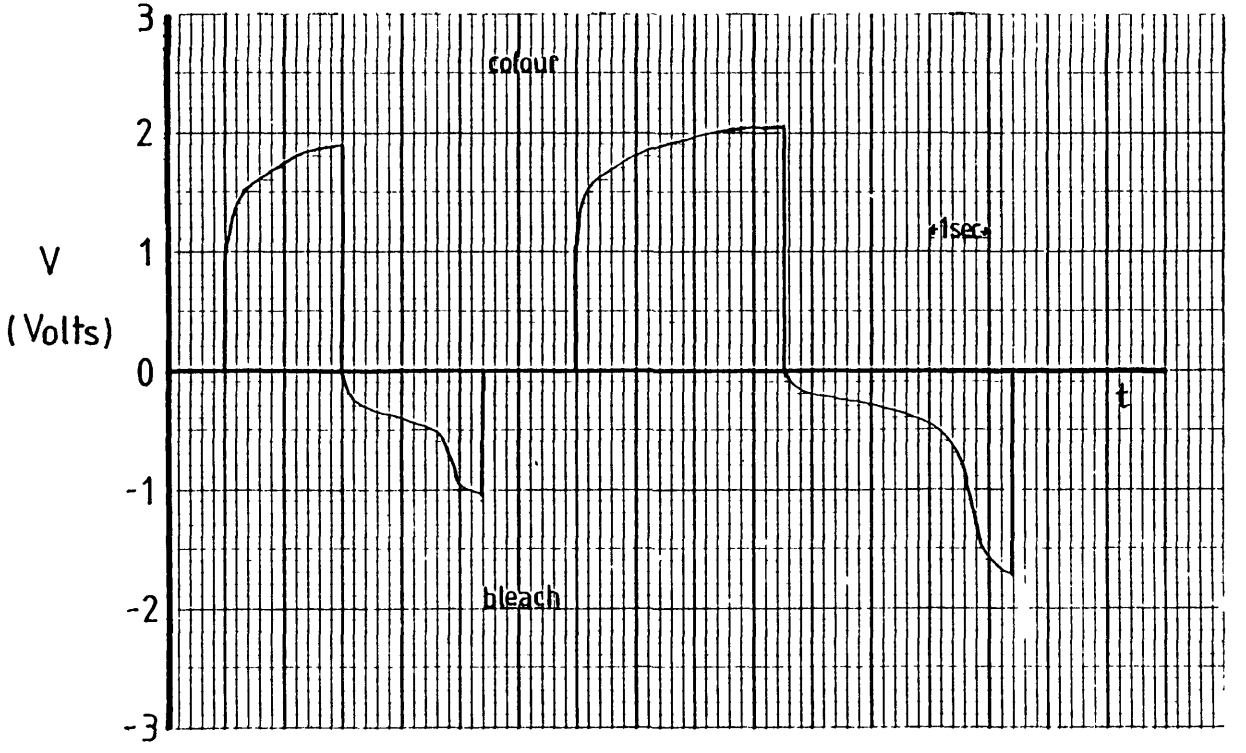

Fig. 2.2.11 : Colouring and bleaching curves of a WO_3 film under constant current (10^{-5}A) conditions

The interpretation of the exact slope of sections II and III of the curves depends on the particular model used to describe the process. We used the "grain model" as developed by Green [12] because it can satisfactorily explain all our observations, taking into account the polycrystalline nature of the films.

According to this model the diffusion of sodium ions out of the film occurs much faster through the grain boundaries than through the grains and therefore in the limit the rate of out-diffusion from each grain is constant (Fig. 2.2.12).

Fig (2.2.13) shows a schematic picture of the sodium concentration in the film at various times during bleaching.

The concentration in the grains is lowered to some very small value before the start of a complete depletion region around each grain. The creation of this depletion region increases the resistivity of the film and gives rise to the rapid increase of the voltage across the electrodes towards the end of the bleaching process (section III of the curves). At shorter times the concentration of sodium in the film is almost uniform, its resistivity changes very slowly and the voltage change across the electrodes is small (section II of the curve).

The "grain model" is also supported by the fact that films with large grains cannot be bleached completely, by this method. This is because when the depletion region is established around each grain the quantity of sodium remaining inside the grain is considerable and the large voltage needed to continue the extraction initiates electrolysis of water which dominates the process before the completion of the extraction of sodium.

Having established that the sodium is extracted from the film during sections II and III of the bleaching curve the calculation of its

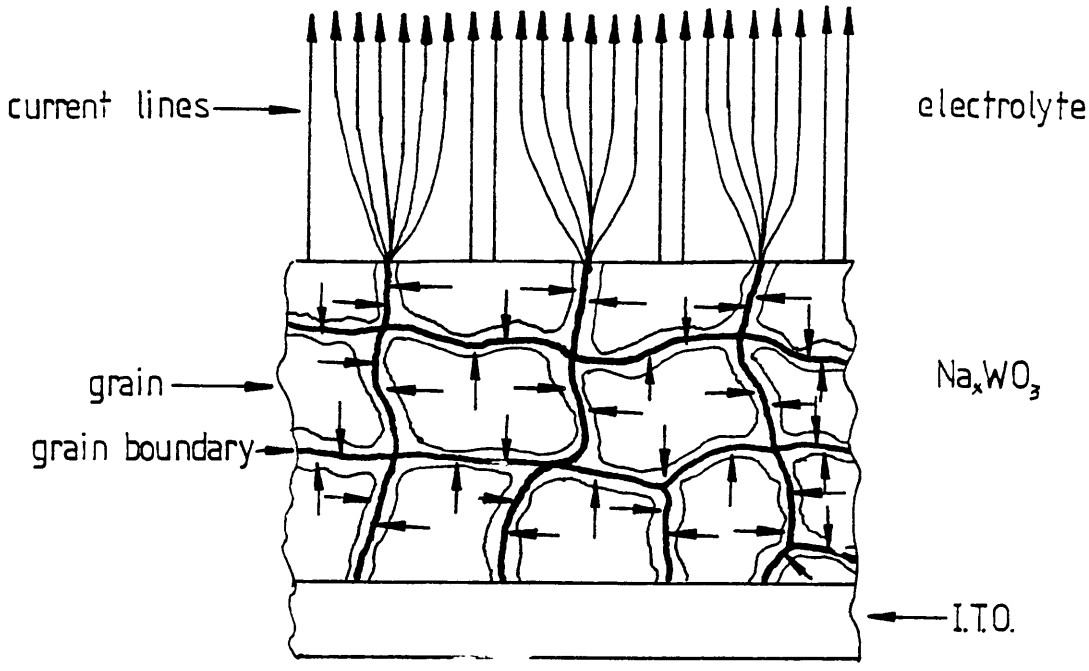

Fig. 2.2.12 : The "grain model" as proposed by Green [12], see text for details.

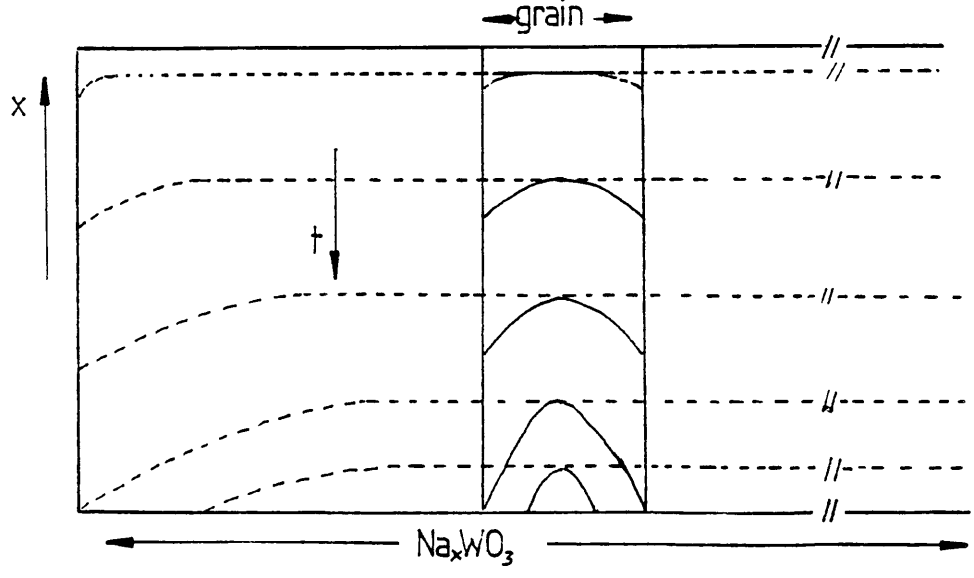

Fig. 2.2.13 : Schematic diagram of the sodium concentration in Na_xWO_3 films at various times during bleaching as predicted by the "grain model"

exact amount is carried out as follows ;

The total charge removed from known volume V of the film is given by:

$$Q_T = I\, t_f \qquad (2.2.5)$$

where

I = constant current flowing through the cell

t_f = time at the end of section III of the curve

since every sodium atom removed is singly ionized the total number of sodium ions extracted is given by

$$N_T = \frac{It_f}{e} \qquad (2.2.6)$$

where e is the electronic charge.

The concentration x is defined as the ratio of the number of moles of sodium to the number of moles of WO_3.

Therefore

$$\langle x \rangle = \frac{N_T/A}{DV/M} \qquad (2.2.7)$$

where A is the Avogadro's constant

M is the molecular weight of WO_3

D is the density of the film

V is the bleached volume of the film .

It has, however, been shown [1,12] that for low concentrations, $x \lesssim 0.2$, there is no significant amount of sodium in the grain boundaries. This is true because of the low binding energy of sodium in the grain boundary and the high binding energy in the grain. Therefore, eqn. (2.2.7) is modified to take into account the absence of sodium from the grain boundaries:

$$x = \frac{N_T/A}{D_G V_G/M} \quad , \tag{2.2.8}$$

From eqns.(2.2.7) and (2.2.8) for the same N_T we have

$$x = \langle x \rangle \frac{D\ V}{D_G V_G} \tag{2.2.9}$$

using eqn. (2.2.3)

$$x = \langle x \rangle \frac{D}{D_G} \left(1 + \frac{\kappa}{L}\right) \tag{2.2.10}$$

and combining equations (2.2.6), (2.2.7) and (2.2.10) we obtain

$$x = \frac{I\ t_f\ M}{Ae\ D_G V}\left(1 + \frac{\kappa}{L}\right) \quad . \tag{2.2.11}$$

In order to calaulate x from the bleaching curves we use the following values for the constants in eqn. (2.2.11)

$$M = 231.85\times10^{-3}\ \text{Kg/mole}$$

$$D_G = 7.3\times10^{3}\ \text{Kg cm}^{-3}$$

$$\kappa = 44\times10^{-10}\ \text{m}$$

$$L = 50\times10^{-10}\ \text{m}$$

$$A = 6.0225\times10^{23}\ \text{mole}^{-1}$$

$$e = 1.6\times10^{-19}\ \text{C}$$

substituting in eqn. (2.2.11) we obtain

$$x = 6.19\times10^{-10}\ \frac{It_f}{V} \tag{2.2.12}$$

for $x \lesssim 0.2$

and the number density N_d of sodium atoms in the grain is given by

$$N_d = 1.9\times10^{28}x \qquad (\text{in } m^{-3}). \qquad (2.2.13)$$

The thickness of the films has been measured with a Taylor-Hobson Talysurf 4 and their area with the travelling stage of an optical microscope. Taking into account the uncertainties in the measurements of V and in the values quoted for κ and L, the values of x calculated from eqn. (2.2.12) are correct to within ±8%.

The determination of x by extracting electrochemically the sodium from the films has been employed successfully for films with concentrations up to 0.2. It is not, however, possible to employ this method for films with higher values of x because they craze when they contact the electrolyte. The reason of this behaviour is not absolutely clear. It is, however, possible that water molecules react with sodium ions in the grain boundaries thereby disolving parts of the film and undermining its continuity. If this is the case, then, the use of a water-free electrolyte could extend the usefulness of this method to much higher values of x.

Another electrochemical method which we employed in order to determine x is the measurement of the chemical potential of sodium in our Na_xWO_3 films, since its variation as a function of x up to x = 0.25 has been established both experimentally and theoretically [1,12,20]. To this purpose we used the following technique : A cell containing saturated sodium amalgam and with the one end sealed with a polished piece of Na-β-alumina which is a good solid ionic conductor, (Fig. 2.2.14), was placed in contact with the film under examination and the equilibrium potential difference between the film and the sodium amalgam was measured with a Keithbey electrometer. Adding to this potential difference 1.76V which is the difference in potential between saturated sodium amalgam and pure sodium, the chemical potential of sodium in the film was obtained. From the curve shown in Fig.2.2.1

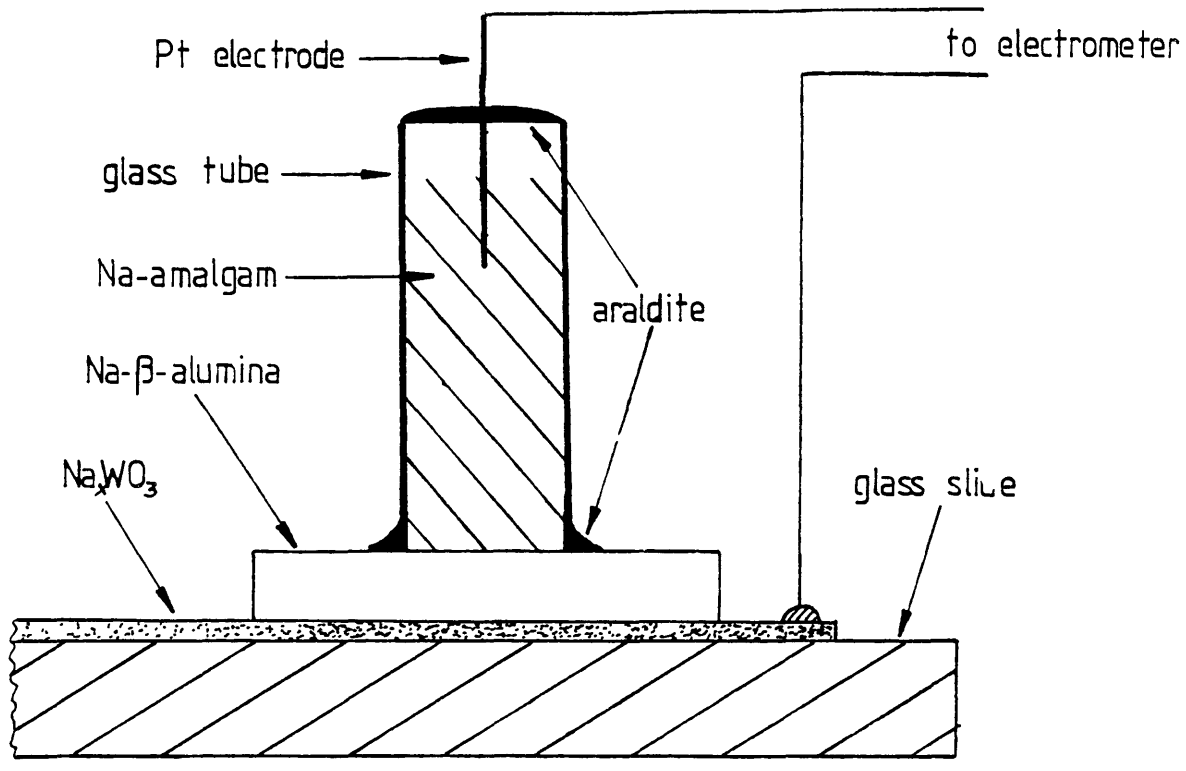

Fig. 2.2.14 : Electrochemical cell used in the measurement of the chemical potential of sodium in the Na_xWO_3 films

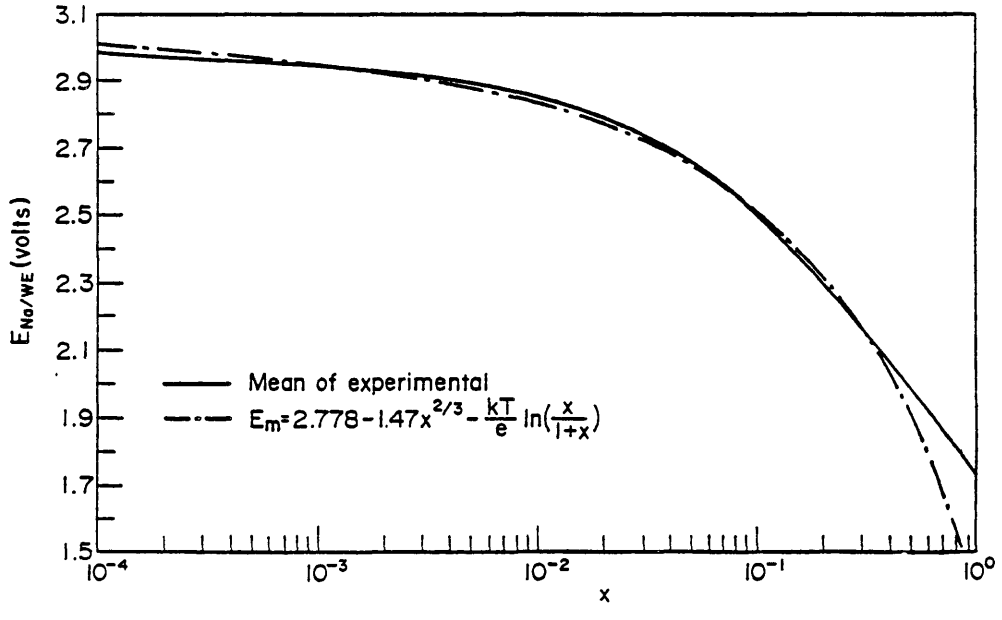

Fig. 2.2.15 : The cell e.m.f. (Na|Na-β-alumina|Na_xWO_3) for Na_xWO_3 electrodes of varying sodium content at 25^0C (After M. Green [20]).

which has been established by Green [20], the value of x can be directly obtained using the measured value of the chemical potential of Na in the film. This method has been successfully employed [1,12] previously, but with the Na_xWO_3 film evaporated on the Na-β-alumina slab. In our case, however, we found that the results obtained were not always reproducible. The main reason is the poor contact between the Na_xWO_3 film and the solid electrolyte, because of the presence of a very thin layer of sodium oxide which covers the surface of the films exposed to air as well as the presence of water both on the surface of the Na-β-alumina and the film. Attempts to minimize the water, by performing the measurement in vacuum improved the results but not to a satisfactory extent.

In order to verify the results obtained by the electrochemical method we attempted to measure the sodium content of our films using atomic absorption spectrometry.

The Na_xWO_3 were disolved in NH_3 solution in doubly distilled water, and the so prepared samples were analysed for sodium in a Perkin-Elmer-atomic-absorption spectrophotometer (Model 2380).

The instrument has been callibrated using several solutions of NaCℓ in distilled water with sodium concentrations equivalent to $x = 0$ up to $x = 0.1$.

The accuracy of the values of x obtained with this method is approximately 10%. This is due to possible sodium contamination of the glassware in which the solutions were prepared as well as uncertainties in the actual measurement.

When compared with the values of x obtained by the electrochemical method, the later are found systematically 15% lower. We believe that this is due to the sodium which outdiffuses from the films and forms a thin layer of sodium oxide at their surface. This sodium is measured by the

atomic absorption method because it is dissolved into the NH_3 solution but it is not measured by the electrochemical method since it dissolves into the electrolyte without contributing to the current passed through the cell. It is very difficult to eliminate the cause of this discrepency because the outdiffusion of sodium is fast when the film is first exposed to air and therefore one does not have time to measure x before the sodium oxide layer is formed.

However, even if the agreement in the measurement of x is not better than 15%, it can be considered as a good substantiation of the electrochemical method.

References

[1] K.S. Kang, Ph.D. thesis. London University (1979)

[2] M. Green and D. Richman, Thin Solid Films, 24, 545(1974).

[3] R.J. Ackermann and E.G. Rauth, J. Phys. Chem., 67, 2596(1963).

[4] G.R. St Pierre, Trans. Metallurgical Joc. of A.I.M.E., 224, 259(1962).

[5] M.R. Goulding and C.B. Thomas, Thin Solid Films 62. 175(1979).

[6] J.P. Randin, J. Electronic Mat. 7, 47(1978).

[7] M. Manfredi, C. Paracchini, G.S. Salvioti and G. Schianchi, Thin Solid Films, 79, 161(1981).

[8] D.K. Deb, Phil. Mag., 27, 801(1973).

[9] M. Shiojiri, T. Mijano, C. Kaito and Y. Saito, Proc. of the 8th International Vacuum Conference p. 413(1980).

[10] M. Shiojiri et al, Japanese Journal of Applied Physcis, 18, 1937(1979).

[11] S. Tanisaki, J. of Phys. Soc. of Japan, 15, 4(1960).

[12] M. Green and K.S. Kang, Solid State Ionics, in press.

[13] H.R. Zeller and B.V. Beyeler, Appl. Phys., 13, 231(1977).

[14] A. Nakamura and S. Yamada, Appl. Phys., 24, 55(1981).

[15] R.S. Crandall and B.W. Faughnan, Applied Phys. Lett., 28, 95(1976).

[16] B.W. Faughnan, R.S. Crandall and M.A. Lampert, Applied Physics Lett., 27, 275(1975).

[17] H. Morita and H. Washida, Japenese Journal of Applied Physics, 19, L228(1980).

[18] M.L. Hitchman, Thin Solid Films, 61, 341(1979).

[19] S. Yamada, T. Nakamura, Y. Hiruta, K. Urabe and M. Kitao, Jap.J. Appli. Phys., 22, 789, (1983)

[20] M. Green, J. Res. Inst. Catalysis, 28, 163(1980).

CHAPTER 3

OPTICAL AND ELECTRICAL MEASUREMENTS

3.1 Optical measurements

3.1.1 Experimental data and refinement of results

The transmission and reflection spectra of Na_xWO_3 films were measured in the wavelength range of 0.3μm to 2.7μm. The instrument used, was a Beckmann DK2A spectrophotometer which is of the double beam type. It was operated at its highest sensitivity.

A schematic diagram of the spectrophotometer is shown in Fig. 3.1.1. Light from the monochromator enters the integrating sphere alternatively through A and B so that the detector receives light pulses of equal duration. The ratio of the signals from every two consecutive light pulses is plotted on the chart recorder. The transmission, T_{obs}, of a film is measured by placing it in front of the entrance A of the intergrating sphere, while a slide identical to the slide of the film is placed in front of the entrance B. Entrances C and D are covered with thick MgO films, which have a reflectivity of unity, evaporated on silica slides. The values of T_{obs} obtained do not include the absorption of the slides. The reflection, R_{obs} is obtained by placing the film at the entrance C, the film facing the beam, while entrance D is covered with the MgO film and entrances A and B are left open.

Both transmission and reflection measurements are measured at near normal incidence (about 5^o off normal).

Transmission and reflection measurements were also carried out for a few films in the wavelength range of 2.5μm to 5μm using a Perkin-Elmer 580B infrared spectrophotometer. The operating and experimental

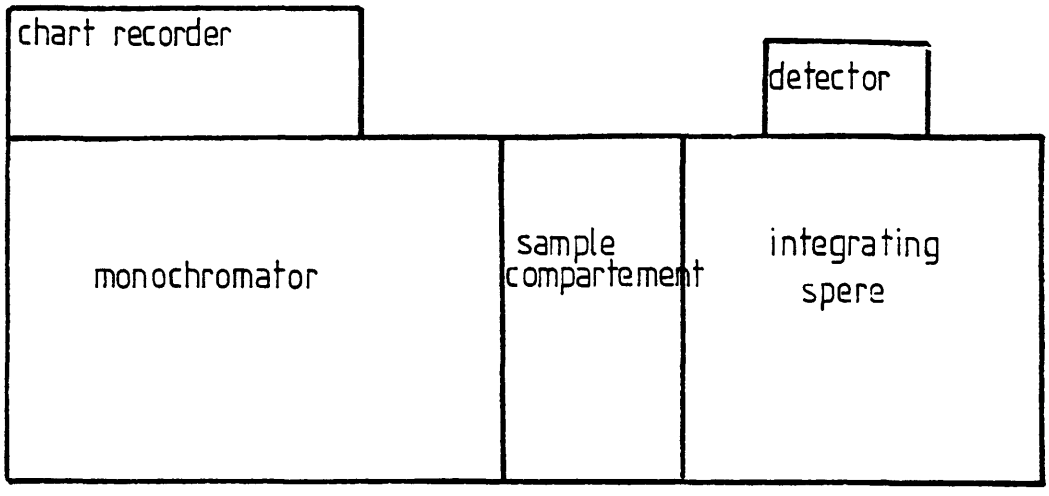

(a)

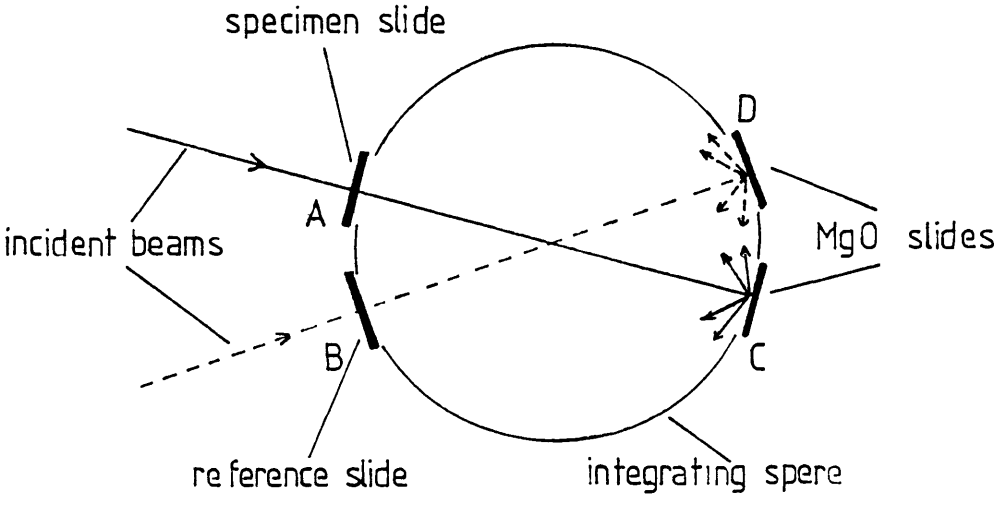

(b)

Fig. 3.1.1 : (a) Schematic diagram of the Beckmann DK2A spectrophotometer. (b) Experimental arrangement for transmission measurements (see text for details)

arrangement of this instrument is similar in principle to that of the Beckmann DK2A spectrophotometer. The reflection measurements carried out with this spectrophotometer were on a relative scale because there was no reference used. They were subsequently converted to an absolute scale using the overlap of these measurements with the measurements obtained with the Beckmann DK2A in the wavelength range of 2.5μm to 2.7μm.

All the optical measurements were carried out on films which were evaporated on silica substrates. Silica is an excellent substrate and non-absorbing in the wavelength range used. Its reflection is approximately 3.5% over the same range, as calculated from its mean refractive index of 1.46 [1].

Typical unrefined spectra showing the experimental T_{obs} and R_{obs} are shown in Figs. 3.1.2, 3.1.3 and 3.1.4. These values of T_{obs} and R_{obs} were treated in three stages in order to obtain the absorbing coefficient of the films as a function of wavelength.

Firstly, the interference maxima and minima were averaged out by taking the arithmetic mean of consecutive extreme values so that $\langle T_{obs} \rangle$ and $\langle R_{obs} \rangle$ are obtained. Secondly, $\langle T_{obs} \rangle$ and $\langle R_{obs} \rangle$ values were corrected for the effect of multiple reflections inside the substrate, and reflections from the back surface of the substrate.

The true values of transmission, T_f, were obtained using the expression [2, 3]

$$T_f = \langle T_{obs} \rangle \frac{1-R'_s R'_f}{1+R'_s} \qquad (3.1.1)$$

where

$$R'_s = \frac{(n_s-1)^2}{(n_s+1)^2} = 0.035 \ ;$$

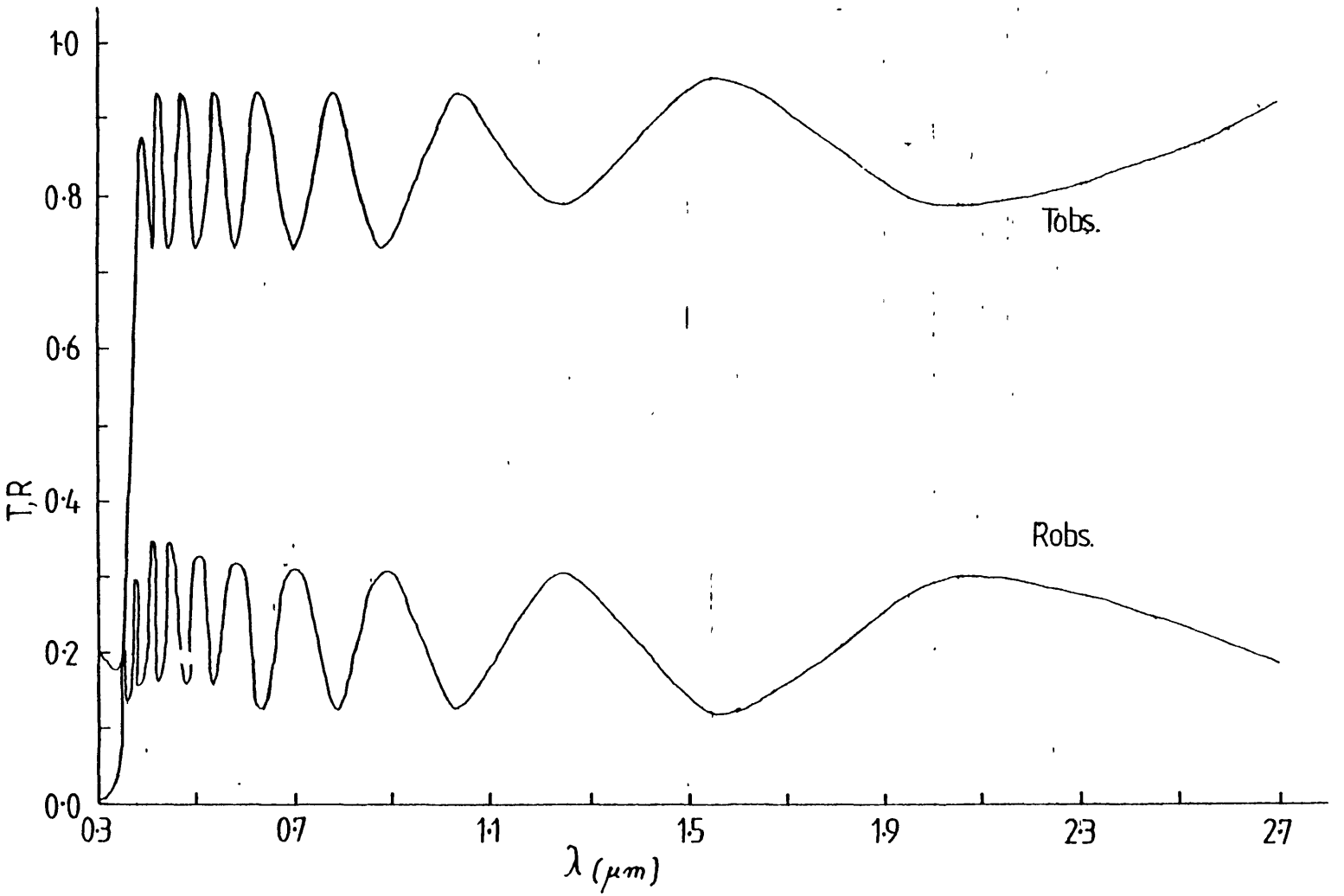

Fig. 3.1.2 : Measured transmission and reflection vs wavelength of the WO_3 film A1 (see table 3.1.1)

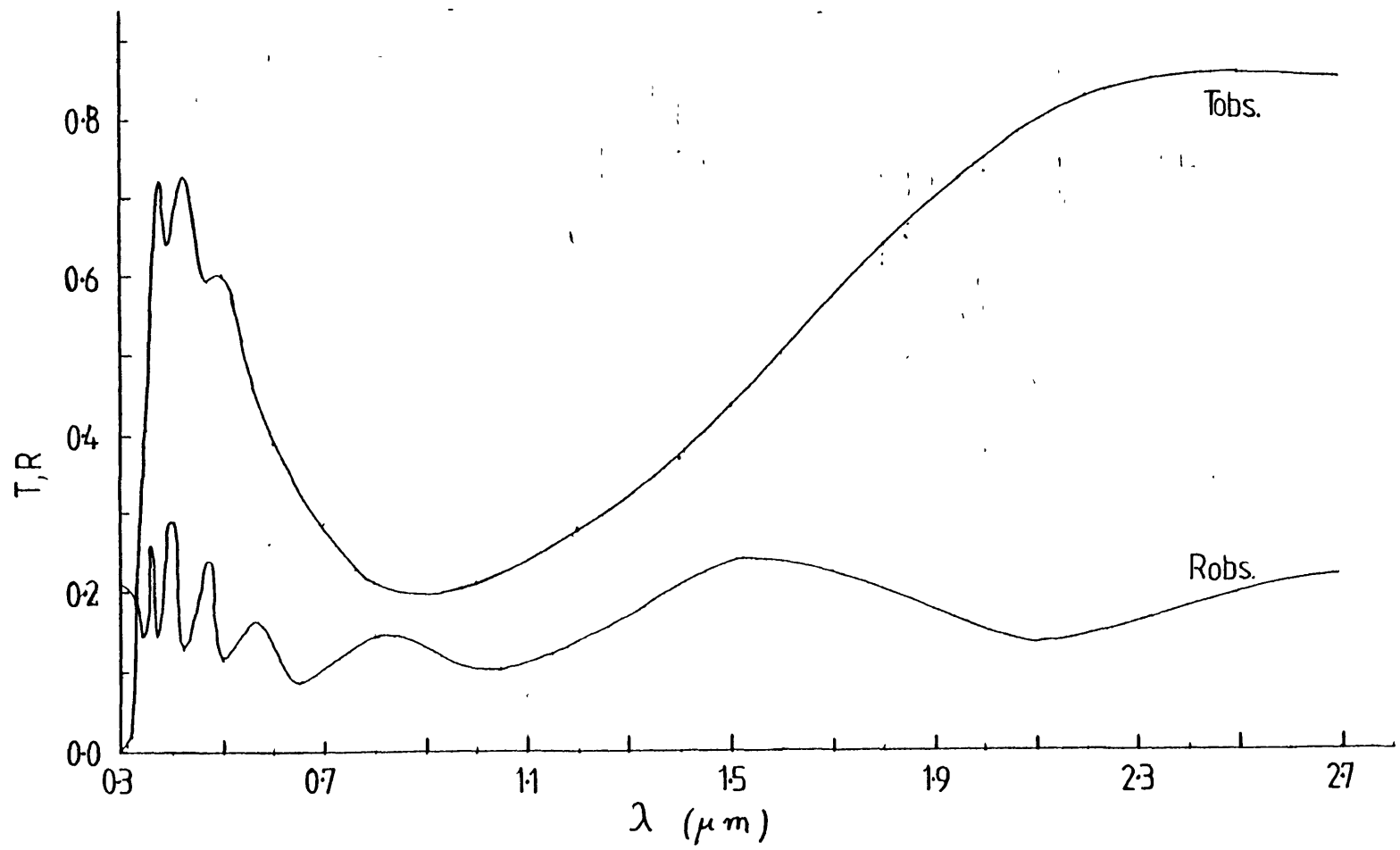

Fig. 3.1.3 : Measured transmission and reflection vs wavelength of the film A9 (see table 3.1.1), x = 0.055.

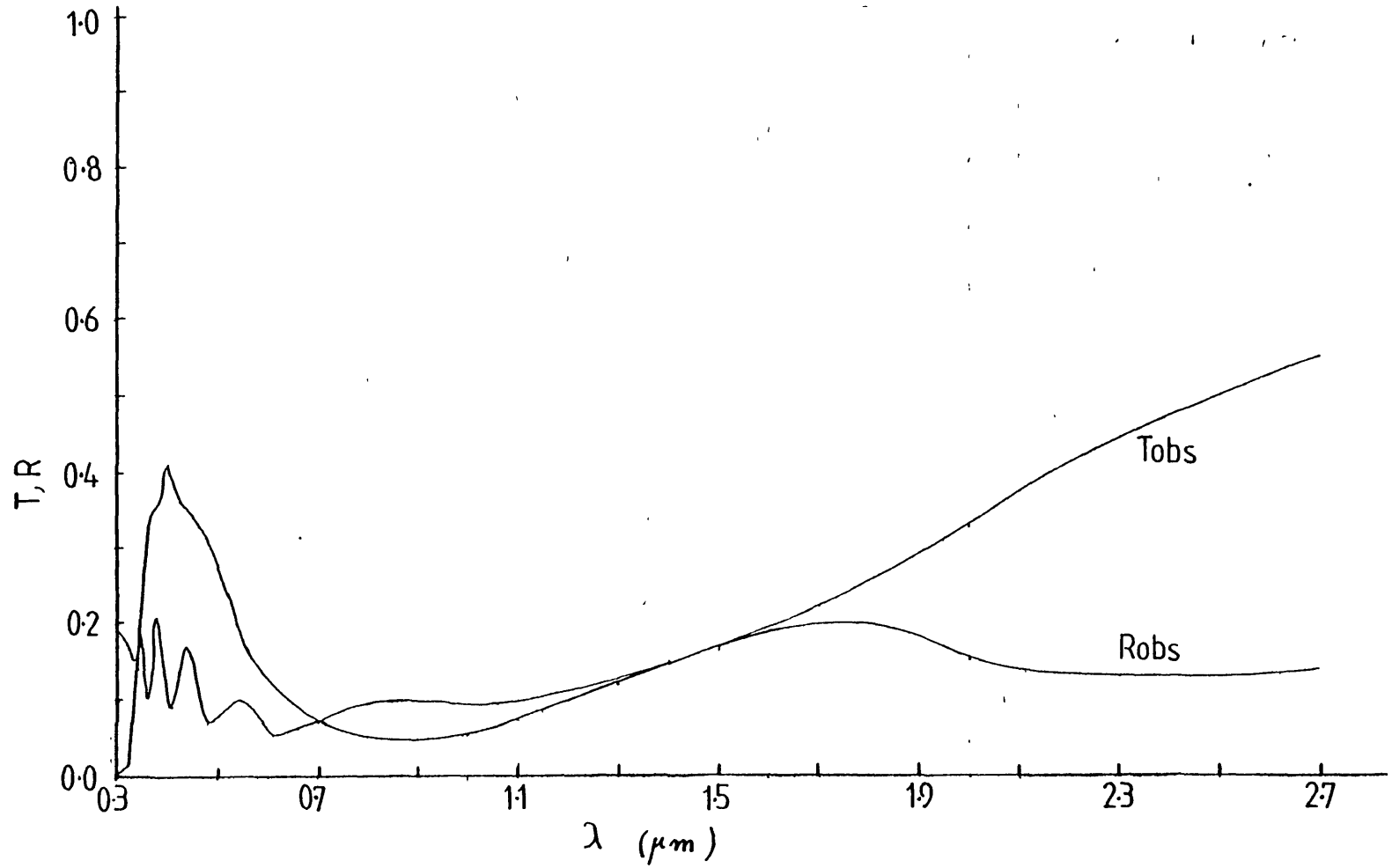

Fig. 3.1.4 : Measured transmission and reflection vs wavelength of the film A17 (see table 3.1.1), x = 0.22.

n_s = 1.46 the index of refraction of silica; and R'_f is the reflection at the film-substrate interface.

The values of R'_f are not known exactly but they are sufficiently close to $\langle R_{obs} \rangle$ which varies from 0.07 to 0.23.

Therefore

$$1 - R'_s R'_f = 0.995 \pm 0.003$$

and Eqn. (3.1.1) can be written as,

$$T_f = 0.96 \langle T_{obs} \rangle \quad . \tag{3.1.2}$$

The true values of reflection, R_f, were calculated using the expression

$$R_f = \langle R_{obs} \rangle - R_s T_f^2 \tag{3.1.3}$$

where R_s is the reflection of a bare silica slide which includes both front and rear face effects.

R_s was measured to be approximately 0.12 over the wavelength range of interest. The difference between R_s and R'_s is due to both internal reflections in the slide and reflection at the slide-holder interface so that Eqn. (3.1.3) now becomes

$$R_f = \langle R_{obs} \rangle - 0.12 T_f^2 \quad . \tag{3.1.5}$$

Figs. 3.1.5, 3.1.6 and 3.1.7 show the spectra of Figs. 3.1.2, 3.1.3 and 3.1.4 after the above two stages of analysis.

It should be pointed out that the values of R_f obtained from equation (3.1.4) are expected to contain an error due to limitations of the experimental arrangement used to measure R_{obs}. An estimate of this error can be obtained by comparing R_f with the values of the reflection calculated from the expression

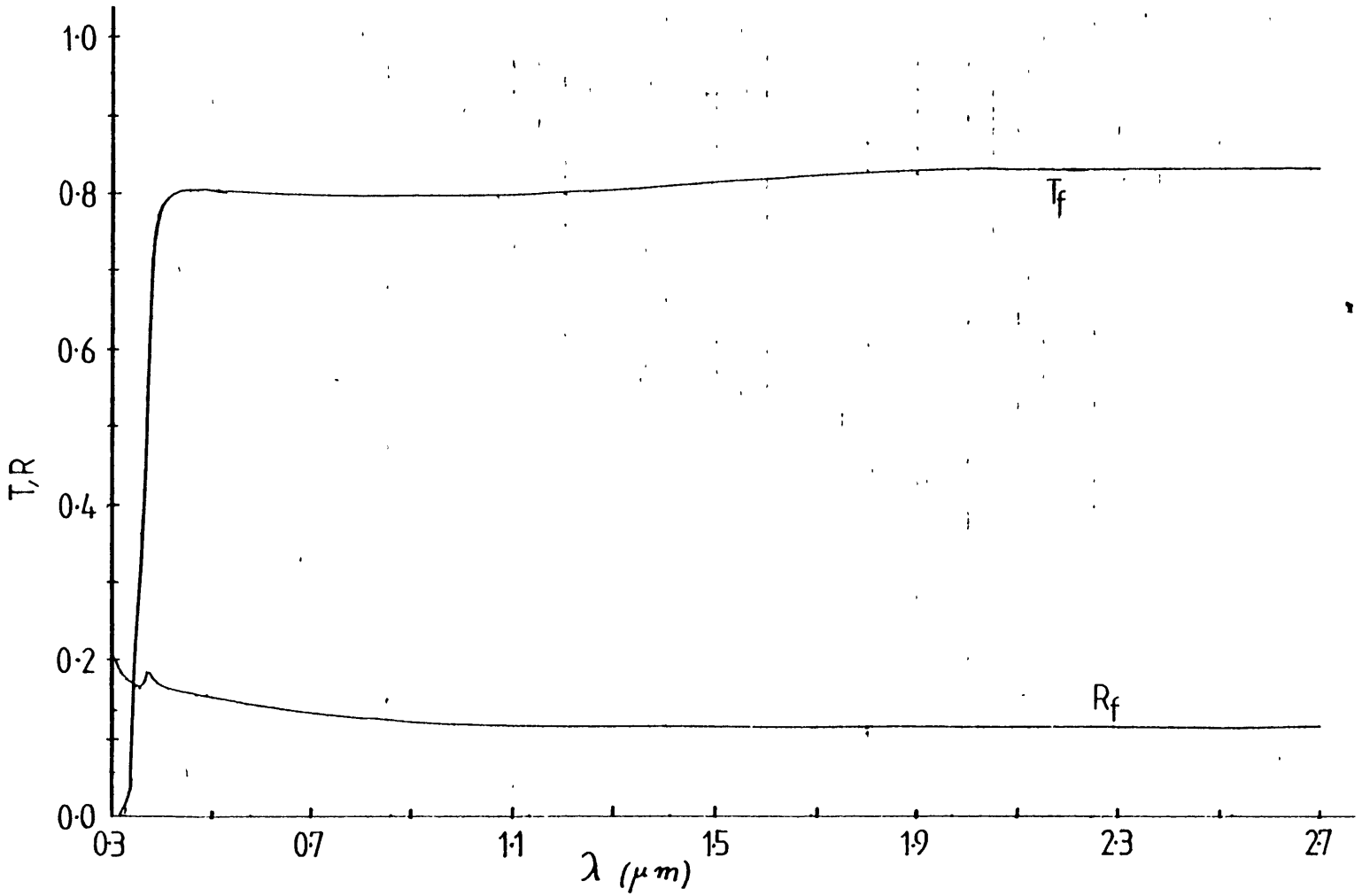

Fig. 3.1.5 : Transmission and reflection vs wavelength of the film A1 (see table 3.1.1) obtained after refinement using equ. (3.1.1) and (3.1.4).

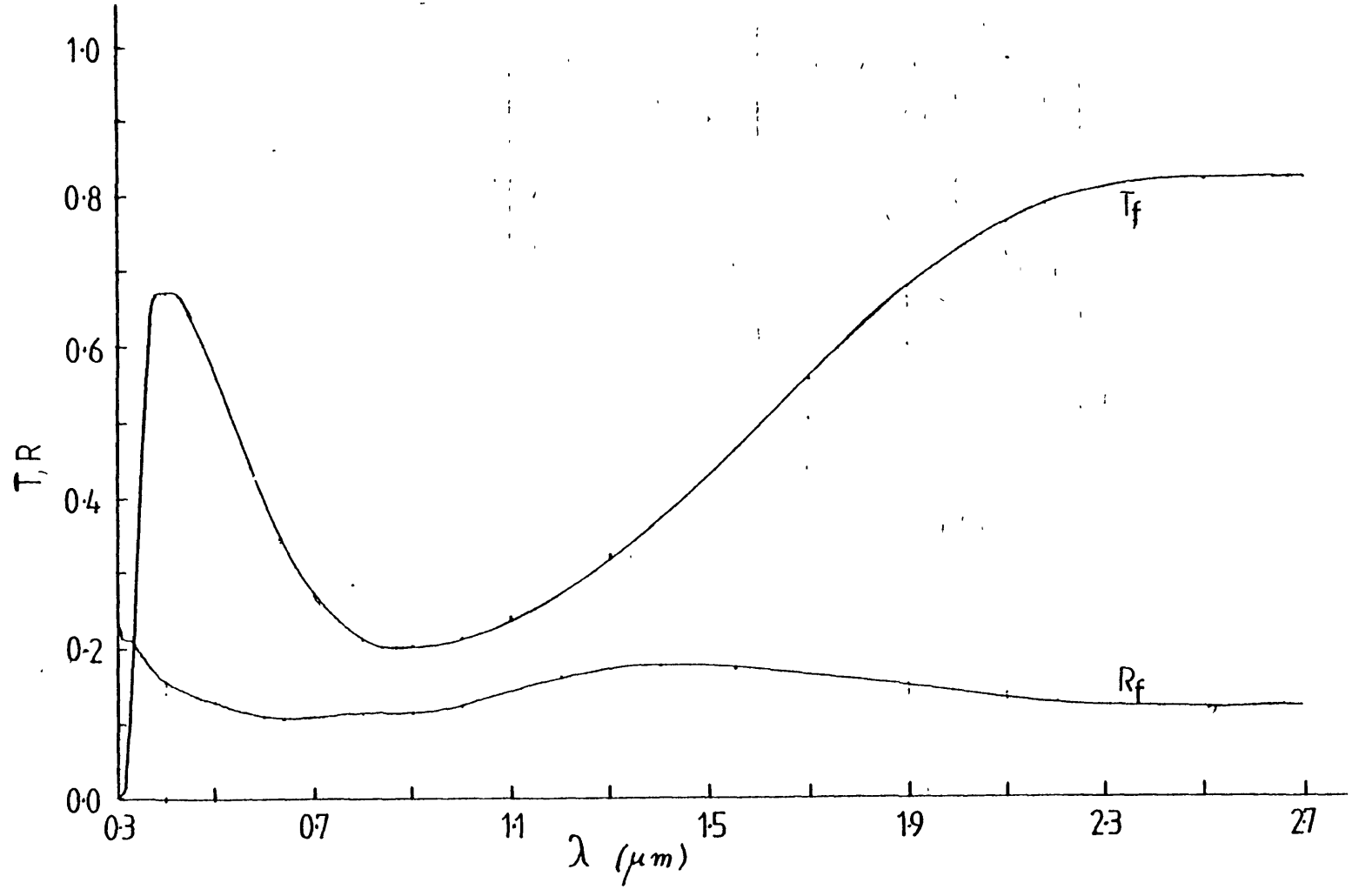

Fig. 3.1.6 : Transmission and reflection vs wavelength of the film A9 (see table 3.1.1), x = 0.055, obtained after refinement using equ. (3.1.1) and (3.1.4).

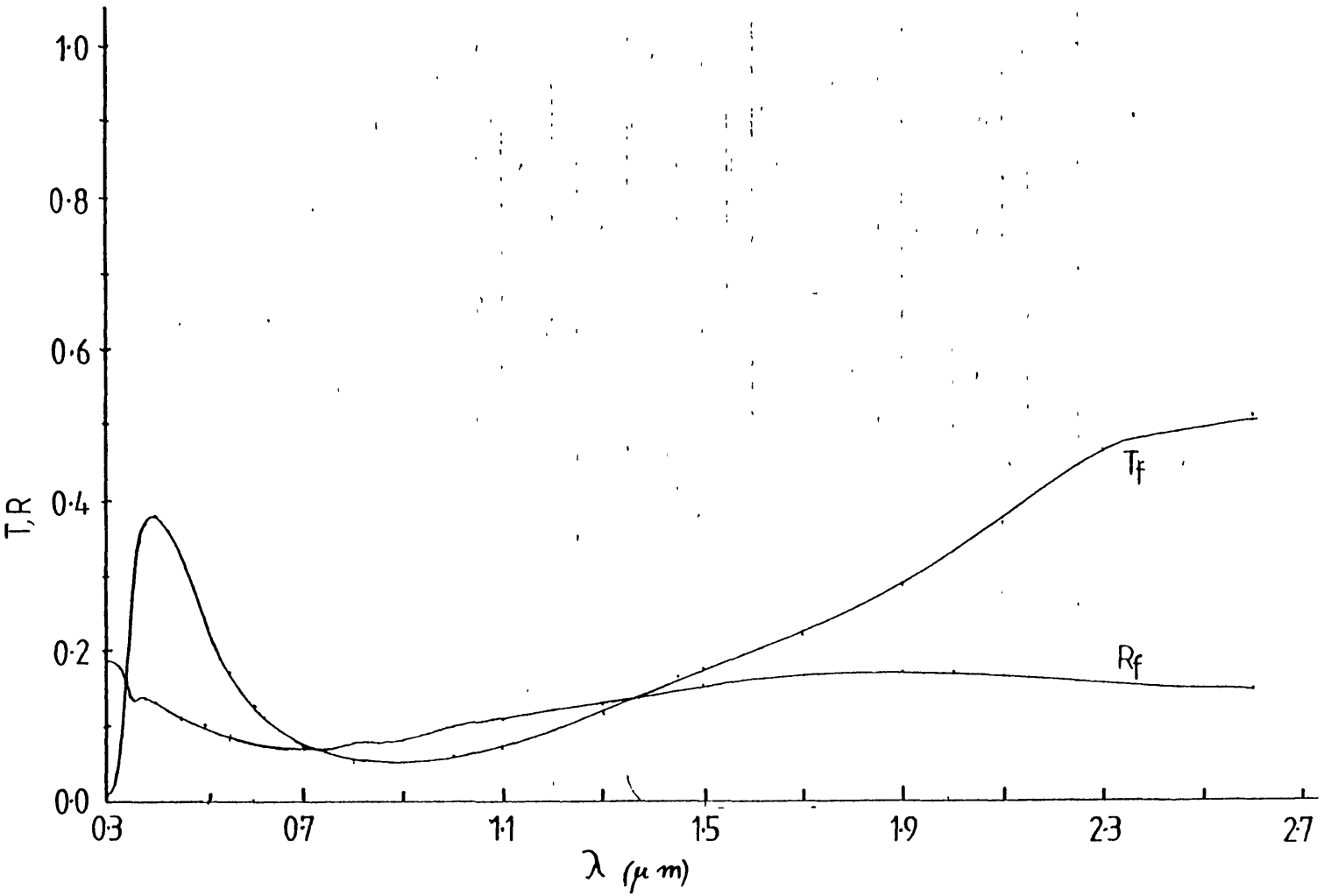

Fig. 3.1.7 : Transmission and reflection vs wavelength of the film A17 (see table 3.1.1, x = 0.22, obtained after refinement using equ (3.1.1) and (3.1.4)

$$R = \frac{(1-n)^2}{(1+n)^2} \tag{3.1.5}$$

in the transparent region of the spectrum, provided that the real part of the index of refraction, n, is known.

n has been obtained from the position, on the wavelength scale, of the maxima and minima of the reflection spectrum using the expressions [4, 5]

$$d = \frac{(m + \frac{1}{2})}{2n} \lambda_{min} \tag{3.1.6}$$

and

$$d = \frac{m}{2n} \lambda_{max} \tag{3.1.7}$$

where

d is the thickness of film;

λ_{min} is the wavelength at which minimum occurs;

λ_{max} is the wavelength at which maximum occurs;

m is the integer representing the order of the interference fringe.

From these values, R can be computed using eqn. (3.1.5) and compared with R_f. R_f is found to be approximately 8% higher than R.

However, in the third stage of treatment which is the calculation of the absorption coefficient, the error of 8% in R_f only introduces an error of less than 1% in the absorption coefficient.

The absorption coefficient α is

$$\alpha = \frac{4\pi k}{\lambda} \tag{3.1.8}$$

where k the extinction coefficient is the imaginary part of the refractive index n_c,

$$n_c = n - ik \tag{3.1.9}$$

and λ is the wavelength.

α has been calculated from the expression [4, 5]

$$T_f = \frac{(1-R_f)^2 \exp(-\alpha d)}{1-R_f^2 \exp(-2\alpha d)} \tag{3.1.10}$$

which takes into account multiple reflections inside the film.

The values of α were computed with a CBM Commodore 3032 microprocessor using the program of Appendix I.

The absorption coefficient versus photon energy for the films of Figs. 3.1.2, 3.1.3 and 3.1.4 is shown in Fig. 3.1.8. The accuracy of the values of α depends primiraly on the accuracy of determination of T_f. Therefore we expect the largest and smallest values of α to contain an error of ~ 10%. These values of α correspond to $T_f \geq 0.75$ and $T_f \leq 0.005$. In the first case the interference effects are very pronounced and in the second case the noise level of the amplifier of the spectrophotometer is reached. One could overcome this problem by using films of identical composition but different thickness, it is however very difficult to achieve such a state of affairs in practice.

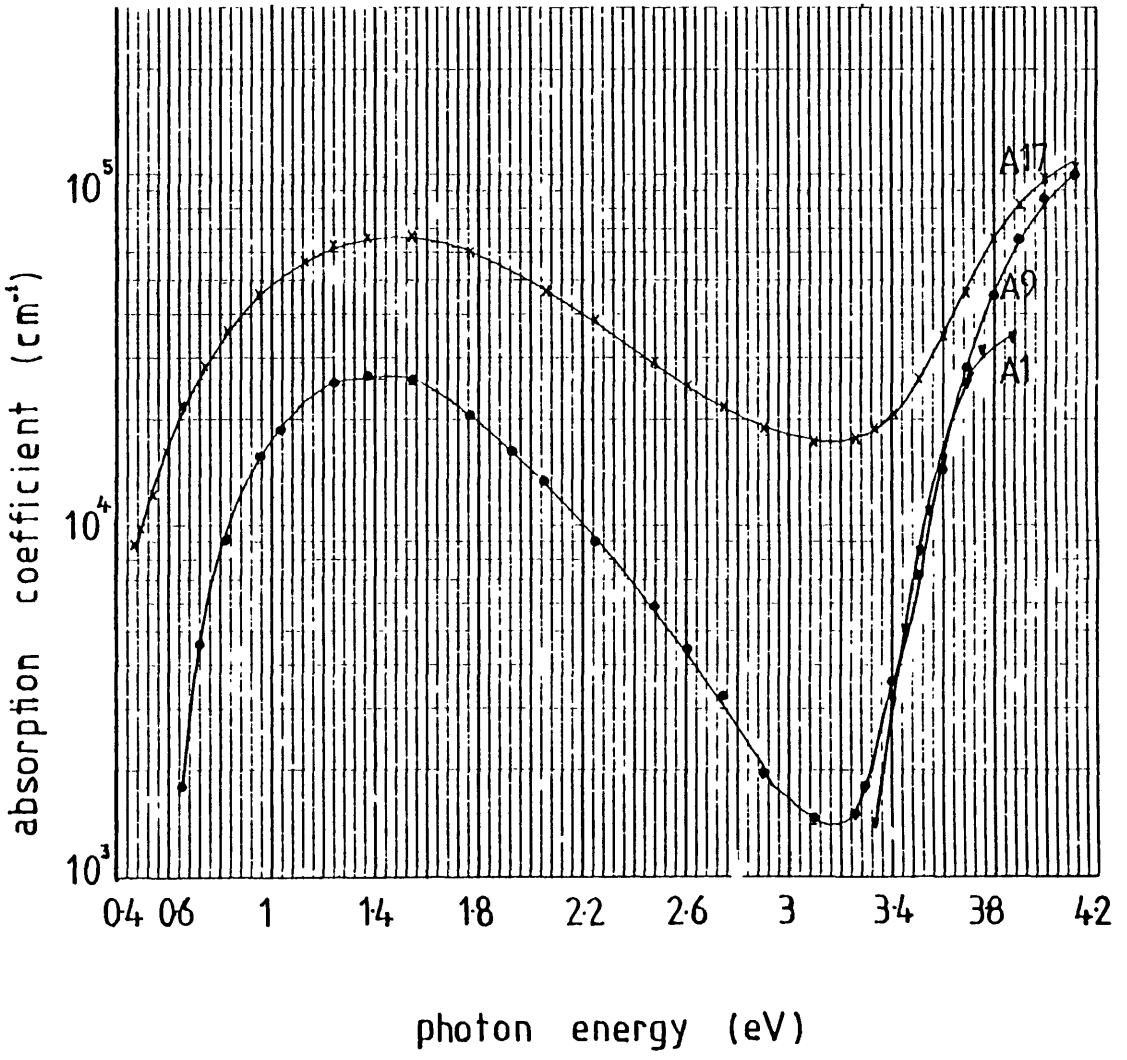

Fig. 3.1.8 : Absorption coefficient vs photon energy of the films A1, A9 and A17, (see table 3.1.1). The corresponding values of x are 0, 0.055 and 0.22.

3.1.2 Optical results

Optical measurements have been carried out on a range of Na_xWO_3 films which can be classed into two groups according to their method of preparation.

Films of group A have been prepared with the evaporation method as described in section 2.1.2. The conditions of preparation were identical for all the films except for the substrate temperature and the temperature of the sodium source. By varying these two parameters films of different grain sizes and x-values were obtained. Table 3.1.1 shows the measured x-values and thickness as well as the substrate temperature and mean grain size of the films in group A. The grain sizes have been inferred from the electron microscope work of section 2.2. The x-values have been obtained from equ.(2.2.12) which has been obtained for the 50Å m.g.s. films. Therefore, the value of the films of 120Å m.g.s. reported in table 3.1.1 are smaller than the actual x-values by ~10%.

Films of group B have been prepared as described in section 2.1.2 but they have been annealed prior to sodium insertion from the vapour phase. Their sodium content could not be measured, but an estimate of their x-value was obtained by comparison of their reflectivity spectra with the reflectivity measurements of Na_xWO_3 powder of known x-value [6].

The thickness, x-value and annealing conditions of these films are shown in table 3.1.2. The absorption spectra of group A are presented in two energy ranges for the sake of clarity. For the same reason they are presented on different figures so as to avoid excessive overlap. They are shown in Fig. 3.1.9 to Fig. 3.1.15.

The reflection spectra obtained from eqn. 3.1.4 and their index

of refraction (real part) as obtained from equations (3.1.6) and (3.1.7) are shown in Figures 3.1.16 to 3.1.21 and in Figures 3.1.22 to 3.1.25 respectively.

The corresponding spectra and index of refraction of films in group B are shown in Figures 3.1.26 to 3.1.29.

In the energy range of 3.2 eV to 4.1 eV the absorption coefficient was found to obey the relation of the 50Å m.g.s. films

$$\alpha(h\nu) = \frac{A(h\nu - E_0)^2}{h\nu} \qquad (3.1.11)$$

where A and E_0 are material constants, and $h\nu$ is the photon energy.

Figures 3.1.30 to 3.1.32 show a plot of $(\alpha h\nu)^{\frac{1}{2}}$ versus $h\nu$ for the different films. From these plots both constants E_0 and A can be obtained from the zero intercept and the slope respectively. The values of E_0 and A so obtained are tabulated in table 3.1.3.

It can be seen, however, that the fit to the relation (3.1.11) is gradually restricted to a smaller range as x increased from zero to $x = 0.22$. In the same energy range 3.2eV to 4.1eV and below the range of applicability of relation (3.1.11) the logarithm of α of all films was found to be a linear function of $h\nu$. The values of the slope $\frac{d(\log \alpha)}{d(h\nu)}$ obtained from figures 3.1.9, 3.1.10, 3.1.11 and 3.1.26 are also tabulated in table 3.1.3.

The absorption coefficient of the 2-3μ m.g.s. films follows equ. (3.1.11) up to ~ 3.75 eV. The quantities A and E_0 for these films are shown in table 3.1.3.

In the energy range 3.75 eV to 4.1 eV the absorption coefficient of the 2-3μ m.g.s. films obeys the relation:

$$\alpha h\nu = B(h\nu - E_d)^{\frac{1}{2}} \qquad (3.1.12)$$

The material constants B and E_d are shown in table 3.1.4.

Table 3.1.1

Sodium content, thickness, m.g.s and substrate temperature of Na_xWO_3 films prepared by the coevaporation method and used in optical measurments

Film N°	x	thickness d(μm)	substrate temperature °C	mean grain size Å
A1	0	0.78	60	50
A2	5.6×10^{-3}	0.5	60	50
A3	8×10^{-3}	0.53	60	50
A4	1×10^{-2}	0.53	60	50
A5	1.3×10^{-2}	0.63	60	50
A6	1.9×10^{-2}	0.44	60	50
A7	3.4×10^{-2}	0.4	60	50
A8	5×10^{-2}	0.44	60	50
A9	5.5×10^{-2}	0.48	60	50
A10	7.2×10^{-2}	0.5	60	50
A11	8.2×10^{-2}	0.51	60	50
A12	8.4×10^{-2}	0.34	300	120
A13	9.5×10^{-2}	0.29	60	50
A14	1.1×10^{-1}	0.35	60	50
A15	1.2×10^{-1}	0.63	60	50
A16	1.4×10^{-1}	0.45	60	50
A17	2.2×10^{-1}	0.45	300	120
A18	$> 2.2\times10^{-1}$	0.42	300	120

Table 3.1.2

Thickness, x-value and annealing conditions of the Na_xWO_3 films of 2-3μm m.g.s. used in optical measurements

Film	x*	d(μm)	annealing conditions
B1	0	0.24	$T_a = 500^oC$ t_a = 20 hours in dry N_2
B2	~ 0.05	0.38	$T_a = 500^oC$ t_a = 4 hours in dry N_2
B3	~ 0.1	0.45	$T_a = 500^oC$ t_a = 4 hours in dry N_2
B4	~ 0.2	0.24	$T_a = 500^oC$ t_a = 20 hours in dry N_2

* The x-values were not obtained by direct measurement. See text for details.

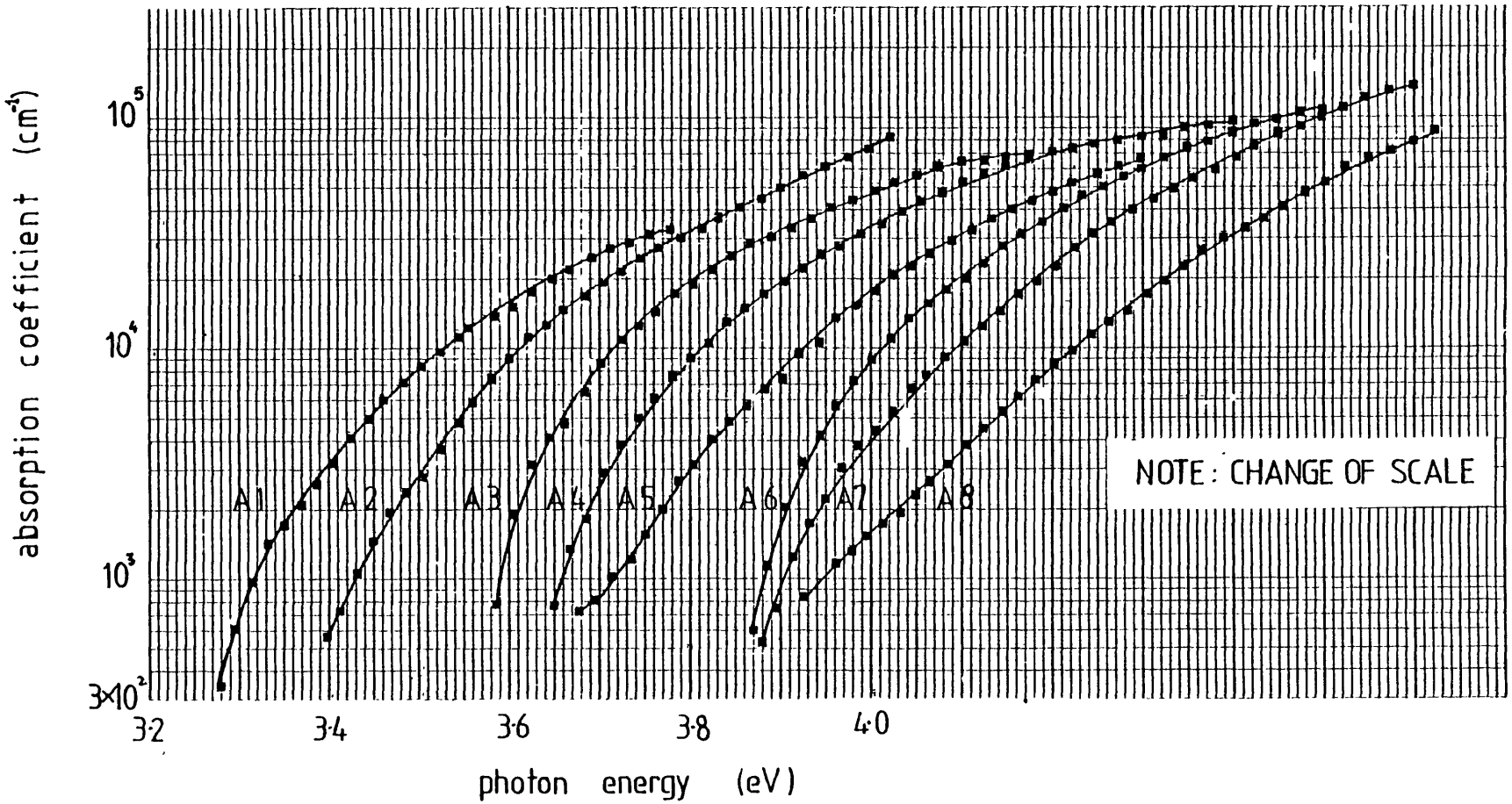

Fig. 3.1.9 : Absorption coefficient vs photon energy of the films A1, A2, A3, A4, A5, A6,A7 and A8 (see table 3.1.1). The corresponding values of x are 0, 0.0056, 0.008, 0.01, 0.019, 0.034 and 0.05. The energy scale is shifted to the right by steps of 0.1 eV for everv film after A1

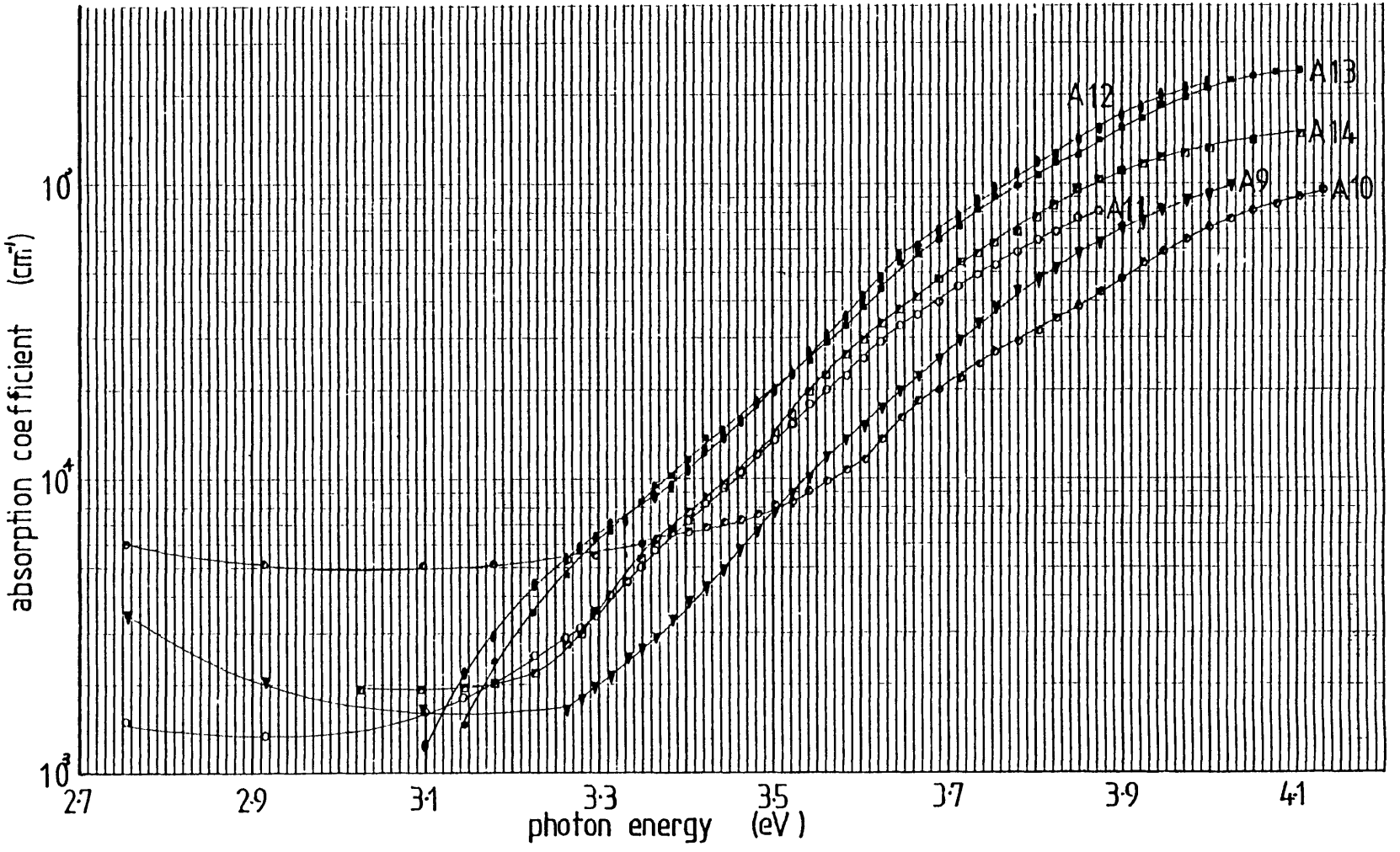

Fig. 3.1.10 : Absorption coefficient vs photon energy of the films A9, A10, A11, A12, A13 and A14 (see table 3.1.1). The corresponding values of x are 0.055, 0.072, 0.082, 0.084, 0.095 and 0.11

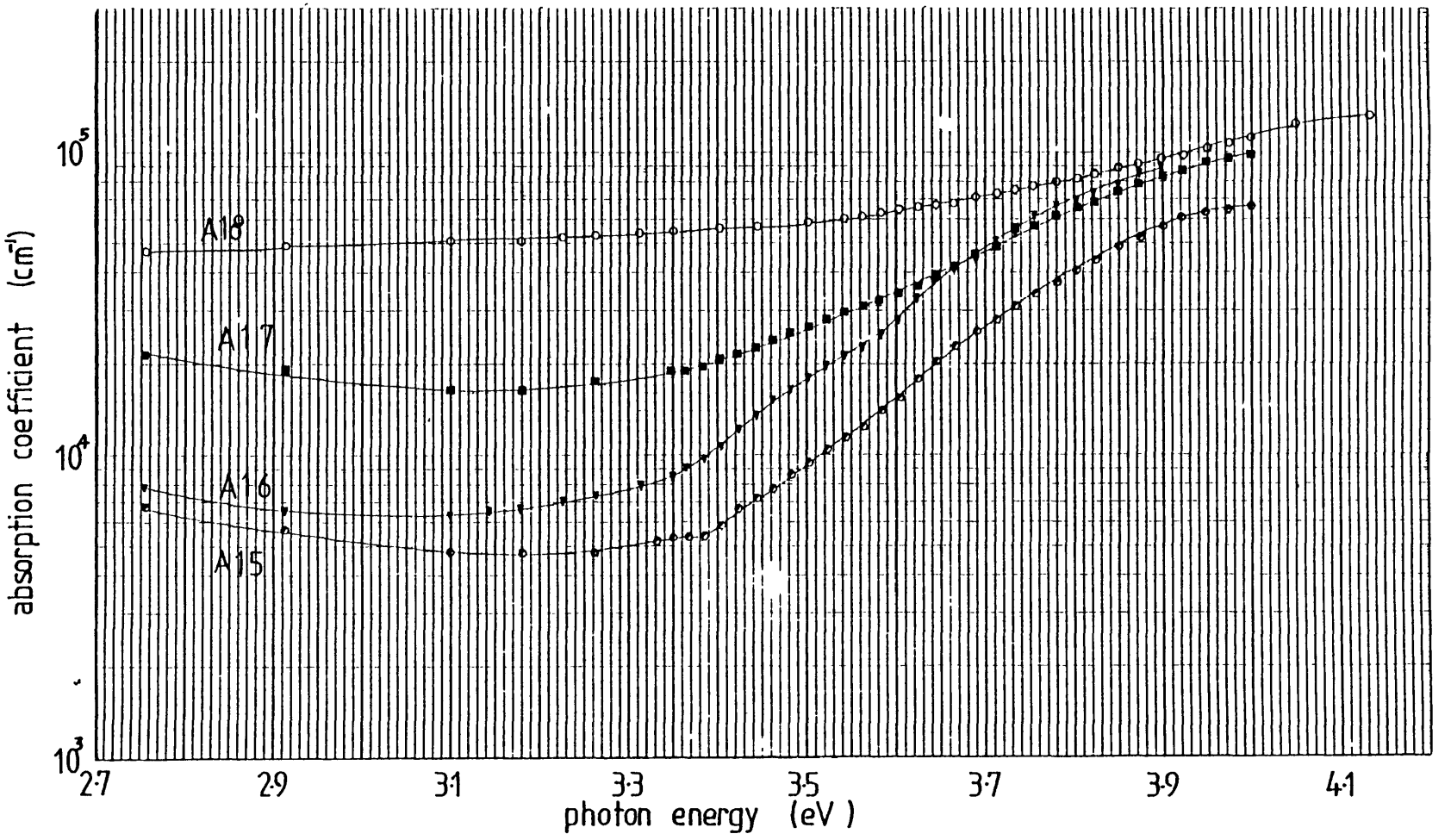

Fig. 3.1.11 : Absorption coefficient vs photon energy of the films A15, A16, A17 and A18 (see table 3.1.1). The corresponding values of x are 0.12, 0.14 and 0.22. The x value of A18 is not exactly known but is larger than 0.22

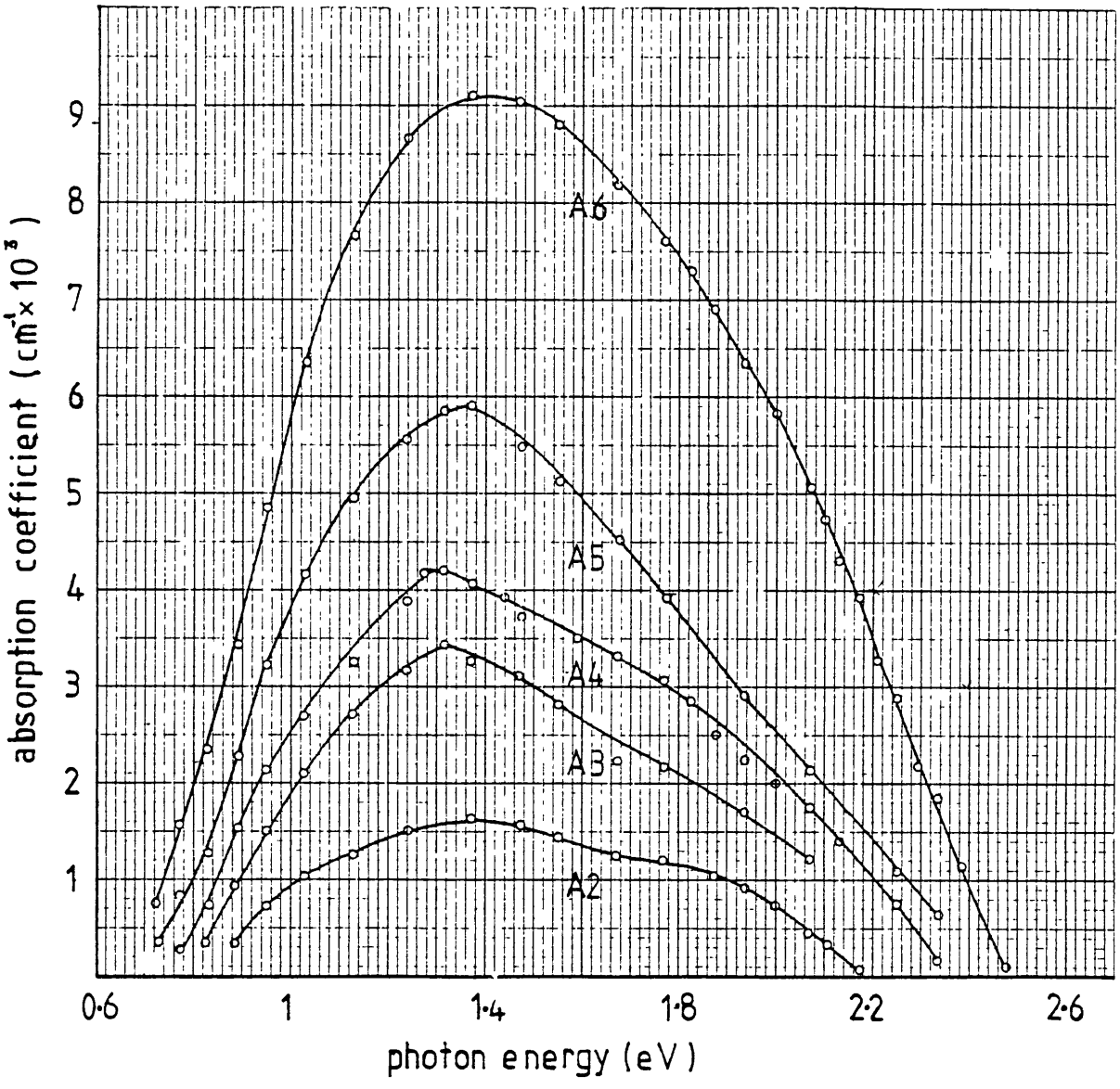

Fig. 3.1.12 : Absorption coefficient vs photon energy of the films A2, A3, A4, A5 and A6 (see table 3.1.1). The corresponding values of x are 0.0056, 0.008, 0.01, 0.013 and 0.019

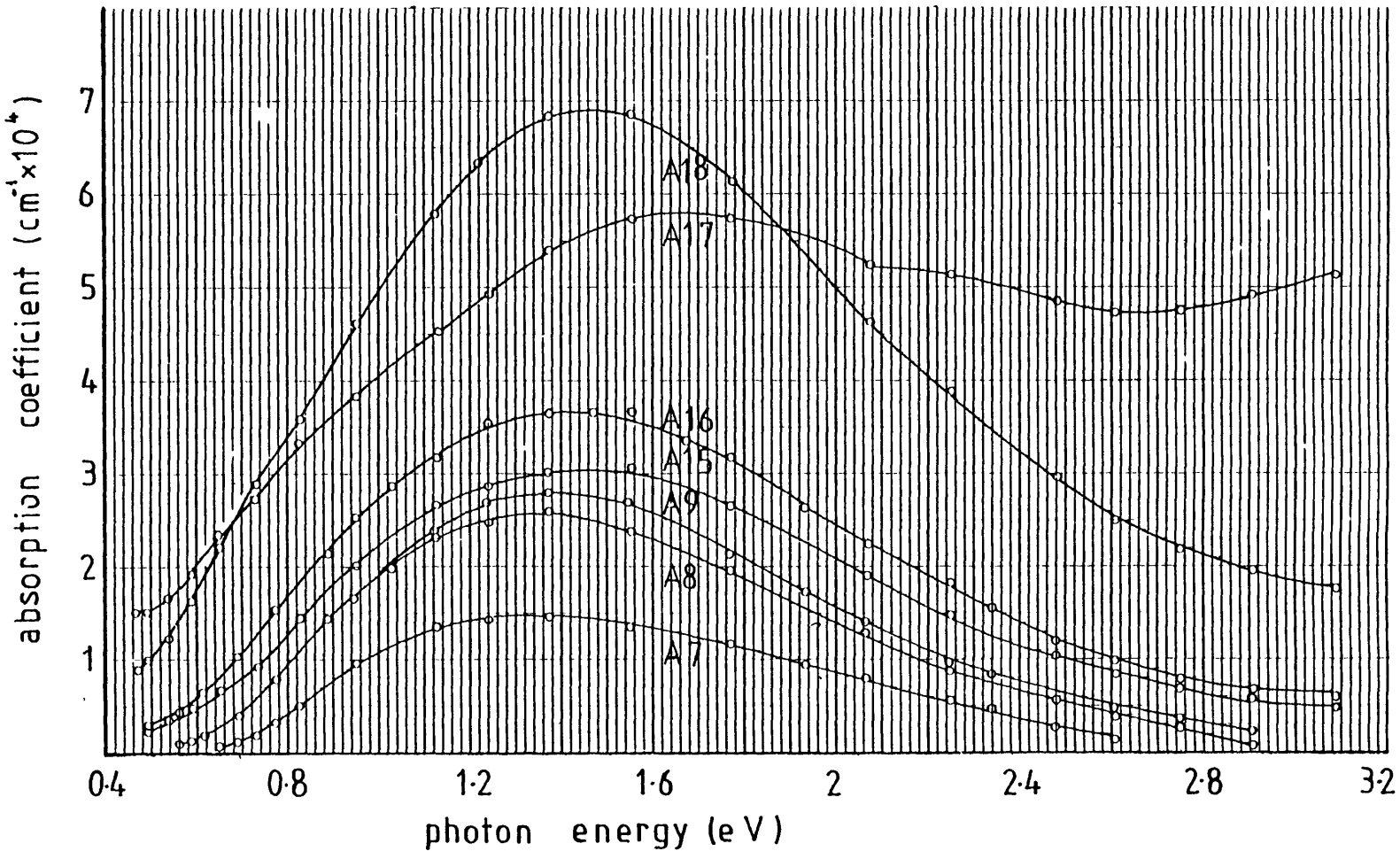

Fig. 3.1.13 : Absorption coefficient vs photon energy of the films A7, A8, A9, A15, A16, A17 and A18 (see table 3.1.1). The corresponding values of x are 0.034, 0.05, 0.055, 0.12, 0.14, 0.22 and $x > 0.22$

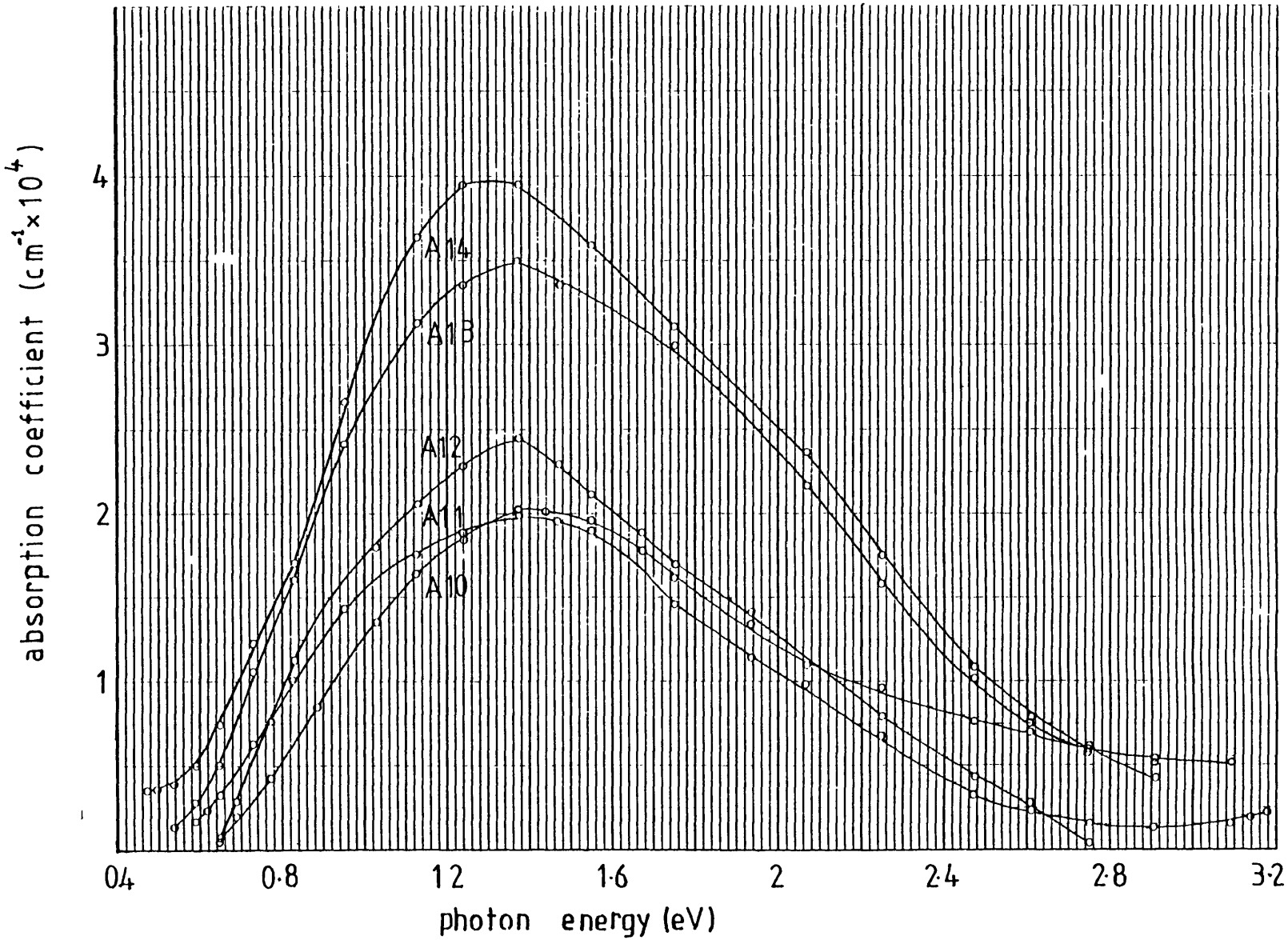

Fig. 3.1.14 : Absorption coefficient vs photon energy of the films A10, A11, A12, A13 and A14 (see table 3.1.1). The corresponding values of x are 0.072, 0.082, 0.084, 0.095 and 0.11

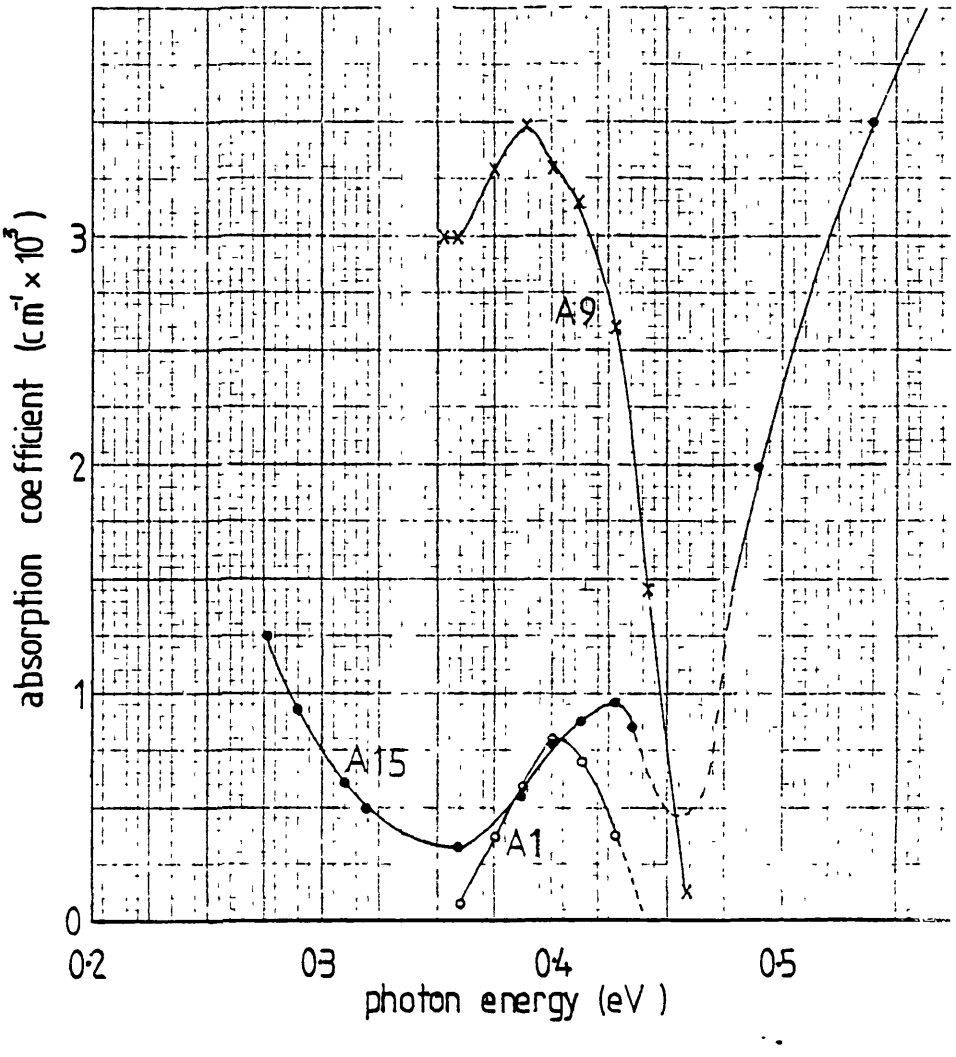

Fig. 3.1.15 : Absorption coefficient vs photon energy of the films A1, A9 and A15 (see table 3.1.1). The corresponding values of x are 0, 0.055 and 0.12

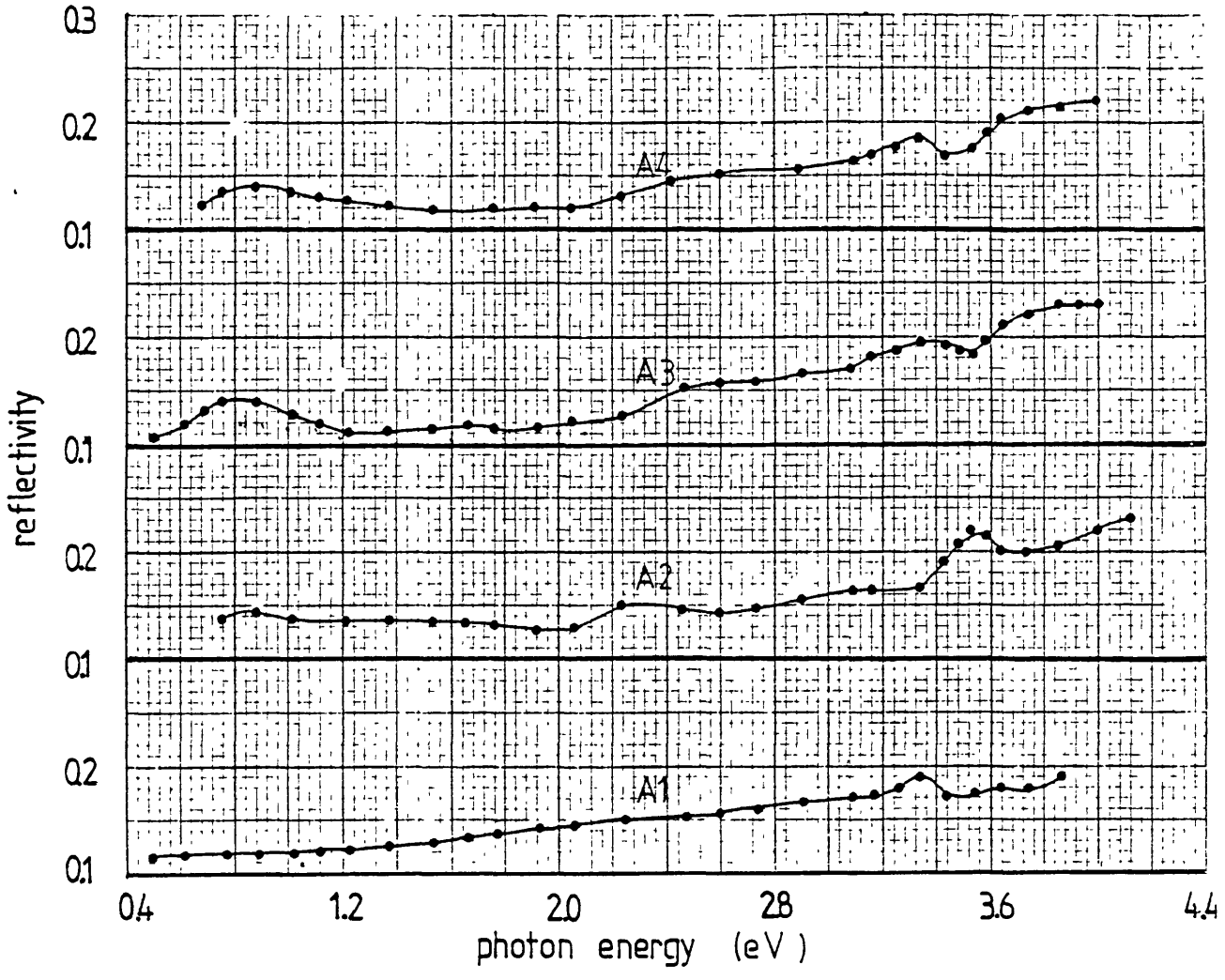

Fig. 3.1.16 : Reflectivity vs photon energy for the films A1, A2, A3 and A
(see table 3.1.1). The corresponding values of x are 0, 0.0056, 0.008 a
0.01

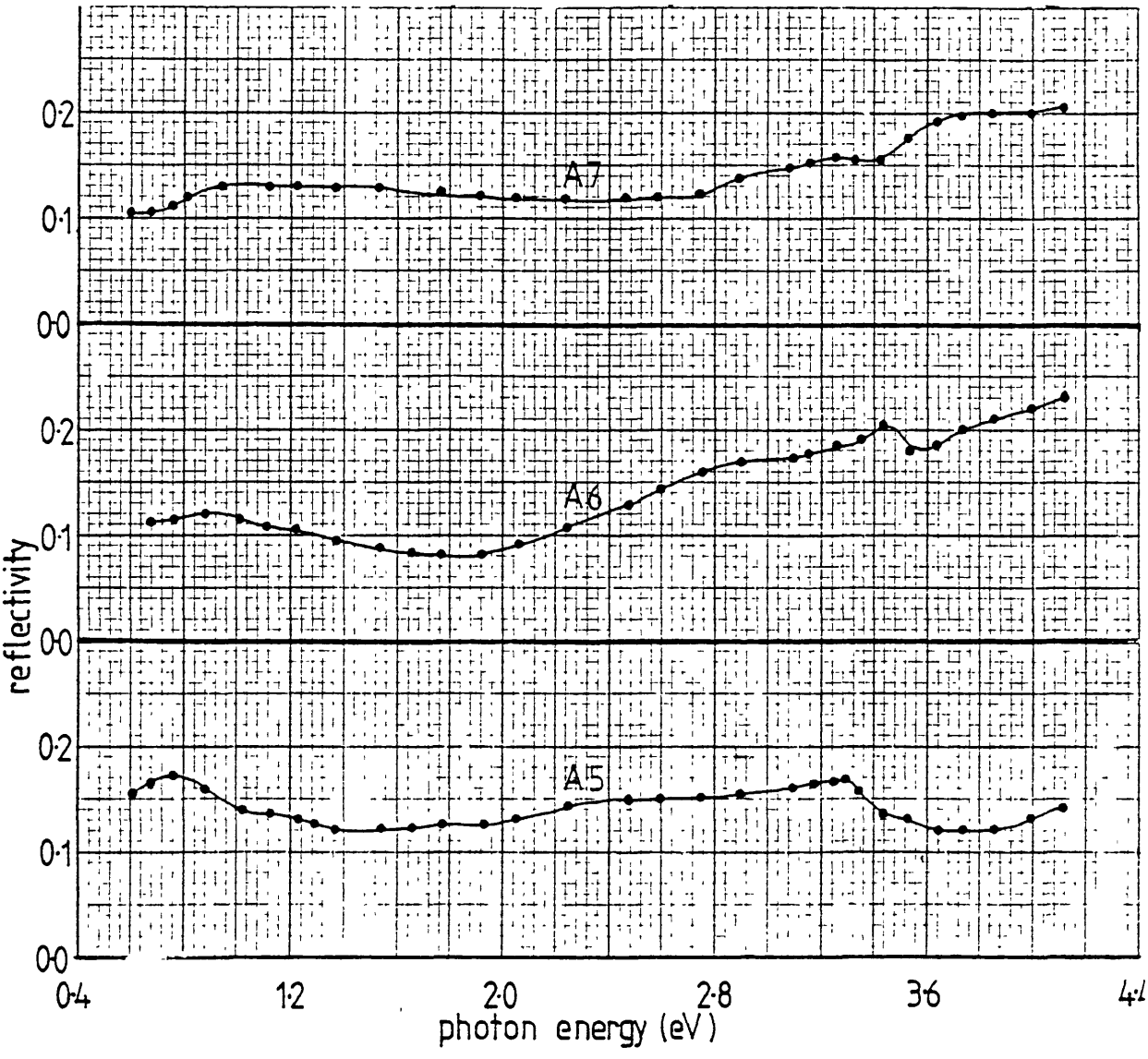

Fig. 3.1.17 : Reflectivity vs photon energy for the films A5, A6 and A7 (table 3.1.1). The corresponding values of x are 0.013, 0.019 and 0.034

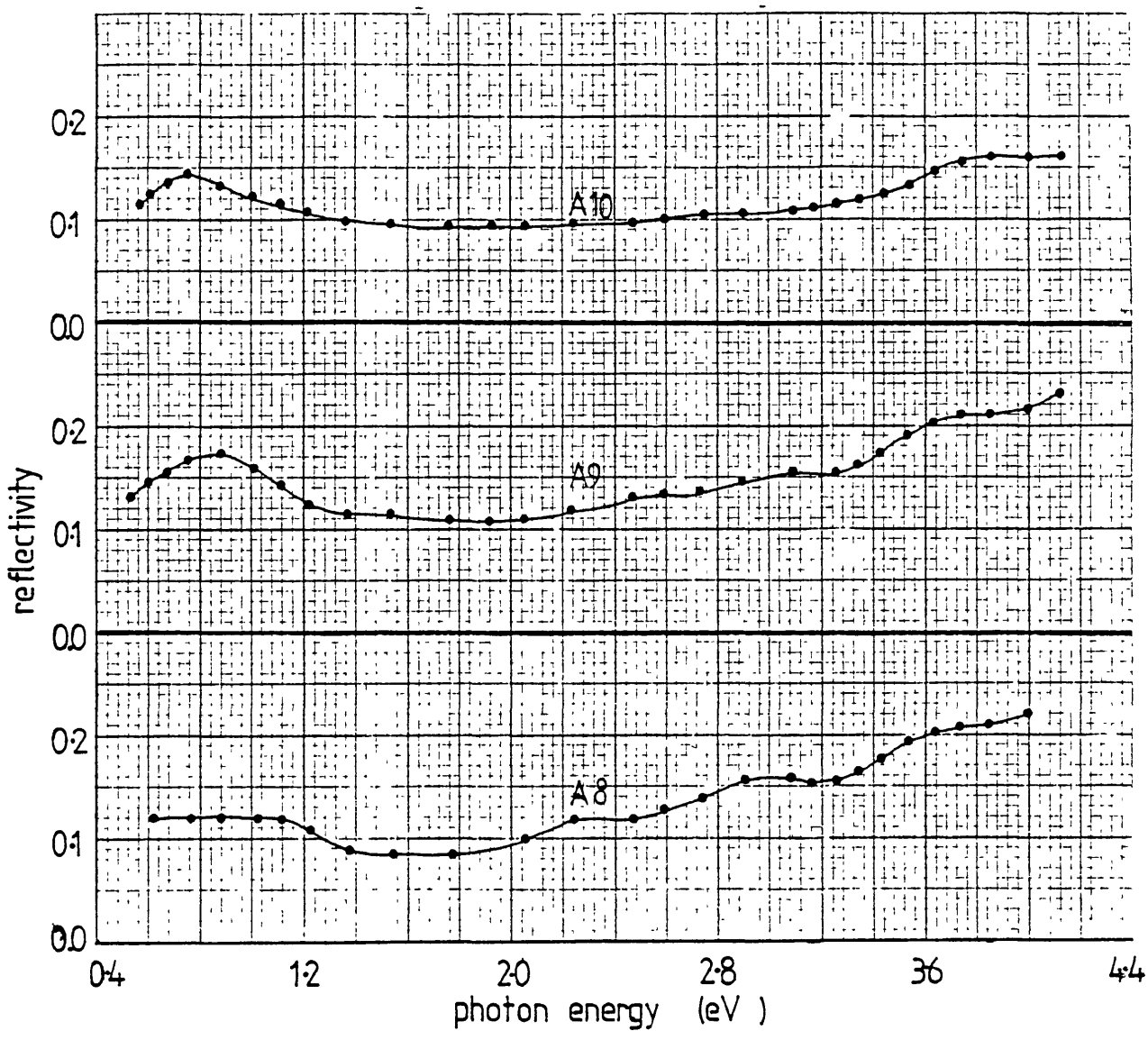

Fig. 3.1.18 : Reflectivity vs photon energy of the films A8, A9 and A10 (see table 3.11). The corresponding values of x are 0.05, 0.055 and 0.072

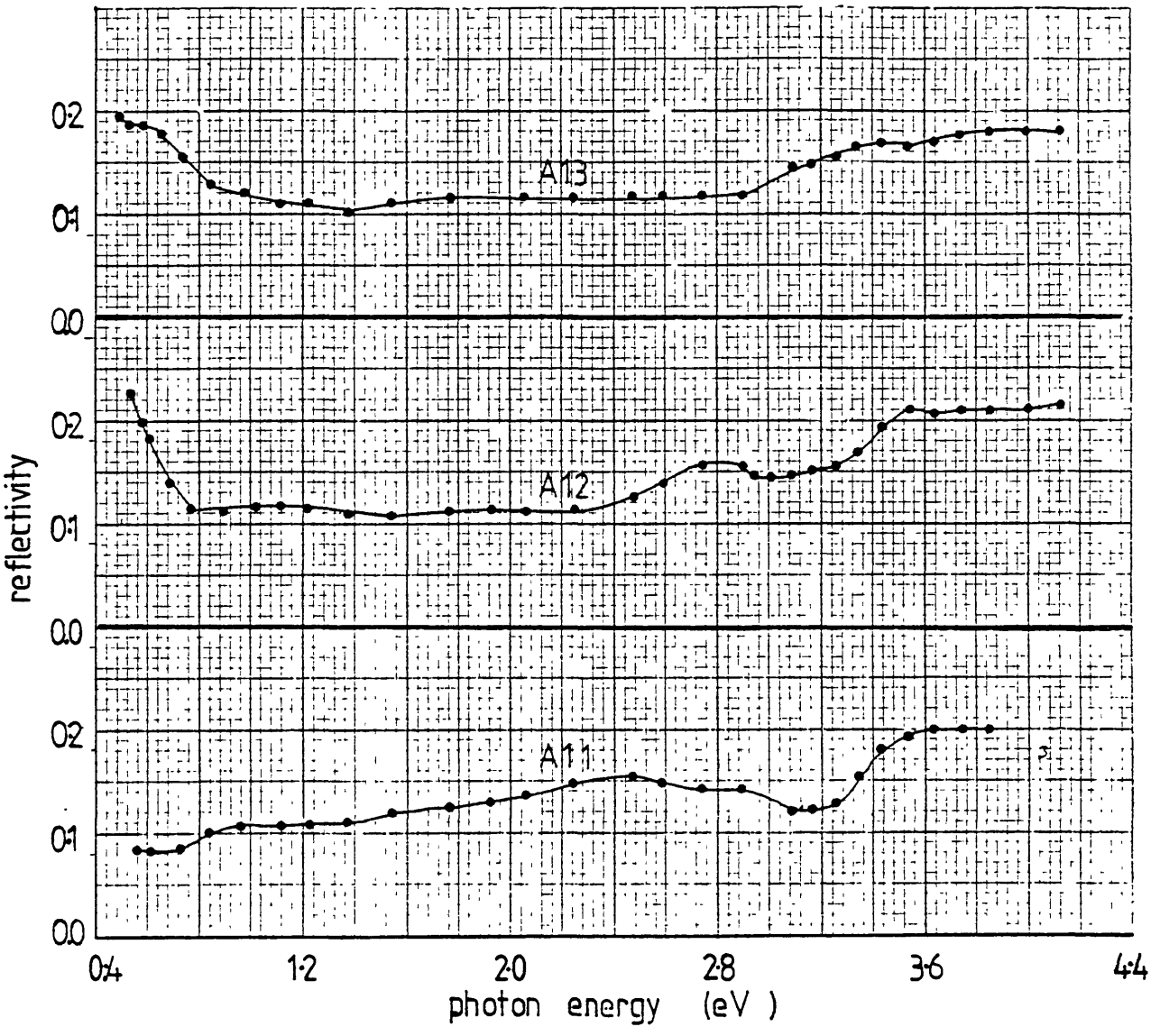

Fig. 3.1.19 : Reflectivity vs photon energy of the films A11, A12, and A13 (see table 3.1.1). The corresponding values of x are 0.082, 0.084 and 0.095

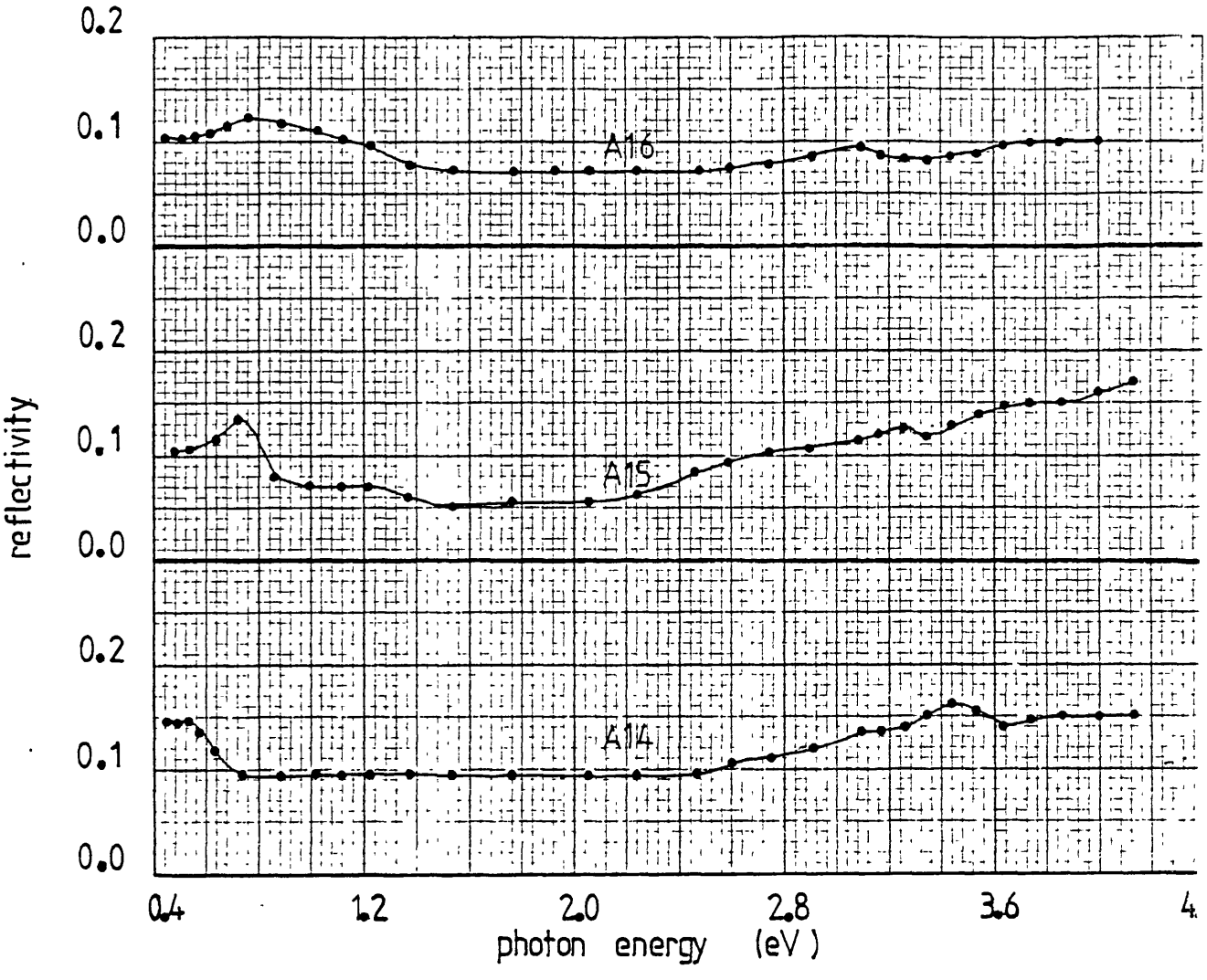

Fig. 3.1.20 : Reflectivity vs photon energy of the films A14, A15 and A16 (see table 3.1 1). The corresponding values of x are 0.11, 0.12 and 0.14

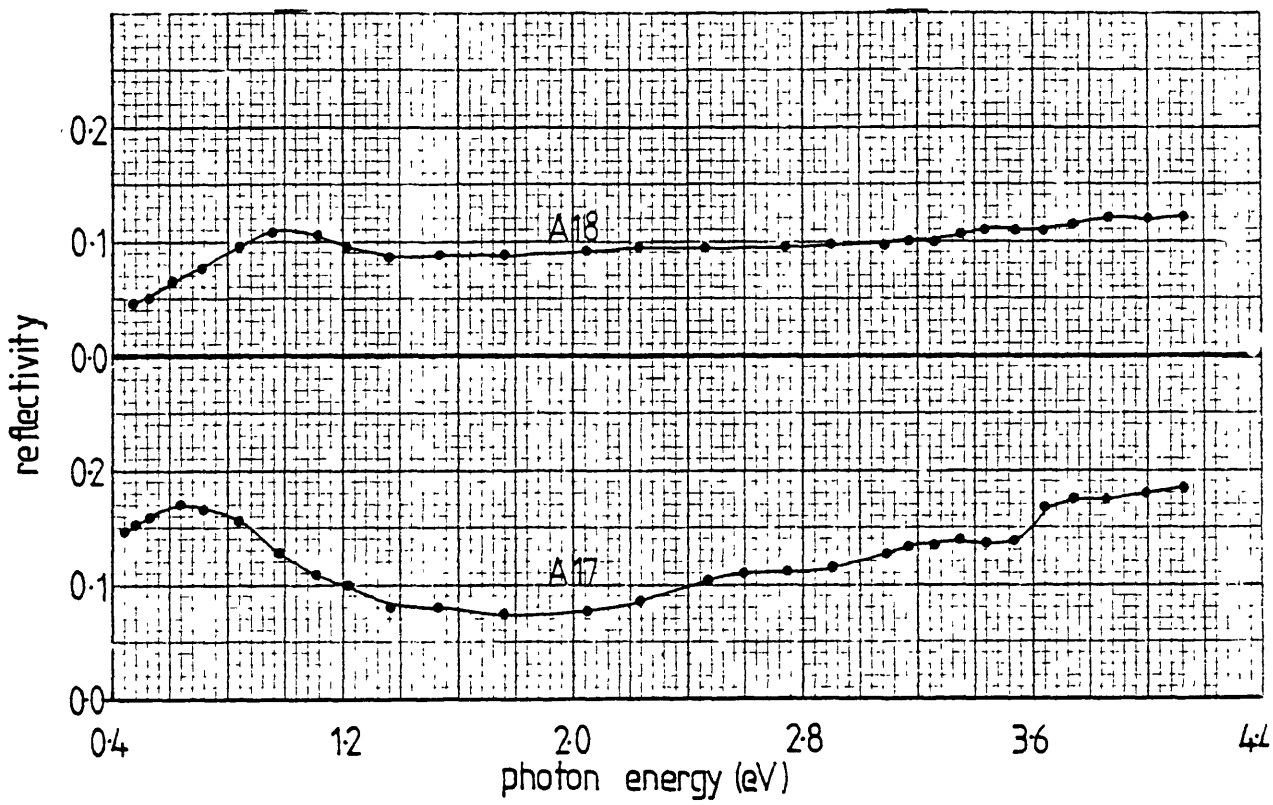

Fig. 3.1.21 : Reflectivity vs photon energy of the films A17 and A18 (see table 3.1.1). The x values are 0.22 and x > 0.22 respectively.

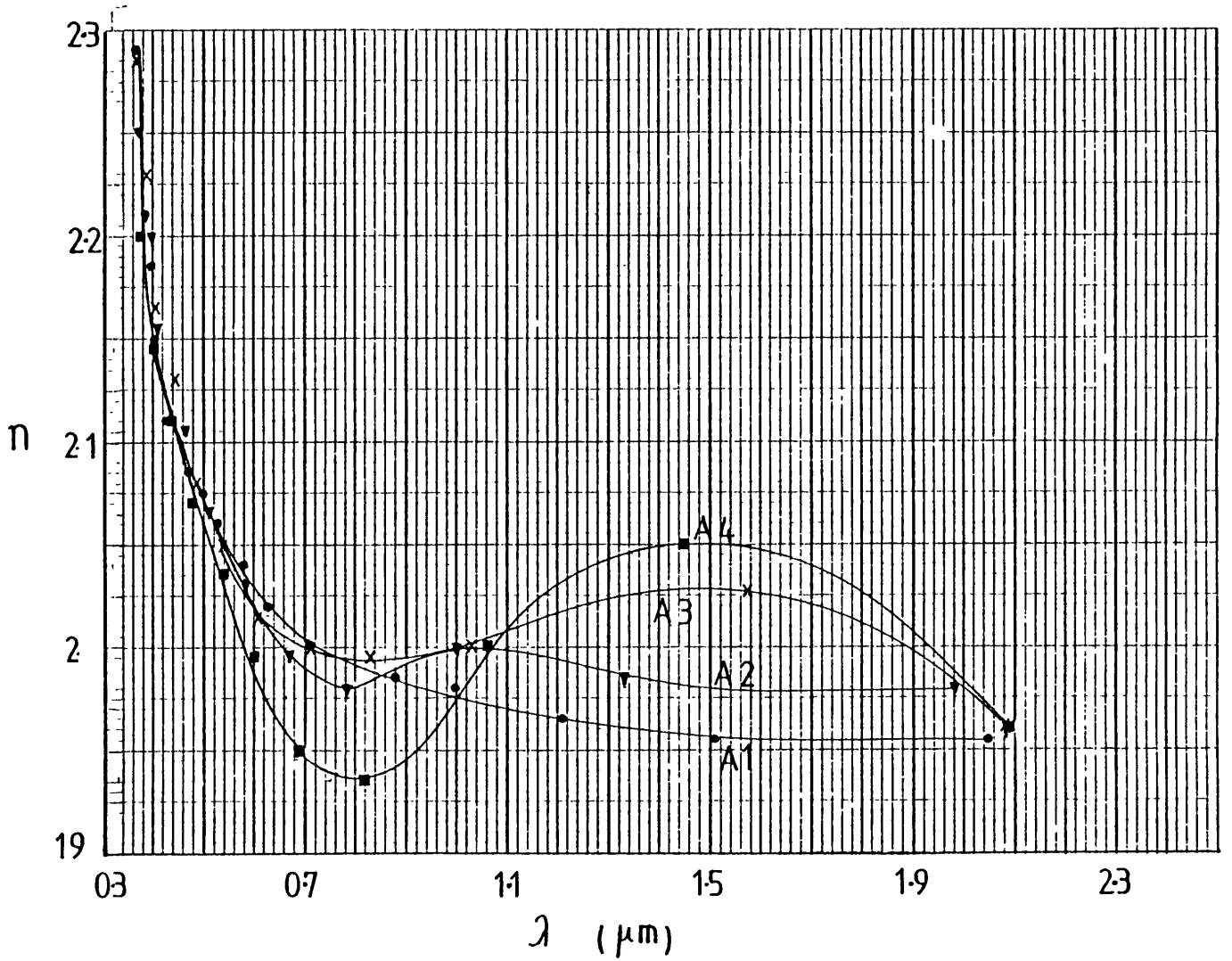

Fig. 3.1.22 : Real part of refractive index vs wavelength of the films A1, A2, A3 and A4 (see table 3.1.1). The corresponding values of x and 0, 0.0056, 0.008, and 0.01

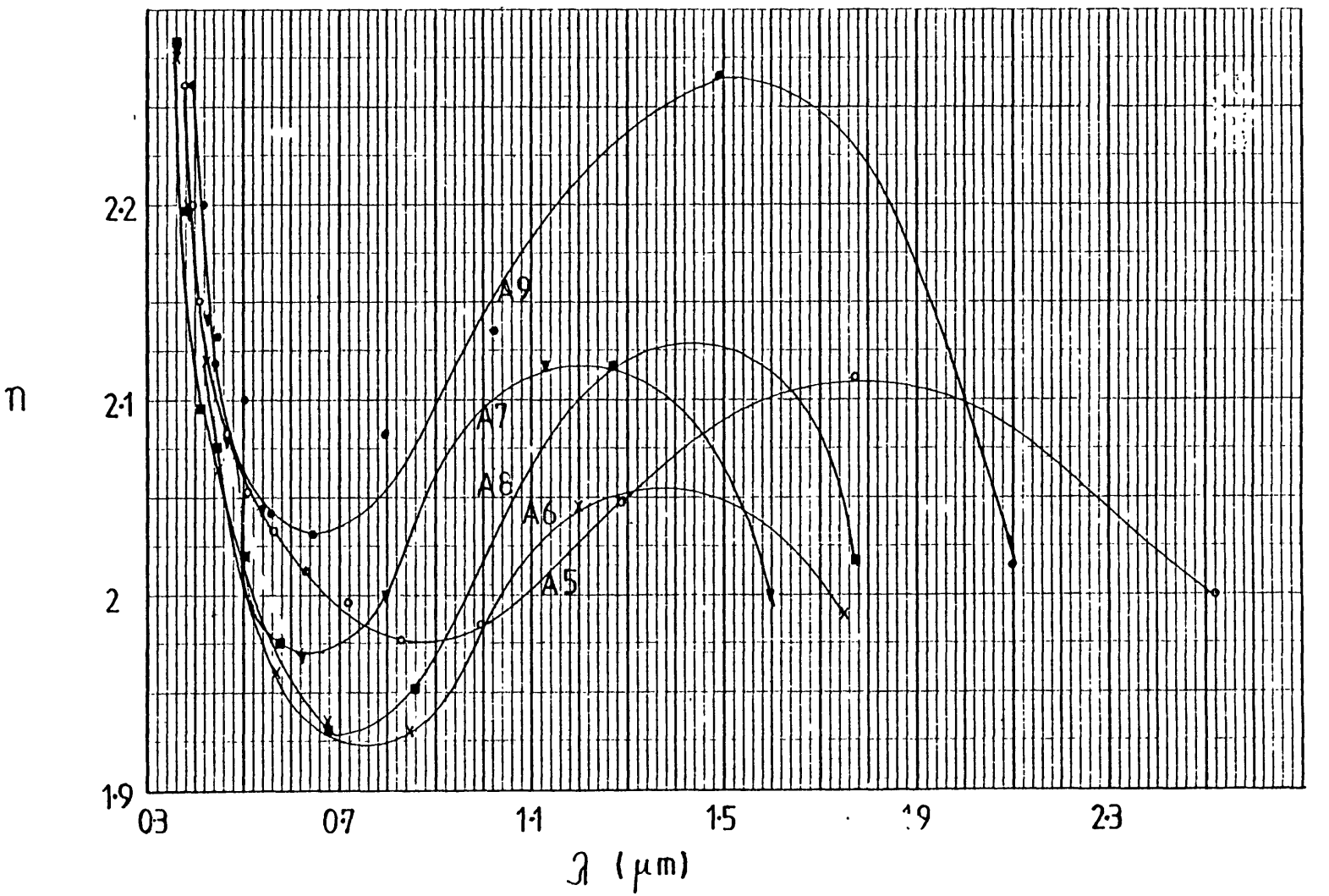

Fig. 3.1.23 : Real part of refractive index vs wavelength of the films A5, A6, A7, A8 and A9 (see table 3.1.1). The corresponding values of x are 0.013, 0.019, 0.034, 0.05 and 0.55.

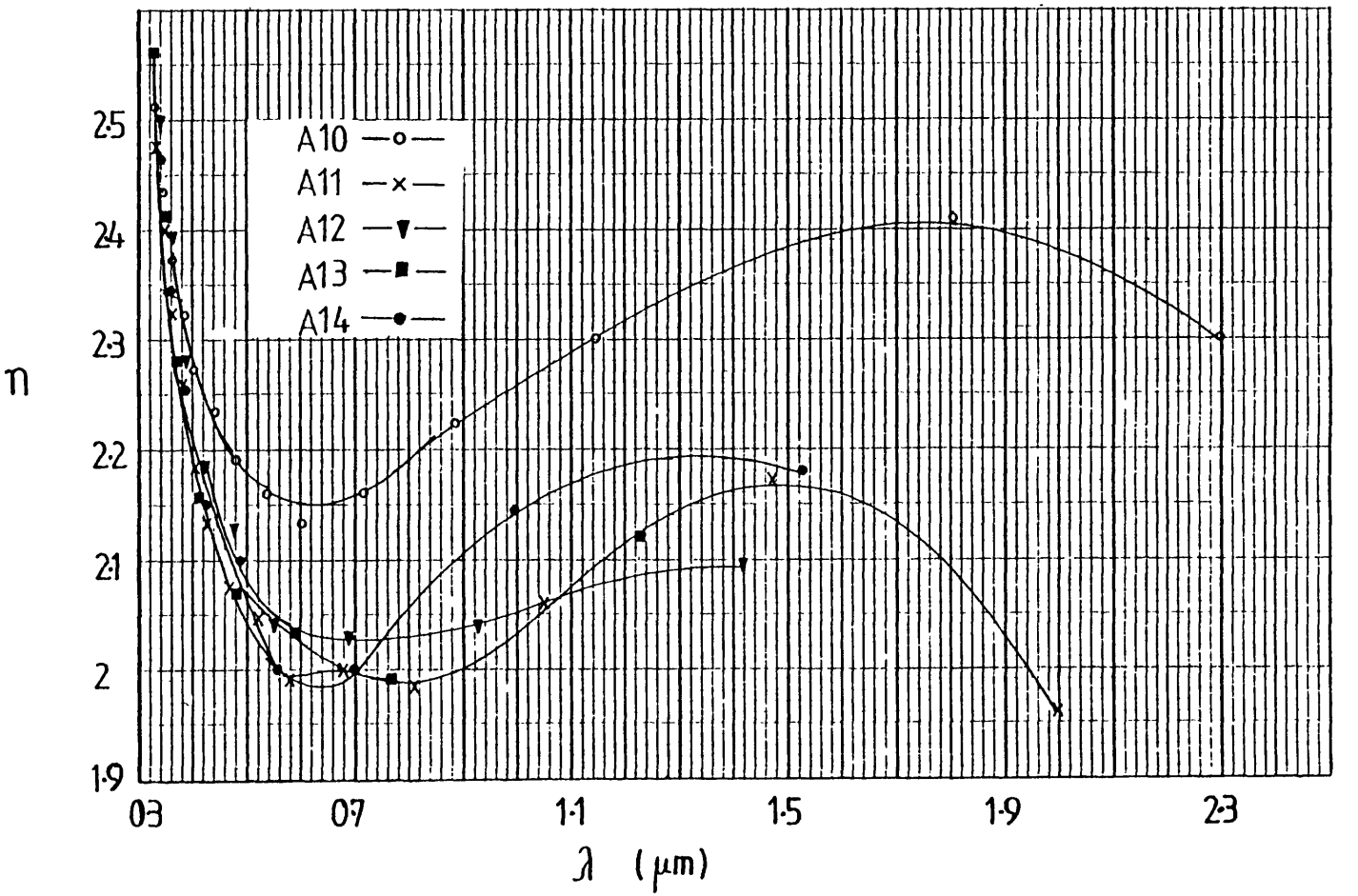

Fig. 3.1.24 : Real part of the refractive index vs wavelength of the films A10, A11, A12, A13 and A14, (see table 3.1.1). The corresponding values of x are 0.072, 0.082, 0.084, 0.095 and 0.11.

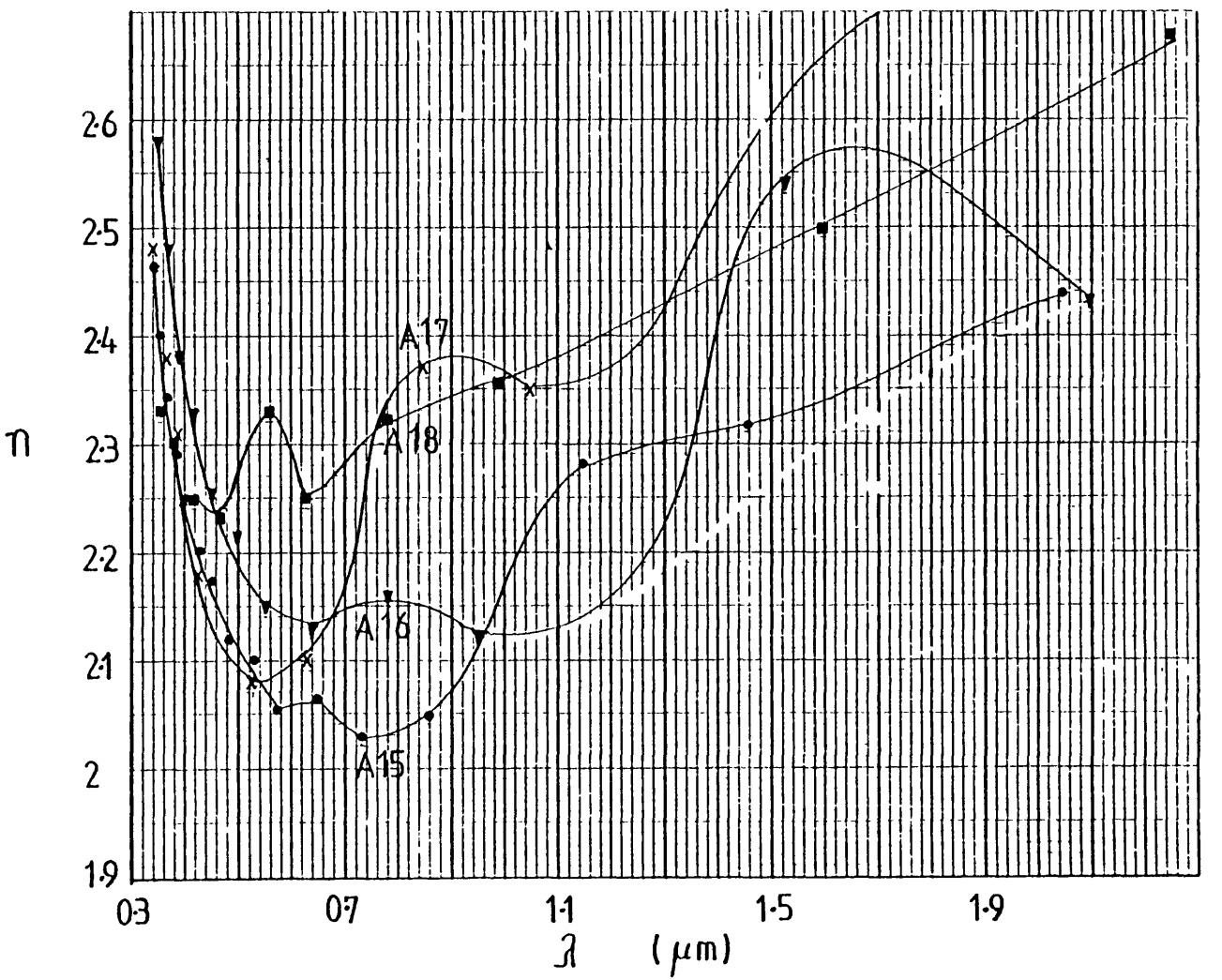

Fig. 3.1.25 : Real part of the refractive index vs wavelength of the fims A15, A16, A17 and A18, (see table 3.1.1). The corresponding values of x are 0.12, 0.14, 0.22 and x > 0.22.

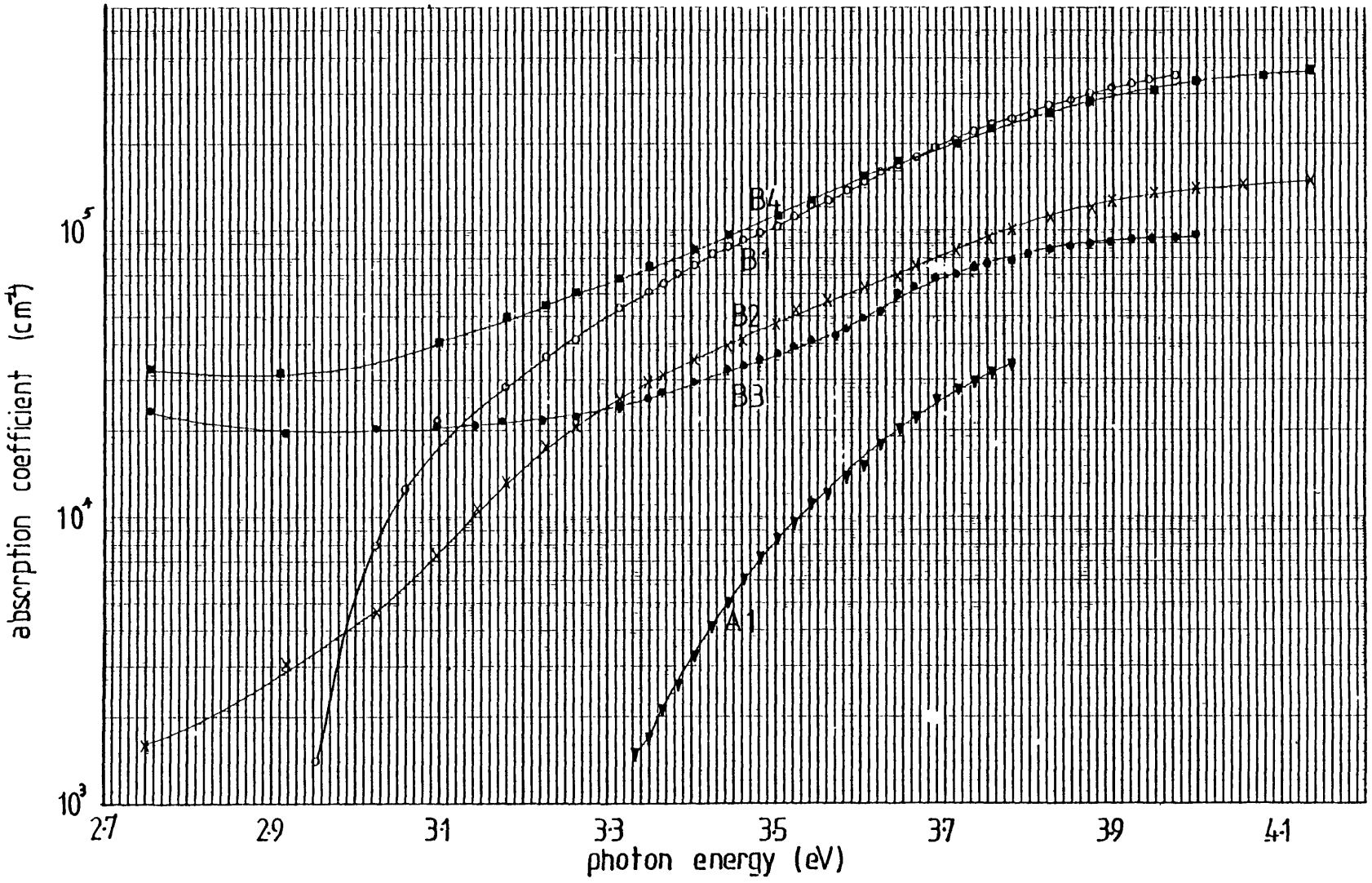

Fig. 3.1.26: Absorption coefficient vs photon energy of the films B1, B2, B3 and B4, (see table 3.1.2). The absorption coefficient of the film A1 is included for comparison.

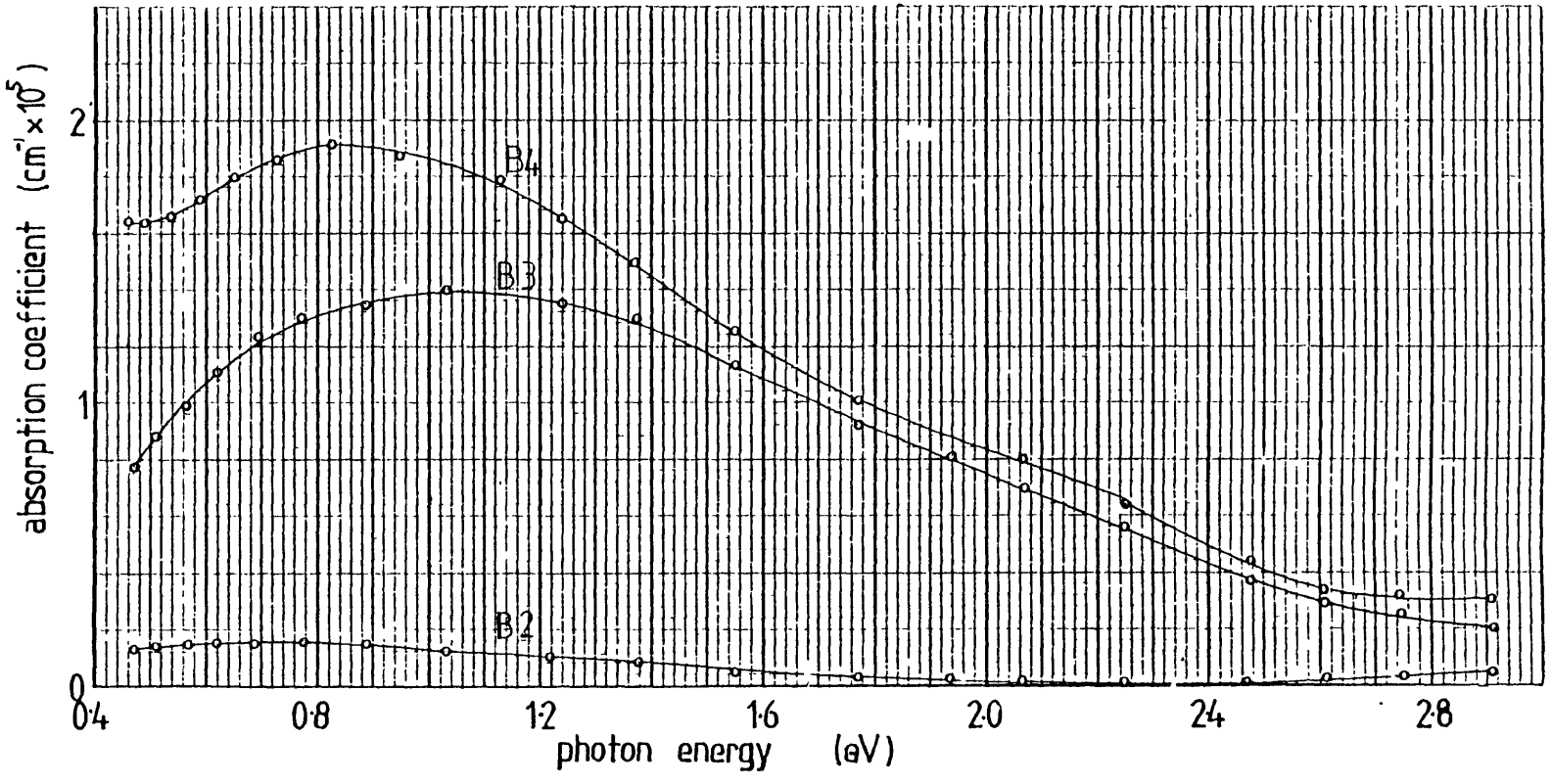

Fig. 3.1.27: Absorption coefficient vs photon energy of the films B2, B3 and B4, (see table 3.1.2)

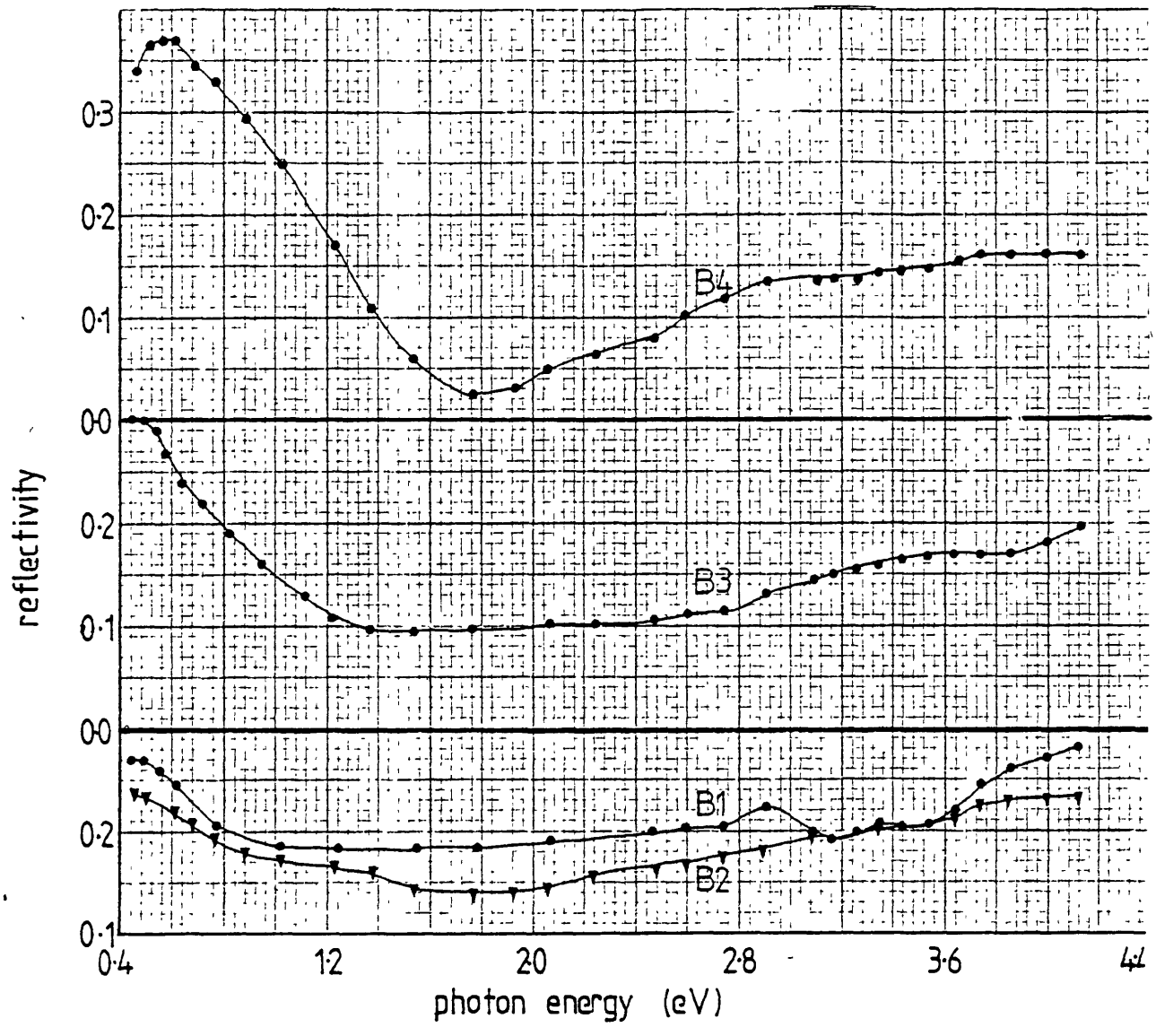

Fig. 3.1.28 : Reflectivity vs photon energy of the films B1, B2, B3 and B4 (see table 3.1.2)

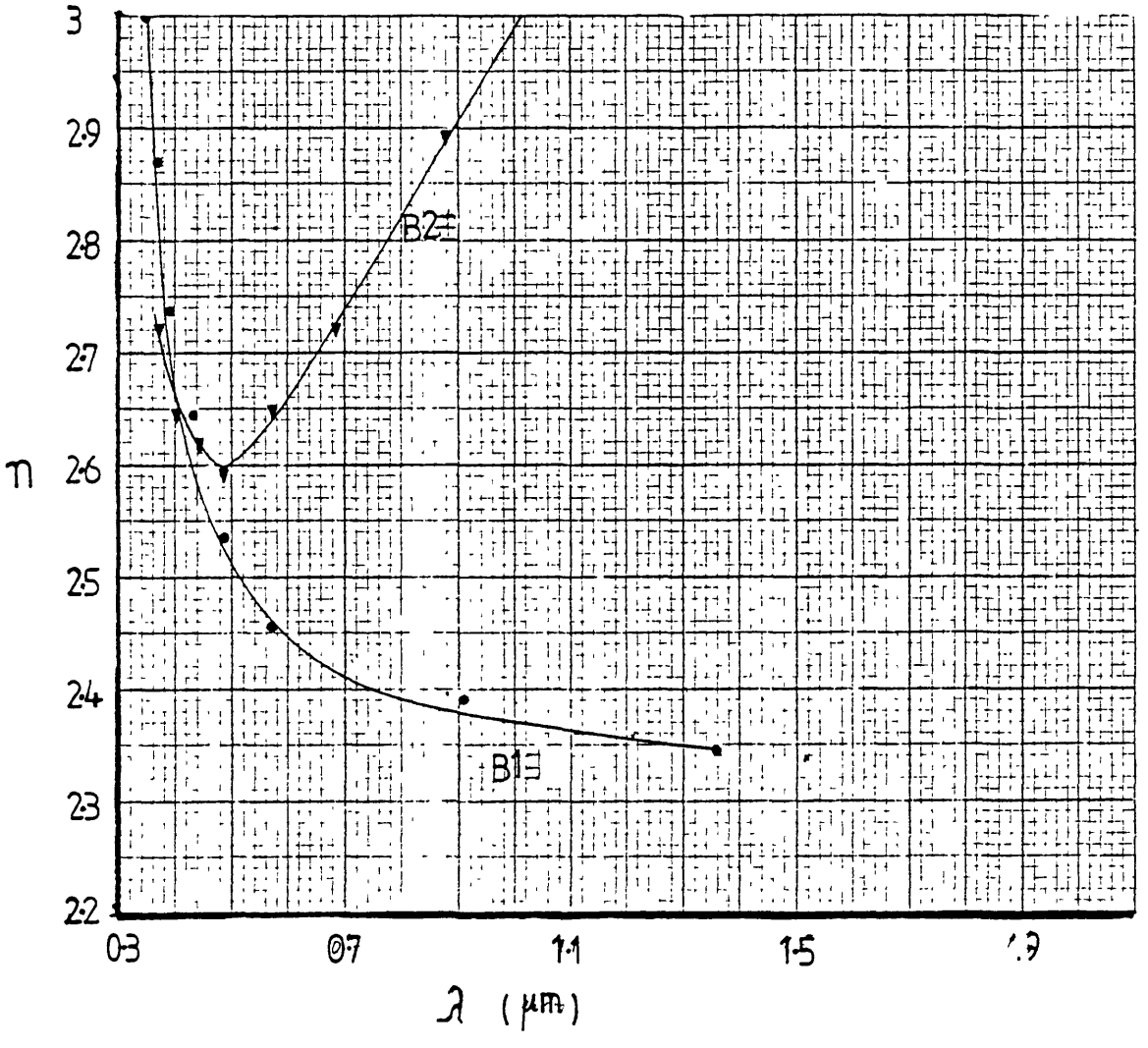

Fig 3.1.29 : Real part of the refractive index vs wavelength of the films B1 and B2 (see table 3.1.2)

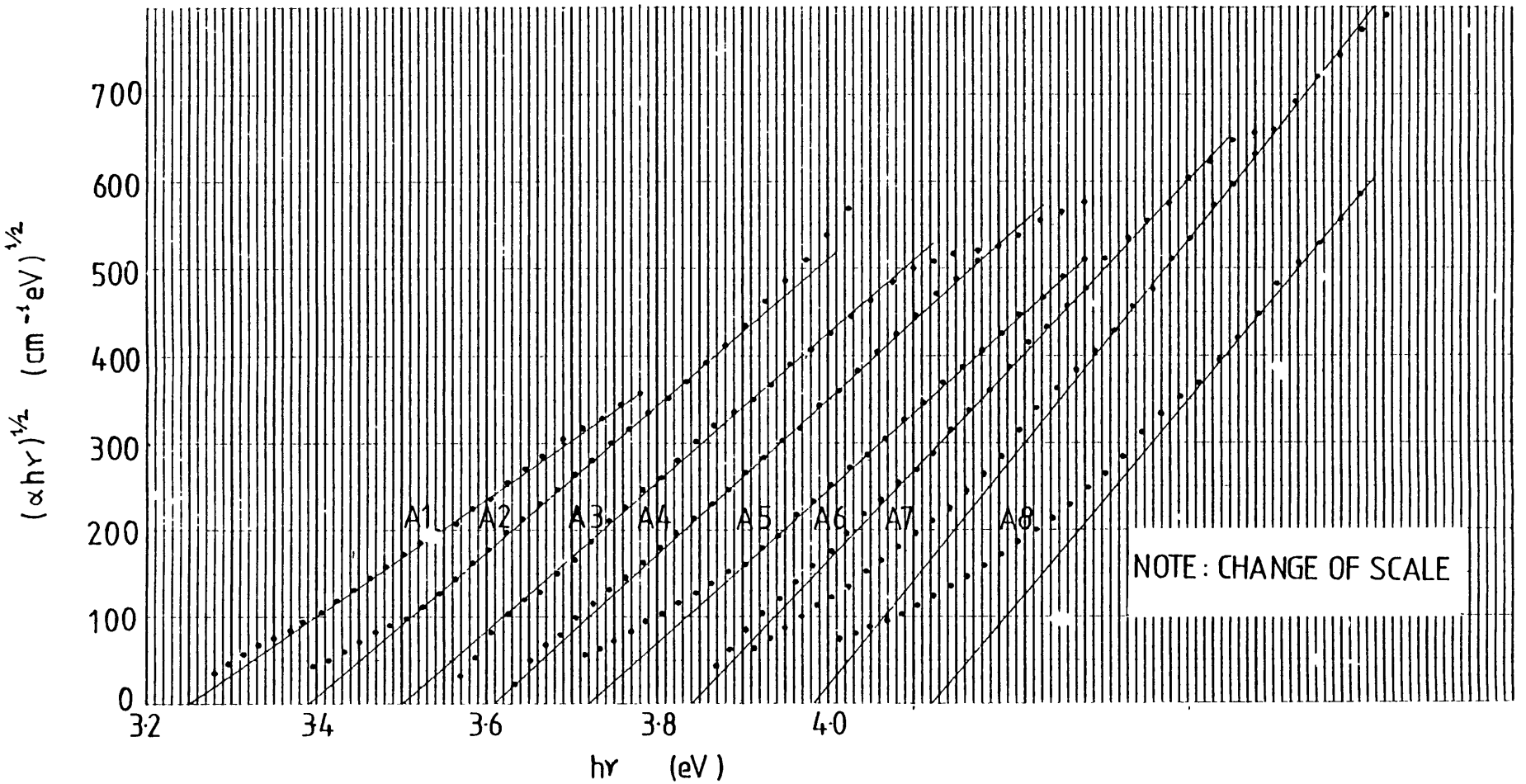

Fig. 3.1.30 : $(\alpha h\nu)^{\frac{1}{2}}$ vs photon energy of the films A1, A2, A3, A4, A5, A6, A7 and A8 (see table 3.1.1). The corresponding values of x are 0, 0.0056, 0.008, 0.01, 0.013, 0.019, 0.034 and 0.05. The energy scale is shifted by 0.1 eV to the right for every film after A1

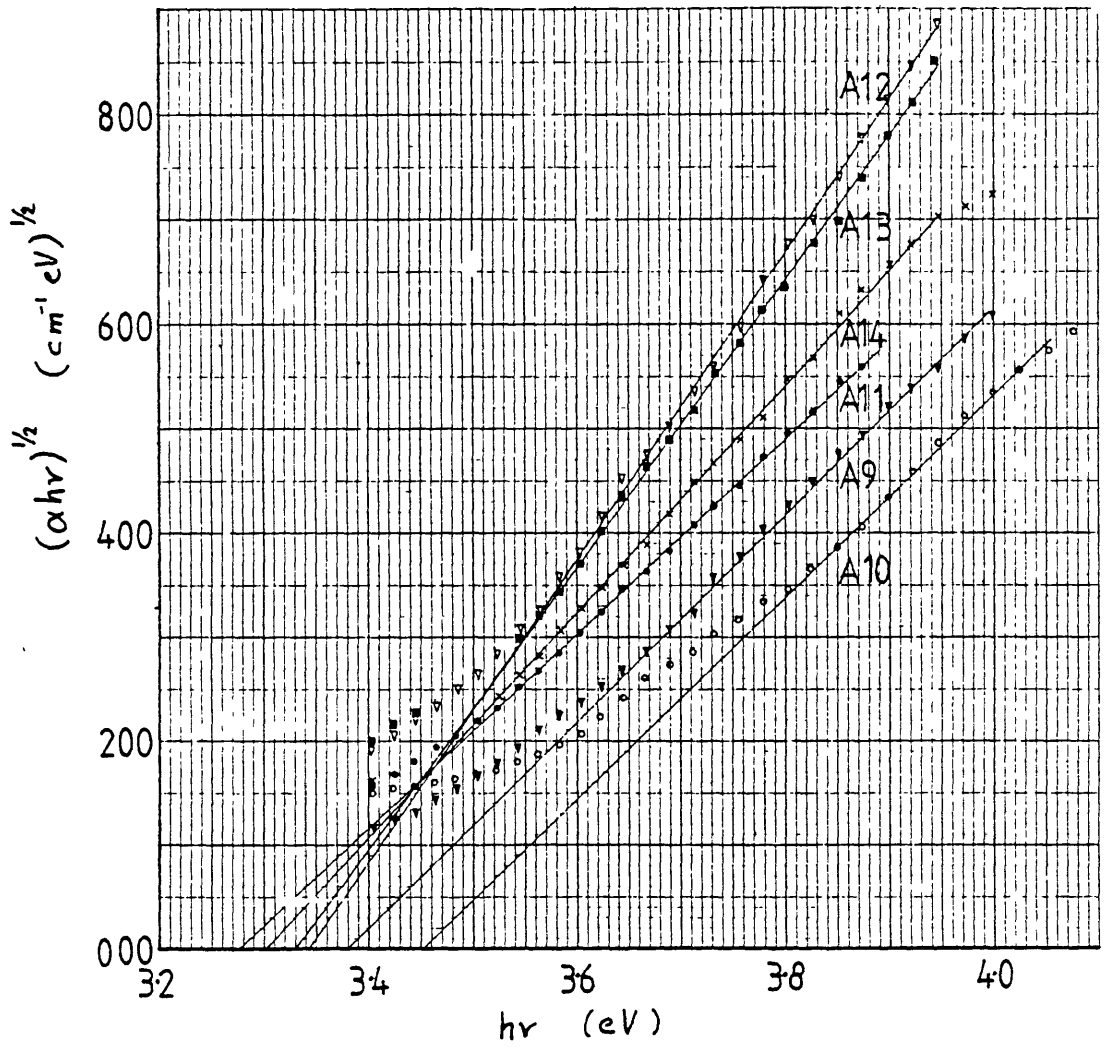

Fig. 3.1.31 : $(\alpha h\nu)^{\frac{1}{2}}$ vs photon energy of the films A9, A10, A11, A12, A13 and A14 (see table 3.1.1). The corresponding values of x are 0.055, 0.072, 0.082, 0.084, 0.095 and 0.11

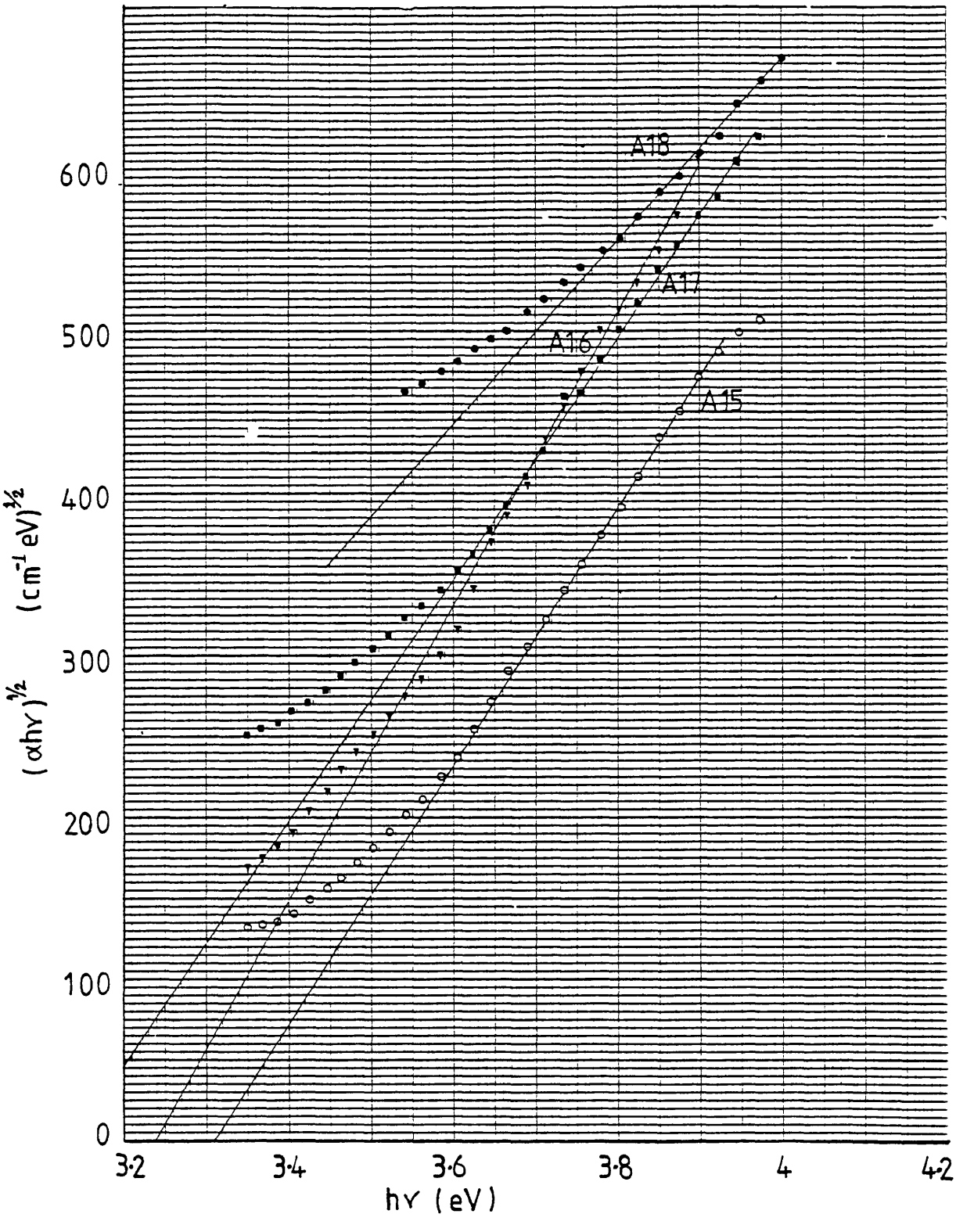

Fig. 3.1.32 : $(\alpha h\nu)^{\frac{1}{2}}$ vs photon energy of the films A15, A16, A17 and A18 (see table 3.1.1). The corresponding values of x are 0.12, 0.14, 0.22 and x > 0.22

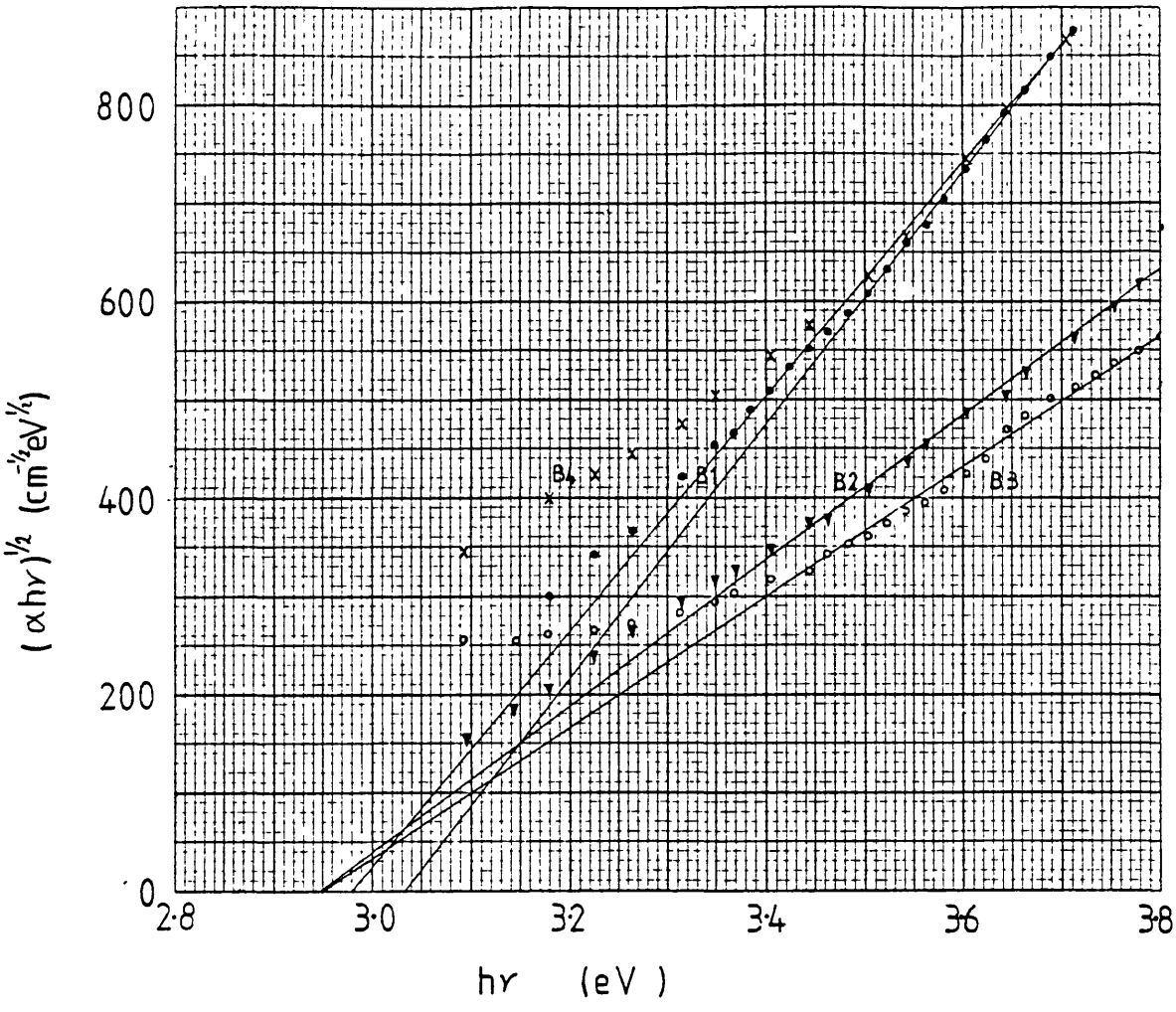

Fig. 3.1.33 : $(\alpha h\nu)^{\frac{1}{2}}$ vs photon energy of the films B1, B2, B3 and B4 (see table 3.1.2)

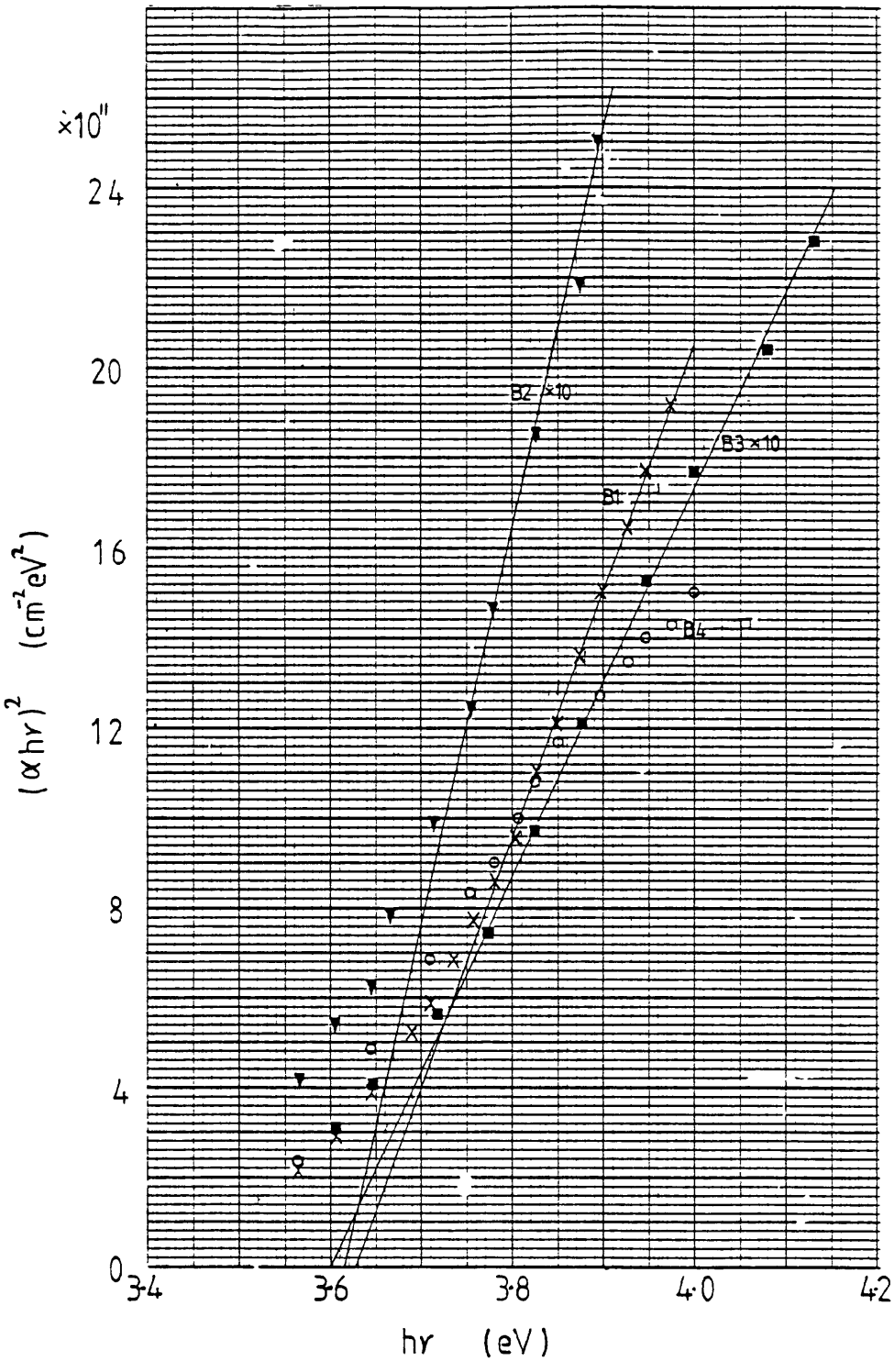

Fig. 3.1.34 : $(\alpha h\nu)^2$ vs photon energy of the films B1, B2, B3 and B4 (table 3.1.2). $(\alpha h\nu)^2$ of films B2 and B3 is multiplied by 10

Table 3.1.3

The material constants E_0, A and $\frac{d\log \alpha}{dh\nu}$ defined in the text as obtained from the optical measurements.

Film N°	x	E_0(eV)	A($cm^{-1}eV^{-1}$)	$\left(\frac{d \log \alpha}{dh\nu}\right)$ (eV^{-1})
A1	0	3.25	4.53×10^5	12.82
A2	0.0056	3.29	7×10^5	7.75
A3	0.008	3.30	7.22×10^5	6.896
A4	0.01	3.31	7.93×10^5	6.06
A5	0.013	3.32	7.73×10^5	5.61
A6	0.019	3.34	1.07×10^6	5.263
A7	0.034	3.385	1.48×10^6	4.273
A8	0.05	3.42	1.36×10^6	3.861
A9	0.055	3.38	9.92×10^5	3.226
A10	0.072	3.452	9.35×10^5	1.118
A11	0.082	3.278	8.83×10^5	2.932
A12	0.084	3.345	2.17×10^6	2.864
A13	0.095	3.33	1.87×10^6	2.543
A14	0.11	3.302	1.18×10^6	2.9
A15	0.12	3.31	6.4×10^5	2.18
A16	0.14	3.24	8.3×10^5	1.814
A17	0.22	3.14	5.6×10^5	1.145
A18	>0.22	2.82	3.2×10^5	-
B1	0	3.036	1.68×10^6	1.908
B2	~0.05	2.948	5.5×10^5	1.51
B3	~0.1	2.952	4.46×10^5	0.957
B4	~0.2	2.98	1.43×10^6	1.137

Table 3.1.4

The material constants B, E_d defined in the text as obtained from the optical measurements

Film	x	E_d(eV)	B(cm^{-1} $eV^{\frac{1}{2}}$)
B1	0	3.63	2.35×10^6
B2	~ 0.05	3.615	2.98×10^6
B3	~ 0.1	3.6	2.08×10^6
B4	~ 0.2	-	-

3.2 Electrical measurements

3.2.1 Experimental thechnique

The d.c. resistivity and the thermoelectric power of the sodium tungsten bronze films was measured using the apparatus shown in Fig.3.2.1.

The copper blocks could be heated with electrical heaters up to 500°K and cooled down to 200°K via the copper rod which was immersed in liquid nitrogen. Blocks 2 and 3 could also be kept at different temperatures by varying the current passing through the heaters. For thermoelectric power measurements, the specimen slide was placed across the gap of blocks 2 and 3 so that a temperature gradient of several degrees was mentioned between the ends of the film. For conductivity measurements only block 2 was used, so that the film was kept at a uniform temperature. In order to ensure good thermal contact between the specimen slide and the copper blocks a thin layer of ZnO paste was spread between them.

The whole apparatus was inside a vacuum chamber which could be evacuated to 10^{-3} Torr.

Temperature measurements were carried out by Cromel-Alumel thermocouples which were glued onto the slide with silver "dag".

Resistance and voltage measurements were made with a Keithley 616 electrometer.

The WO_3 and Na_xWO_3 films were evaporated on silica slides and electrical contacts were made using either evaporated thin metal films (Al or Cr) or silver "dag" . The resistivity values obtained were found to be independent of the nature of the contacts as well as the method of measurement. Both the four probe [7,8] and two probe methods were used

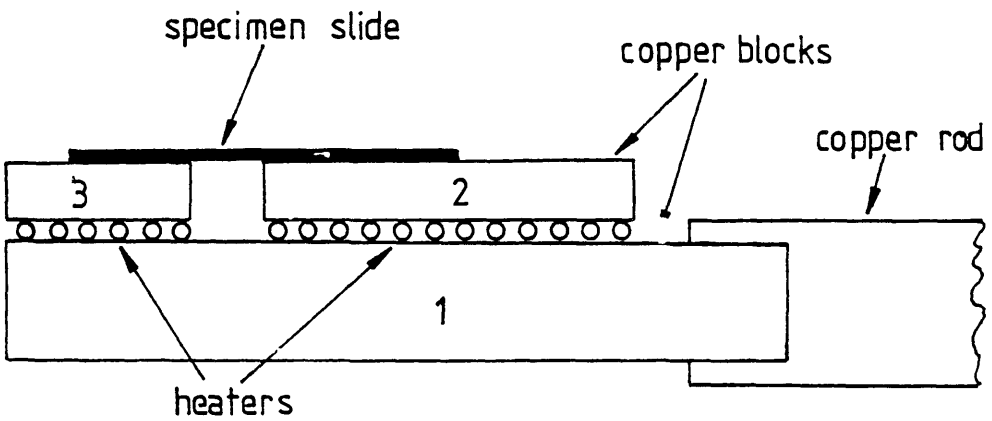

(a)

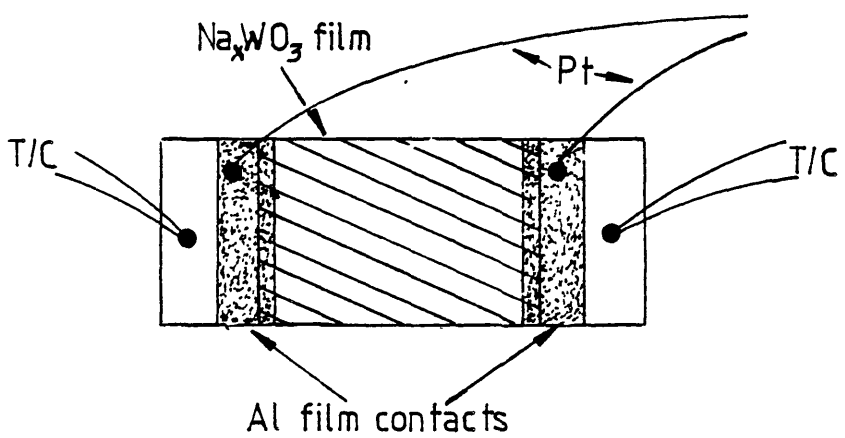

(b)

Fig. 3.2.1 : (a) Apparatus used for the electrical measurements of Na_xWO_3 films, showing the position of the specimen slide relative to the copper blocks of the heaters for the thermo-electric power measurements. The size of the gap between blocks 2 and 3 is 5mm.
(b) Arrangement of the electrodes and thermocouples on the specimen slide.

to measure the room temperature resistivity of several WO_3 and Na_xWO_3 films and it was found that their results were identical within experimental error. Therefore, the two probe method was adopted and the experimental arrangement is shown in Fig. 3.2.1b.

3.2.2 Resistivity measurements

The resistivity of the Na_xWO_3 films was found to be thermally activated over the range of x-values investigated, i.e. from zero to 0.22. The magnitude of the resistivity as well as its activation energy were found to depend on :

a) the partial water vapour pressure during evaporation

b) any subsequent heat treatment of the film

c) the mean grain size of the film and

d) the sodium concentration of the film.

The effect of the partial water vapour pressure on the resistivity of the films can be seen in Fig. 3.2.2. . Curve (a) shows the temperature dependence of the resistivity of the 50Å m.g.s. WO_3 film A1 which was prepared with liquid nitrogen in the water vapour trap. Curve (b) shows the temperature dependence of the resistivity of the 50Å m.g.s. . WO_3 film A21 which was prepared without any liquid nitrogen in the water vapour trap.

The 50Å m.g.s. Na_xWO_3 films exhibit changes in the magnitude of the resistivity and the activation energy when heated above 70°C. Fig. 3.2.2 shows the effect of heat treatment on the resistivity of film A21. Curve (c) shows the temperature dependence of the resistivity of film A21 after it had been heated at 170°C in vacuum of 10^{-3} Torr for 15 minutes. The changes in the resistivity and activation energy can be partly reversed by heating the film in air. Curve (d) of Fig. 3.2.2 shows the resistivity of the film A21 after it had been heated at 170°C in air for 10 minutes. On the other hand, heat treatment of 50Å m.g.s. Na_xWO_3 films either in air or in vacuum results in irreversible changes of the resistivity and the activation energy, to larger values, accompanied by partial bleaching of the films. Fig. 3.2.3 shows the temperature

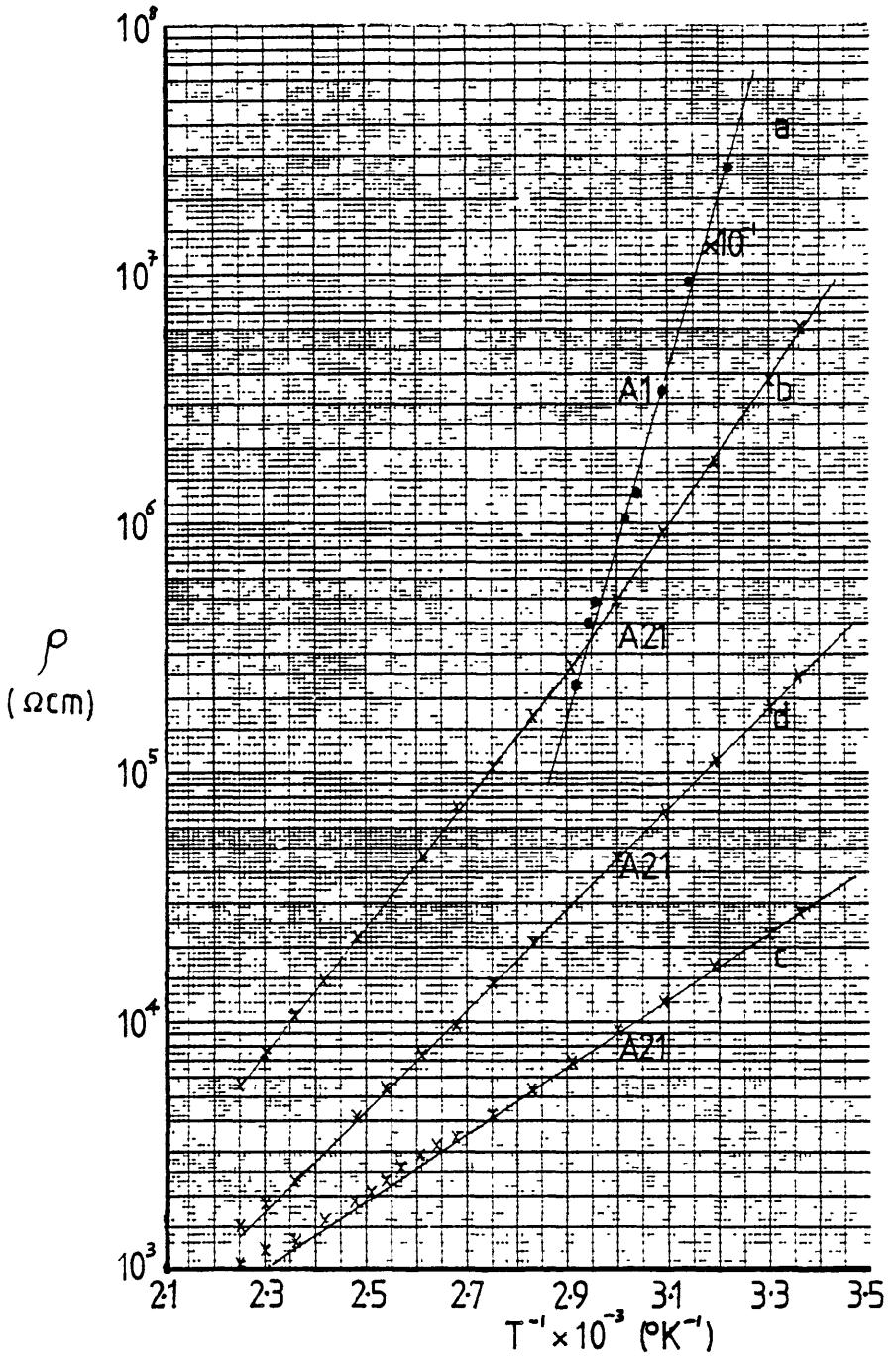

Fig. 3.2.2: Resistivity vs inverse absolute temperature of WO_3 films A1 and A2 (see Table 3.2.1). (a) Film A1, $\times 10^{-1}$ denotes that all resistivity values have been multiplied by 10^{-1} (b) Film A21 of Table 3.2.1 (c) Film A21 after it has been heated at 170°C for 15min in vaccum (d) Film A21 after is has been heated in air at 170°C for 10 min.

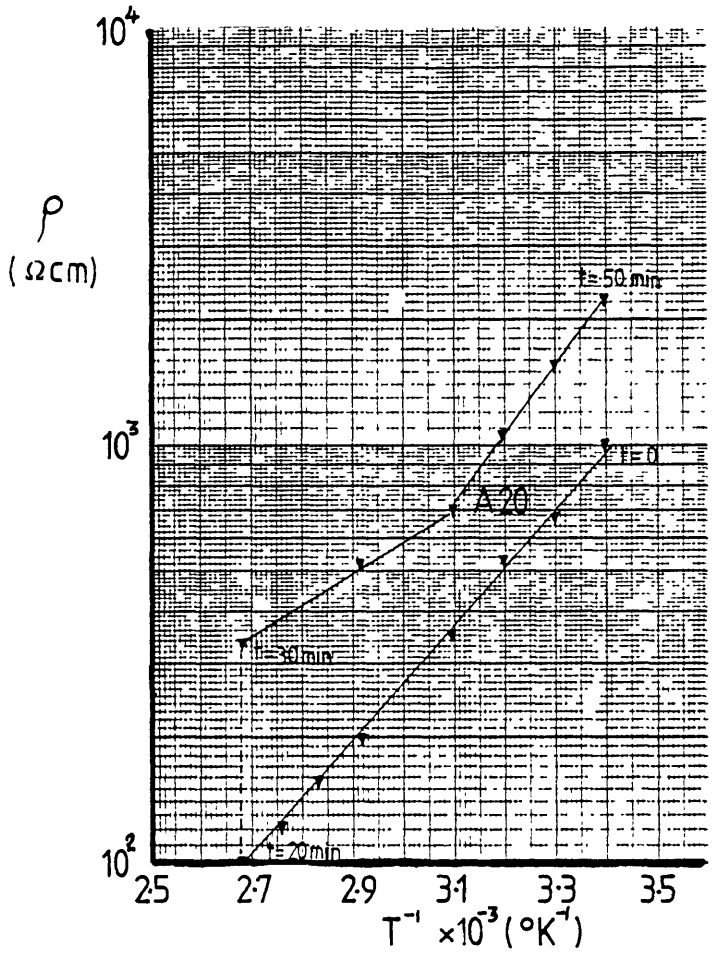

Fig. 3.2.3 : Resistivity vs inverse absolute temperature of Na_xWO_3 film A20 (see Table 3.2.1) as a function of heating time, in air.

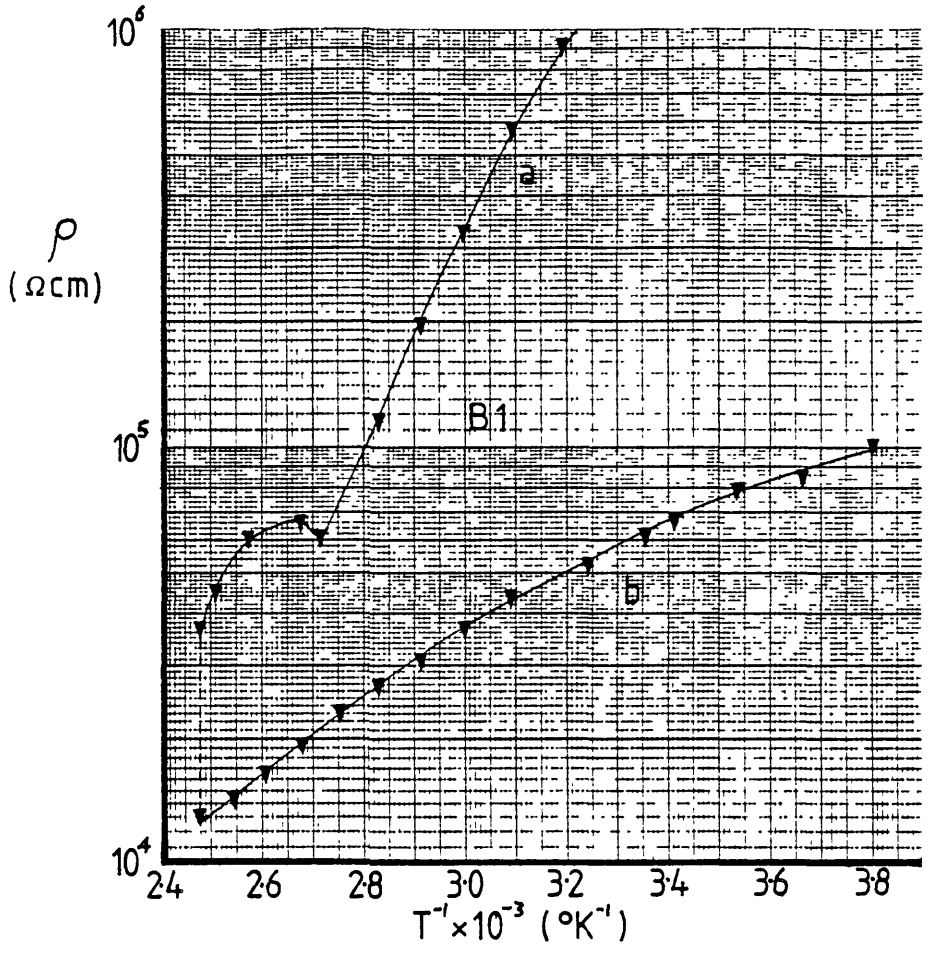

Fig. 3.2.4 : Resitivity vs inverse absolute temperature of WO_3 film B1 (see Table 3.2.2). Measurements performed in vaccum of 10^{-3} Torr.

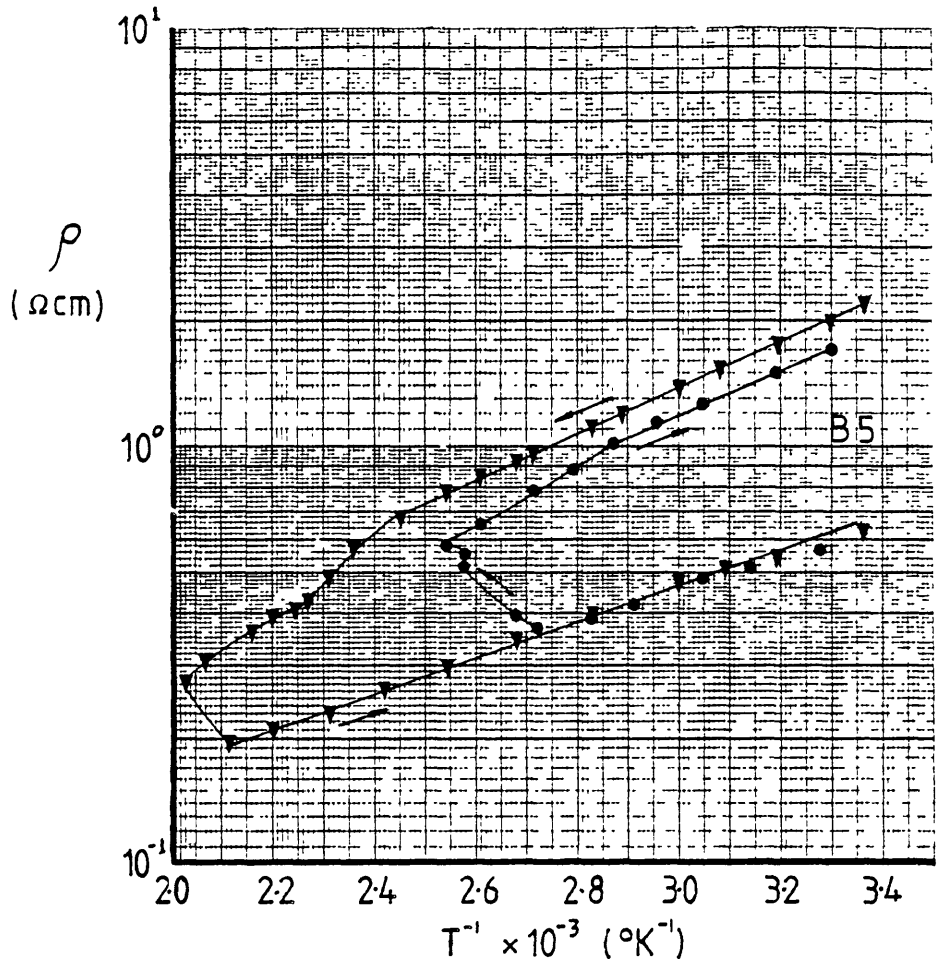

Fig. 3.2.5 : Resistivity vs inverse absolute temperature of Na_xWO_3 film B5 (see Table 3.2.2).
-▼- measurements performed in vaccum of 10^{-3}Torr
-●- measurements performed in air
Arrows indicate the direction of temperature change.

dependence of the resistivity of the 50Å m.g.s. $Na_{0.08}WO_3$ film (A20) heated in air.

In the case of the 2-3μm m.g.s. WO_3 films the effect of the heat treatment is less pronounced than in the case of the 50Å m.g.s. films, see Fig. 3.2.4. Moreover, heat treatment in air of the Na_xWO_3 films with 2-3μm m.g.s. particularly reverses the effects on the resistivity of the heat treatment in vacuum, see Fig. 3.2.5.

In order to investigate the effect of the sodium concentration on the resistivity and the activation energy, the temperature dependence of the resistivity of several small m.g.s. Na_xWO_3 films was measured. All these films were prepared by the co-evaporation method as described in section 2.1.2. Prior to the measurement of their resistivity in vacuum of 10^{-3}Torr, they have been exposed to air for several days. Their temperature was never raised above 60°C in order to avoid any rapid outdiffusion of sodium. The x-value, thickness, substrate temperature and m.g.s. of these films are shown in table 3.2.1. The temperature dependence of their resistivity is shown in Fig. 3.2.6 to Fig. 3.2.9.

Resistivity measurements were also performed on 2-3μm m.g.s. Na_xWO_3 films. These films were prepared by diffusing sodium ions into anealed WO_3 films as described in section 2.1.2. Their thickness, x-value and conditions of preparations are shown in table 3.2.2. The temperature dependence of their resistivity is shown in Fig. 3.2.10.

As can be seen from Fig. 3.2.6 to Fig. 3.2.10 the resistivity of all the films in the high temperature regime changes with temeprature according to the relation

$$\rho = \rho_0 \; e^{\frac{E_A}{kT}} \qquad (3.2.1)$$

where :-

ρ_0, is a constant for each film;

E_A, is the thermal activation energy;

T , is the absolute temperature;

k , is the Boltjmann's constant.

At lower temperatures the experimental values of the resistivity deviate from the relation (3.2.1).

The resistivity values at 303°K as well as the thermal activation energies of all the films are given in table 3.2.3.

Table 3.2.1

Thickness, x-value, substrate temperature and mean grain size of the Na_xWO_3 films prepared by the co-evaporation method, used for electrical measurements

Film†	d(μ)	x	substrate temperature °C	m.g.s Å°
A1	0.78	0	60	50
A2	0.5	5.6×10^{-3}	60	50
A4	0.53	0.01	60	50
A6	0.44	0.019	60	50
A7	0.4	0.034	60	50
A8	0.44	0.05	60	50
A9	0.48	0.055	60	50
A11	0.51	0.082	60	50
A12	0.34	0.084	300	120
A13	0.29	0.095	60	50
A14	0.35	0.11	60	50
A15	0.63	0.12	60	50
A16	0.45	0.14	60	50
A17	0.45	0.22	300	50
A18	0.42	> 0.22	300	120
A19	0.34	0.009	60	50
A20	0.76	0.08	60	50
A21*	0.8	0	60	50

† the numbers used are the same as those in table 3.1.1 and they represent the same films

* A21 was prepared without liquid nitrogen in the water vapour trap

Table 3.2.2

Thickness, x-value and annealing conditions of the large grain films (2-3μm) used in electrical measurements.

Film†	d(μm)	x*	annealing conditions
B1	0.24	0	T_a = 500°C t_a = 20 hours in dry N_2
B2	0.38	~ 0.05	T_a = 500°C t_a = 4 hours in dry N_2
B3	0.45	~0.01	T_a = 500°C t_a = 4 hours in dry N_2
B5	0.52	?	T_a = 500°C t_a = 4 hours in dry N_2

* The x-values were not obtained by direct measurement. See section 3.1.2.

† The numbers used are the same as those in table 3.1.2 and they represent the same films

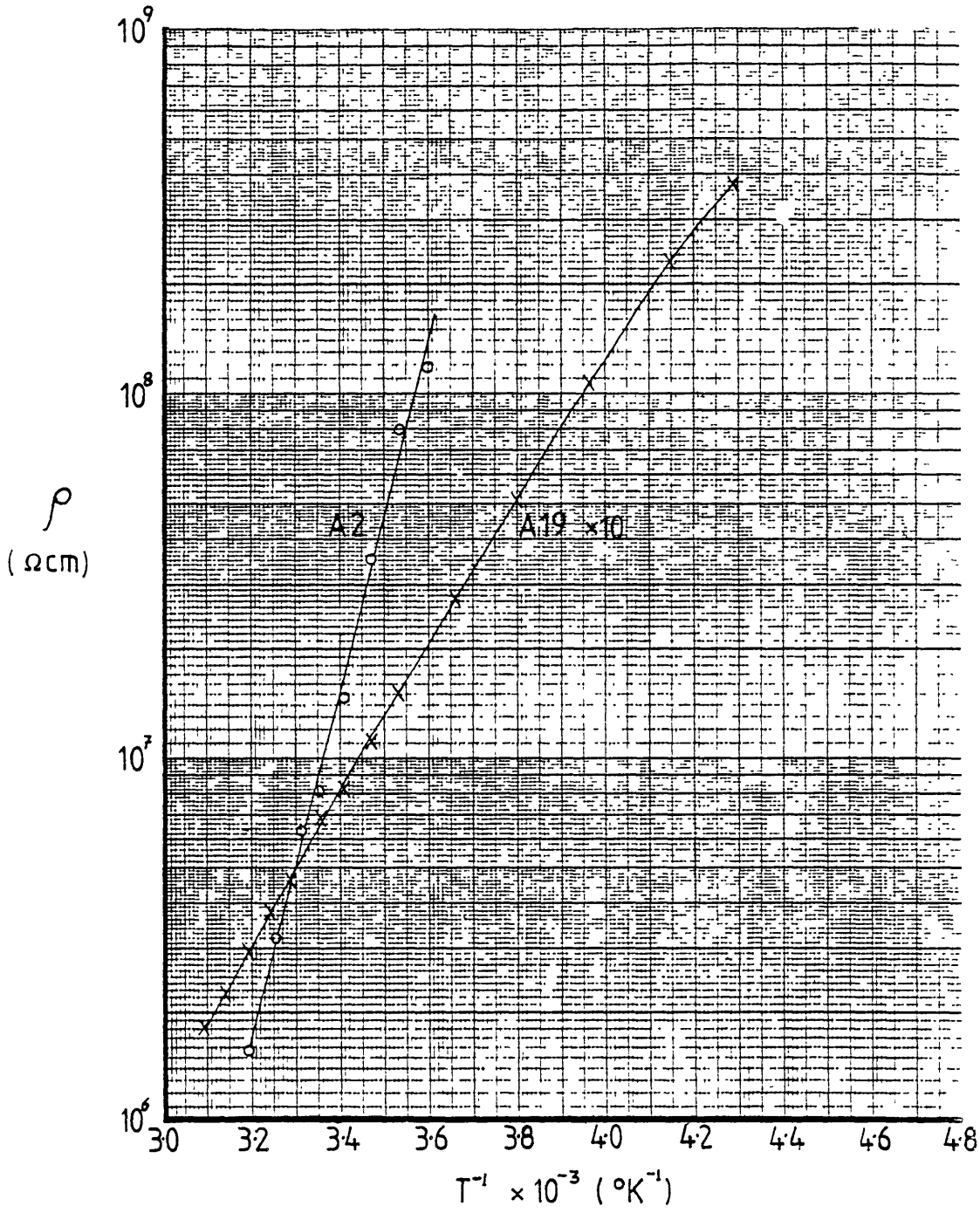

Fig. 3.2.6 : Resistivity vs inverse absolute temperature of Na_xWO_3 films A2 ($x=5.6\times10^{-3}$) and A19 ($x=9\ 10^{-3}$) of Table 3.2.1. ×10 denotes that ρ is multiplied by 10.

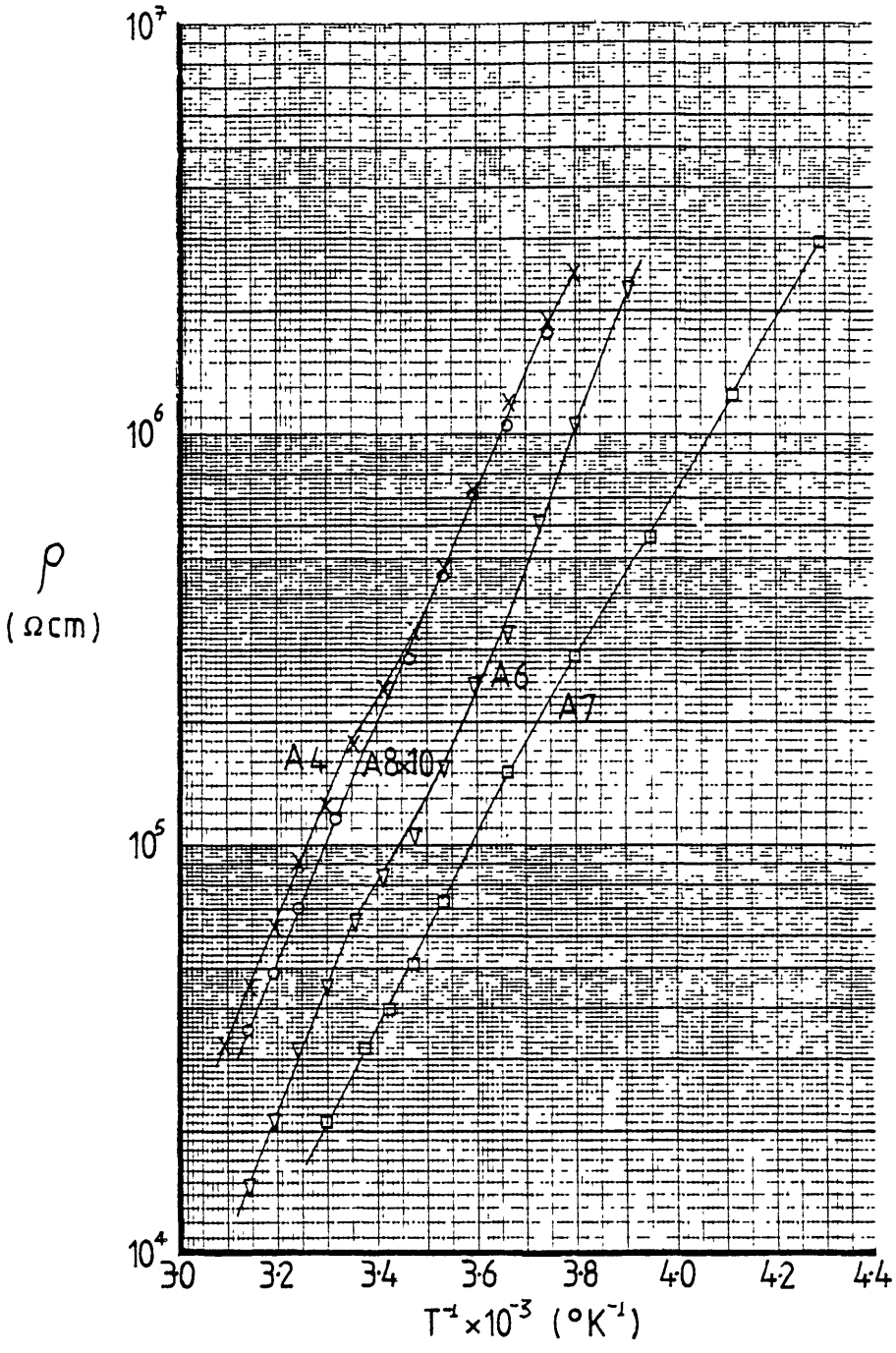

Fig. 3.2.7 : Resistivity vs inverse absolute temperature of Na_xWO_3 films A4(x00.01), A6(x=0.019), A7(x=0.034) and A8(x=0.05) of Table 3.21. Values of ρ of film A8 are multiplied by 10

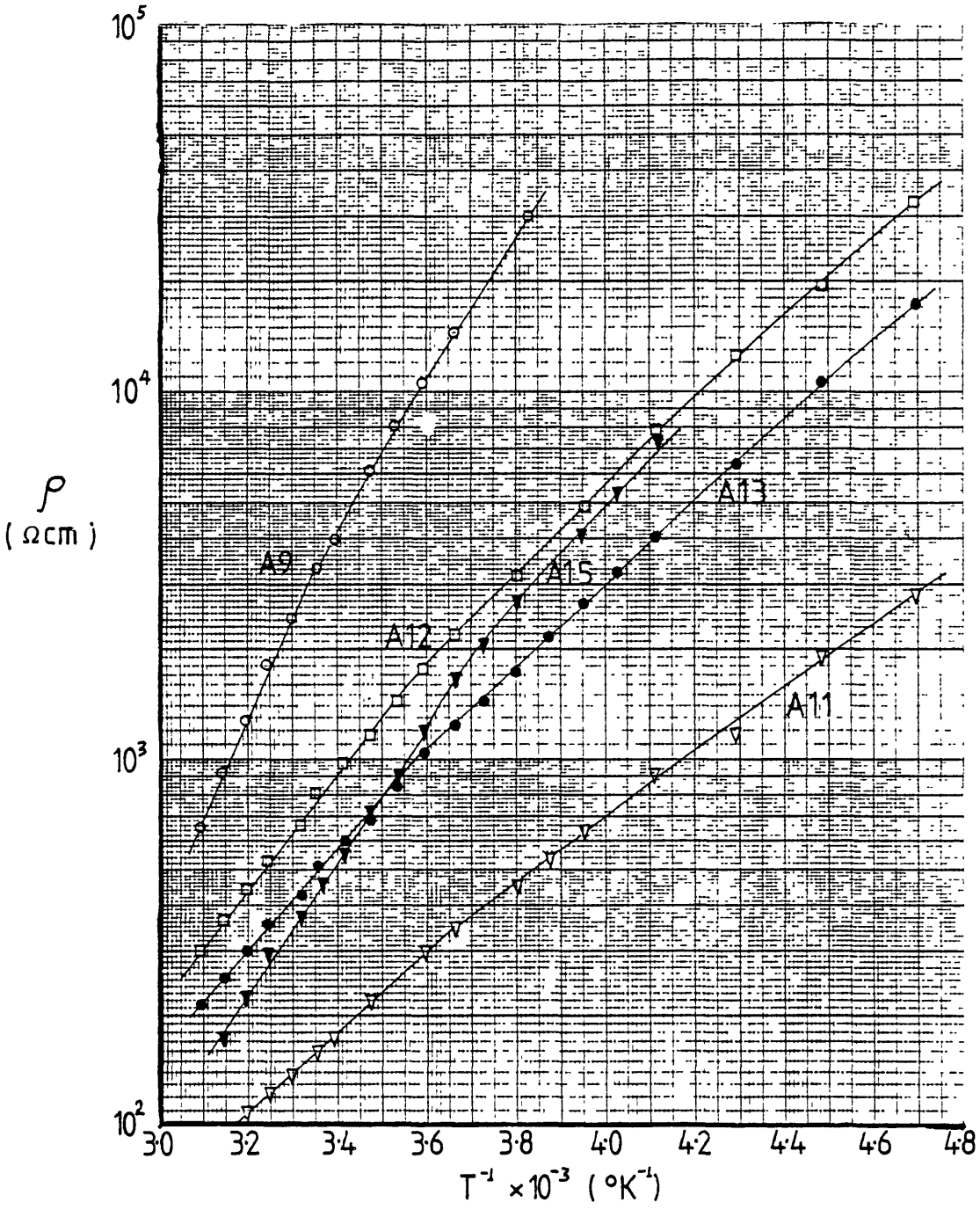

Fig. 3.2.8 : Resistivity vs inverse absolute temperature of Na_xWO_3 films A9(x=0.055), A11(x=0.082), A12(x=0.094), A13(x=0.095) and A15(x=0.12) of Table 3.2.1.

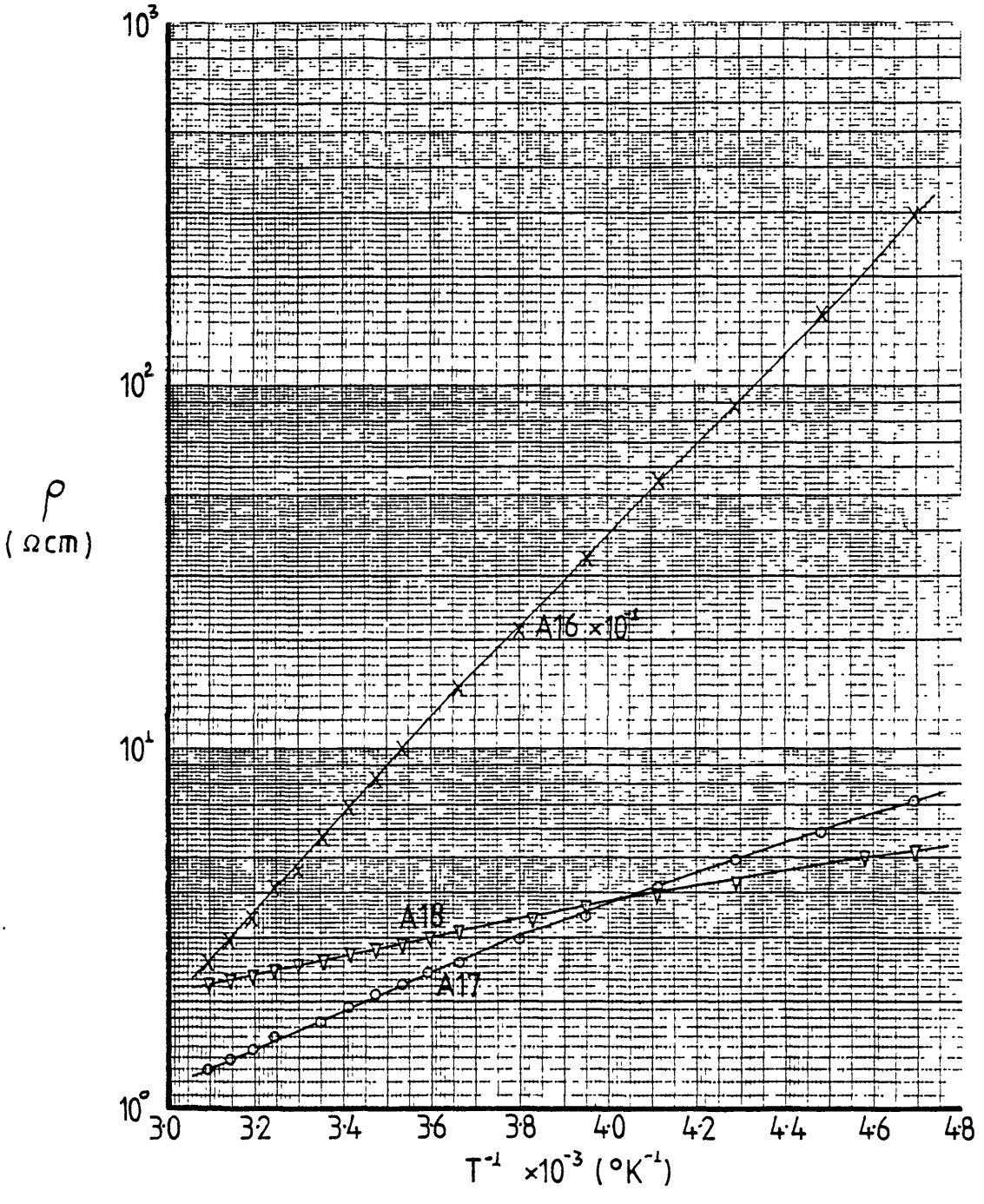

Fig. 3.2.9 : Resistivity vs inverse absolute temperature of Na_xWO_3 films A16(x=0.14), A17(x=0.22) and A18(x>0.22) of Table 3.2.1 ρ of film A16 is multiplied by 10^{-1}.

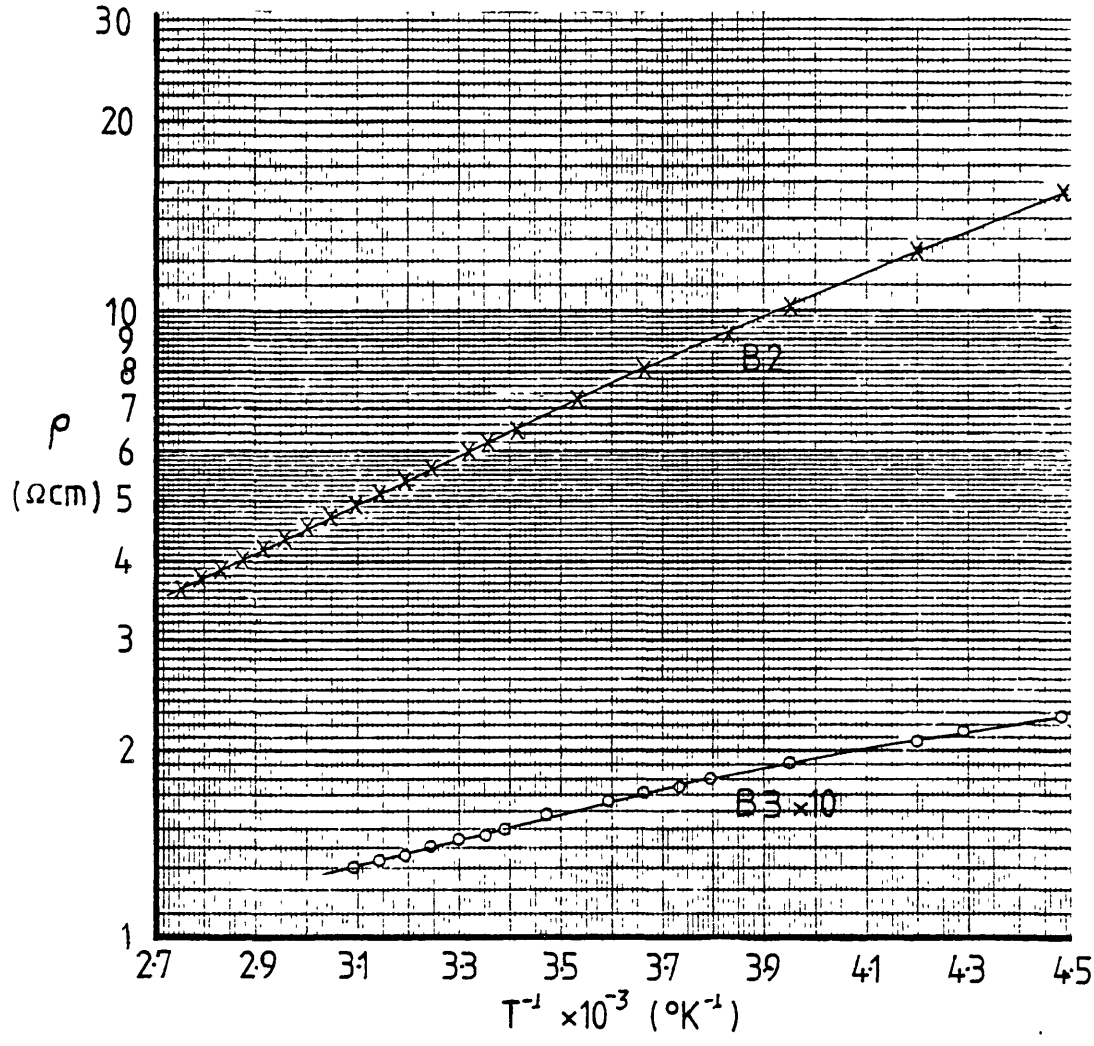

Fig 3.2.10 : Resistivity vs inverse absolute temperature of Na_xWO_3 films B2(x~0.05) and B3(x~0.1) of Table 3.2.2. ρ of film B3 is multiplied by 10

Table 3.2.3

Resistivity at 303°K and thermal activation energy of the Na_xWO_3 films of tables 3.2.1 and 3.2.2.

Film	x	$\rho_{303°K}(\Omega cm)$	$E_A(eV)$
A1	0	1×10^{9}	1.4
A2	5.6×10^{-3}	5×10^{6}	0.94
A4	1×10^{-2}	1.25×10^{5}	0.6
A6	1.9×10^{-2}	4.6×10^{4}	0.6
A7	3.4×10^{-2}	2.1×10^{4}	0.465
A8	5×10^{-2}	9.4×10^{3}	0.59
A9	5.5×10^{-2}	2.4×10^{3}	0.542
A11	8.2×10^{-2}	1.4×10^{2}	0.22
A12	8.4×10^{-2}	6.2×10^{2}	0.32
A13	9.5×10^{-2}	4.1×10^{2}	0.29
A15	1.2×10^{-1}	3.4×10^{2}	0.353
A16	1.4×10^{-1}	48	0.264
A17	2.2×10^{-1}	1.65	0.105
A18	> 0.22	2.5	0.054
A19	0.009	5×10^{5}	0.4
A20	0.08	7×10^{2}	0.27
A21	0	4×10^{6}	0.57
B1	0	1.4×10^{6}	0.366
B2	~ 0.05	5.9	0.076
B3	~ 0.1	0.14	0.041
B5	?	2	0.107

3.2.3 Thermoelectric power measurements

The thermoelectric power measurements have been taken using the apparatus described in section 3.2.1. The Na_xWO_3 films used were some of the films of tables 3.2.1 and 3.2.2.

The accuracy of the measurements was approximately 10 - 20% : this was mainly due to fluctuations in the voltage measurement with the Keithley electrometer, which were caused by the electrical noise picked up by the sample during measurements and instabilities of the temperature gradient across the sample.

The values of the Seebeck coefficient at 300°K for different films is shown in table 3.2.4.

The temperature dependence of the Seebeck coefficient of some of the films is shown in Fig. 3.2.11 and Fig. 3.2.12.

Table 3.2.4

Seebeck coefficient of Na_xWO_3 films at 300° K.

Film	x	S(μvK^{-1})
A19	9×10^{-3}	- 550±60
A9	5.5×10^{-2}	- 212±24
A11	8.2×10^{-2}	- 100±10
A12	8.4×10^{-2}	- 185±10
A14	1.1×10^{-1}	- 120±7
A15	1.2×10^{-1}	- 72±8
A17	2.2×10^{-1}	- 20±2
A18	> 0.22	- 25±2
B2	~ 0.05	- 76±3
B3	~ 0.1	- 20±2

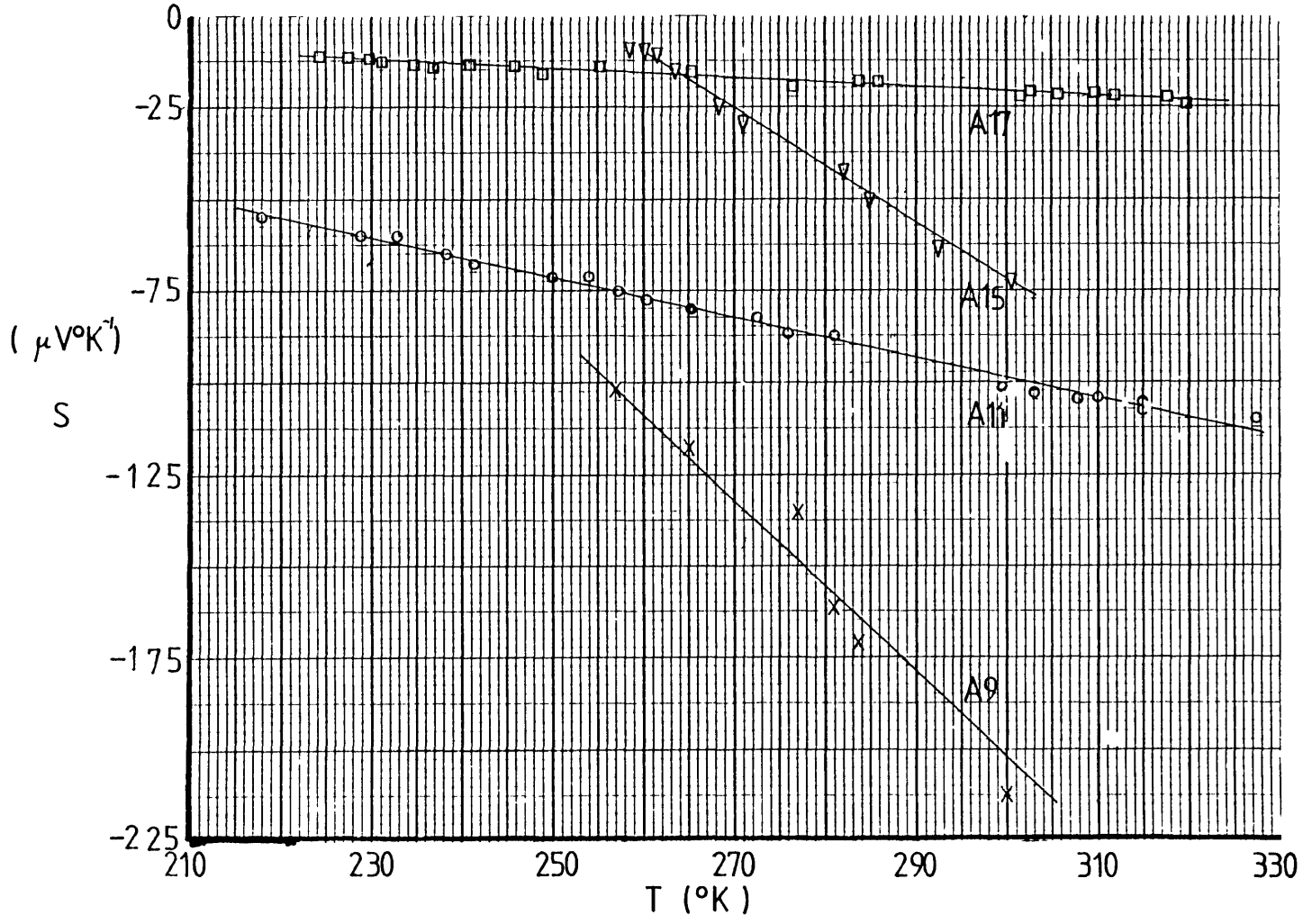

Fig. 3.2.11 : Seebeck coefficient vs absolute temperature of Na_xWO_3 films A9(x=0.055), A11(x=0.082), A15(x=0.12) and A17(x=0.22) of Table 3.2.1.

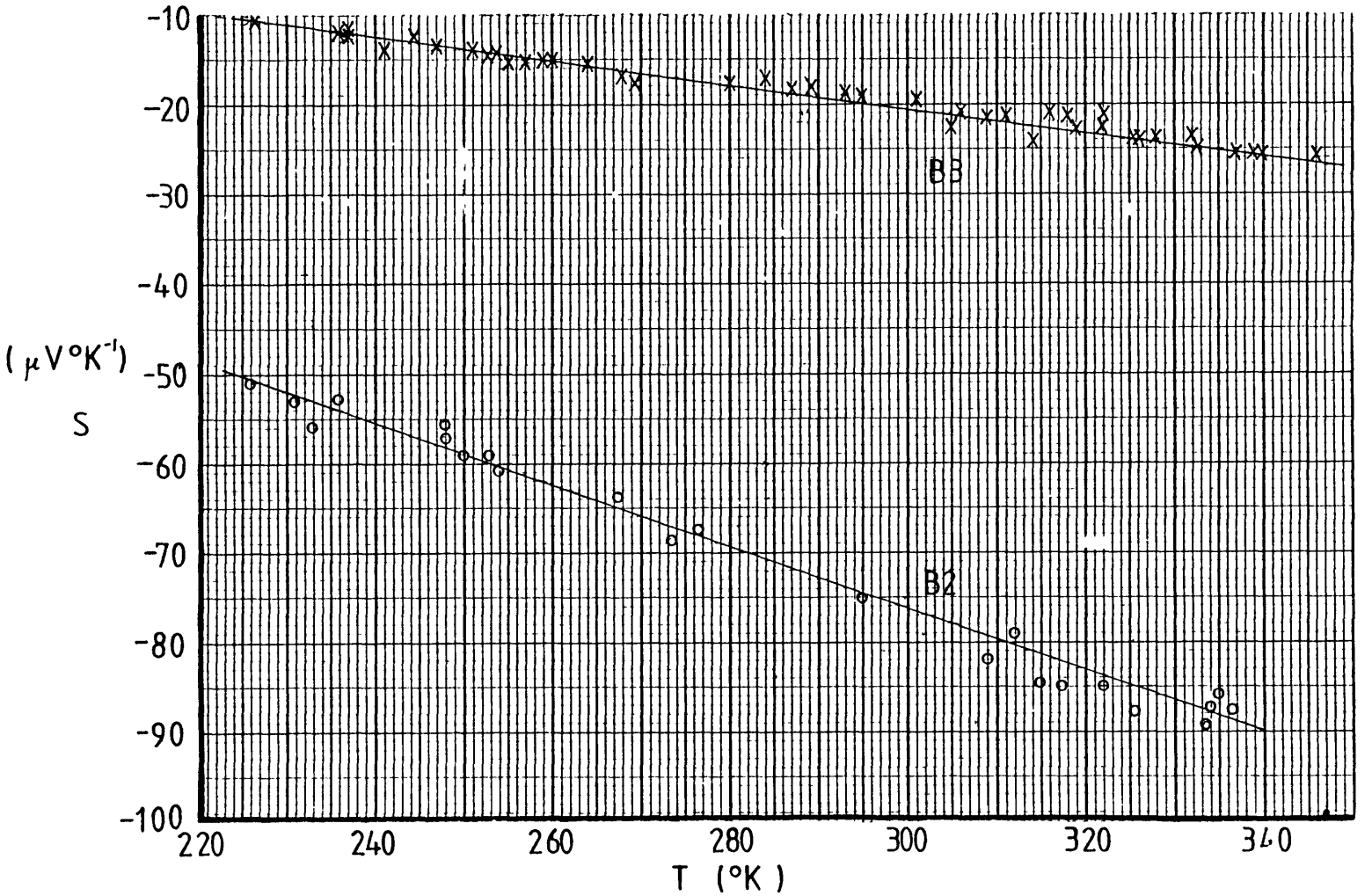

Fig. 3.2.12 : Seebeck coefficient vs absolute temperature of Na_xWO_3 films B2 (x~0.05) and B3(x~0.1) of Table 3.2.2.

APPENDIX 1

List of programme used in the calculation of the absorption coefficient, $\alpha(h\nu)$, from equ. (3.1.10).

```
 1 DIML 170 ,TC 170 ,GC 170 ,T 170 ,P 170 ,PC 170 ,E 170 ,A 170
 2 OPEN1,4
 5 PRINT"□"
 6 DATA.3,.302,.304,.306,.308,.310,.312,.314,.316,.318,.320,.322,.324,.326,.328
 8 DATA.330,.332,.334,.336,.338,.340,.342,.344,.346,.348
 10 DATA.35,.352,.354,.356,.358,.36,.362,.364,.366,.368,.37,.372,.374,.376,.378
 20 DATA.38,.382,.384,.386,.388,.39,.392,.394,.396,.398,.4,.405,.41,.415,.42,.42
5
 30 DATA.43,.435,.44,.445,.45,.455,.46,.465,.47,.475,.48,.485,.49,.495,.5
 40 DATA.51,.52,.53,.54,.55,.56,.57,.58,.59,.6,.62,.64,.66,.68,.7,.72,.74,.76,.7
8
 50 DATA.8,.82,.84,.86,.88,.9,.92,.94,.96,.98,1.1.025,1.05,1.075,1.1,1.125,1.15
 60 DATA1.175,1.2,1.225,1.25,1.275,1.3,1.325,1.35,1.375,1.4,1.425,1.45,1.475
 70 DATA1.5,1.525,1.55,1.575,1.6,1.625,1.65,1.675,1.7,1.725,1.75,1.775,1.8
 80 DATA1.825,1.85,1.875,1.9,1.925,1.95,1.975,2,2.025,2.05,2.075,2.1,2.125
 100 DATA2.15,2.175,2.2,2.225,2.25,2.275,2.3,2.325,2.35,2.375,2.4,2.425,2.45
 110 DATA2.475,2.5,2.525,2.55,2.575 2.6,2.625,2.65,2.675,2.7
 200 FORI=1TO169 TC I)=1 NEXT
 290 FORI=1TO169 READL I NEXT
 293 FORI=1TO72 GC I)=0 NEXT
 294 FORI=73TO102 GC I)=0 NEXT
 295 FORI=103TO169 GC I)=0 NEXT
 300 INPUT"FILM THICKNESS (MICRONS)",D
 390 I=1
 410 PRINT"LAMBDA("I")="L I
 415 GETA$ IFA$=""THEN415
 416 IFA$="U"THENI=I+1 PRINT GOTO410
 417 IFA$="D"THENI=I-1 PRINT GOTO410
 418 IFA$="P"THEN500
 420 PRINT"P("I")=" INPUT"□■■■■■■■(",P(I)
 430 PRINT"T("I")=" INPUT"□■■■■■■■(",T(I)
 435 PRINT PRINT I=I+1
 440 GOTO410
 500 INPUT"□INDEX OF ALPHA",N1
 502 FORI=1TO170
 510 IFP(I)=0THEN560
 515 PC(I)=R(I)*TC(I)-GC(I)
 520 E(I)=1.239854/L(I)
 530 C=T(I)/(1-PC(I))/(1-PC(I))
 535 B=LOG((1+SQR(1+4*C*C*PC(I)*PC(I)))/2/C)
 536 A(I)=B/D
 540 A(I)=A(I)/2/D*1E4
 560 NEXTI
 590 PRINT
 595 PRINT#1,"" PRINT#1,""
 600 PRINT"E EV  ALPHA("N1")  (AHF)^"N1
 605 PRINT#1,"E EV          ALPHA("N1")          (AHF)^"N1
 610 PRINT"_____ __________ _____"
 615 PRINT#1,"----- ---------- ---------"
 620 FORI=1TO170
 625 IFP(I)=0THEN640
 627 C=1.2399
 628 IFA(I)<0THENA(I)=-A(I) A=-1
 630 IFA=<0THENPPRINTINT(E(I)*1E4)/1E4,INT(A(I)*N1),INT((A(I)*2/L(I))*N1*100)/100
 632 IFA>0THENPPRINTINT(E(I)*1E4)/1E4,INT(A(I)*N1),INT((A(I)*2/L(I))*N1*10)/10" -
"
 635 IFA=<0THENPPRINT#1,INT(E(I)*1E4)/1E4,INT(A(I)*N1),INT((A(I)*2/L(I))*N1*10)/1
0
 637 IFA>0THENPPRINT#1,INT(E(I)*1E4)/1E4,INT(A(I)*N1),INT((A(I)*2/L(I))*N1*10)/10
" _"
 639 A=0
 640 NEXTI
 650 GETA$ IFA$=""THEN650
 660 IFA$="N"THENCLP GOTO1
 670 IFA$="P"THEN500
 680 IFA$="E"THENEND
 690 IFA$="D"THEN1000
 700 END
 1000 PRINT"FILM THICKNESS (MICRONS)"D
 1001 PRINT#1,"FILM THICKNESS (MICRONS)"D
 1002 PRINT"□LAMBDA MICRONS      P        T"
 1003 PRINT#1,   "LAMBDA MICRONS      P        T"
 1005 PRINT"--------------      -        -
 1006 PRINT#1,"--------------      -        -
 1010 FORI=1TO145
 1015 IFR(I)=0THEN1040
 1020 PRINTL(I),P(I),T(I)
 1030 PRINT#1,L(I),P(I),T(I)
 1040 NEXTI
 1050 GOTO500
```

References

[1] Handbook of Chemistry and Physics, CRC Press, 60^{th} edition, p. E387(1980)

[2] H.E. Bennett and J.H. Bennett, Physics of Thin Films, 4, 1(1967)

[3] S. Sharma, D.K. Pandye, H.K. Sehgal and K.L. Chopra Thin Solid Films, 62, 97(1079)

[4] T.S. Moss, "Optical properties of seniconductors" Pub. Butterworths (1961)

[5] J.T. Pankove, "Optical processes in semiconductors" Dover Publications Inc. (1971)

[6] P.G. Dickens, R.M.P. Quilliam and M.S. Whittingham Mat. Res. Bull., 3, 941(1968)

[7] L.J. van de Pauw, Philips, Res. Repts., 13, 1(1958)

[8] E. Hesse, Solid State Electronics, 21, 637,(1978)

CHAPTER 4

DISCUSSION OF THE OPTICAL AND ELECTRICAL PROPERTIES OF $Na_x WO_3$ FILMS

4.1 Optical properties

4.1.1 Introduction

It has already been shown in chapter 2 that the "as evaporated" WO_3 films are polycrystalline with grains of approximatelly 50Å in average linear dimensions with grain boundaries of perhaps 8 to 10Å thickness.

Measurements of the sodium diffusion into the films [1] are consistant with the model that the grains are small crystallites with the bulk WO_3 density, while the grain boundary regions have a much smaller effective density (cf. table 2.1).

Electron diffraction studies confirm that the grains are small WO_3 crystallites which can assume different crystallographic configurations, triclinic [2], monoclinic [3] and orthorombic [4],depending on the conditions of evaporation, while the grain boundary material is highly disordered.

For the purpose of discussion of the optical properties we will treat the "as evaporated" WO_3 and $Na_x WO_3$ films as a collection of crystalline particles embedded in a matrix of grain boundary material.

Webman et. al. [5] developed an effective medium theory appropriate to this situation which relates the effective complex dielectric function of a composite material to the complex dielectric functions of its components. For the binary case of WO_3 and $Na_x WO_3$ films we obtain:

$$c\left\{\frac{\varepsilon_g(h\nu) - \varepsilon(h\nu)}{\varepsilon_g(h\nu) + 2\varepsilon(h\nu)}\right\} + (1-c)\left\{\frac{\varepsilon_{gb}(h\nu) - \varepsilon(h\nu)}{\varepsilon_{gb}(h\nu) + 2\varepsilon(h\nu)}\right\} = 0 \qquad (4.1.1)$$

where $\varepsilon(h\nu)$, $\varepsilon_g(h\nu)$ and $\varepsilon_{gb}(h\nu)$ are the complex dielectric function of the film, the grain and the grain boundary material respectively. c is the volume fraction of the film occupied by the grains and (1-c) is the volume fraction occupied by the grain boundary material.

We believe that the dielectric function of the grains is approximately the same as the dielectric function of the corresponding single crystal. It is, however, expected that the strain field introduced by the grain boundaries modifies the structure of the grains causing small changes in the optical properties as well.

Because of the large amount of disorder in the grain boundary material, we expect its electronic states to be strongly localized. The probability of electronic transitions between such states is negligibly small and therefore the imaginary part of the dielectric function ε_{gb} can be set equal to zero and its real part can be taken as independent of the photon energy.

The dielectric functions ε_g, ε_{gb} and ε can be written as :

$$\begin{aligned} \varepsilon(h\nu) &= \varepsilon_1(h\nu) + i\varepsilon_2(h\nu) \\ \varepsilon_g(h\nu) &= \varepsilon_{1g}(h\nu) + i\varepsilon_{2g}(h\nu) \\ \varepsilon_{gb} &= \varepsilon_{1gb} = \text{constant} \end{aligned} \qquad (4.1.2)$$

The volume fraction occupied by the grains can be calculated from eqn. (2.2.3). For the 50Å m.g.s. films, $c \approx 0.53$

Using this value for c and equ. (4.1.2), equ. (4.1.1) can be written, after separation of the real and imaginary parts, as follows:

$$\varepsilon_{1g} = \frac{2\varepsilon_1^2 - 1.47\varepsilon_2^2 + 0.06\varepsilon_2\varepsilon_{2g} - 0.41\varepsilon_{1gb}\varepsilon_1}{\varepsilon_{1gb} + 0.59\varepsilon_1} \qquad (4.1.3)$$

$$\varepsilon_{2g} = \varepsilon_2 \left(\frac{4\varepsilon_1 - 0.41\varepsilon_{1gb} - 0.59\varepsilon_{1g}}{\varepsilon_{1gb} + 0.59\varepsilon_1} \right) . \qquad (4.1.4)$$

The indication of phonon energy dependence has been omitted for the sake of brevity.

The real and imaginary parts of the dielectric function are related to the corresponding parts of the complex index of refraction, n_c, through the following relations :

$$\varepsilon_1 = n^2 - k^2 \qquad (4.15)$$

$$\varepsilon_2 = 2nk \qquad (4.1.6)$$

where $$n_c = n - ik. \qquad (4.1.7)$$

In the photon energy range $0.5 \leq h\nu \leq 4$ eV, we find experimentaly that

$$n^2 >> k^2 \qquad (4.1.8)$$

and therefore

$$\varepsilon_2^2 << \varepsilon_1^2 . \qquad (4.1.9)$$

Using the relation (4.1.9), equ. (4.1.3) can be written as

$$\varepsilon_{1g} \simeq \varepsilon_1 \left(\frac{2\varepsilon_1 - 0.41\varepsilon_{1gb}}{\varepsilon_{1gb} + 0.59\varepsilon_1} \right) \qquad (4.1.10)$$

and substitution of equ. (4.1.10) into equ.(4.1.4) leads to

$$\varepsilon_{2g} \simeq \varepsilon_2 \left(\frac{1.3\varepsilon_1^2 + 4\varepsilon_1 \varepsilon_{1gb} - 0.41\varepsilon_{1gb}^2}{(\varepsilon_{1gb} + 0.59\varepsilon_1)^2} \right) \qquad (4.1.11)$$

Eqns. (4.1.10) and (4.1.11) can be written as

$$\varepsilon_{1g} \simeq G_1 \varepsilon_1 \tag{4.1.12}$$

$$\varepsilon_{2g} \simeq G_2 \varepsilon_2 \tag{4.1.13}$$

where

$$G_1 = \frac{2\varepsilon_1 - 0.41\,\varepsilon_{1gb}}{\varepsilon_{1gb} + 0.59\varepsilon_1} \tag{4.1.14}$$

and

$$G_2 = \frac{1.3\varepsilon_1^2 + 4\varepsilon_1\varepsilon_{1gb} - 0.41\varepsilon_{1gb}^2}{(\varepsilon_{1gb} + 0.59\varepsilon_1)} \quad . \tag{4.1.15}$$

The quantities G_1 and G_2 can be evaluated using the experimently determined values of n and the value of ε_{1gb} found in section 4.1.4. They are found to be slowly varying functions of n, in the range $0.5 \leq h\nu \leq 4$ eV, and to a first approximation, they can be considered constants.

The change in G_1 and G_2 over the photon energy range $0.5 \leq h\nu \leq 4$ eV is less than 15%. A change of the same magnitude is found in G_1 and G_2 for any photon energy as x of the $Na_x WO_3$ films is varied from zero to 0.2.

Equ. (4.1.13) can be used to relate the experimentaly determined absorption coefficient, α, of the films to the absorption coefficient, α_g, of the grains.

The absorption coefficient is defined by the relation

$$\alpha = \frac{4\pi k}{\lambda} \tag{4.1.16}$$

where λ is the wavelength of the light.

Using eqns. (4.1.16) and (4.1.6), eqn. (4.1.13) can be written as

$$\alpha_g \approx \frac{n}{n_g} G_2 \alpha \qquad (4.1.17)$$

where n_g is the real part of the index of refraction of the grains.

Using equs. (4.1.5), (4.1.8) and (4.1.12) we find that

$$\alpha_g \simeq \frac{G_2}{\sqrt{G_1}} \alpha \ . \qquad (4.1.18)$$

Therefore the experimentaly determined absorption coefficient of the 50Å m.g.s. films is proportional to the absorption coefficient of the grain with a constant of proportionality of the order of 2.

In the case of the 2-3μ m.g.s. films, one can easily show using equ. (2.3) that $c \approx 1$ and therefore eqn. (4.1.1) leads to

$$\varepsilon_g(h\nu) = \varepsilon(h\nu)$$

i.e. the optical properties of the film are identical to the optical properties of the grains.

In what follows the optical properties of WO_3 and $Na_x WO_3$ are interpreted in terms of three interband electronic tranisitions.

In WO_3 the only possible transitions are those from the occupied valence band to the empty conduction band, giving rise to the main absorption edge. When sodium is inserted into the WO_3 lattice, it becomes ionised creating a new band of states above the conduction band minimum and it liberates electrons which occupy some of the empty conduction band states. Transitions from the occupied conduction band states to the empty sodium states and to empty states in the conduction band manifold give rise to the absorption band below the main absorption edge of $Na_x WO_3$

(Fig. 4.1.1). Superimposed on this absorption band there is the free carrier contribution which is significant only in the large grain $Na_x WO_3$ films.

The abrupt changes in the absorption and reflection spectra at $x \approx 0.07$ and $x \approx 0.1$ are attributed to the phase changes of $Na_x WO_3$ occuring at these x values [6] .

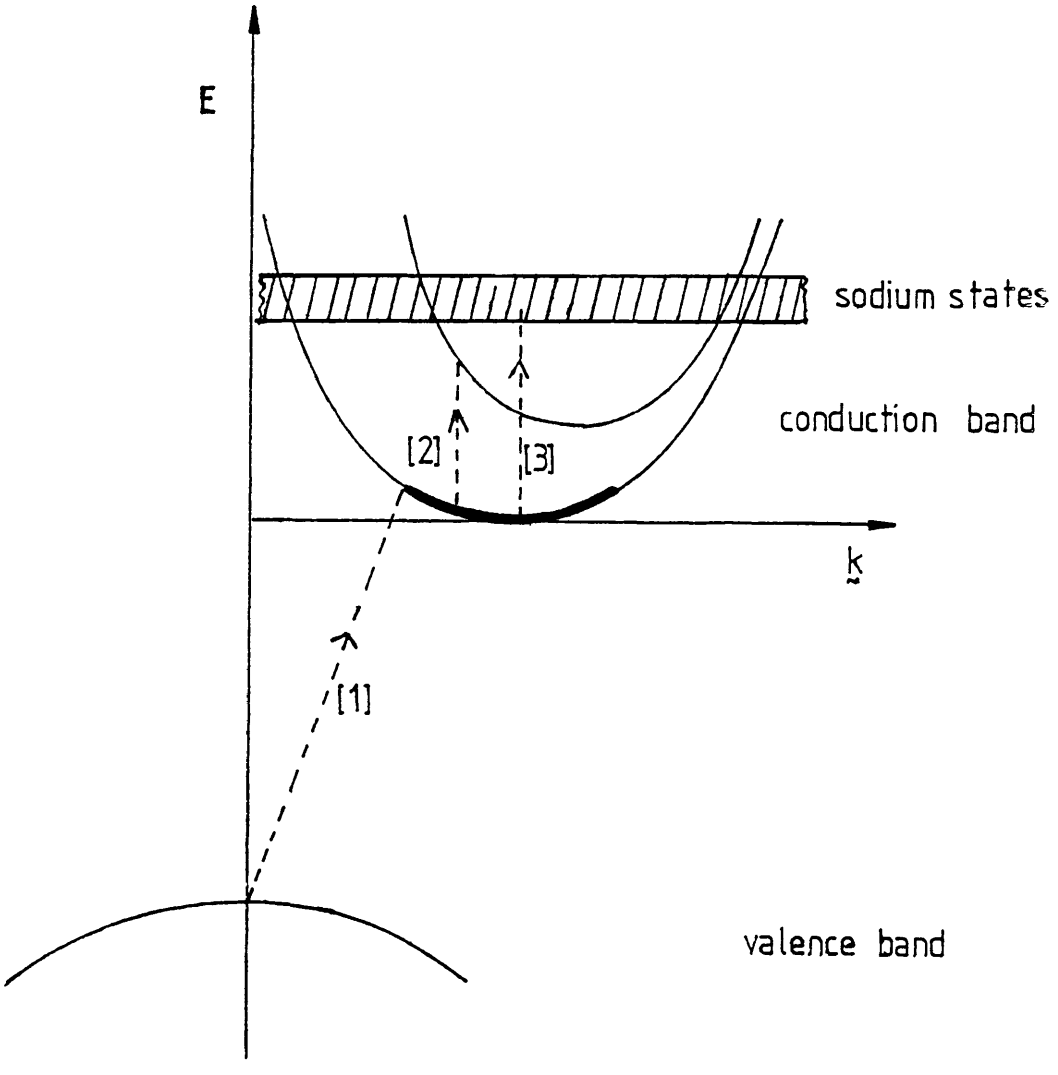

Fig. 4.1.1: Schematic band diagram of the grain of 50Å mgs Na_xWO_3 film, showing the electronic transitions involved in the absorption of light in the photon energy range of 0.4 to 4eV. [1] Valence to conduction band transitions, giving rise to the main absoprtion edge. [2], [3] transitions from the conduction band minimum to a higher conduction subband and to the sodium states

4.1.2 Main Absorption Edge

a. WO_3 films

The absorption coefficient of 50Å m.g.s. WO_3 films in the photon range of 3.25 eV to 3.8 eV is found in section 3.1.2 to vary over three orders of magnitude and to obey the relation (3.1.11) which, using eqn. (4.1.18) can be written as

$$\alpha_g \, h\nu = \frac{G_2}{\sqrt{G_1}} A(h\nu - E_0)^2 \qquad (4.1.19)$$

where A and E_0 are material constants.

The rapid variation of the absorption coefficient with energy and the form of eqn. (4.1.19) indicate that this is the region of the main absorption edge of WO_3, due to electronic transitions from the top of the valence band to the bottom of the conduction band.

The theoretical description of the absorption spectrum near the main absorption edge of solids [7,8] predicts that the absorption coefficient will obey a relation of the form of equ. (4.1.19) if the electronic transitions invloved in the absorption process of the light occur between parabolic bands and are *indirect*.

An indirect transition is one occurring between states with different crystal momentum. In such transitions momentum is conserved by scattering of the electrons with phonons or ionised impurities or crystal imperfections. According to the theory of indirect transitions the constant A of eqn. (4.1.19) depends on the momentum matrix element between the initial and final states of the transition, the effective masses of the electron and hole and the scattering mechanism involved in the momentum

conservation process. The constant E_0 is a measure of the energy gap between the top of the valence band and the bottom of the conduction band. If the scattering mechanism involves phonons, E_0 is given by

$$E_0 = E_g \pm E_p \qquad (4.1.20)$$

where E_0 is the energy gap and E_p is the energy of the phonon involved in the process. The plus and minus signs correspond to emission or absorption of the phonon. On the other hand, if the scattering does not involve phonons E_0 is equal to the energy gap.

In the light of the discussion above, we conclude that the minimum energy gap of the grain in the 50Å m.g.s. WO_3 films is an indirect one, i.e. the minimum of the conduction band and the maximum of the valence band occur at different values of the wavevector $\underset{\sim}{k}$, and that these bands are parabolic for a limited range around their respective minimum and maximum points. The dominant scattering mechanism in WO_3 films is not known and cannot be determined by our experimental data. However, given the high density of grain boundaries and impurities which are likely to exist in the films, it is not unreasonable to assume that they will dominate the scattering processes. In such a case the value of E_0 = 3.25 eV given in table 3.1.3 for the 50Å m.g.s. WO_3 film should correspond to the energy gap.

In the case of 2-3μ m.g.s. WO_3 films the absorption coefficient in the photon range of 3 eV to 3.75 eV is described by equ. (3.1.11). The energy gap, however, is decreased to 3.036 eV and the constant A is increased compared with the value of $\frac{G_2}{\sqrt{G_1}}$ A ≈ 2A of the 50Å m.g.s. films (cf. table 3.1.3), indicating that grain growth by annealing produces changes in the band structure of the films. This is confirmed by the fact that at 3.63 eV there is a second, direct, energy gap in the band structure of the 2-3μ m.g.s. WO_3 films. Fig. 3.1.34 shows that the absorption coefficient of these films above 3.75eV varies as

$$\alpha h\nu = B(h\nu - E_d)^{\frac{1}{2}} \qquad (4.1.21)$$

which is characteristic of direct transitions i.e. transitions occurring between electronic states with the same $\underset{\sim}{k}$ vector [7,8].

As in the case of eqn. (4.1.19), the derivation of eqn. (4.1.21) assumes that the bands are parabolic near their maximum and minimum points. The constant E_d is the energy gap between the top of the valence band and the bottom of the conduction band and B is a function of the electron and hole effective masses and the constant momentum matrix element of the states involved in the transitions.

The variation of the gap with grain size is confirmed by other workers as well. Deb [9] reports that the energy of the "as evaporated" WO_3 films is indirect and has a value of 3.25 eV while annealing at 650^oK shifts the gap to smaller energies. Nakamura et. al. [10] find an indirect gap of 3.41 eV for the "as evaporated" WO_3 films and 3.27 eV for the annealed at 200^oC films. It should be pointed out that the films used by Nakamura et. al. have a smaller density than ours, indicating a smaller mean grain size.

Kang [2] also reports a decrease of 0.38 eV in the indirect gap of WO_3 films when annealed at 350^oC. The values of the indirect gap for the "as evaporated " and annealed films found by Kang are 3.15 eV and 2.78eV respectively, which are smaller than the gap found for our films. This is due to the fact that Kang's films were evaporated on ordinary microscope slides which have an optical cut-off very close to the energy gap of WO_3.

The optical gap of WO_3 films prepared by R.F. reactive sputtering is found to be in the range of 3 to 3.03 eV [11],but the rate of deposition is 10 to 50 times smaller than ours and the m.g.s of these films is $\sim$ 300Å.

Measurements of the photoelectrolysis spectra of sintered polycrystalline WO_3 yield an indirect optical gap at 2.62 eV and two direct ones at 3.52 eV and 3.74 eV [12]. Spichiger-Ulmann et. al. [13] find that

the indirect gap of thermally grown polycrystalline WO_3 is 2.5 eV.

Using the same method, i.e. photoelectrolysis, Butler [14, 15] found that the optical gap of WO_3 single crystal is indirect and has a value of 2.77 eV. On the other hand, Hoppemann et. al. [16] report that the transmission measurements on single crystal WO_3 yield a direct gap of 2.77 eV.

Finally, we would like to point out that band structure calculations for the single crystal WO_3 [17, 18] show that the band gap increases by non-cubic crystallographic distortions. This is in agreement with our results which show that a decrease in the m.g.s. leads to an increase of the energy gap, since the distortions of the structure of the grains, brought about by the influence of the grain boundaries, are expected to lower their cyrstallographic symmetry.

b. $Na_x WO_3$ films

The absorption coefficient of the 50Å m.g.s. $Na_x WO_3$ films in the region of the main absoprtion edge is found to follow equ. (4.1.19), (cf. section 3.1.2). Therefore the main absorption edge of $Na_x WO_3$ films is due to indirect transitions from the top of the valence band to the conduction band as in the case of WO_3.

The constant A and the optical gap E_0 are found to vary with x (cf. table 3.1.3). Fig. (4.1.2) shows the variation of E_0 with x, which is found to be :

$$E_0 = 3.25 + 1.3\ x^{2/3} \text{(in eV)} \qquad \text{for } x \lesssim 0.05 \qquad (4.1.22)$$

It should be noted that when the uncertainties in the measurement of E_0 and x are taken into consideration the value to the second term in eqn. (4.1.22) becomes 1.3 ± 0.14.

This shift, of E_0 with $x^{2/3}$ can be explained in terms of the increased occupation of the c.b. states by free electrons.

The sodium atoms in $Na_x WO_3$ are ionised and the liberated electrons occupy the lowest states in the conduction band of WO_3, thereby making these states inaccessible to the electronic transitions from the valence band. Therefore the optical energy gap, E_0, will increase by the ammount the Fermi level E_F rises inside the conduction band states. From Fig. 4.1.1 we can see that

$$E_0 = E_g + E_F \ . \qquad (4.1.23)$$

Taking E_g to be the minimum energy gap of WO_3, viz. $E_g = 3.25$ eV, equ. (4.1.23) can be written as

$$E_0 = 3.25 + E_F \text{ (in eV)} \qquad (4.1.24)$$

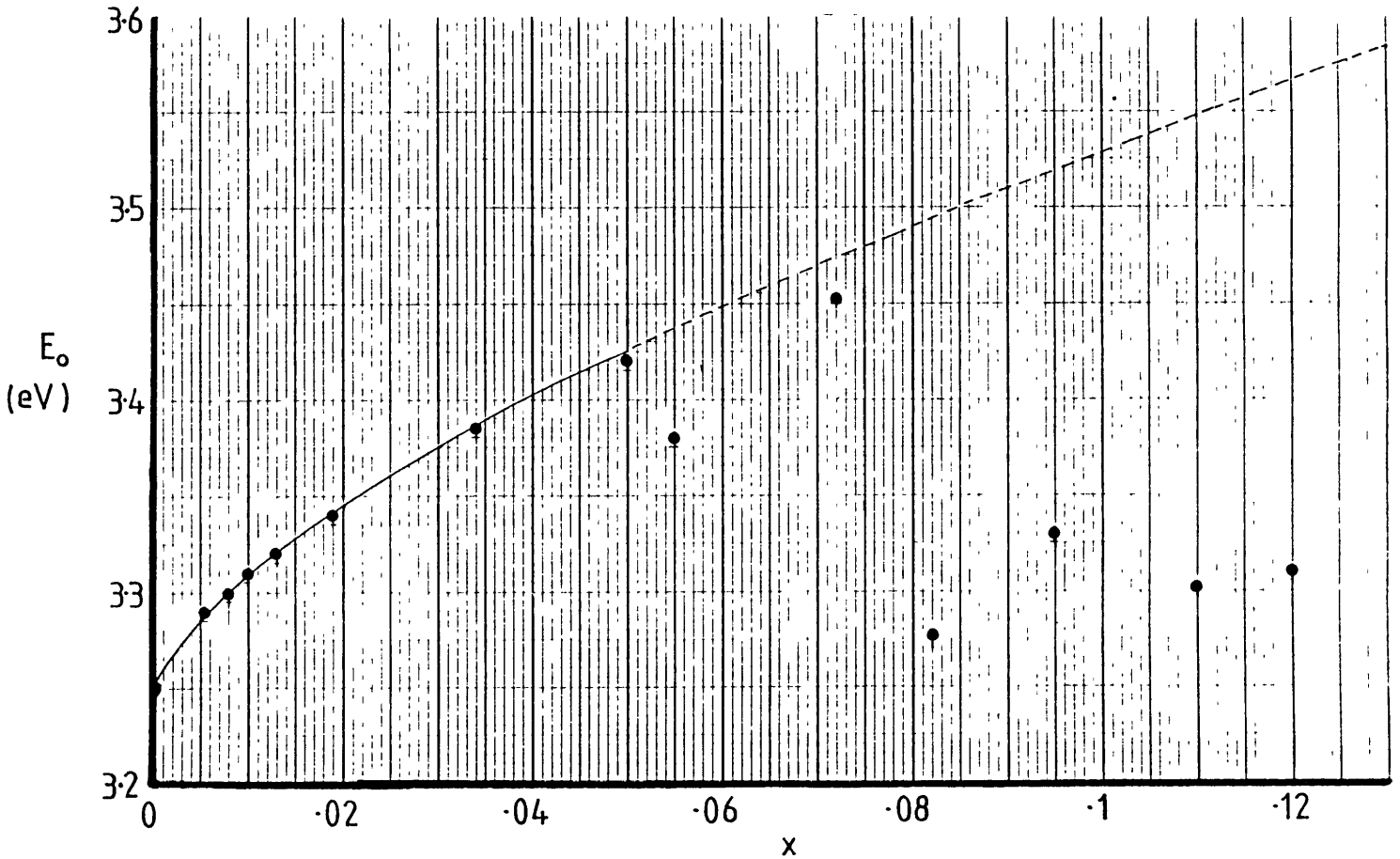

Fig. 4.1.2 : The optical gap, E_0, (see Table 3.13), of the 50Å m.g.s. Na_xWO_3 films as a function of x. The curve through the experimental points is given by $E_0 = 3.25 + 1.3x^{2/3}$, equ. (4.1.22), indicating that for $x \lesssim 0.05$ the Fermi level in Na_xWO_3 rises in the conduction band as $x^{2/3}$

The Fermi level in a heavily degenerate semiconductor with parabolic bands can be written in terms of the free electron density, N_e, as [19]

$$E_F = \frac{(3\pi^2)^{2/3} \hbar^2}{2\, m^*} N_e^{2/3} \qquad (4.1.25)$$

where m^* is the density of states effective mass of the electron.

The sodium concentration is given by equ. (2.2.13). Assuming that each sodium atom liberates one electron in the grain, the free electron density is related to x by

$$N_e = 1.9\times10^{28} x \qquad (\text{in } m^{-3}) \qquad (4.1.26)$$

Combining equs. (4.1.24), (4.1.25) and (4.1.28) we obtain

$$E_0 = 3.25 + 2.597\left(\frac{m}{m^*}\right) x^{2/3} \text{ in eV} \qquad (4.1.27)$$

$$\text{for } x \lesssim 0.05$$

where m is the mass of the free electron.

Equ. (4.1.27) has exactly the same form as the experimental relation (4.1.22), confirming therefore, that the shift of the optical gap in Na_xWO_3 films is a direct effect of the increase of free electrons in the grains of the film.

Combining equ. (4.1.22) and equ. (4.1.27) one can obtain an estimate of the effective mass ratio of the electrons in the conduction band of $Na_x WO_3$ films :

$$\frac{m^*}{m} \simeq 2 \pm 0.22 \qquad \text{for } 0 \lesssim x \lesssim 0.05$$

The variation of the constant A of equ. (4.1.19) with x is shown in Fig. 4.1.3. For $x \lesssim 0.04$, A is linearly increasing with x, indicating that the dominant scattering mechanism in $Na_x WO_3$ is scattering by the ionised sodium atoms.

For $x \gtrsim 0.05$, there is no simple relation between the optical properties of Na_xWO_3 and x. This is due to three effects caused by the increase of the sodium concentration :

[1] The WO_3 lattice is continuously deformed by the presence of the sodium ions. Therefore the band structure is perturbed causing changes in the optical properties. This effect is expected to be a gradually increasing function of x and it will be negligible at low x values.

[2] The electronic transitions within the conduction band and to the sodium states (see Fig. 4.1.1), which at low x-values contribute in the asborption coefficient only in the visible and infrared, extend their contribution with increasing x in the region of the main absorption edge. Since it is very difficult to separate the two contributions, the absorption coefficient around 3.2 eV becomes less and less representative of the transitions between valence and conduction bands. Furthermore, the presence of strong internal electric fields causes deviations of the absorption edge from the shape predicted by equ. (4.1.19), (cf. see 4.1.3). The influence of these fields extends to higher energies as the sodium concentration increases (see Fig. 3.1.30), thereby making the extraction of accurate information from the main absorption edge progressively more difficult.

[3] The perovskite-type structure of Na_xWO_3 is well known [6,20] to exhibit several phase changes as x varies from zero to one. We believe that the abrupt changes observed in the optical properties of Na_xWO_3

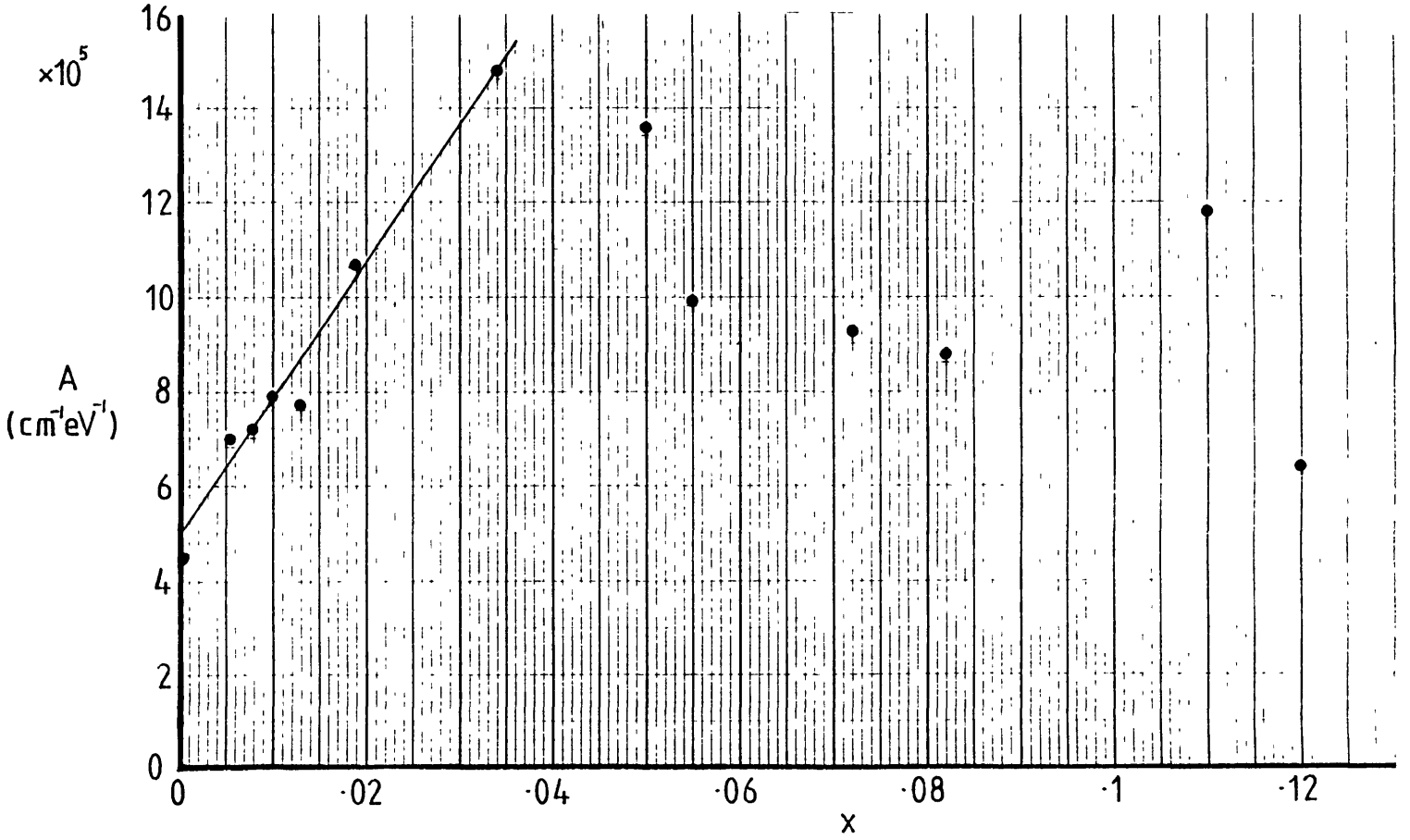

Fig. 4.1.3 : The constant A of equ. (4.1.19), (see Table 3.1.3), for the 50Å m.g.s. Na_xWO_3 films as a function of x. The linear variation of A with x for $x \leq 0.04$ indicates that the dominant scattering mechanism in Na_xWO_3 is ionised impurities scattering

at certain x values are caused by band structure changes due to the phase changes. The optical gap, E_0, is seen in Fig. 4.1.2 to exhibit two abrupt discontiuities at $x \approx 0.07$ and $x \approx 0.11$.

At these x-values Na_xWO_3 changes from orthorombic to tetragonal I and from tetragonal I to tetragonal II respectively [20].

The discussion of the main absorption edge of the Na_xWO_3 films with m.g.s. larger than 50Å is hindered by the lack of data covering a wide enough x-range, and by the fact that all our data are for films with $x \gtrsim 0.05$ where the effects of the phase changes and the lattice deformation by the sodium ions play an important role. It can, however, be seen from table 3.13 that both A and E_0 for these films follow the same trend as the corresponding quantities of the 50Å m.g.s. films. The change of the direct optical gap of the 2-3μ m.g.s. films with x (cf. table 3.1.4) conform our postulate that the increase of sodium concentration above $x \approx 0.05$ deforms the electronic band structure of Na_xWO_3. Note that for film B4 ($x \approx 0.2$) is not possible to distinguish between the direct and indirect gap.

There are no optical data near the main absorption edge of Na_xWO_3 thin films in the literature against which to compare our results. There are, however, some reports on other tungsten bronze thin films which should behave in a way similar to Na_xWO_3 near the main absorption edge. Gabrusenoks et. al. [21] report that colouration of WO_3 films with H shifts the fundamental absorption edge to the higher energy side.

Nakamura et. al. [10] found that that the optical gap of Li_xWO_3 and H_xWO_3 films increases witn x, but the magnitude of the shift is much smaller than that expected from the filling of a parabolic conduction band. However, the values of x they used are not correct, because they were obtained using Smakula's equation from the infrared absorption band of the films. As it will be shown in section 4.1.4 this band is a composite

one and therefore it cannot be used as it is for determination of the x-value. Furthermore the value of the oscillator strength used by Nakamura et. al. has not been determined experimentaly.

Our results are also in agreement with measurements of the chemical potential of Na_xWO_3 films by Green and Kang [1]. They find that sodium atoms are ionised and the liberated electrons occupy conduction band states with their Fermi level varying as $x^{2/3}$.

Studies of H_xWO_3 films by X-ray electron spectroscopy [22, 23] show that they exhibit a small band near the Fermi level which grows proportionally with the colouration, but it is placed only 2eV above the valence band. However, in view of the fact that X-ray electron spectroscopy samples only a surface layer ~ 10Å in thickness and since the experimental resolution in these studies was no better than 0.6 eV, the energy assignment of the Fermi level relative to the valence band cannot be taken as representative of the bulk of the film.

Electronic structure calculations of Na_xWO_3 single crystal [17, 18] show extra electrons occupy the t_{2g} conduction band of WO_3 although this band is not parabolic for high x-values. These results are confirmed by optical measurements [24, 25, 26], nuclear magnetic resonance studies [27] and ultraviolet photoemission spectroscopy [28].

Our results indicate that for low x-values Na_xWO_3 behaves as a degenerate semiconductor. For $x \lesssim 0.05$ the density of states is parabolic in energy and a "rigid band" approximation is applicable although it has to be abandoned for higher x-values.

It should be pointed out that these results are in direct contrast with suggestions that the Fermi level in low x-values ($x \lesssim 0.2$) Na_xWO_3 is pinned below the conduction band [17] or that the electrons donated by the sodium in Na_xWO_3 films are strongly localized forming a small polaron band in the energy gap [22, 23, 29, 30].

4.1.3 Tail of the main absorption edge

The absorption coefficient of WO_3 and Na_xWO_3 films, below the energy range where it follows equ. (4.1.19), exhibits a tail of the form,

$$\alpha = \alpha_0 \exp\left(\frac{h\nu}{E_e}\right) \qquad (4.1.28)$$

where α_0 and E_e are constants.

Such an exponential tail is observed in all non-crystalline semiconductors and in several crystalline materials as well. Much theoretical effort has been devoted to explaining the origin of this absorption tail [31, 32], but several questions still remain unanswered.

It has been suggested that the absorption tail, or Urbach's spectral rule as it is known, originates from electronic transitions between tails of the densities of states [8, 33]

This model requires that the densities of states extend inside the gap and that they vary exponentially with energy. Such a distribution of states can originate from localized fluctuations of the density of impurities which on the average are uniformly distributed throughout the sample, provided that attractive forces exist between the electrons and the impurity atoms [19]. There are many published reservations about the validity of the above explanation [31] mainly because the slope of the absorption tail observed in a variety of materials both crystalline and non-crystalline is almost the same.

A second explanation, which looks more promising, is based on the existence of strong internal electric fields which can arise from charged impurity states or from strain fluctuations or the vibrating atoms of the material. The presence of an electric field can modify the absorption edge in two ways : a) In the case of direct allowed transitions the

presence of an electric field will introduce a small "red shift" in the absorption edge (Franz-Keldysh effect) and an exponential tail. Similar effects occur in indirect transitions although they are less pronounced.

b) When exciton effects are present, an electric field will broaden the exciton line and the absorption coefficient will vary exponentially with photon energy [34].

Although, (b) gives quite satisfactory results for some materials, there are still aspects of the theory which require further investigation [31]. Prominent among these are the question of the existence of excitons in all non-crystalline materials and the question whether the random fields which are likely to exist in a non-crystalline material, average to give the same result as a constant uniform field which the above theory requires.

The above mentioned uncertainties in those theoretical models, attempting to employ the origin of the Urbach's spectral rule, as well as the lack of data for smaller values of the absorption coefficient than those appearing in Figs. 3.1.9 and 3.1.10, limit our ability to discuss conclusively the exponential tail of the absorption coefficient of WO_3 and Na_xWO_3 films. Several useful comments can, however, be made about its origin, based on the following experimental observations:

i) The tail extends both below and above the expected optical gap.

ii) The extent of the tail above the optical gap is an increasing function of x

iii) The constant E_e of eqn. (4.1.28), obtained from the values of the slope $\frac{d \log\alpha}{dh\nu}$ given in table 3.1.3, is an increasing function of x and the grain size. The values of E_e versus x for the 50Å m.g.s. film are shown in Fig. 4.1.4.

Although we expect that both the conduction and the valence band

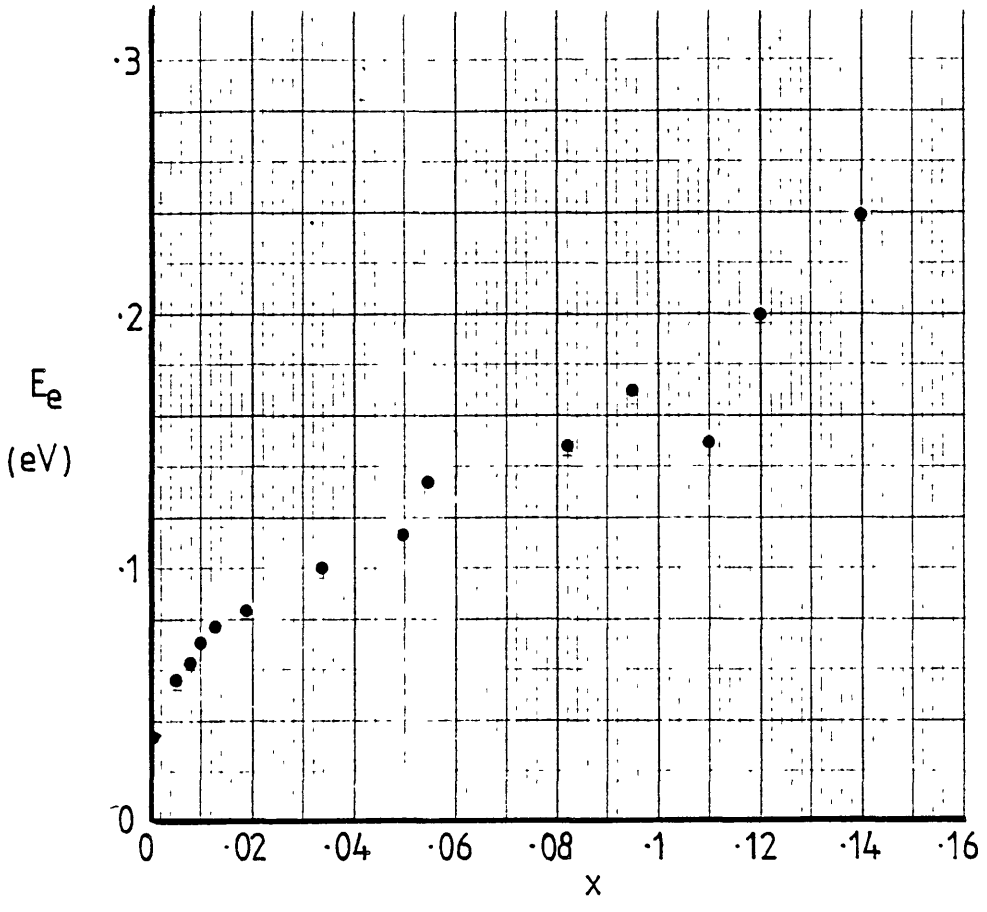

Fig. 4.1.4 : The constant E_e of equ. (4.1.28) for the 50Å m.g.s. Na_xWO_3 films as a function of x

densities of states of WO_3 and Na_xWO_3 films exhibit small tails because of the disorder, we cannot attribute the absorption tail to transitions involving these states for the following reasons :

a) The magnitude of the absorption coefficient in the region described by eqn. (4.1.28) would have required that the density of states in the tails was of the same order of magnitude as the density of states in the parabolic portion of the bands. However, such a states of affairs is contrary to the findings of section 4.1.1 where the density of states near the bottom of the conduction band and the top of the valence band were found to vary experimentally as $E^{\frac{1}{2}}$ and not exponentially with energy.

For the same reason the experimental absorption tail cannot be attributed to tails of the densities of states created by the presence of the Na ions.

b) As can be seen from table 3.1.3, E_e increases with grain size. Similar behaviour was reported by Nakamura et. al. [10] although their values of E_e are larger then those obtained from table 3.1.3.

If the absorption tail were due to tails of the densities of states, E_e would have been a measure of the extent of these tails inside the forbidden gap [8], and therefore it should have been increasing with disorder.

On the other hand, the highly disordered regions of the grain boundaries as well as the sodium ions are expected to induce electric fields of considerable strength [35] which may influence the absorption edge in one of the two ways described above.

The origin of the electric fields, as shown in section 4.2, is the trapping of free carriers in localized states in the grain boundary which creates a space charge region around each grain and establishes high electric fields ($\sim 10^7$ Vcm^{-1}) at the interface of two grains.

The magnitude of the field, given by eqn. (4.2.19), increases with the sodium concentration and therefore the nearly exponential tail introduced in the absorption edge [36] is expected to extend further away from the optical gap as x increases.

Finally it should be noted that if excitons exist in WO_3 and Na_xWO_3 films, their binding energy will be small because of the high relative permitivity and therefore will become ionized in the presence of the strong internal fields.

As a consequence, electric field broadening of the exciton peak is not likely to be the cause of the exponential absorption tail.

4.1.4 Transitions above the main absorption edge

Although, optical measurements have not been extended above 4eV in photon energy, some information about the nature of electronic transitions contributing to the optical constants on the high energy side of the main absorption edge can be obtained from the variation of the real part of the refractive index with photon energy on the low energy side of the absorption edge.

The electrons in a solid can be treated as damped harmonic oscillators with natural frequency ω_0 and a damping constant γ. In this simple Lorentzian model the electrons are considered to be bound to the nucleus in much the same way as a small mass can be bound to a large mass by a spring. The driving force of the electrons is the time varying electric field of the electromagnetic wave. From this model the complex dielectric function of a solid is derived to be [7, 37]

$$\varepsilon = \varepsilon_1 + i\varepsilon_2 = 1 + \frac{\omega_p^2}{\omega_0^2-\omega^2-i\gamma\omega} \quad . \tag{4.1.29}$$

The real and imaginary parts of the complex index of refraction, $n_c = n - ik$, are related to ε_1 and ε_2 by the following equations

$$\varepsilon_1 = n^2 - k^2 = 1 + \frac{\omega_p^2(\omega_0^2 - \omega^2)}{(\omega_0^2-\omega^2)^2 + \gamma^2\omega^2} \tag{4.1.30}$$

$$\varepsilon_2 = 2nk = \frac{\omega_p^2\,\gamma\omega}{(\omega^2-\omega^2)^2 + \gamma^2\omega^2} \tag{4.1.31}$$

where

$$\omega_p = \left(\frac{N_e e^2}{\varepsilon_0 m} \right)^{\frac{1}{2}} \tag{4.1.32}$$

is the plasma frrquency of the electron ensemble and N_e their density.

In a real solid, electrons absorb radiation by making transitions between different sets of levels and with different relative probabilities. Therefore, eqn. (4.1.29) is modified so as to include the sum of the contributions of all these transitions occurring at different ω_0, ω_p and γ. Moreover, each term has to be multiplied by the corresponding oscillator strength, f, which is a measure of the relative probability of a quantum mechanical transmission. Hence the quantum mechanical equation for the dielectric constant ε is given by [7, 37]

$$\varepsilon = 1 + \frac{4\pi e^2}{m^*} \sum_j \frac{N_j f_j}{\omega_{0j}^2 - \omega^2 - i\gamma_j \omega} \qquad (4.1.33)$$

where m^* is the effective mass of the electron. Equs. (4.1.30) and (4.1.31) can, however, be used if the different ω_{0j} are separated by wide frequency intervals so that at a particular range only one of the contributions in the sum of equ. (4.1.33) is dominant.

In the case of WO_3 films the electrons occupying the valence band states are treated as damped Lorentzian oscillators and the transitions between the valence and conduction band states are described by equ. (4.1.29).

For $\omega << \omega_0$, $k^2 << n^2$ and equ. (4.1.30) becomes

$$\varepsilon_1 \approx n^2 \approx 1 + \frac{\omega_p^2}{\omega_0^2 - \omega^2} \quad . \qquad (4.1.34)$$

Equ. (4.1.36) can be written in terms of the photon energy $\hbar\omega$ as

$$(n^2 - 1)^{-1} = \left(\frac{\hbar\omega_0}{\hbar\omega_p}\right)^2 - \left(\frac{\hbar\omega}{\hbar\omega_p}\right)^2 \qquad (4.1.35)$$

Fig. 4.1.5 shows the variation of $\frac{1}{n^2-1}$ with the square of the photon energy for the 2-3 μm m.g.s WO_3 film B1 of Table 3.1.2. The linear

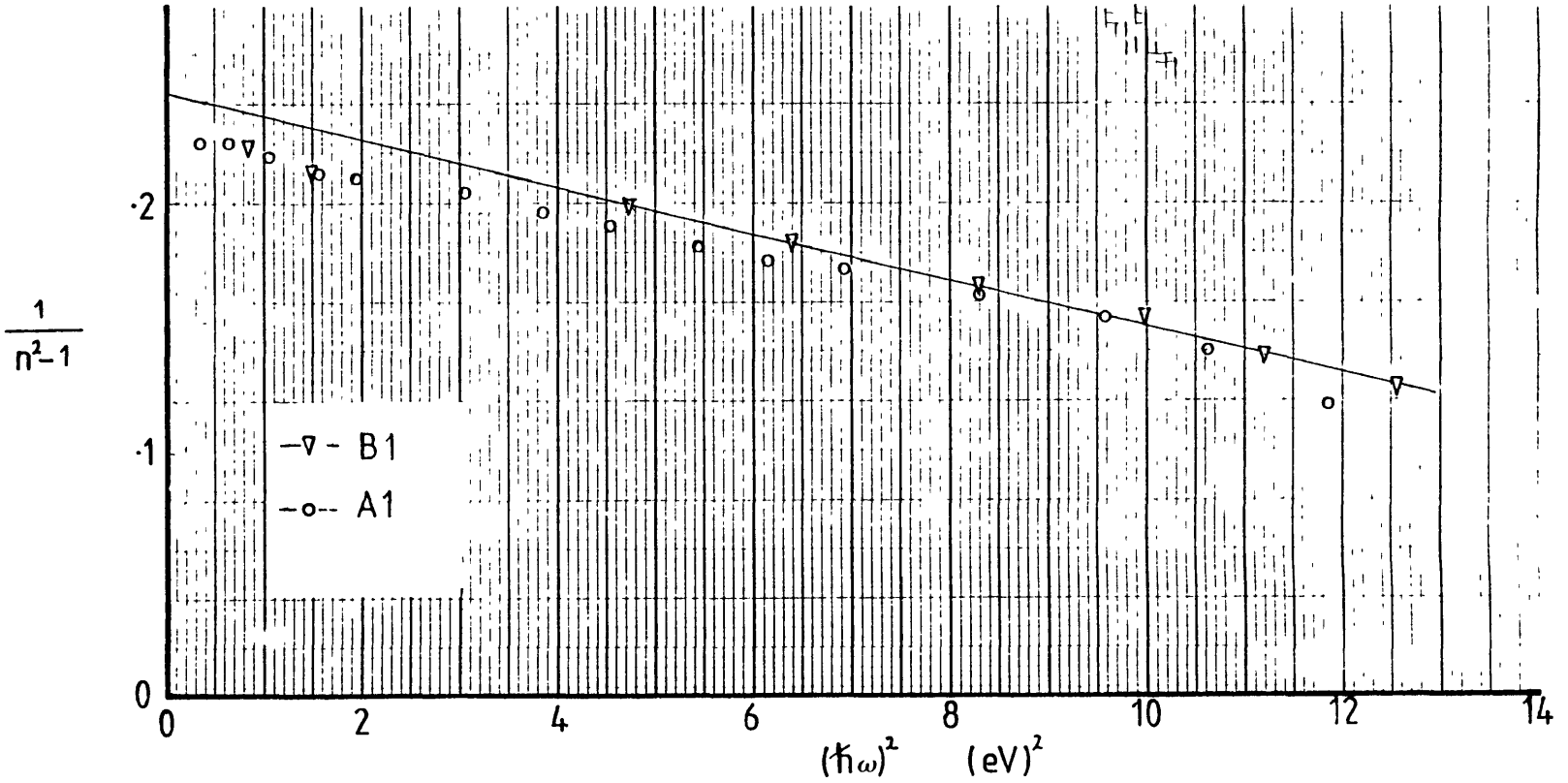

Fig. 4.1.5 : $\frac{1}{n^2-1}$ vs $(h\omega)^2$ for the 2-3μm m.g.s. WO_3 film (B1) and $\frac{1}{n_g^2-1}$ vs $(h\omega^2)$ for 50Å m.g.s. WO_3 film (A1).

The straignt line is given by equ. (4.1.35) with $h\omega_p$ = 10.35 eV and $h\omega_0$ = 5.11eV in agreement with the Lorentz' model.

variation of $\frac{1}{n^2-1}$ with $(\hbar\omega)^2$ provides justification for our assumption that the dielectric function of WO_3 can be treated in terms of a single Lorentz oscillator and permits us to calculate the quantities $\hbar\omega_p$ and $\hbar\omega_0$ from the slope and intercept with the y-axis of the straight line in Fig. 4.1.5, which are found to be 10.35 eV and 5.11 eV respectively.

The dielectric function of the 50Å m.g.s. WO_3 film A1 of Table 3.1.1 was found to behave in a similar way, indicating that the grains of both films have similar, but not identical, electronic structure.

The values of n_g, the real part of the index of refraction of the grains in the 50Å m.g.s. film, were calculated using equ. (4.1.10) assuming that $\varepsilon_{1g} \approx n^2$ and $\varepsilon_1 \approx n^2$. An estimate of the value of ε_{1gb} of equ. (4.1.10) was obtained as follows:

The value of n_g at 2.88 eV was taken equal to the value of the real part of the refractive index of the 2-3 μm m.g.s. WO_3 film, and ε_{1gb} was then calculated using equ. (4.1.10) to be 2.4. It was assumed that the material of the grain in the two films had the same index of refraction.

The values of n_g obtained from the above calculations are presented as $\frac{1}{n_g^2-1}$ vs $(\hbar\omega)^2$ in Fig. 4.1.5.
The deviation of $\frac{1}{n_g^2-1}$ from $\frac{1}{n^2-1}$ of the large grain film indicates that there is a small shift of the natural frequency, $\hbar\omega_0$, of the 50Å m.g.s. film towards smaller energies. This is in agreement with the shift found in the optical gap of the two films (cf. section 4.1.2)

4.1.5 Absorption below the main absorption edge

The characteristic blue colour of the 50Å m.g.s. sodium bronze films is due to an absorption band below the main absorption edge, which extends from the visible part of the spectrum down to the near infrared as shown in Fig. 2.3.12, 13, 14. It is proposed that this absorption band is due to electronic transitions from the occupied conduction band states to a higher lying conduction band and to the empty sodium states which are also located above the minimum of the conduction band (cf. Fig. 4.1.1).

This interpretation of the asborption band is based on the behaviour of ε_2 of the films as a function of the photon energy, $\hbar\omega$, and the value of x.

ε_2, which is proportional to ε_{2g}, (cf. section 4.1.1), is calculated from the experimentally determined quantities α and n using the relation :

$$\varepsilon_2 = 1.972\times10^{-5}\,\frac{\alpha n}{\hbar\omega} \qquad (4.1.36)$$

where the absorption coefficient, α, is measured in cm^{-1} and $\hbar\omega$ in eV.

$\hbar\omega\varepsilon_2$ as a function of $\hbar\omega$ is shown in Fig. 4.1.6, 4.1.7 and 4.1.8 for the films A2, A3 and A4 of Table 3.1.1. It is found that $\hbar\omega\varepsilon_2$ is made up of two bands and obeys the relation :

$$\hbar\omega\,\varepsilon_2(\hbar\omega) = \frac{C\Gamma\hbar^2\omega^2}{(\hbar^2\omega_0'^2 - \hbar^2\omega^2)^2 + \Gamma^2\hbar^2\omega^2} + \hbar\omega\varepsilon_2^{Na}(\hbar\omega) \qquad (4.1.37)$$

The first term of the right hand side of equ. (4.1.39) is of the form of equ. (4.1.31) describing the imaginary part of the dielectric function

Table 4.1.1

Parameters obtained from the application of the Lorentz' model to the optical spectra in the near infrared of the films, A2, A3 and A4

Film	x	$\hbar\omega_0'$ (eV)	C $(eV)^2$	Γ (eV)	$\hbar\omega\varepsilon_2$ at 2eV
A2	5.6×10^{-3}	1.31	0.053	0.827	0.0085
A3	8×10^{-3}	1.3	0.1	0.8	0.018
A4	1×10^{-2}	1.293	0.134	0.87	0.023

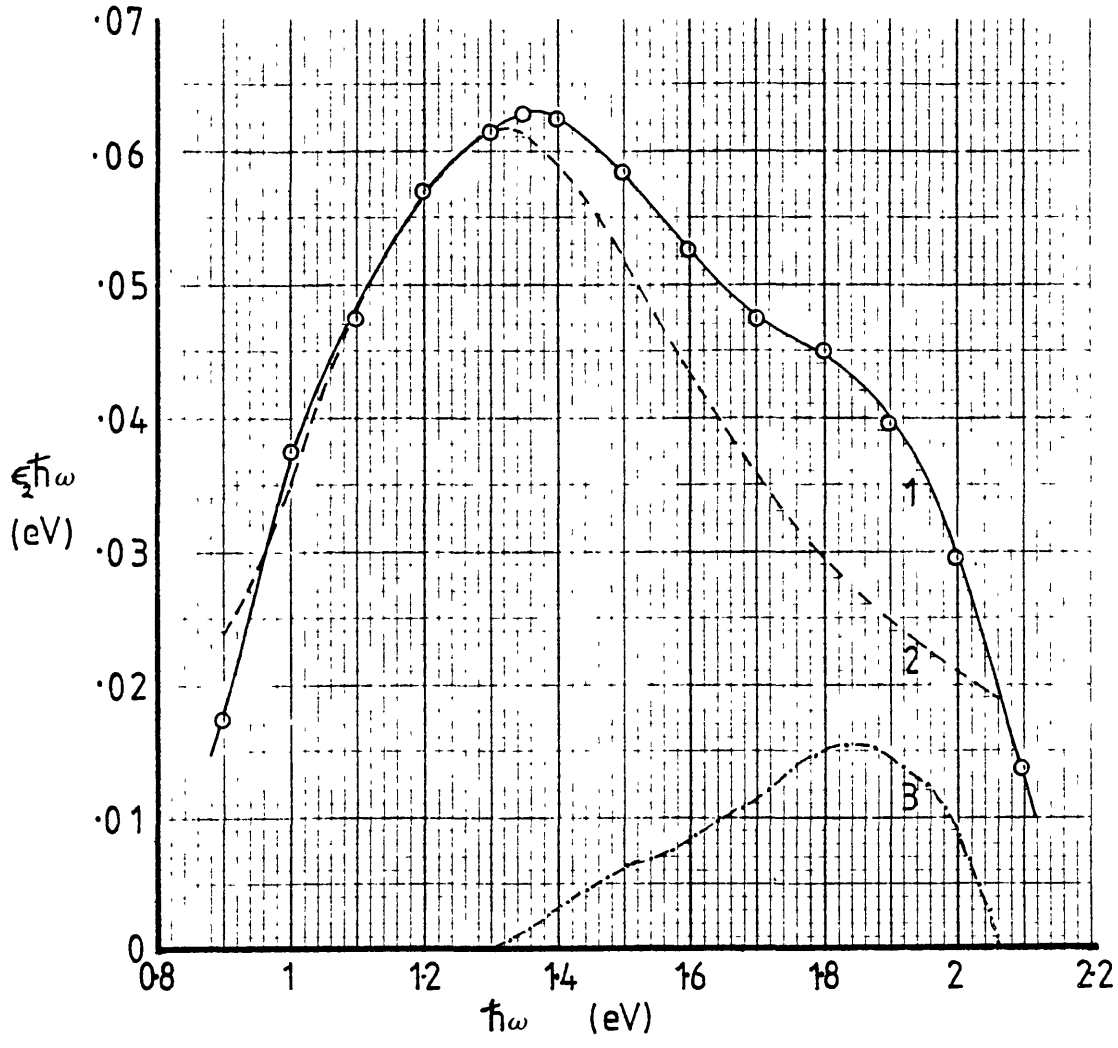

Fig. 4.1.6 : Deconvolution of $\hbar\omega\varepsilon_2$ of the 50Å m.g.s. Na_xWO_3 film A2 (curve 1) in terms of a Lorentzian oscillator (curve 2) and the contribution of the electronic transitions to the sodium states(curve 3). Curve (1) : experimental data from Fig 3.1.12. Curve (2) : calculated from the first term of equ. (4.1.37) using the parameters of Table 4.1.1. Curve (3) : obtained by substraction of curve (2) from curve (1).

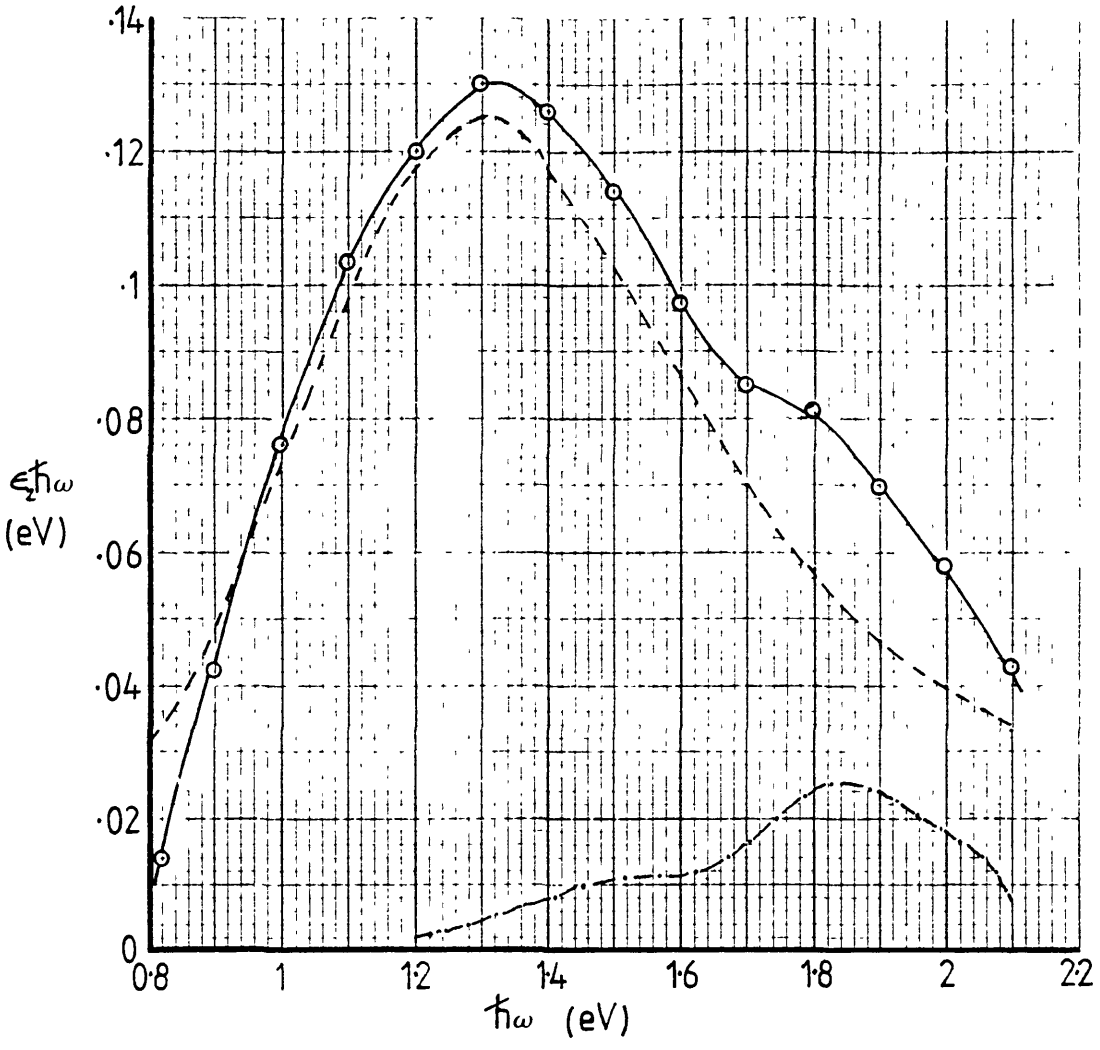

Fig. 4.1.7 : Deconvolution of $\hbar\omega\varepsilon_2$ of the 50Å m.g.s. Na_xWO_3 film A3 (curve 1) in terms of a Lorentzian oscillator (curve 2) and the contribution of the electronic transitions to the sodium states (curve 3). Curve (1) : experimental data from Fig. 3.1.12. Curve (2) : calculated from the first term of equ. (4.1.37) using the parameters of Table 4.1.1. Curve (3) : obtained by substraction of curve (2) from curve (1).

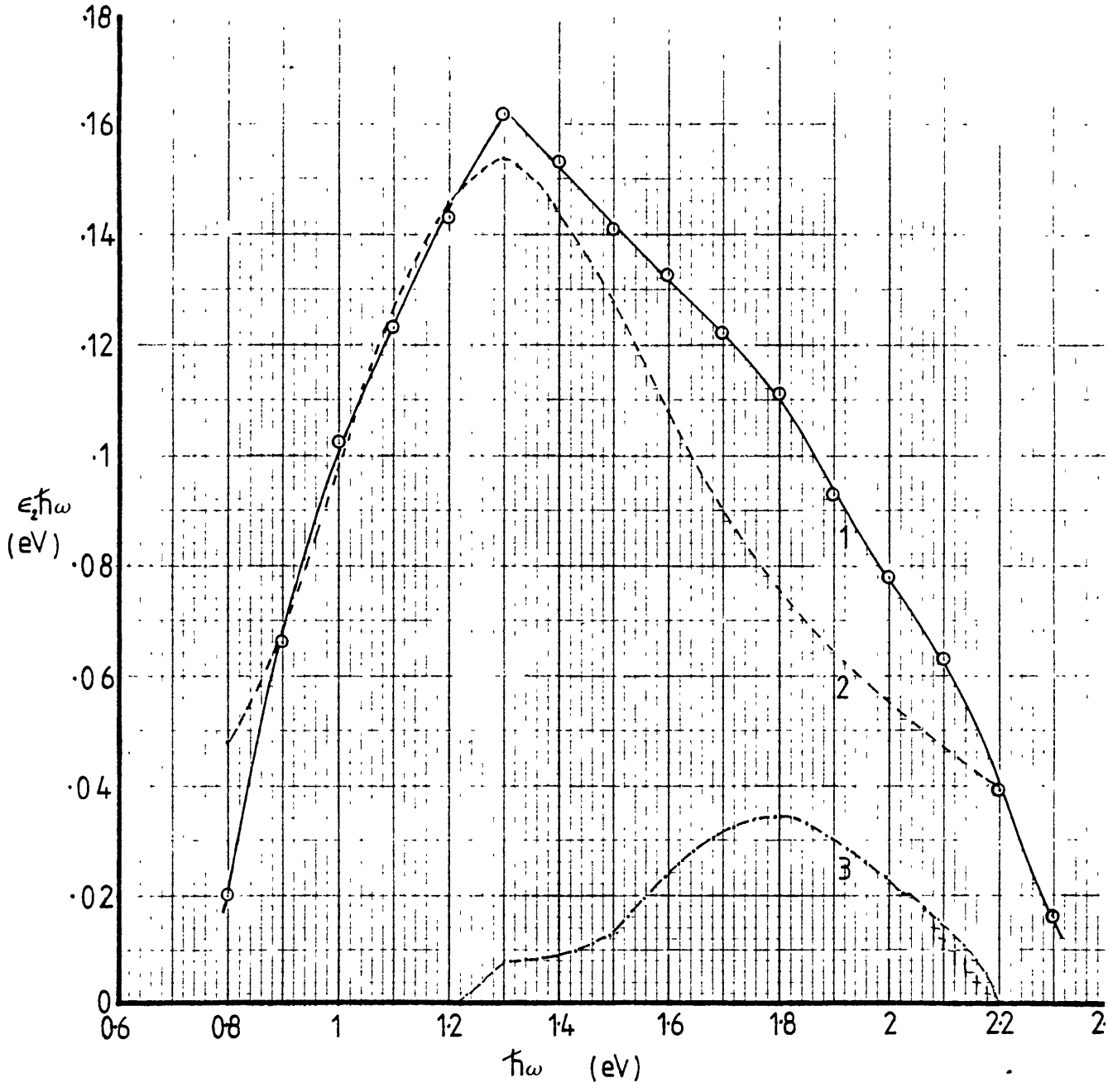

Fig. 4.1.8 : Deconvolution of $\hbar\omega\varepsilon_2$ of the 50Å m.g.s. Na_xWO_3 film A4 (curve 1) in terms of a Lorentzian oscillator (curve 2) and the contribution of the electronic transitions to the sodium states (curve 3). Curve (1) : experimental data from Fig. 3.1.12. Curve (2) : calculated from the first term of equ. (4.1.37) using the parameters of Table 4.1.1. Curve (3): obtained by substraction of curve (2) from curve (1).

of an ensemble of bound electrons in the context of the Lorentz model. The values of the constants C, $\hbar\omega_0'$ and Γ are shown in Table 4.1.1. $\hbar\omega_0'$ can be seen from Table 4.1.1 to increase with x by amounts equal to the shift of the Fermi level inside the conduction band. A similar shift towards smaller energies can be seen from Figs. 4.1.6, 7 and 8 to occur in the low energy cut-off of the experimental absorption band.

The constant C, which is proportional to the square of the plasma frequency of the electrons contributing to the transitions, is found to be proportional to x as predicted by equ. (4.1.34). Therefore the transitions described by the first term of equ. (4.1.37) have their initial states at the conduction band minimum and their final states at a conduction subband. The two conduction bands are separated by an energy difference of approximately 0.8 eV.

The second band of Figs. 4.1.8, 7 and 8 is obtained by substraction of the contribution of the Lorentz oscillator from the experimental data.

The fact that its low energy side is shifting towards lower energies as x increases, indicates that the initial states of the transitions contributing to this band are the occupied conduction band states as well. On the other hand, the final states of these transitions are assigned to the empty sodium states because $\hbar\omega\varepsilon_2^{Na}$ is found to be proportional to x^2 (cf. Table 4.1.1). $\hbar\omega\varepsilon_2$ is proportional to the joint density of initial and final states. Therefore, since the initial states are proportional to x the final states have to be proportional to x as well. The only empty states which are a function of x are the sodium states. From the position of the $\hbar\omega\varepsilon_2^{Na}$ band, the sodium states are expected to have the maximum of their distribution approximately 1.8eV, above the conduction band minimum.

At values of x larger than 0.01, the two bands contributing to $\hbar\omega\varepsilon_2$ overlap to such an extend that their separation is not possible. It was found, however, that $\hbar\omega\varepsilon_2$ has the x-dependence predicted by equ. (2.1.37) for $x \lesssim 0.05$.

Fig. (4.1.9) shows $\hbar\omega\varepsilon_2$ at 2eV and 1eV as a function of x. For $x \lesssim 0.05$, $\hbar\omega\varepsilon_2$ is given by

$$\hbar\omega\varepsilon_2(x) = 7x + 80x^2 \qquad \text{at } \hbar\omega = 2\text{eV} \qquad (4.1.38)$$

$$\hbar\omega\varepsilon_2(x) = 15.4x - 0.03 \quad \text{at } \hbar\omega = 1\text{eV} \quad . \qquad (4.1.39)$$

Equ. (4.1.38) and (4.1.39) can be understood in terms of equ. (4.1.37) as follows:

The terms linear in x correspond to the first term of eq . (4,1.37) which has a linear dependence in x because of the plasma frequency included in C.

The quadratic term in x of equ. (4.1.40) corresponds to $\hbar\omega\varepsilon^{Na}$ which is zero at 1eV and therefore does not appear in equ. (4.1.39). We, therefore, expect that $\hbar\omega\varepsilon_2$ can be described by equ. (4.1.37)) for x-values up to 0.05.

It should be pointed out that equ. (4.1.39) gives $\hbar\omega\varepsilon_2 = 0$ at $x = 1.95\times10^{-3}$, rather than at x = 0. Since x is a measure of the sodium concentration in the films and C a measure of the electrons in the conduction band states, the fact that C and consequently $\hbar\omega\varepsilon_2$, become zero at $x = 1.95\times10^{-3}$ can only be interpreted as evidence that some of the electrons donated by the sodium atoms occupy states other than the conduction band states. Possible candidates of such states include the interface states likely to exist in the grain boundary region because of the lack of full coordination of the tungsten and oxygen ions induced by

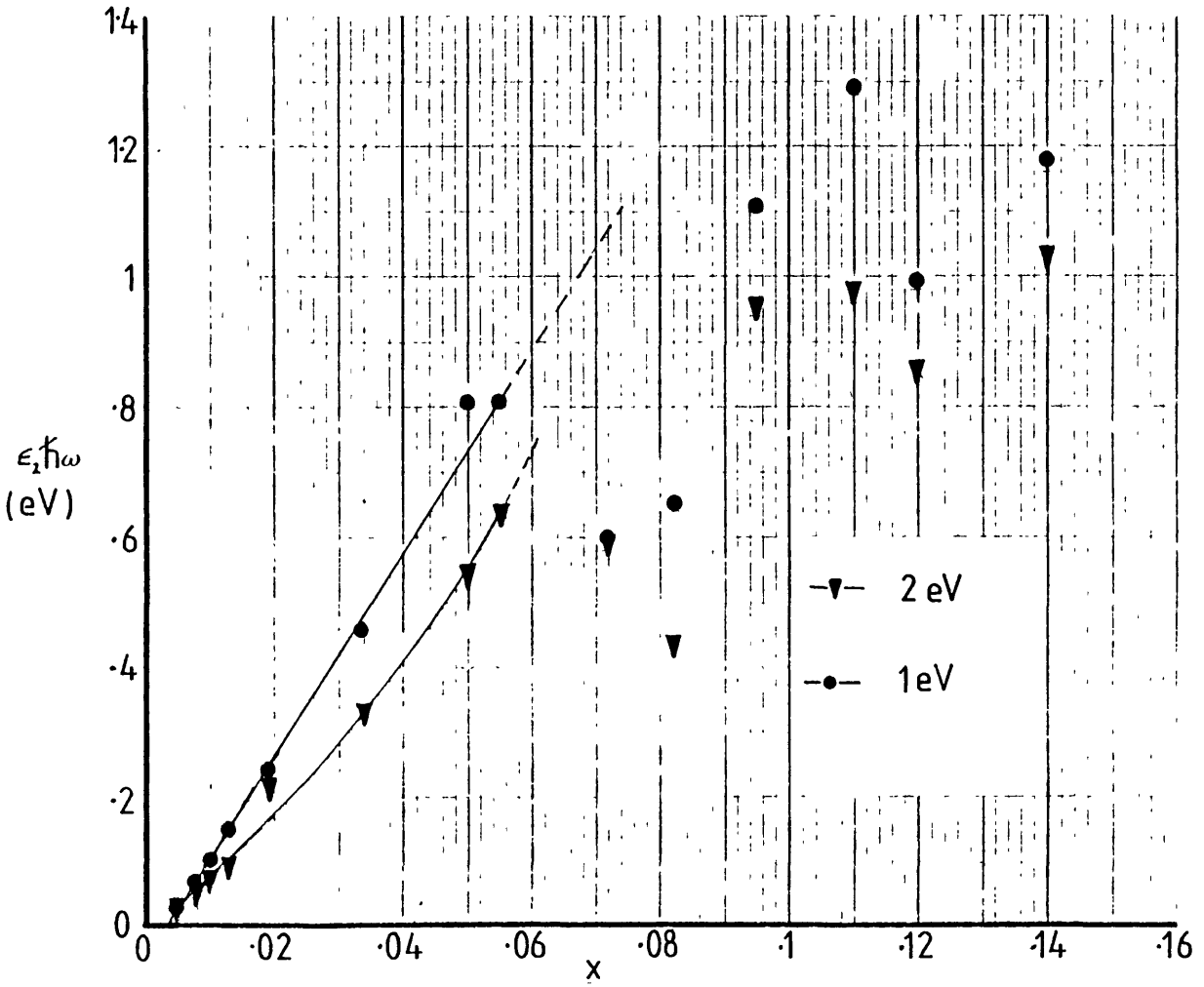

Fig. 4.1.9: $\hbar\omega\epsilon_2$ vs x for the 50Å m.g.s. Na_xWO_3 films at 1eV and 2eV. The curve through the experimental points at 2eV is given by equ. (4.1.38) and the straight line through the experimetnal points at 1eV is given by equ. (4.1.39)

the extreme disorder of the material in the grain boundary.

At values of x higher than 0.05, the absorption band is still due to electronic transitions from the filled conduction band states to the sodium states and to the states of higher lying conduction sub-band. The applicability, however, of equs. (4.1.39),(4.1.41) is severely limited by the phase changes occurring at x = 0.07 and 0.11 and by the increasing deformation of the electronic band structure of Na_xWO_3 as the sodium concentration is increased (cf. section 4.1.2). It should, also, be pointed out that as the Fermi level rises inside the conduction band, at certain x-value, it will reach the bottom of the higher lying conduction band, (see Fig. 4.1.1). When this happens, the number of available final states will be reduced and the absorption band will start decreasing in magnitude with x, (see Fig. 3.1.14 A18).

Further evidence in support of the model proposed above, to explain the absorption band in the visible and infrared, comes from the behaviour of the real part, n, of the index of refraction.

As can be seen from Figs. 3.1.22, 23, 24, n exhibits a minimum and a maximum which can be explained in terms of the above model as follows:

Since $k^2 << n^2$, $n^2 \approx \varepsilon_1$ where ε_1 is the real part of the dielectric constant of the film which is proportional to the corresponding quantity of the grains (cf. section 4.1.1 equ. 4.1.12). In terms of the Lorentz model, if ε_2 is described by equ. (4.1.37), ε_1 will be given by:

$$n^2 \approx \varepsilon_1 = \varepsilon_1^{uv} + \frac{C(\hbar^2\omega_0'^2 - \hbar^2\omega^2)}{(\hbar^2\omega'^2 - \hbar^2\omega^2) + \Gamma^2\hbar^2\omega^2} + \varepsilon_1^{Na} \qquad (4.1.40)$$

ε_1^{uv} is the contribution of the electronic transitions giving rise to the absorption above the main absorption edge and it is given by an equation of the form of equ. (4.1.34).

The second term in equ. (4.1.40) describes the contribution of the electronic transitions between the two conduction bands.

ε_1^{Na} is the contribution from the transitions to the sodium states.

ε_1^{uv} is positive in this spectral region, while the second and third terms of equ. (4.1.40) assume both negative and positive values so that ε_1 and therefore n, exhibit a maximum and a minimum as the experimental data.

In the case of Na_xWO_3 films with 120Å m.g.s., the infrared absorption band and the real part of the index of refraction are similar to the corresponding quantities of the 50Å m.g.s. films (see Figs. 3.1.13 and 3.1.14). The magnitude of the absorption is however larger in agreement with equ. (4.1.1) which predicts that an increase in the volume fraction of the film occupied by grains will result in an increase of the dielectric function of the film.

On the other hand, the optical properties of the 2-3μ m.g.s. films show some features which cannot be accounted for, only by the interband transitions described above. The absorption coefficient does not become zero at the low energy side of the band (Fig. 3.1.27) and the reflectivity shows a well defined minimum (Fig. 3.1.28) which moves to higher energies as x increases.

We believe that both of these features are manifestations of free carrier transitions occurring co-currently with the interband ones. Free carrier transitions, i.e. indirect electronic transitions between states of the same conduction band valley occur in all degenerate semiconductors and metals. Their existence is well established in Na_xWO_3 single crystal [25, 26] and in large grain polycrystalline H_xWO_3 films [29]. Their effect is however, suppressed in the 50Å m.g.s. Na_xWO_3 films because of the small grain size. Similar suppression of the

free carrier asborption has been observed in discontinuous gold films [38], in composite $Ni/A\ell_2O_3$ films [39] and in Na_xWO_3 powder when mixed with MgO [24].

The real and imaginary parts of the dielectric function, ε, of the 2-3μ m.g.s Na_xWO_3 films, in the spectral region of 0.4 to 3eV can be written as follows:

$$\varepsilon_1 = \varepsilon_1^{uv} + \varepsilon_1^{c} + \varepsilon_1^{Na} + \varepsilon_1^{f} \qquad (4.1.41)$$

$$\varepsilon_2 = \varepsilon_2^{c} + \varepsilon_2^{Na} + \varepsilon_2^{f} \qquad (4.1.42)$$

where ε_1^{uv} is the contribution form the transitions between the calence and conduction bands, ε_1^{c}, ε_2^{c} are due to transitions between the two conduction bands, ε_1^{Na} , ε_2^{Na} are due to transitions from the occupied conduction band states to the sodium states and ε_1^{f} ,ε_2^{f} are the free carrier contributions given by the relation [7]:

$$\varepsilon_1^{f} = 1 - \frac{\hbar^2\omega_{pf}^2}{\hbar^2\omega^2 + \hbar^2\gamma_f^2} \qquad (4.1.43)$$

$$\varepsilon_2^{f} = \frac{\hbar^2\omega_{pf}\,\hbar\gamma_f}{\hbar^3\omega^2 + \hbar^2\gamma_f^2\hbar\omega} \quad . \qquad (4.1.44)$$

γ_f is the inverse of the relaxation time of the electron distribution and $\omega_{pf} = \left(\frac{N_e e^2}{\varepsilon_0 m^*}\right)^{\frac{1}{2}}$ is their plasma frequency.

Comparison of equs. (4.1.43) and (4.1.44) with our experimental data is not possible because ε^{c}, ε^{Na} and ε^{f} cannot be separated. In order to investigate the free carrier effects, one would have to measure $\alpha(\hbar\omega)$ and $n(\hbar\omega)$ at energies lower than 0.4 eV, where the contribution of the

interband transitions is negligible.

There are no optical data in the visible and near infrared on sodium tungsten bronze thin films with 50Å m.g.s. in the literature against which to compare our results.

Recently, some ellipsometric studies at 0.63μm have been performed on Na_xWO_3, Li_xWO_3 and H_xWO_3 thin films with small grain sizes [40]. The values of ε_2 and ε_1 of Na_xWO_3 films are in excellent agreement with our results. Moreover, the small differences found between the optical constants of the different bronzes are in agreement with our model of the absorptions band in the infrared. The position of the donor states relative to the conduction band depends on the ionisation energy of the donor atom. Therefore the position of the absorption band resulting from the electronic transitions to the donor states is expected to be different for each bronze. A similar difference in the shape of the absorption bands of Li_xWO_3 and H_xWO_3 thin films can be seen in the optical results reported by Nakamura et. al. [10].

K. Kang and M. Green [41] report the optical absorption spectra of 300Å m.g.s. R.F. sputtered Na_xWO_3 films, in which the sodium has been electrochemically inserted. Their absorption bands for different x-values are similar in shape with those in Figs. 3.1.12, 3.1.13 and 3.1.14, but the magnitude of the absorption is twice that of our 50Å m.g.s. films with the same x-values. This large difference in the magnitude of the absorption is due to the difference in the grain size of the films in agreement with equ. (4.1.1).

The data reported by Kang and Green extend to x-values up to 0.96. The absorption bands corresponding to x-values larger than 0.5 show a change in shape and a continuous decrease in magnitude as x increases. This is in agreement with our prediction that both the shape and magnitude of the absorption with change when the states of the second

band will become occupied.

The absorption in the near infrared of Li_xWO_3 and H_xWO_3 in thin film form has also been reported [14, 32, 33] but detailed comparison with our results is inhibited by the lack of information about the films or the absolute magnitude of the absorption. The shape, however, of the absorption bands is similar to the absorption bands obtained for the 50Å m.g.s. films in this work.

Schirmer et. al. [34] report that the absorption bands of H_xWO_3 thin films, when annealed at 300°C shift to lower energies and become broader compared with the absorption bands of the "as evaporated" H_xWO_3 films. The reflectivity spectra of the "crystallized" films are also in agreement with the reflectivity of our 2-3μ m.g.s. films shown in Fig. 3.1.28.

The optical properties of Na_xWO_3 single crystal in the visible and near infrared have been studied for x-values larger than 0.5. At these high concentrations of sodium both the absorption and reflection spectra are dominated by Drude-type transitions. It has, however, been found[20], that there is a significant contribution to the dielectric function from 0 to 2.5eV from direct transitions within the conduction band. Calculations of the joint density of states of $Na_{0.9}WO_3$ [20] show similar contributions in the same energy range. Camagni and Manara [35] have also found it necessary to invoke electronic transitions within the conduction band in order to explain their electroreflectance measurements on Na_xWO_3 single crystal

An absorption band around 1.2 eV has also been found superimposed on the free carrier absorption of H_xWO_3 single crystal by Salje and Hoppmann [6]. This absorption band becomes more prominent as the temperature of the crystal is lowered.

Absorption bands in the near infrared and visible, superimposed on the free carrier absorption have also been found in the optical spectra of impure MoO_3 single crystals [42] and ReO_3 single crystals [43]. Both

of these oxides have an electronic structure similar to Na_xWO_3. Band calculations of WO_3 and Na_xWO_3 single crystal [17, 18] show that the t_{2g} conduction band manifold of these materials consist of two overlaping bands. On the basis of these calculations, one would expect that when the states of the lower sub-band are occupied there will be direct optical transitions from these states to the higher sub-band, as shown in Fig. 4.1.1. Furthermore, the same band structure calculations indicate that the sodium states in Na_xWO_3 lie well above the Fermi level. The same conclusion can be drawn from the statement of Mott [44] that the potential of the electrons near the lattice site of a sodium ion is repulsive.

The origin of the absorption band of thin film tungsten bronzes in the infrared has been attributed to intervalence transfer absorption (I.T) [30] or to charge transfer absorption from the valence band to a "split off" W^{+5} state [23, 30] or to small polaron absorption [29].

All three models require that the electrons donated by the sodium atoms are localized at states below the conduction band minimum. There are, however, several objections to this hypothesis :

i) The results on the main absorption edge of Na_xWO_3 films (cf. 4.1.2) show that the extra electrons occupy states in the conduction band of WO_3. This is also confirmed by studies of the variation of the chemical potential of Na_xWO_3 films [1].

ii) Electron spin resonance studies of H_xWO_3 thin films [45], show that the electrons are not localized on single atomic sites.

iii) The intervalence transfer and small polaron models require strong correlation between the optical absorption band and the electrical conductivity of the material [30, 45, 47].

We found no such correlation for any value of x. Furthermore, the temperature dependence of the absorption band was found to be very small [40]

and one can easily attribute it to the temperature dependence of the electronic bands of Na_xWO_3.

We therefore conclude that the above mentioned models i.e. inter-valence transfer, charge transfer and small polaron formation are not applicable in Na_xWO_3 thin films.

4.1.6 Absorption arising from water (?)

Fig. 3.1.15 shows a small absorption band around 0.4eV, found both on WO_3 and Na_xWO_3 films.

We believe that this infrared band is due to the OH stretching vibration of the H_2O molecules which are likely to be trapped mainly in the grain boundary regions of the films during evaporation and on the surface of the film when exposed to air.

Similar absorption bands have been observed in WO_3 films and have been correlated to the partial pressure of water vapour during evaporation [48].

It should be pointed out that the absorption bands of Fig. 3.1.15 occur at smaller energies than the stretching vibration of OH in gas phase water which occurs at 0.45eV [49]. Similar shifts in the vibrational frequencies OH have been observed to occur when the OH groups are in liquid or solid enviroments [50] as a result of the interaction with neighbouring molecules. It is therefore expected that the OH groups are strongly bound to the WO_3 films. The exact form of the interaction of water with WO_3 is not known and the understanding of this process as well as its quantitative analysis requires further investigation.

4.2 Electrical properties

4.2.1 Introduction

For the purpose of discussion of the electrical properties the "as evaporated" WO_3 and Na_xWO_3 films are treated as a collection of crystalline particles embedded in a matrix of grain boundary material. (see section 4.1.1).

It is expected that the disorder in the grain boundary material gives rise to a large number of defects which in turn form a large number of localized electronic states in the forbidden gap of the grain boundary material. These states can capture free carriers thereby creating a potential barrier and reducing the conductivity of the film as compared to that of the single crystal.

A one dimensional sketch of the band diagram in polycrystalline Na_xWO_3 films is shown in Fig. 4.2.1. It is assumed that all the grains have the same dimensions and that the thickness of the grain boundary is small compared with the m.g.s.

The resistivity and Seebeck coefficient of the film can be approximated by the following relations :

$$\rho = \left(\frac{L-2\ell_0}{L}\right)\rho_g + \left(\frac{2\ell_0}{L}\right)\rho_{gb} \qquad (4.2.1)$$

$$S = \left(\frac{L-2\ell_0}{L}\right)S_g + \left(\frac{2\ell_0}{L}\right)S_{gb} \qquad (4.2.2)$$

where L is the mean grain size, $2\ell_0$ is the width of the region around the grain boundary depleted from free carriers, ρ_g and S_g are the resistivity

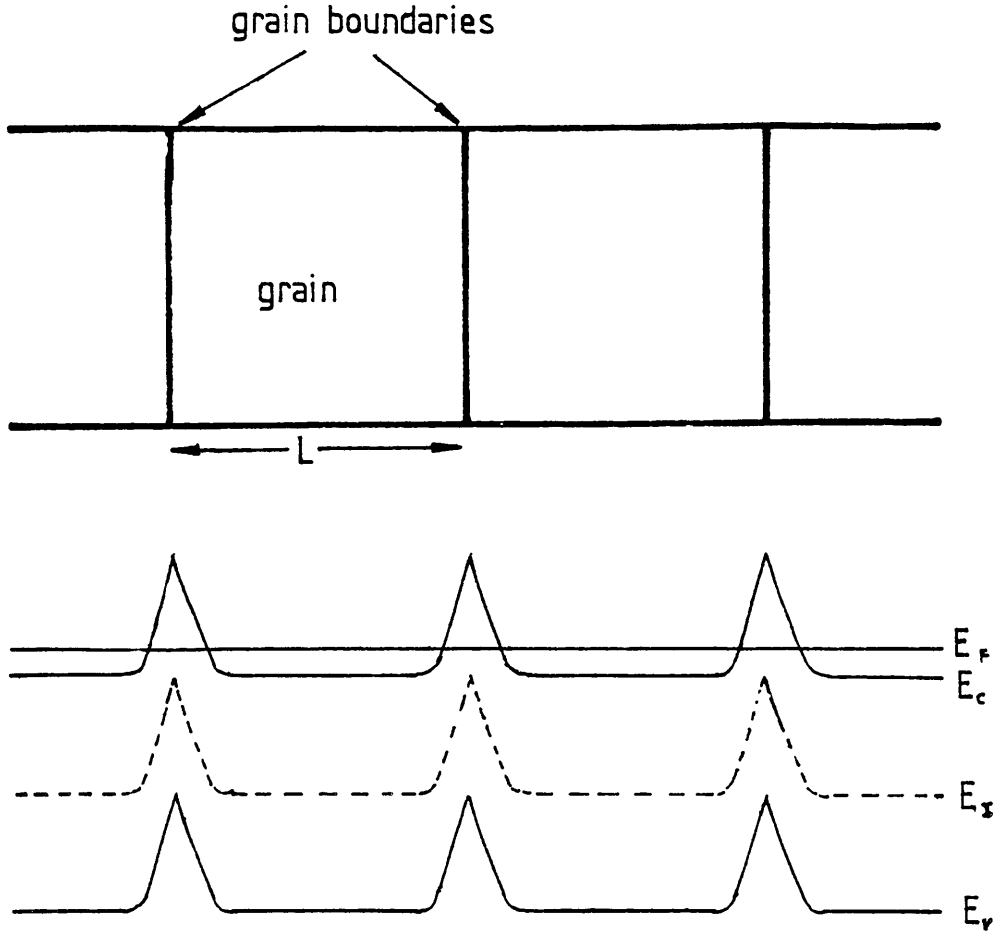

Fig. 4.2.1 : Sketch of the band diagram in polycrystalline Na_xWO_3 films

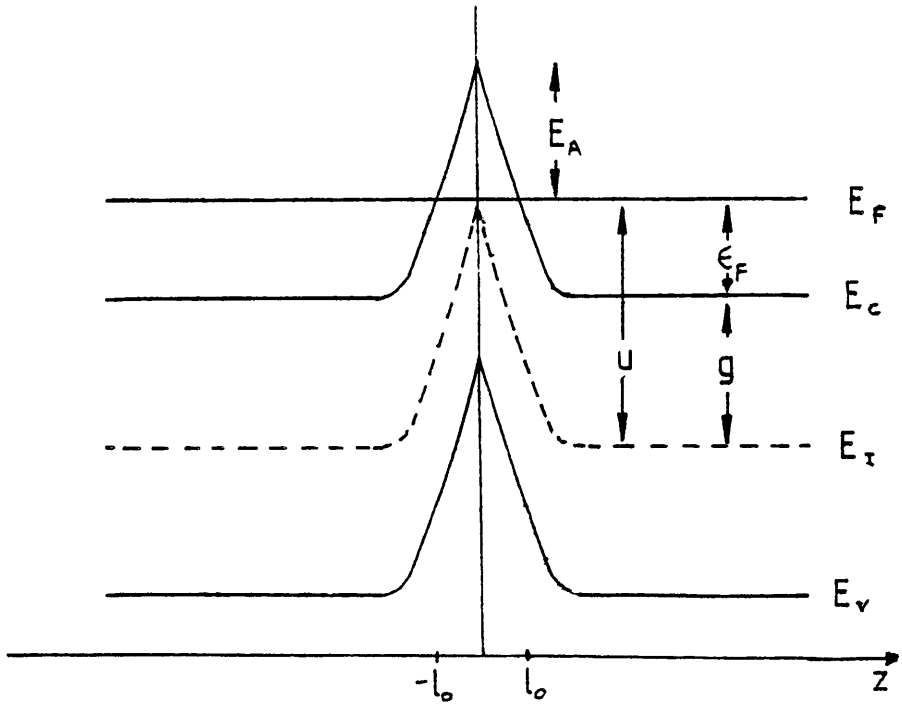

Fig. 4.2.2 : Sketch of the band diagram in polycrystalline Na_xWO_3 films around a grain boundary, showing the quantities used in the calculation of the space charge.

and Seebeck coefficient of the material at the centre of the grain and ρ_{gb}, S_{gb} are the corresponding quantities of the material in the region of the grain boundary depleted from carriers.

The electrical properties of the degenerate material of the grain are determined by the position of the Fermi level relative to the conduction band. On the other hand the electrical properties of the depletion region are determined by the properties of the potential barrier. The shape and height of the potential barrier can be obtained, in the one dimensional case, under certain simplifying approximations from a space charge calculation of the grain.

It is assumed that the electron distribution at the centre of the grain is not affected by the presence of the space charge region and that the distribution of sodium is uniform throughout the grain right up to the interface with the next grain. Any non-uniformity in the distribution of sodium is ignored for the purpose of this calculation. Under these assumptions we follow the space charge calculation of Seiwatz and Green [51].

The energy and potential terms used are shown in Fig. 4.2.2. E_F is the Fermi level, E_c and E_V are the energies at the bottom and top of the conduction and valence bands respectively and E_I is the energy that E_F would assume if the grain were intrinsic. The following quantities are used:

$$u = \frac{E_F - E_I}{kT} \tag{4.2.3}$$

$$g = \frac{E_c - E_I}{kT} \tag{4.2.4}$$

$$\epsilon_F = \frac{E_F - E_c}{kT} \quad . \tag{4.2.5}$$

The charge density, ρ_c, at any point inside the grain is given by

$$\rho_c = eN_D - eN_e \qquad (4.2.6)$$

where e is the electronic charge, N_D is the concentration of the sodium atoms which are assumed to be ionized at all temperatures and N_e is the electron concentration in the conduction band.

We assume that the concentration of the acceptor-like impurities and the hole concentration are negligibly small.

The electron concentration, N_e, at any point inside the grain is given by [51] :

$$N_e = 4\pi \left(\frac{2m^* kT}{h^2}\right)^{3/2} F_{\frac{1}{2}}(u-g) \qquad (4.2.7)$$

where m^* is the effective mass of the electron and the function $F_{\frac{1}{2}}(u-g)$ is defined by the relation

$$F_j(\eta) = \int_0^\infty \frac{x^j dx}{1+\exp(x-\eta)} \quad . \qquad (4.2.8)$$

Equ. (4.2.7) is applicable to solids with parabolic conduction bands and therefore can be applied to Na_xWO_3 since such an approximation was shown to be valid (see section 4.1.2).

Poisson's equation in one dimension can be written as

$$\frac{d^2u}{dz^2} = - e^2\rho_c/\varepsilon_s\varepsilon_0 kT \qquad (4.2.9)$$

where ε_s and ε_0 are the permitivities of WO_3 and free space.

Using equ. (4.2.6) and equ. (4.2.7), equ. (4.2.9) can be written as

$$\frac{d^2u}{dz^2} = -A + BF_{\frac{1}{2}}(u-g) \qquad (4.2.10)$$

where

$$A = \frac{e^2 N_D}{\varepsilon_s \varepsilon_0 kT} \qquad (4.2.11)$$

and

$$B = \frac{e^2 4\pi \dfrac{(2m^* kT)^{3/2}}{h^2}}{\varepsilon_s \varepsilon_0 kT} \quad . \qquad (4.2.12)$$

Equ. (4.2.10) can be integrated using the relation

$$\frac{\partial F_j(\eta)}{\partial \eta} = j\, F_{j-1}(\eta) \qquad (4.2.13)$$

and the fact that at the centre of the grain $\frac{du}{dz} = 0$ and $u = g + \epsilon_F$ to give :

$$\frac{du}{dz} = \{2A(g + \epsilon_F - u) + \frac{4B}{3}[F_{3/2}(u-g) - F_{3/2}(\epsilon_F)]\}^{\frac{1}{2}} \qquad (4.2.14)$$

Equ. (4.2.14) evaluated at z = 0 gives

$$\left.\frac{du}{dz}\right|_{z=0} = \{2A(\epsilon_A + \epsilon_F) + \frac{4B}{3}[F_{3/2}(-\epsilon_A) - F_{3/2}(\epsilon_F)]\}^{\frac{1}{2}} \qquad \ldots (4.2.15)$$

where $\epsilon_A = g - u$ at $z=0$ is the activation energy over the potential barrier in units of kT.

The numerical evaluation of $\frac{du}{dz}$ requires that the functions $F_j(\eta)$ be known for particular values of η. These functions have been evaluated for $j = \frac{1}{2}$ and $3/2$ in the range $\eta = -4$ to 20 by McDougall and Stoner [52] and tables for their evaluation can also be found in ref [51] and [53]. For values of η outside the range -4 to 20 the limiting forms of $F_j(\eta)$ can be used.

$$\lim_{\eta \to -\infty} F_{\frac{1}{2}}(\eta) = \tfrac{1}{2}\pi^{\frac{1}{2}} e^{\eta} \qquad (4.2.16)$$

and

$$\lim_{\eta \to -\infty} F_j(\eta) = (j+1)^{-1} \eta^{j+1} \quad . \qquad (4.2.17)$$

For the experimentally found values of ϵ_A and ϵ_F (see Table 3.2.3) $F_{3/2}(-\epsilon_A) \ll F_{3/2}(\epsilon_F)$ and equ. (4.2.15) can be written as

$$\left.\frac{du}{dz}\right|_{z=0} \approx \{2A(\epsilon_A+\epsilon_F) - \frac{4B}{3}F_{3/2}(\epsilon_F)\}^{\frac{1}{2}} \quad . \qquad (4.2.18)$$

The electric field E_s at the interface is given by the relation

$$E_s = -\frac{kT}{e} \left.\frac{du}{dz}\right|_{z=0} \qquad (4.2.19)$$

Using Gauss' law we can obtain the net space charge per unit interface area

$$Q_s = \frac{2\varepsilon_s\varepsilon_0 kT}{e} \left.\frac{du}{dz}\right|_{z=0} \qquad (4.2.20)$$

which can be related to the density of filled interface states.

The distribution of the interface states in Na_xWO_3 is not known. For the purpose of this discussion we shall assume that the mobility gap of the grain boundary material is the same as the intrinsic gap of the grain material and that both the conduction and valence bands densities of states of the grain boundary material have tails which extend towards the middle of the gap and which vary exponentially with energy. Therefore, the conduction band tail will be of the form :

$$N_s = N_0 \exp\left(\frac{E-E_I}{E_s} \right) \qquad (4.2.21)$$

where N_0 is the number of interface states per unit area at $E = E_I$ and E_s is a constant with the units of energy.

Assuming that each state can accommodate one electron, the number of filled states, above E_I, is given by

$$N_{ss} = \int_{E_I}^{E_F} N_s(E) f(E) dE \qquad (4.2.22)$$

where f(E) is given by

$$f(E) = \{1 + \exp(\frac{E-E_F}{kT}) \}^{-1} \qquad (4.2.23)$$

taking $f(E) \approx 1$, equ. (4.2.22) can easily be inregrated to give

$$N_{ss} = N_0 E_s \exp \left(\frac{(g-\epsilon_A)kT}{E_s} \right) . \qquad (4.2.24)$$

The interface charge given by equ. (4.2.20) is related to N_{ss} by the following equation :

$$Q_s = e\, N_{ss} \qquad (4.2.25)$$

which, using equ. (4.2.24), (4.2.20) and (4.2.18) can be written as

$$\exp\left(\frac{-\epsilon_A kT}{E_0}\right) = \frac{\varepsilon_s \varepsilon_0 kT}{e^2 N_0 E_s} \exp\left(\frac{gkT}{E_s}\right) \left\{ 2A(\epsilon_A + \epsilon_F) - \frac{4B}{3} F_{3/2}(\epsilon_F) \right\}^{\frac{1}{2}} \qquad \ldots(4.2.26)$$

Equ. (4.2.26) can be used to calculate ϵ_A, once N_0 and E_s are known.

The calculation of the shape of the potential barrier can only be achieved by solving the differential equ. (4.2.14). However, this is not easily done.

In the region $0 \leq z \leq \ell_0$, the following approximation can be made

$$F_{3/2}(u-g) \ll F_{3/2}(\epsilon_F) \quad . \qquad (4.2.27)$$

The physical meaning of the approximation (4.2.27) is that the density of free carriers in the region $0 \leq z \leq \ell_0$ is much smaller than the density of the free carriers in the region $\ell_0 \leq z \leq L-\ell_0$.

Using the relation (4.2.27), equ. (4.2.14) can be written as :

$$\frac{du}{dz} = \left\{2A(g+\epsilon_F-u) - \frac{4B}{3} F_{3/2}(\epsilon_F)\right\}^{\frac{1}{2}} \qquad \text{for } 0 \leq z \leq \ell_0 \qquad \ldots(4.2.28)$$

Equ. (4.2.28) can be simplified making the substitution

$$v = \{2A(g + \epsilon_F) - \frac{4B}{3} F_{3/2}(\epsilon_F) - 2Au\}^{\frac{1}{2}} \qquad (4.2.29)$$

$$\frac{dv}{dz} = -A \qquad 0 \leq z \leq \ell_0 \quad . \qquad (4.2.30)$$

Equ. (4.2.30) can be solved, taking into account that at $z = 0$ $u = g - \epsilon_A$, to give

$$u = g + \epsilon_F - \frac{2B}{3A} F_{3/2}(\epsilon_F) - \frac{1}{2A}\left\{[2A(\epsilon_A+\epsilon_F) - \frac{4B}{3}F_{3/2}(\epsilon_F)]^{\frac{1}{2}} - Az\right\}^{\frac{1}{2}} \qquad \ldots (4.2.31)$$

which gives the shape of the potential barrier in the region $0 \leq z \leq \ell_0$.

Making use of the fact that $u = g$ at $z = \ell_0$, an expression for ℓ_0 can be obtained from equ. (4.2.31), in terms of ϵ_A and ϵ_F.

$$\ell_0 = \frac{1}{A}\{[2A(\epsilon_A + \epsilon_F) - \frac{4B}{3} F_{3/2}(\epsilon_F)]^{\frac{1}{2}} - [2A\epsilon_F - \frac{4B}{3} F_{3/2}(\epsilon_F)]^{\frac{1}{2}}\} \quad . \qquad \ldots (4.2.32)$$

The values of ϵ_A and ℓ_0 obtained from equ. (4.2.26) and (4.2.32) respectively are expected to provide reasonable approximations to the activation energy and the width of the depletion region at low sodium concentrations. At higher x-values, several conditions used in the derivation of these two equations are not satisfied:

a) For $x \gtrsim 0.08$, $\epsilon_F \gtrsim \epsilon_A$ and the approximation of ℓ_0 obtained from equ. (4.2.32) for $x \gtrsim 0.08$ cannot be considered as accurate.

b) It was shown in section (4.1.2) that for $x \gtrsim 0.05$ the band gap of Na_xWO_3 changes with x. Therefore, equ. (4.2.26) cannot be used for $x \gtrsim 0.05$ without taking into account the changes in the band gap.

c) It should also be pointed out that the electric field at the interface is expected to assume quite large values ($\sim 10^7$ V cm^{-1})

as x increases above 0.05. At these high values of the electric field the energy spectrum of Na_xWO_3 is expected to display Stark splitting of the order of several kT [50] thereby making a simple description of the band structure invalid.

Bearing the above limitations in mind, equs.(4.2.26) and (4.2.32) can be used in order to calculate the electrical properties of the depletion region and therefore the electrical properties of the Na_xWO_3 films can be compared with the experimentally obtained ones.

4.2.2 Resistivity of Na_xWO_3 films

The resistivity of Na_xWO_3 films can be approximated by equ. (4.2.1). The resistivity, ρ_g, of the central part of the grain, $\ell_0 < z < L-\ell_0$, is given by the relation

$$\rho_g = \frac{1}{e\mu_e N_e} \qquad (4.2.33)$$

where μ_e is the mobility of the electrons and N_e is the density of electrons in the conduction band.

In the range of x-values $0.0056 \leq x \leq 0.22$, the Fermi level is above the conduction band minimum, (c.f. section 4.1.2) and therefore N_e is given by equ. (4.1.26). The electron mobility is not known at low x-values, if however, we use the value of 15 $cm^2/Vsec$ found for $Na_{0.3}WO_3$ single crystal [55], equ. (4.2.33) becomes :

$$\rho_g \approx \frac{2.2\times10^{-4}}{x}\ \Omega\ cm \quad . \qquad (4.2.34)$$

ρ_g is therefore several orders of magnitude smaller than the resistivity of the film found experimentally (see table 3.2.3). Equ. (4.2.1) can be written as

$$\rho \approx \left(\frac{2\ell_0}{L}\right)\rho_{gb} \quad . \qquad (4.2.35)$$

There are two possible current transport mechanisms in the region of the barrier: termionic emission over the barrier and electron tunnelling through the barrier. We believe that both of these mechanisms contribute to the electronic current in the region of the potential barrier. The

relative proportion of the current density due to the two mechanisms depends on the thickness and height of the barrier as well as on the temperature and electric field applied to the sample.

For small electric fields, at temperatures above 300°K the thermionic emission current is expected to be the dominant component. At lower temperatures and/or low and thin potential barriers, the tunnelling component is ecpected to be significant too.

Therefore the resistivity, ρ_{gb}, of the depletion region, for $T \geq 300\,°K$, will be of the form:

$$\rho_{gb} = \rho_{gb}^{0} \exp\left(\frac{E_A}{kT}\right) \qquad (4.2.36)$$

as in the case of discontinuous thin metal films [56]. The constant ρ_{gb}^{0} is a function of the properties of the potential barrier and the sodium concentration of the film.

Therefore equ. (4.2.35) can be written as

$$\rho \approx \left(\frac{2\ell_0}{L}\right)\rho_{gb}^{0} \exp\left(\frac{E_A}{kT}\right) \qquad (4.2.37)$$

$$\text{for } T \geq 300°K$$

Equ. (4.2.37) is of the form of the experimental equations (3.2.1) provided that E_A is identified as the thermal activation energy and ρ_0 of equ. (3.2.1) is set equal to $\left(\frac{2\ell_0}{L}\right)\rho_{gb}^{0}$.

At temperatures lower then 300°K the tunnelling contribution becomes increasingly important and the resistivity deviates from Equ. (4.2.37), see Fig. (3.2.6) to (3.2.10). Furthermore, this deviation becomes larger and sets in at higher temperatures as the sodium concentration of the films increases. This is in agreement with the fact that the

tunnelling current increases as the height and width of the potential barrier become smaller.

Equ. (4.2.37) cannot be used to calculate the value of the resistivity of the films because ρ_{gb}^{0} is not known. It does, however, predict correctly the dependence of the resistivity on the mean grain size of the films. As can be seen from table (3.2.3), the ratio of the room temperature resistivity of the 50Å m.g.s. Na_xWO_3 films to that of the 2-3μ m.g.s. films with the same x-value is equal, to within a factor of five, to the inverse of the ratio of their m.g.s.

The values of the thermal activation energy of the 50Å m.g.s. Na_xWO_3 films, prepared under the same conditions, of table (3.2.3) are shown in Fig. (4.2.3). The line through the experimental points in Fig. (4.2.3) is obtained from equ. (4.2.26). The quantities used in this calculation are as follows :

g = 63 in kT units at 300°K has been obtained from the optical gap of 50Å WO_3 films (c.f. see 4.1.2)

ε_s the relative permitivity of WO_3 is taken to be 8, from measurements of WO_3 polycrystalline pellets [57]. Measurements of the dielectric properties of WO_3 films [58] also show that ε_s varies from 4 to 30 depending on the density of the films and the frequency at which the measurement was taken. It should, however, be pointed out that the relative permitivity of single crystal WO_3 is reported to be very large ($230 < \varepsilon_s < 1000$) at room temperature [59, 60]. This large value of the relative permitivity of single crystal WO_3 is possibly due to small amounts of hydrogen or other impurities which are incorporated in the WO_3 forming a dilute bronze. In such a case, the crystal is expected to behave like a metal and the

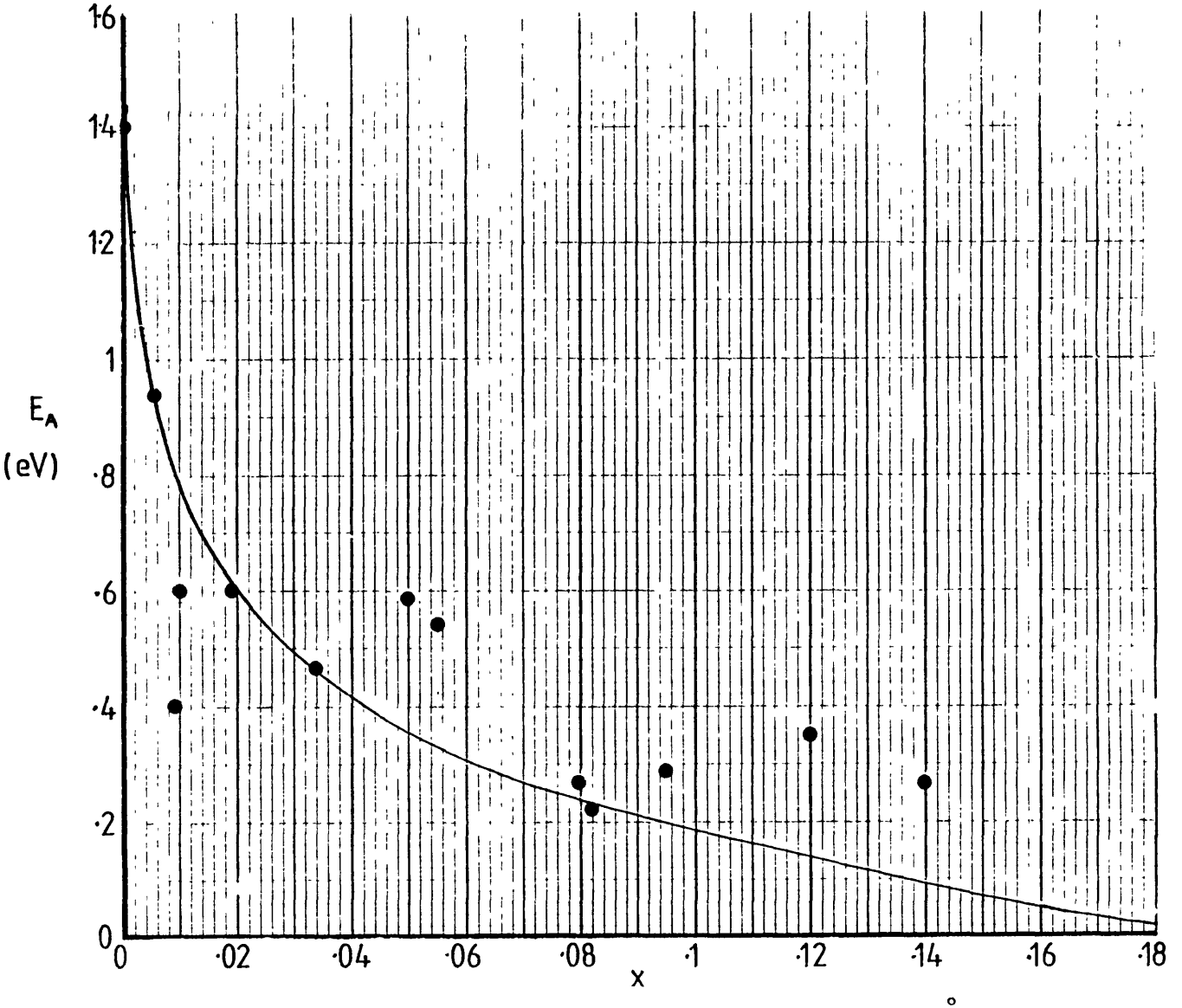

Fig. 4.2.3 : Thermal activation energy E_A vs x for the 50Å m.g.s. Na_xWO_3 films. The curve through the experimental points is calculated from Eqn. 4.2.38.

measured relative permitivity will be quite large.

ϵ_F, the reduced Fermi energy is calculated from the relation $\epsilon_F = \frac{1.3x^{2/3}}{kT}$ which was found from the optical properties of Na_xWO_3 to be valid for x-values at least up to 0.05 (c.f. section 4.12).
m* is taken equal to the free electron mass

$E_s = 0.782$ eV

$N_0 = 9.94\times10^{35}\ m^{-2}J^{-1}$.

E_s and N_0 have been obtained by fitting equ. (4.2.26) to the experimental results at the low x-value side of Fig. (4.2.3), where the assumptions in the derivation of equ. (4.2.26) are at their best.

Using the above quantities equ. (4.2.26) becomes

$$\exp(-0.033\ \epsilon_A) = 0.02\ \{10^3 x(\epsilon_A+\epsilon_F) - F_{3/2}(\epsilon_F)\}^{\frac{1}{2}} \quad \ldots \quad (4.2.38)$$

Taking into account the limitations of equs.(4.2.26) and (4.2.38) (c.f. section 4.2.1), the theoretical curve obtained from equ. (4.2.38) is in satisfactory agreement with the experimental results. Equ. (4.2.38) predicts that as $x \to 0$, E_A tends to the value of half the optical gap of 50Å m.g.s. WO_3 films which was found to be 1.625 eV. This is also in agreement with the value of the activation energy of WO_3 film Al (see table 3.2.3) found to be 1.4eV, considering that WO_3 films contain small amounts of hydrogen which will decrease their thermal activation energy.

At high x-values, $x \sim 0.2$, equ. (4.2.38) predicts that the activation energy tends to zero as it is expected to happen when all the localized interface states are filled. Note that the experimental data tend to zero as well, but at higher x-values, see table (3.2.3).

It is expected that when the activation energy becomes zero the resistivity of the Na_xWO_3 films will become metallic and it will be given by equ. (4.2.23) approaching the resistivity of the single crystal Na_xWO_3.

It should be pointed out that the density of interface states was considered to be the same for all the films. This however, may not be the case: The interface states arise from incomplete bonding in the region of the grain boundary and their density is expected to be a sensitive function of the conditions of preparation of the films, and their subsequent history, e.g. heat treatment. This is well illustrated by the fact that the activation energy of the 2-3μ m.g.s. films is much smaller than the activation energy of the 50Å m.g.s. films with the same x-value, indicating that the density of the interface states in the annealed films is smaller. Therefore, the deviation of the experimental points from the theoretical curve in Fig. (4.2.3) can be partly attributed to small variations in the conditions of preparation of the films.

The effect of the water vapour partial pressure during evaporation on the resistivity of the WO_3 films, see Fig. (3.2.2), as well as the effect of the heat treatment of the films in vacuum and air, Figs. (3.2.2), (3.2.4) and (3.2.5) can be explained in terms of hydrogen bronze formation. We believe that water molecules adsorbed on the surface of the films and in the grain boundary regions, at low pressures, act as a source of protons which diffuse inside the film to form dilute hydrogen bronze.

It is expected that the hydrogen bronze formation is more favourable when the WO_3 film is oxygen deficient so that the reaction of water with the WO_3 is as follows:

$$\frac{x}{2} H_2O + WO_{3-y} \longrightarrow H_x WO_{3-y+\frac{x}{2}}$$

Heat treatment of these hydrogen bronze films in air results in partial outdiffusion of the hydrogen thereby increasing their resistivity and activation energy. In the case of large grain WO_3 films, the process of H_xWO_3 formation is much slower because the diffusion of hydrogen in and out of the film is much slower.

In view of the above discussion we conclude that the resistivity of the Na_xWO_3 films is mainly derermined by the presence of the potential barriers in the grain boundary region.

There are no electrical measurements of Na_xWO_3 films in the literature against which to compare our results. There is, however, good agreement between the behaviour of the resistivity of our films and the resistivity of H_xWO_3 films [61, 62, 63] which are expected to behave in a way similar to Na_xWO_3 films.

The dependence of the resistivity of H_xWO_3 films on the electric field applied to the film, [63, 64, 65], shows that the resistivity decreases as the electric field increases above $\sim 10^3$ V cm^{-1} and that the decrease of the resistivity is larger at lower temperatures. This is in agreement with the model of the electrical properties of Na_xWO_3 films discussed above, since the tunnelling contribution to the electric current is expected to be field dependent.

Resistivity measurements of single crystal bronzes [6, 27, 55, 66, 67, 68, 69] indicate that they are metallic i.e. their resistivity increases with temperature, in agreement with our assumption that the central part of the grains of Na_xWO_3 films behave as degenerate semiconductors. It has been reported that the single crystal bronzes with $x < 0.25$ exhibit semiconducting behaviour [5, 55, 66]. These reports, however, are based on the resistivity measurements of a few crystals with x-values lower than 0.25 and in view of the difficulties involved in obtaining good single crystals of tungsten bronzes with low x-values, have

to be treated with caution. There are, for example, electrical studies of $Rb_{0.18}WO_3$ [68] and $Ag_{0.01}WO_3$ [27] single crystals which show that these bronzes are metallic.

Several models put forward in order to explain the electrical properties of tungsten bronzes thin films have been influenced by the above reports of semiconducting behaviour of the single crystal bronzes with $x < 0.25$. Crandal et. al [62], Manfredi et.al.[70] and Dallacasa et. al. [65] propose that electric conduction in $HxWO_3$ films takes place in a set of localized levels below the conduction band by variable range hopping Goulding et. al. [63] suggest that the conduction occurs by small polaron hopping near the Fermi level in an impurity band. Gritsenka et. al. [61] explain the nature of the resistivity of H_xWO_3 films in terms of thermally activated tunnelling between deep centers.

There are several objections to the above models.

i) They do not take into account the polycrystalline nature of the films and the effect of the grain boundaries on their electrical properties. Instead, they consider the films to be amorphous and homogenious.

ii) They cannot explain the large variation of the thermal activation energy with x.

iii) The optical properties of Na_xWO_3 films (c.f. section 4.1.2) indicate that the electrons occupy conduction band states rather than localized states in the gap.

Mott [42] explains the experimental results of Lightsey et. al. [55] and the electrical properties of $Na_xTa_yW_{1-y}O_3$ investigated by Doumerc [71, 72] in terms of an Anderson type transition to a non-metalic state when $x \lesssim 0.2$. Although, the tantalum substitution may cause enough disorder in the lattice of the sodium bronzes for an Anderson transition to be possible, there is no evidence from our measurements that such a

metal-nonmetal transition occurs in Na_xWO_3 films.

Fuchs [73] and Webman et. al. [74] propose a model based on nonrandom clustering of the alkali atoms into metalic regions in order to interpret the electronic properties of alkali tungsten bronzes. This model is however, discounted by Tunstall [75, 76) on the basis of nuclear-resonance measurements and x-ray results and has been criticized by others as well.

Crowder et. al. [77] explain the electrical properties of WO_3 single crystal in terms of a shallow donor level and strong electron-phonon ınteraction. Polaronic conduction at low temperatures in WO_3 has also been proposed by Gehlic et. al. [57]. The resistivity of WO_3 films is dominated by the presence of the potential barriers in the grain boundary region and therefore the nature of the carriers in the grains cannot be determined unambiguously. However, in view of the fact that the electrical properties of single crystal WO_3 are very sensıtive to oxygen substochio-metry and the formation of crystallographic shear planes [71], further investigatıon of the properties of WO_3 single crystal is needed.

4.2.3 Thermoelectric power of Na_xWO_3 films

The Seebeck coefficient of Na_xWO_3 films is given by Equ. (4.2.2.). We expect that the Seebeck coefficient, S_g, of the undepleted part of the grains of the films will be given by the usual equation for a degenerate semiconductor [53]

$$S_g = -\frac{\pi^2}{3}\frac{k}{e}\frac{(3/2 + \lambda_s)}{\epsilon_F} \qquad (4.2.39)$$

where k is Boltjman's constant, e is the electronic charge and λ_s is a constant depending on the scattering process of the charge carriers in the semiconductor.

The scattering mechanism in Na_xWO_3 is not known but it will be assumed to be the sodium ions. In such a case λ_s takes the value of 3/2 [53] and equ. (4.2.39) becomes :

$$S_g = -\frac{851}{\epsilon_F}\ \mu V\ K^{-1} \quad . \qquad (4.2.40)$$

The use of ϵ_F in equ. (4.2.39) and (4.2.40) is only correct insofar, the extension of the space charge inside the undepleted part of the grain is very small. It is expected that because of the large number of free carriers, the space charge does not penerate more than 2-3Å inside the undepleted part of the grain.

The Seebeck ceofficient of the depleted region, S_{gb}, is not easy to calculate exactly. An approximate expression for S_{gb} can be obtained as follows:

The depleted region is treated as an extrinsic semiconductor. The Seebeck coefficient of an extrinsic semiconductor is given by [53]

$$S_e = \pm \frac{k}{e} [\eta - (\lambda_s + \frac{5}{2})] \qquad (4.2.41)$$

where η is the reduced potential energy of the carriers

In the case of the depleted region around the grain boundary, η is a function of the distance from the interface (see Fig. 4.2.2) and it is equal to (u-g), where u is given by equ. (4.2.31). The Seebeck coefficient dS_{gb} of a slice of the depletion region of thickness dz and at a distance z from the interface is given by:

$$dS_{gb} = \frac{k}{e} [u(z) - g - 4] \frac{dz}{\ell_0} \qquad (4.2.42)$$

where we set as before $\lambda_s = 3/2$

and

$$S_{gb} = \int_0^{\ell_0} dS_{gb} \quad . \qquad (4.2.43)$$

After substituting equs.(4.2.42) and (4.2.31) into equ. (4.2.43) and performing the integration we obtain :

$$S_{gb} = - 86.2\{\epsilon_A + \frac{A\ell_0^2}{6} - \frac{\ell_0}{2} [2A(\epsilon_A + \epsilon_F) - \frac{4B}{3} F_{3/2}(\epsilon_F)]^{\frac{1}{2}}\} \qquad ...(4.2.44)$$

where ℓ_0 is given by equ. (4.2.32) and S_{gb} is given in $\mu V K^{-1}$.

Equs.(4.2.40) and (4.2.44) are used in conjunction with equ. (4.2.2) in order to calculate the Seebeck coefficient of Na_xWO_3 films at 300°K. The parameters used in this calculations are as follows:

$$\epsilon_F = \frac{1.3x^{2/3}}{kT}$$

$$\epsilon_s = 8$$

m* is taken as the free electron mass

ϵ_A is the experimentally found activation energy in units of kT (see table 3.2.3).

The results of the calculation are shown in table (4.2.1). There is reasonably good agreement between the experimental and the calculated values of the Seebeck coefficient and furthermore the main features of the model discussed above are shown to be correct :

The contribution of S_{gb} to the total Seebeck coefficient of the films is significant for the small grain size with low x-values. As x increases and the barrier becomes smaller and thinner, the electrons can tunnel through it and the Seebeck coefficient is dominated by the contribution of the undepleted region of the grains.

In the case of the large grain films, the Seebeck coefficient is again dominated by the undepleted region of the grains both because of tunelling and the large dimensions of the grains. The above points can be further illustrated by the temperature dependence of the Seebeck coefficient. As can be seen from Figs. (3.2.11) and (3.2.12) the Seebeck coefficient decreases in absolute magnitude with decreasing temperature. This is due to the fact that at temepratures below 300°K, tunnelling becomes significant thereby reducing the contribution of S_{gb} to the total Seebeck coefficient which subsequently approaches the temperature dependence of S_g given by equ. (4.2.40). In the case of the films A17, B2 and B3 where the contribution of S_{gb} is negligible, the Seebeck coefficient follows the temperature dependence of Equ. (4.2.40) very well. From the slope of the curves A17, B2 and B3 of Figs.(3.2.11) and (3.2.12) their reduced Fermi energy, ϵ_F, is calculated to be 22.7, 8.23 and 21.3. These values can be compared with 18.36, 6.84 and 10.85 obtained from the equation $\epsilon_F = \frac{1.3x^{2/3}}{kT}$ (c.f. section 4.1.2), bearing in mind that the x-values of

Table 4.2.1

Quantities used in the calculation of the Seebeck coefficient from equ. (4.2.44)

Film	x	ϵ_F	ϵ_A	ℓ_0 (Å) cal. equ. (4.2.32)	S_{gb} ($\mu V K^{-1}$) equ. (4.2.44)	S ($\mu V K^{-1}$) equ. (4.2.40)	S ($\mu V K^{-1}$) equ. (4.2.2)	S ($\mu V K^{-1}$) experimental
A19	9×10^{-3}	2.18	15.5	10.5	- 892	- 390	- 601	-550±60
A9	5.5×10^{-2}	7.29	21	4.15	-1120	- 116.7	- 283	-212±25
A11	8.2×10^{-2}	9.51	8.53	1.5	- 689	- 89.5	- 125.5	-100±10
A14	1.1×10^{-1}	11.57	6.2*	0.9	- 603	- 73.5	- 92.5	-120±7
A15	1.2×10^{-1}	12.26	13.68	1.67	- 898	- 69.4	- 124.7	- 72±8
A12	8.4×10^{-2}	9.66	12.4	2	- 840	- 88.1	- 113	-185±10
A17	2.2×10^{-1}	18.36	4.07	-	-	- 46.35	- 46.35	- 20±2
B2	$\sim 5\times10^{-2}$	6.84	2.94	0.8	- 474.2	- 124.4	- 24.4	- 76±3
B3	$\sim10^{-1}$	10.85	1.59	-	-	- 78.4	- 78.4	- 20±2

* This value of ϵ_A has been calculated from equ. (4.2.38).

films B2 and B3 are only approximately known.

The values of Seebeck coefficient of Na_xWO_3 obtained experimentally are in good agreement with the Seebeck coefficient of H_xWO_3 films [63, 79].

There are no measurements of the Seebeck coefficient of single crystal tungsten bronzes with low x-values in the literature. However, the Seebeck ceofficient measurements of single crystal sodium tungsten bronzes with $x > 0.25$ [66] show that S varies as $x^{-2/3}$ with the sodium concentration, and that its small negative magnitude varies linearly with temperature which are in agreement with the behaviour of the Seebeck coefficient of films A17, B2 and B3.

We therefore conclude that the Seebeck coefficient of the Na_xWO_3 films shows that the charge carriers in the grains of the films are free electrons occupying conduction band states.

4.3 Conclusion

The optical and electrical properties of WO_3 and Na_xWO_3 thin films discussed in the previous section permit us to draw the following conclusions about the bulk electronic structure of these compounds:

i) The conduction band minima and valence band maxima of WO_3 are parabolic in energy for a limited range of energies and they are separated by both an indirect and a larger direct gap. The magnitude of the gaps depends on the crystal structure.

ii) The conduction band consists of at least two subbands. The energy difference between the minima of the two subbands is approximately 0.8eV.

iii) Sodium in Na_xWO_3, does not contribute in the formation of the conduction and valence bands. The electronic band structure of Na_xWO_3 can be treated in a "rigid band" approximation for $x \lesssim 0.05$. Sodium atoms are ionised forming a set of empty electronic states, 1.8eV above the minimum of the lower conduction subband which is partially filled by the liberated electrons. For $x \gtrsim 0.05$, the "rigid band" approximation is not valid because of changes in the band structure of the WO_3 caused by the deformation of the crystal structure under the influence of the high sodium concentration.

iv) The charge carriers in Na_xWO_3 can be treated as quasi-free electrons, throughout the x-values range i.e. $0 < x \leq 1$.

The above observations are in agreement with the model proposed by Goodenough [80, 81, 82] in order to explain the mechanism of band formation in tungsten bronzes and other oxides with the perovskite structure. According to this model the conduction band of WO_3 and Na_xWO_3 arises from the overlapping of 5d t_{2g} tungsten orbitals via the 2p oxygen orbitals and

the sodium atoms act as donors to this, otherwise empty, conduction band.

Furthermore, the experimental evidence of optical and electrical properties of Na_xWO_3 films, presented in the previous sections, indicates that models which introduce localization of the electrons in order to explain the properties of tungsten bronzes and other related compounds with $x \leq 0.25$ [30, 43, 29] are not applicable in the case of Na_xWO_3.

The use of thin films in the investigation of tungsten bronzes is very promising. However, in order to be able to extract quantitive information about the properties of the bronzes, the effects of the grain boundaries must be known to a satisfactory extent. To this purpose a systematic study of the properties of Na_xWO_3 thin films as a function of their grain size will be very useful.

Further information about the band structure of the bronzes can be obtained by investigating the optical properties of related compounds. The optical properties of tungsten bronzes with different alkali metals, in the visible and near infrared can produce information about the nature and position of the alkali states above the conduction band. On the other hand, information about the conduction band, can be obtained by studying the optical properties of mixed oxides bronzes ($Na_xMo_yW_{1-y}O_3$ or $Na_xTa_yW_{1-y}O_3$ etc), in the region of the main absorption edge.

It should be pointed out that both of these studies are expected to yield useful informatiom about the improvement of the efficiency of electrochromic devices based on WO_3 films, since the position of the absorption band giving rise to the blue colour of tungsten bronzes depends on the energy difference between the conduction subbands and the alkali states.

Finally, infromation about the scattering mechanism of the carriers in the conduction band can be extracted from Seebeck coefficient

and free carrier optical absorption measurements performed on large grain Na_xWO_3 films where the effect of grain boundaries is small.

REFERENCES

[1] M. Green and K.S. Kang, Solid State Ionics, 8, 281, (1983)

[2] K.S. Kang, Ph.D. Thesis, University of London (1979)

[3] R. Le Bihan, G. Grandet and S. Paoli, Proceedings of the 8th Inter. Vacuum Conf. Sept. 1980, p. 409.

[4] L.A. Aleshina, A.D. Fofanov and O.N. Shivrin, Sov. Phys. Sokl., 27, 945, (1982)

[5] I. Webman, J. Jortner and ,.H. Cohen, Physical Rev., B 15, 5712,(1977)

[6] A. Hussain, University of Stockholm Chem. Commun., 2, 1, (1978)

[7] "Optical properties of solids", F. Wooten, Academic Press, (1972)

[8] "Optical processes in semiconductors", J.I. Pankove, Dover Puplications Inc. (1971)

[9] S.K. Deb, Phil. Mag., 27, 801, (1973)

[10] A. Nakamura and S. Yamada, Appl. Phys., 24, 55, (1981)

[11] K. Mijake, H. Kanacko and V. Teramoto, J. Appli. Phys., 53, 1511,(1982

[12] F.P. Koffyberg, K. Dwight and A. Wold, Solid State Commu., 30, 433, (1979)

[13] M. Spichiger-Ulmann and J. Augustynski, J. Appl. Phys., 54, 6061, (1983)

[14] M.A. Butler, J. Appli. Phys., 48, 1914, (1977)

[15] M.A. Bulter, R.D. Nasby and R.K. Quinn, Solid State Comm. 19, 1011, (1976)

[16] G. Hoppmann and E. Salze, Optics Comm., 30, 179, (1979)

[17] D.W. Bullett, Solid State Comm., 46, 575, (1983)

[18] D.W. Bullett, J. Phys. C: Solid State Phys., 16, 2197, (1983)

[19] "The Electronic Theory of Heavily Doped Semiconductors", B.L. Bonch-Bruyevich, Americam Elsevier Publishing Company Inc. 1966.

[20] A.S. Ribnick, B. Post and E. Banks, Advances in Chemistry, Series 39, 246, (1963)

[21] J.V. Gabrusenoks, P.D. Cikmach, A.R. Lusis, J.J. Kleperis and G.M. Ramans, 4th International Conference on Solid State Ionics, Grenoble, France, 1983.

[22] R.J. Colton, A.M. Guzman and J.W. Rabalais, Appli. Phys., 49, 409, (1978)

[23] G. Hollinger, T.M. Duc and A. Deneuville, Phys. Rev. Lett., 37, 1564, (1976)

[24] P.G. Dickens, R.M.P. Quilliam and M.S. Whittingham, Mat. Res. Bull, 3, 941, (1968)

[25] J.F. Owen, K.J. Tecgarden and H.R. Shanks, Phys. Rev. B, 18, 3827, (1978)

[26] P. Camagni, A. Manara, G. Campaguoli, A. Gustinetti and A. Stella, Phys. Rev. B, 15, 4623, (.977)

[27] M.J. Sienko, Advances in chemistry series 39, Amer. Chem. Soc., 224, (1963)

[28] H. Höchst, R.D. Bringans and H.R. Shanks, Phys. Rev. B, 26, 1802, (1982)

[29] O.F. Schirmer, V. Wittwer, G. Baur and G. Brandt, J. Electrochem. Soc., 124, 749, (1977)

[30] B.W. Faughnan, R.S. Crandall and P.M. Heyman, R.C.A. Review, 36, 177, (1975)

[31] "Electronic Processes in Non-crystalline Materials", N.F. Mott and E.A. Davis, Clarendon Press, 2nd Ed. (1979)

[32] J.J. Hopfield, Comments on Solid State Physics, 1, 16, (1968)

[33] J. Tauc, L. Štourač, V. Vorlíček and M. Zavětova, Proc. Intern. Semiconductor Conf. Moscow, 1251, (1968)

[34] J.D. Dow and D. Redfield, Phys. Rev. B, 1, 3358, (1970)

[35] D. Redfield, Phys. Rev., 130, 914, (1963)

[36] D. Redfield, Phys. Rev., 130, 916, (1963)

[37] "Optical properties of semiconductors", T.S. Moss, Pub. Butterworths, (1961)

[38] D.N. Jarrett and L. Ward, J. Phys. D, 9, 1515, (1976)

[39] H.G. Craighead and R.A. Buhrman, Appli. Phys. Lett., 31, 423,(1977)

[40] Z. Hussain, Ph.D., Unpublished data

[41] K. Kang and M. Green, in press

[42] R. Juryska, Phys. stat. sol., 72, K161, (1975)

[43] J.H. Weaver and D.W. Lynch, Phys. Rev. B, 6, 3620, (1972)

[44] N.F. Mott, Phil. Mag., 35, 111, (1977)

[45] J.H. Pifer and E.K. Sichel, J. Elect. Mat., 9, 129, (1980)

[46] "Polarons in Ionic Crystals and Polar Semiconductors" ed. J.T. Devreese, North-Holland Publishing Company 1972

[47] J. Appel, Solid State Physics, 21, 193, (1968)

[48] P. Schlotter and L. Pickelmann, J. of Elect. Mat. 11, (1982)

[49] S.S. Penner, "Quantitative molecular spectroscopy and gas emissivities" Addison-Wesley Pub. Co. (1959)

[50] G. Herzberg, "Molecular Spectra and Molecular Structure", D. Van Nostrand Co., 3rd Ed., (1947)

[51] R. Seiwatz and M. Green, J. Appl. Phys. 29, 1034, (1958)

[52] J. McDougall and E.C. Stoner, Trans. Roy. Soc. A237, 67, (1938)

[53] "Thermoelectric Refrigeration" H.J. Goldsmid, Temple Press Books Ltd, 1964

[54] "Electrical properties of semiconductor surfaces" D.R. Frankl, Pergamon Press 1967

[55] P.A. Lightsey, D.A. Lilenfeld and D.F. Holcomb, Phys. Rev. B, 14, 4730, (1976)

[56] "Thin Film Phenomena" K.L. Chopra, McGeaw-Hill Book Co. 1969

[57] R. Gehlic and E. Salze, Phil. Mag. B, 47, 229, 1983

[58] Krishnaji and P. Kant and R. Srivastava, Thin Solid Film 30, 319, 1975

[59] I. Lefkowitz, M.B. Dowell and M.A. Shields, J. Solid State Chem., 15, 24, 1975

[60] E. Salze, Acta Cryst., A31, 360, 1975

[61] V.A. Gritsenko, Y. O. Roisin, L.E. Semenchuk and N.L. Schwartz, Solid State Comm. 38, 351, 1981

[62] R.S. Crandall and B.W. Faughnan, Physical Rev. Lett., 39, 232.(1977)

[63] M.R. Goulding and C.B. Thomas, Thin Solid Films 62, 175, 1979

[64] S. Benci, M. Manfredi and G.C. Salviati, Solid State Comm. 33, 107, 1980

[65] V. Dallacasa, M. Manfredi and G. Schianchi, Thin Solis Films,

[66] H.R. Shanks, P.H. Sidles and G.C. Danielson, "Advances in chemistry" series 39, Amer. Chem Soc., 1963

[67] L.D. Muhlestein and G.C. Danielson, Phys. Rev. 158, 825, 1967

[68] R.K. Stanley, R.C. Morris and W.G. Moulton, Phys. Rev. B, 20, 1903, 1979

[69] L.D. Ellerbeck, H.R. Shanks, P.H. Sidles and G.C. Danielson, The Journal of Chemical Physics 35, 298, 1961

[70] M. Manfredi, C. Paraccini, G. Salviati and G. Schianchi, Thin Solid Films, 79, 161, 1981

[71] J.P. Doumerc, "Tungsten Bronzes : Fluorine or Tantalum Substitution", from "The Metal-nonmetal Transitions in Disordered Systems", Ed. L.R.Friedman and D.P Tungtall, 1978

[72] D.P. Dordor, J.P. Doumerc and G. Villeneuve, Phil. Mag. B, 315,(1983)

[73] R. Fuchs, J. Chem. Phys. 42, 3781, 1965

[74] I. Webman, J. Jortner and M. Cohen, Phys. Rev. B, 13, 713,(1976)

[75] D.P. Tunstall, Phys. Rev. B, 14, 4735, (1976)

[76] D.P. Tunstall, Phys. Rev. B, 11, 2821, (1975)

[77] B.L. Crowder and H.J. Sienko, J. Chem. Phys., 38, 1576, (1963)

[78] W. Sahle and M. Nygren, J. Solid State Chem., 48, 154, (1983)

[79] M.R. Goulding, C.B. Thomas and R.J. Hurditch, Solid State Comm. 46, 451, (1983)

[80] J.B. Goodenough, Metalic Oxides, Progress in Solid State Chemistry, H. Reiss, Pergamon Press, 5, 145, (1971)

[81] J.B. Goodenough, J. Appl. Physics, 37, 1415, (1966)

[82] C.N.R. Rao and G.V.S. Rao, Phys. Sol. (a) 1, 597, 1970